

Novel Sample Formulations for Pure and Persistent Hyperpolarized Solutions via Dissolution Dynamic Nuclear Polarization

THÈSE N° 7507 (2017)

PRÉSENTÉE LE 10 FÉVRIER 2017

À LA FACULTÉ DES SCIENCES DE BASE

LABORATOIRE DE RÉSONANCE MAGNÉTIQUE BIOMOLÉCULAIRE

PROGRAMME DOCTORAL EN CHIMIE ET GÉNIE CHIMIQUE

ÉCOLE POLYTECHNIQUE FÉDÉRALE DE LAUSANNE

POUR L'OBTENTION DU GRADE DE DOCTEUR ÈS SCIENCES

PAR

Basile VUICHOUD

acceptée sur proposition du jury:

Prof. S. Gerber, présidente du jury

Prof. G. Bodenhausen, Prof. J.-Ph. Ansermet, directeurs de thèse

Dr J. Kempf, rapporteur

Dr A. Gossert, rapporteur

Prof. L. Helm, rapporteur



ÉCOLE POLYTECHNIQUE
FÉDÉRALE DE LAUSANNE

Suisse
2017

à Mirella

Abstract

Nuclear Magnetic Resonance (NMR) spectroscopy allows one to study and analyze the structure, motions and interactions of a broad variety of molecules. However, this technique has a major inconvenience: its low sensitivity, which therefore often results in the use of highly concentrated samples in order to observe tiny signals.

As recently as 2003, a new technique known as dissolution-DNP or d-DNP was invented by Ardenkjaer-Larsen *et al.* to overcome this drawback and to get more intense NMR signals in solution with enhancements factors larger than 10'000. This method consists essentially in mixing paramagnetic species (radicals) with samples containing the metabolites to be analyzed. These mixtures are then rapidly frozen at very low temperatures ($T = 1.2 - 4.2$ K) in liquid helium and, by applying a proper microwave irradiation, the polarization of the electrons can be transferred to nuclei such as ^1H or ^{13}C . This allows one to build up and store the enhanced magnetization of these nuclei and then to dissolve the samples by injecting a superheated solvent via a dissolution stick. The resulting hyperpolarized solution can be finally transferred to an NMR spectrometer where the signals can be recorded.

In the first two chapters of this thesis, the principles of NMR are introduced and the theory of DNP is explained in some detail. The dissolution equipment used in our laboratory and its different parts are shown, in particular the DNP polarizer where the transfer of polarization from electrons to nuclei occurs, the microwave source that is connected to the polarizer, and the dissolution system itself, which comprises the dissolution stick and the dissolution transfer line.

Another chapter is dedicated to the optimization of our DNP setup in order to achieve the highest possible polarization before the dissolution process. Several radicals are tested under carefully controlled conditions to identify the best suited for our DNP system. Furthermore, the modulation of the microwave frequency has been optimized in order to enhance the polarization transfer.

Finally, a number of dissolution experiments are presented that relate to different projects that have been carried out in the course of this thesis. The extent of the polarization can be determined accurately by looking directly at the hyperpolarized NMR spectrum. Filterable polymers containing suitable radical moieties have been synthesized in order to obtain pure hyperpolarized solutions. A final chapter outlines future applications and projects that can benefit from dissolution Dynamic Nuclear Polarization.

Keywords

Nuclear Magnetic Resonance (NMR), Dynamic Nuclear Polarization (DNP), Dissolution Dynamic Nuclear Polarization (d-DNP), Hyperpolarization, Cross-Polarization (CP), Hyperpolarized water, Radical-free solutions.

Résumé

La spectroscopie par Résonance Magnétique Nucléaire (RMN) permet d'étudier et d'analyser la structure, les mouvements et les interactions d'une grande variété de molécules. Cependant, cette technique possède un inconvénient majeur: sa faible sensibilité, qui résulte la plupart du temps dans l'utilisation d'échantillons très concentrés afin d'observer de minuscules signaux.

En 2003, une nouvelle technique communément appelée dissolution par polarisation dynamique nucléaire ou d-PDN inventée par Ardenkjaer-Larsen *et al.* fait son apparition. Elle permet de surmonter l'immense désavantage de la RMN et d'obtenir, en solution, des signaux plus intenses d'un facteur supérieur à 10'000. Cette méthode consiste essentiellement à mélanger des espèces paramagnétiques (comme des radicaux) avec des échantillons contenant les métabolites à analyser. Ces mélanges sont ensuite rapidement gelés à très basses températures ($T = 1.2 - 4.2$ K) dans de l'hélium liquide et, au moyen d'une irradiation par micro-ondes, la polarisation des électrons peut être transférée aux noyaux (^1H ou encore ^{13}C). Cela permet de construire et de stocker la magnétisation de ces noyaux et de dissoudre ensuite ces échantillons en injectant, via une canne de dissolution, un solvant surchauffé. La solution hyperpolarisée peut être finalement transférée vers un spectromètre RMN ou les signaux peuvent être enregistrés.

Dans les premiers chapitres de cette thèse, les principes de la RMN sont introduits et la théorie de la PDN est expliquée en plus de détails. L'équipement de dissolution utilisé dans notre laboratoire, ainsi que ces différentes parties sont exposés, et en particulier le polariseur PDN où le transfert de polarisation des électrons aux noyaux se fait, la source micro-ondes qui est connectée elle-même au polariseur et le système de dissolution qui comprend la canne de dissolution et la ligne de transfert.

Un chapitre est dédié à l'optimisation de notre système PDN afin d'obtenir la plus haute polarisation possible avant le processus de dissolution. Plusieurs radicaux sont testés avec attention pour identifier les meilleurs candidats pour notre système PDN. En plus, la modulation en fréquence micro-onde a été optimisée afin d'améliorer le transfert de polarisation.

Finalement, un grand nombre d'expériences de dissolution effectuées durant cette thèse sont présentées. Le gain en polarisation a pu être déterminé précisément en regardant directement le spectre RMN hyperpolarisé. Des polymères pouvant être filtrés et contenant les radicaux ont été synthétisés dans le but d'obtenir de pures solutions hyperpolarisées. Un chapitre final met en évidence les futures applications et projets qui pourront bénéficier de la dissolution par polarisation dynamique nucléaire.

Mots-clés

Résonance Magnétique Nucléaire (RMN) Polarisation Dynamique Nucléaire (PDN), Dissolution-PDN (d-PDN), Hyperpolarisation, Polarisation Croisée, Eau hyperpolarisée, Solutions sans radicaux

Contents

Abstract/Résumé	I
Contents	III
Chapter 1: Introduction	1
1.1 Nuclear Magnetic Resonance	1
1.2 Improvements in NMR	3
1.3 Structure of the Thesis	3
Chapter 2: Nuclear Magnetic Resonance and Dynamic Nuclear Polarization	5
2.1 Theory of NMR	5
2.1.1 Boltzmann distribution	7
2.2 Dynamic Nuclear Polarization (DNP)	9
2.2.1 Dynamic Nuclear Polarization theory	9
2.2.2 Electron Spin Resonance (ESR) line shape	12
2.3 Dynamic Nuclear Polarization Mechanisms	14
2.3.1 The Solid Effect (SE)	14
2.3.2 The Cross Effect (CE)	18
2.3.3 The Thermal Mixing (TM)	19
2.3.4 The Overhauser Effect (OE)	23
2.3.5 DNP mechanisms that are favored in our laboratory	24
2.4 Magic Angle Spinning-DNP (MAS-DNP)	25
2.5 Dissolution Dynamic Nuclear Polarization (d-DNP)	27
2.5.1 TEMPOL: a new radical	29
2.5.2 Hartmann-Hahn Cross-Polarization	31
2.5.3 Cross-Polarization applied to d-DNP	31
2.5.4 Cross-Polarization at 3.35 T	34
2.5.5 Cross-Polarization at 6.7 T	35
2.5.5 Cross-Polarization at 9.4 T	35
2.6 Dissolution-DNP Setup at the EPFL	36
2.6.1 Preparation of DNP samples	36
2.6.2 DNP polarizer	37
2.6.3 Dissolution stick	40
2.6.4 Magnetic tunnel	41
2.6.5 Injector and NMR spectrometer	43
References	45

Chapter 3: Improvements in Dynamic Nuclear Polarization	51
3.1 Introduction	51
3.2 Optimization of Radicals for Dissolution-DNP	52
3.2.1 TEMPOL, TOTAPOL and AMUPOL	53
3.2.2 Nitroxide radicals derived from TEMPOL	55
3.2.3 Conclusions concerning TEMPOL derivatives	56
3.3 Microwave Frequency Modulation for Dissolution Dynamic Nuclear Polarization	58
3.3.1 Optimization of microwave frequency modulation	58
3.3.2 Experimental results for microwave frequency modulation	60
3.3.3 Conclusions concerning microwave frequency modulation	63
References	65
Chapter 4: Improvements in Dissolution Dynamic Nuclear Polarization	69
4.1 Introduction	69
4.2 Spin Polarimetry Magnetic Resonance (SPY-MR)	70
4.2.1 Why use SPY-MR	70
4.2.2 Traditional determination of the polarization	71
4.2.3 Asymmetry of doublets for non-equilibrium populations	72
4.2.4 Eigenstates of a coupled two-spin system	72
4.2.5 Transitions frequencies and amplitudes	74
4.2.6 Signal amplitudes as a function of the populations	75
4.2.7 Asymmetry of doublets	77
4.2.8 Low temperature DNP and uniform spin temperature	78
4.2.9 The initial DNP polarizations	79
4.2.10 Initial asymmetry and polarization at time $t = 0$	80
4.2.11 Relaxation after dissolution	80
4.2.12 Asymmetry after dissolution	82
4.2.13 Asymmetry in arbitrary two-spin systems	83
4.2.14 Experimental results of SPY-MR	85
4.2.15 Conclusions concerning SPY-MR	89
4.3 Remote Cross-Polarization for Deuterated Metabolites	90
4.3.1 Extending the lifetimes by deuteration	91
4.3.2 Hyperpolarization of deuterated metabolites	91
4.3.3 Conclusions concerning remote hyperpolarization	95

4.4 HYper Polarizing Solids (HYPSO)	96
4.4.1 The HYPSO family	97
4.4.2 Hyperpolarization of [1- ¹³ C] sodium pyruvate using HYPSO-1	98
4.4.3 Hyperpolarization of metabolites with HYPSO-1	100
4.4.4 Optimization of HYPSO materials	101
4.4.5 Conclusions concerning HYPSO	103
4.5 Filterable Labeled Agents for Polarization (FLAP)	104
4.5.1 Traditional DNP samples versus FLAP samples	105
4.5.2 Hyperpolarization of water	107
4.5.3 Hyperpolarization of metabolites	110
4.5.4 Hyperpolarization of proteins	111
4.5.5 Stability of FLAP	113
4.5.6 Conclusions concerning FLAP	114
References	115
Chapter 5: Future Developments of Dissolution Dynamic Nuclear Polarization	121
5.1 Introduction	121
5.2 Hyperpolarization of Frozen Hydrocarbon Gases	122
5.2.1 Dissolution-DNP to hyperpolarize gases	123
5.2.2 Hyperpolarization of ethylene and butane	124
5.2.3 Dissolution-DNP attempt of hyperpolarized ethylene	127
5.2.4 Preliminary conclusions concerning the hyperpolarization of ethylene	129
5.3 Hyperpolarization of biological extracts	130
5.3.1 Dissolution-DNP for metabolomics	131
5.3.2 Experimental results for tomato and cancer cells extracts	131
5.3.3 Conclusions concerning d-DNP for metabolomics	133
5.4 In-Cell Dissolution Dynamic Nuclear Polarization	134
5.4.1 D-DNP for macrophages	135
5.4.2 Experimental results for d-DNP on macrophages	135
5.4.3 Conclusions concerning metabolism in cells	137
References	139
Conclusions	145

Supporting Information	147
6.1 Annexes	147
6.1.1 Optimization of radicals for dissolution-DNP	148
6.1.2 Microwave frequency modulation for dissolution Dynamic Nuclear Polarization	149
6.1.3 Spin Polarimetry Magnetic Resonance (SPY-MR)	150
6.1.4 Remote Cross-Polarization for deuterated metabolites	152
6.1.5 HYper Polarizing SOLids (HYPSO)	153
6.1.6 Filterable Labeled Agents for Polarization (FLAP)	155
6.1.7 Hyperpolarization of frozen hydrocarbon gases	156
6.1.8 Hyperpolarization of biological extracts	157
6.1.9 In-Cell dissolution Dynamic Nuclear Polarization	158
References	159
Remerciements	161
Curriculum Vitae	165

Chapter 1: Introduction

1.1 Nuclear Magnetic Resonance

Nuclear Magnetic Resonance Spectroscopy, or simply abridged NMR Spectroscopy, is nowadays one of the most widely used analytical techniques to observe and study matter at a molecular level. It can give a great deal of information on the structures, motions and chemical reactions of molecules without significantly modifying their properties and without damaging the analyzed system, in contrast to other techniques such as Mass Spectrometry (MS) or Gas Chromatography (GC).

The NMR phenomenon was first discovered almost 80 years ago by Rabi in 1938 [1] and was expanded to liquids and solids by Bloch and Purcell in 1946. [2, 3] Its principle relies on the absorption and re-emission of an electromagnetic radiation by nuclei in a magnetic field at a specific resonance frequency which depends on the magnetic properties of the atoms. Typically, this frequency is contained in the radio-wave range (60-1000 MHz) of the electromagnetic spectrum (see Fig. 1.1) and thus has a lower energy or longer wavelength in comparison with γ -rays, X-rays, UV, Visible or Infrared frequencies.

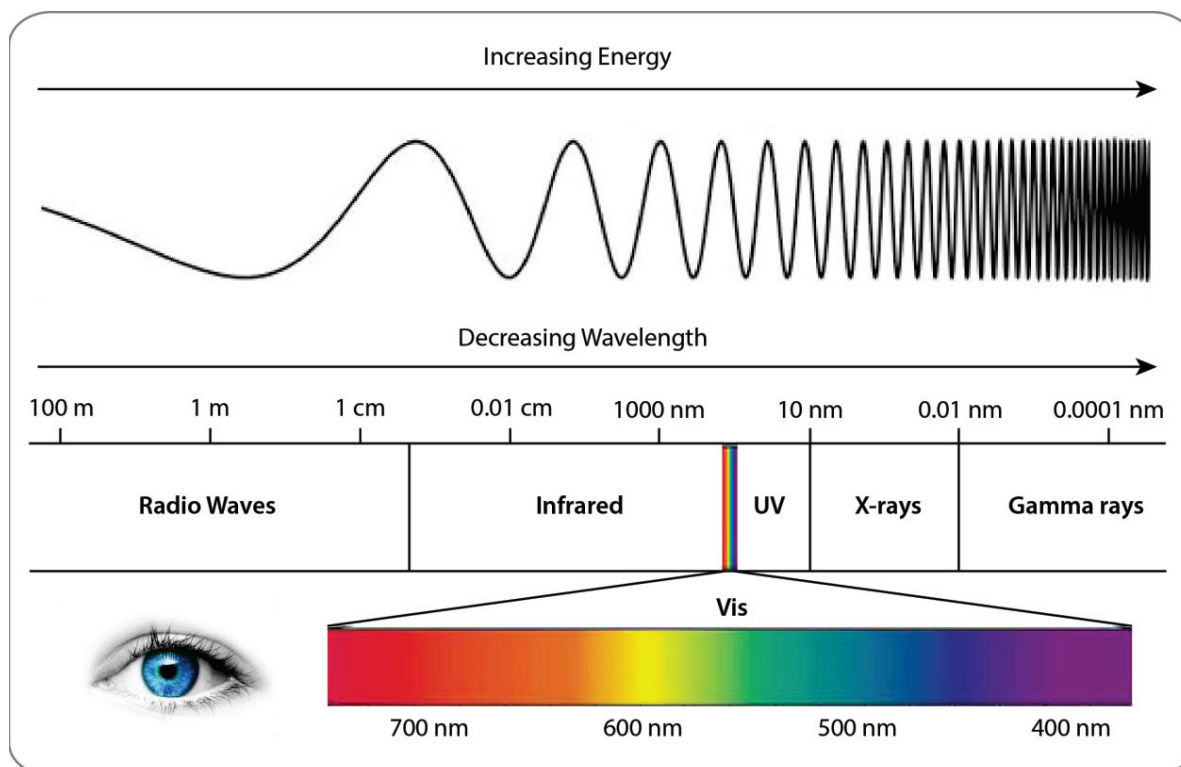


Figure 1.1: Complete electromagnetic spectrum including the different frequencies from radio-waves (low energy) to γ -rays (high energy). To illustrate the magnitude of the electromagnetic spectrum, the visible spectrum is presented and is only contained in 400 nm between the Infrared and UV frequencies. For our interest, the Nuclear Magnetic Resonance (NMR) and Electron Spin Resonance (ESR) are contained in the radio-wave domain with wavelengths varying from 1 cm to 100 m.

This absorption and re-emission of radiofrequency depend mainly on the type of nucleus observed (^1H , ^{13}C , ^{15}N , ^{29}Si , ^{31}P , ^{129}Xe , etc...) because of its characteristic magnetic moment μ , and are also specific to its chemical environments in the molecule, known as "chemical shifts" (see Fig 1.2). [4]

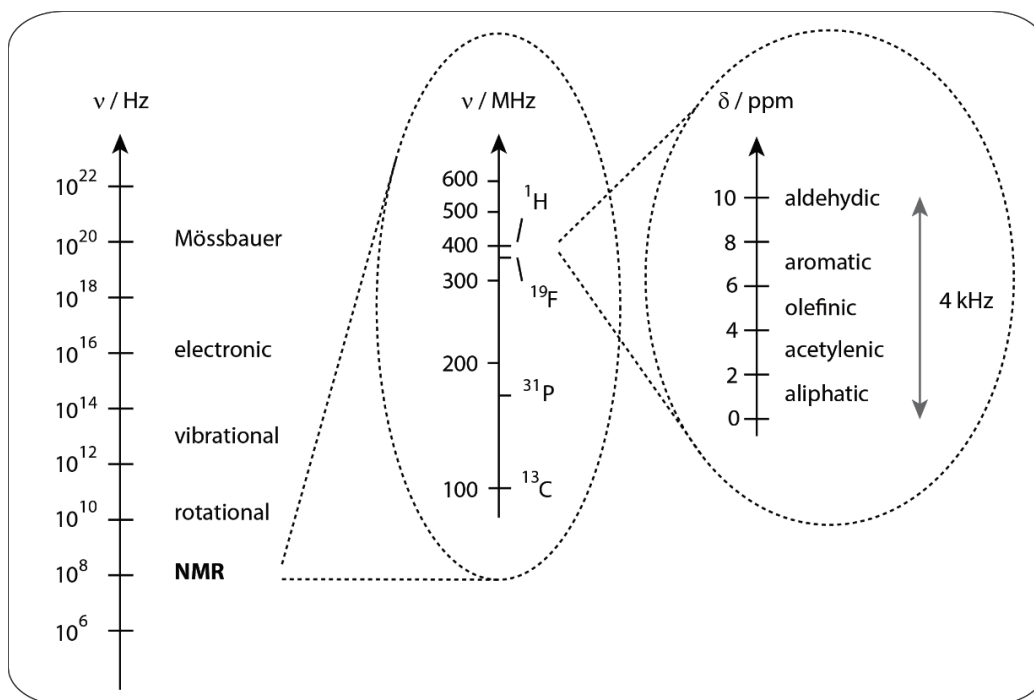


Figure 1.2: Illustration of the electromagnetic spectrum involving different methods of analytical spectroscopies at different specific frequencies (Mössbauer, electronic, vibrational, rotational and NMR). (Center) Zoom of the NMR region of interest for a 9.4 T field with the different isotopes (^1H , ^{19}F , ^{31}P and ^{13}C). (Right) The ^1H chemical shifts for different possible functional groups in molecules are represented, which are only separated by 4 kHz.

NMR is routinely used in chemistry and biochemistry for various sets of experiments from the simple determination of the structure of a small molecule to the motions and reactions of more complex systems such as proteins or even entire cells.

In the domain of radiology, Magnetic Resonance Imaging (MRI), resulting from NMR, is widely used to collect pictures of the body and physiological processes in living organisms without being invasive like PET-scan or X-rays that use ionizing radiation. It may allow one to record a three-dimensional image of a part of a body or an entire body in real time in order to detect diseases like tumors and even to monitor the blood flow in vessels.

1.2 Improvements in NMR

One of the most critical problems in Nuclear Magnetic Resonance Spectroscopy, where all experts in the field tend to agree with each other, is the low sensitivity of this method. Indeed, only relatively weak signals can be observed using conventional NMR techniques in comparison for example with Mass Spectrometry. To overcome this main drawback, Dynamic Nuclear Polarization, often simply called DNP [5, 6], was introduced more than 50 years ago and resulted in a high gain in sensitivity.

In this thesis, different mechanisms leading to DNP like the Solid Effect [7,8], the Cross Effect [9] and Thermal Mixing [10, 11] are discussed in detail and are presented according to the strength of the magnetic field B_0 and the temperature T of the system. Furthermore, a recent method arising from DNP known as dissolution-DNP or d-DNP [12] has been intensively studied. The d-DNP system used in our laboratory at the EPFL [13, 14] was carefully optimized to achieve the maximum enhancement possible for our conditions. During the four years of my research, several optimizations, from the sample preparation to the configuration of the instrumental setup, have been made in order to improve the overall sensitivity of our hyperpolarized system, while reducing the acquisition time in liquid phase.

1.3 Structure of the Thesis

The work presented in this thesis is divided in 5 main chapters. The introduction of this thesis is covered in chapter 1 and chapter 2 deals with the basis of the theory of Nuclear Magnetic Resonance and Dynamic Nuclear Polarization. Furthermore, the d-DNP setup built at EPFL is presented in detail with all its components. In chapter 3, improvements made for the optimization of the DNP process at low temperatures are presented. The different dissolution-DNP experiments performed in the course of the last four years are fully described in chapter 4. Finally, new concepts and ideas for the future of dissolution-DNP are discussed in chapter 5.

Chapter 2: Nuclear Magnetic Resonance and Dynamic Nuclear Polarization

2.1 Theory of NMR

As briefly mentioned earlier, NMR spectroscopy is based on nuclear magnetic moments of nuclei μ and more precisely on their intrinsic angular momentum called "spin", whose magnitude can be defined as follows:

$$\text{Magnitude of spin angular momentum} = \sqrt{I(I + 1)} \hbar \quad (2.1)$$

where \hbar represents the reduced Planck constant ($\hbar = h/2\pi$) and I is the spin quantum number which can only have half or integer values ($I = 0, \frac{1}{2}, 1, \frac{3}{2}, 2, \dots$).

This spin quantum number I is mainly determined by the number of unpaired protons and neutrons of the nucleus; this is why it is possible for isotopes of the same element to have different values for I . This is the case for ^{12}C , which has $I = 0$ and therefore no angular momentum or magnetic moment and finally no observable NMR signal, in contrast to ^{13}C , which exhibits a $I = \frac{1}{2}$ and has therefore an observable NMR spectrum.

The angular momentum denoted I_z (oriented parallel to the z-axis and which should not be mixed up with the spin quantum number I) possesses $(2I + 1)$ projections and represents the "permitted directions or orientations" of the nuclear spin in space:

$$I_z = m\hbar \quad (2.2)$$

where m is the magnetic quantum number comprising $2I + 1$ values between $-I$ and $+I$.

The magnetic moment of a nucleus denoted μ can also be determined; it is proportional to the angular momentum I_z :

$$\mu = \gamma I_z \quad (2.3)$$

where γ is the gyromagnetic ratio that is specific to each nucleus (for example $\gamma(^1\text{H}) = 26.75 \cdot 10^7 \text{ T}^{-1} \text{ s}^{-1}$ and for ^{13}C , the gyromagnetic ratio is roughly four times smaller $\gamma(^{13}\text{C}) = 6.73 \cdot 10^7 \text{ T}^{-1} \text{ s}^{-1}$; note that γ could also possess negative values, which is the case for ^{15}N , where $\gamma(^{15}\text{N}) = -2.71 \cdot 10^7 \text{ T}^{-1} \text{ s}^{-1}$).

Without the presence of an external magnetic field B , these $2I + 1$ orientations have the same energy and no signal can be observed by NMR. This state where there is no splitting in energy levels is known as "degenerate". This situation is lifted when a strong magnetic field is applied to the system. The energy resulting from the magnetic moment μ and the magnetic field B can be calculated:

$$E = -\mu_z B \quad (2.4)$$

where μ_z is the projection of μ onto the z axis (or onto the direction of the B field) and B corresponds to the strength of the external magnetic field.

From the previous Eqs. 2.2 and 2.3, the energy of a nuclear spin can be redefined as follows:

$$E = -m\hbar\gamma B \quad (2.5)$$

where the energy of the nucleus is now split into $2I + 1$ levels which are separated in proportion to the strength of the external magnetic field B and the gyromagnetic ratio γ . In Fig. 2.1, this energy splitting is illustrated for a spin-1/2 and for a spin-1 nucleus.

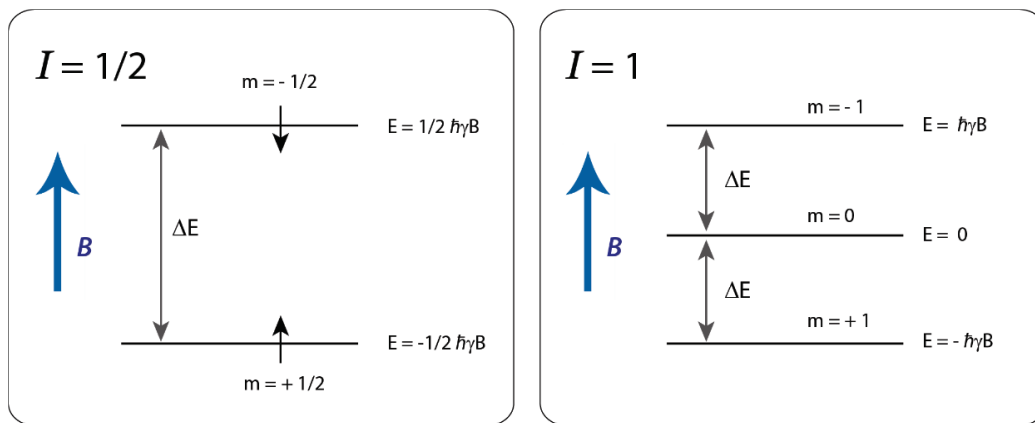


Figure 2.1: Energy splitting for a spin-1/2 (such as ^1H or ^{13}C) and a spin-1 (such as ^2H) nucleus in a strong external magnetic field B . The different spins are separated into $2I + 1$ levels with splittings that are proportional to the strength of the magnetic field and the gyromagnetic ratio.

In NMR, only certain transitions are permitted; these are called "allowed transitions", an expression which is often used in several kinds of spectroscopy. These permitted transitions are defined by "selection rules" and refer in our case to the magnetic quantum number m . Only transitions with $\Delta m = \pm 1$ are allowed between adjacent levels in NMR; these are more commonly described as transitions where the spins flip "up" or "down".

Thus the difference in energy between two levels can be determined:

$$\Delta E = \hbar\gamma B = h\nu \quad (2.6)$$

and can be redefined as function of ν :

$$\nu = \frac{\gamma B}{2\pi} \quad (2.7)$$

where ν corresponds to the frequency of the electromagnetic radiation.

2.1.1 Boltzmann distribution

As discussed previously, nuclear species having a spin I different from zero exhibit splittings between the $2I + 1$ energy levels in an external magnetic field. These separations are relatively small and a transfer between them can occur by thermal collisions, which leads to constant "flip-flops" of nuclear spins at ambient temperatures.

The arrangement of the populations of the states follows the Boltzmann law and (if we take the example of a spin $I = \frac{1}{2}$) can be determined as follows:

$$\frac{n_{upper}}{n_{lower}} = e^{-\Delta E/kT} = e^{-\hbar\gamma B/kT} \quad (2.8)$$

where n_{upper} and n_{lower} represent the populations in the upper and lower energy states (spin "down" and spin "up" with respect with the "up" direction of the external magnetic field), k is the Boltzmann constant ($= 1.38 \cdot 10^{-23} \text{ J}\cdot\text{K}^{-1}$) and T is the temperature in Kelvin.

When considering a spin $I = \frac{1}{2}$, the populations are almost evenly distributed between the two energy levels, since $\Delta E \approx kT$ in NMR, in contrast to electronic or UV/VIS spectroscopy, where $\Delta E > kT$. Nevertheless, a slightly larger fraction of nuclear spins has a tendency to be ordered in the lowest energy level (ground state), resulting in a slight excess of spins. This excess depends on the strength of the magnetic field, the gyromagnetic ratio and the temperature.

With the assumption that $\Delta E \ll kT$, equation 2.8 can be rewritten:

$$\frac{n_{lower} - n_{upper}}{n_{lower} + n_{upper}} = \frac{\Delta E}{2kT} \quad (2.9)$$

Typically for ^1H spins at room temperature in a 9.4 T magnetic field, the population difference between the two energy levels is $3.23 \cdot 10^{-5}$.

This slight difference in populations leads to the possibility of acquiring an NMR signal. Furthermore, the intensity of the signal recorded depends directly on this difference in populations. This means that the larger the difference, the more intense the signal will be, and the easier the detection by NMR spectroscopy. In average, only one nuclear spin in every 10^4 - 10^6 can be observed in the overall system, and this is why NMR signals are rather weak.

In order to overcome this lack of sensitivity, stronger magnetic fields can be used as well as nuclei possessing higher gyromagnetic ratios to maximize ΔE (see Eq. 2.8). However, the strength of the magnetic field cannot be enhanced sufficiently without excessive costs, and the choice of the nuclei to be analyzed is not always free. One last option would be to decrease the temperature T of the system, but this results in a decrease of the NMR resolution due to the frozen state of samples at low temperatures (typically deuterated water is used as an NMR solvent and its melting point is $T_{\text{melting}} = 3.8 \text{ }^\circ\text{C}$ or 276.95 K).

In the last decades, several techniques have emerged to overcome the main drawback of sensitivity in NMR spectroscopy, such as Optical Pumping [15, 16], Para-hydrogen [17], Brute Force [18, 19] and Dynamic Nuclear Polarization (DNP). [5, 6]

In the next chapters, the "*Brain Force*" Dynamic Nuclear Polarization (DNP) will be discussed in more detail, with dissolution Dynamic Nuclear Polarization (d-DNP) in order to obtain highly polarized molecules and new strategies and methods will be presented on how to extend the lifetimes of these enhanced signals.

2.2 Dynamic Nuclear Polarization (DNP)

Since its prediction in 1953 by Overhauser [20] who was confronted with several criticisms from the NMR community, and its successful experimental demonstration by Carver and Slichter in 1953 [21] and by Abraham *et al.* in 1959 [5], Dynamic Nuclear Polarization (DNP) has become a powerful tool to overcome the main drawback of NMR; its lack of sensitivity.

The principle of DNP simply relies on the saturation by irradiation at very low temperatures of the Electron Spin Resonance (ESR) transition of radical impurities present in the sample. It was first realized in metals that contain electrons in the conduction band, like Lithium. [21]

This technique was later extended to organic samples by introducing paramagnetic impurities or so-called "*free electrons*" in the system and therefore allow the transfer of the high polarization of electrons to nuclei by continuous microwave irradiation.

Despite this major step in hyperpolarization and gain in sensitivity, few applications of this promising method were discovered during this period, principally because of the very low temperatures required to boost the enhanced signals (in the order of a few Kelvins) and therefore the solid state of the frozen samples making it impossible to measure in a well-resolved manner as would be the case for liquid-phase samples.

The NMR community had to wait for the new millennium to witness in the reawakening of DNP by the introduction in 2003 of the dissolution Dynamic Nuclear Polarization (d-DNP) by Ardenkjaer *et al.* [12], which consisted of the rapid melting of the frozen sample followed by signal acquisition in solution.

2.2.1 Dynamic Nuclear Polarization theory

In the DNP community, the term "*polarization*" or "*enhancement*" is preferentially used to determine the efficiency of the hyperpolarization, instead of the "*populations*", which is more commonly employed by NMR experts. We can therefore define the polarization P of a system with the Boltzmann equations 2.8 and 2.9:

$$P = \frac{n_{upper} \cdot e^{\frac{\hbar\gamma B}{kT}} - n_{upper}}{n_{upper} \cdot e^{\frac{\hbar\gamma B}{kT}} + n_{upper}} = \frac{e^{\frac{\hbar\gamma B}{kT}} - 1}{e^{\frac{\hbar\gamma B}{kT}} + 1} \cdot \frac{e^{\frac{-\hbar\gamma B}{2kT}}}{e^{\frac{-\hbar\gamma B}{2kT}}} = \frac{e^{\frac{\hbar\gamma B}{2kT}} - e^{\frac{-\hbar\gamma B}{2kT}}}{e^{\frac{\hbar\gamma B}{2kT}} + e^{\frac{-\hbar\gamma B}{2kT}}} = \tanh \frac{\hbar\gamma B_0}{2kT} \quad (2.10)$$

where the polarization ($0 \leq P \leq 1$) is depending on the gyromagnetic ratio, the external magnetic field and the temperature of the system.

As demonstrated by Eq. 2.10, the polarization of a system increases at very low temperatures and high magnetic fields. Nevertheless it becomes challenging for economic reasons or physical limits to build NMR spectrometers with strong magnetic fields ($B_0 = 1.0$ GHz or 23.5 T in Lyon, CRMN) or to reach temperatures in the millikelvin (mK) range in order to scrounge some enhancement (only a few percent). This method is referred as the "Brute Force" technique. Some useful polarization values discussed in this thesis are given as examples in the following Table 2.1 as function of the nucleus, the temperature and the magnetic field.

			Polarization P [%]								
			$B_0 = 3.35$ T			$B_0 = 6.7$ T			$B_0 = 9.4$ T		
Nucleus	Natural abundance [%]	γ [$T^{-1} s^{-1}$]	$T = 1.2$ K	$T = 4.2$ K	$T = 298$ K	$T = 1.2$ K	$T = 4.2$ K	$T = 298$ K	$T = 1.2$ K	$T = 4.2$ K	$T = 298$ K
^1H	99.985	$26.75 \cdot 10^7$	0.29	$8.2 \cdot 10^{-2}$	$1.1 \cdot 10^{-3}$	0.57	0.16	$2.3 \cdot 10^{-3}$	0.80	0.23	$3.2 \cdot 10^{-3}$
^2H	0.015	$4.11 \cdot 10^7$	$4.2 \cdot 10^{-2}$	$1.3 \cdot 10^{-2}$	$1.8 \cdot 10^{-4}$	$8.8 \cdot 10^{-2}$	$2.5 \cdot 10^{-2}$	$3.5 \cdot 10^{-4}$	0.12	$3.5 \cdot 10^{-2}$	$5.0 \cdot 10^{-4}$
^{13}C	1.108	$6.73 \cdot 10^7$	$7.2 \cdot 10^{-2}$	$2.1 \cdot 10^{-2}$	$2.9 \cdot 10^{-4}$	0.14	$4.1 \cdot 10^{-2}$	$5.8 \cdot 10^{-4}$	0.20	$5.8 \cdot 10^{-2}$	$8.1 \cdot 10^{-4}$
^{15}N	0.370	$-2.71 \cdot 10^7$	$2.9 \cdot 10^{-2}$	$8.3 \cdot 10^{-3}$	$1.2 \cdot 10^{-4}$	$5.8 \cdot 10^{-2}$	$1.7 \cdot 10^{-2}$	$2.3 \cdot 10^{-4}$	$8.1 \cdot 10^{-2}$	$2.3 \cdot 10^{-2}$	$3.3 \cdot 10^{-4}$
^{129}Xe	0.264	$-7.40 \cdot 10^7$	$7.8 \cdot 10^{-2}$	$2.3 \cdot 10^{-3}$	$3.2 \cdot 10^{-4}$	0.16	$4.5 \cdot 10^{-2}$	$6.4 \cdot 10^{-4}$	0.22	$6.3 \cdot 10^{-2}$	$8.9 \cdot 10^{-4}$
e^-	100	$1.76 \cdot 10^{11}$	95.4	49.0	0.8	99.9	79.1	1.5	100	90.6	2.1

Table 2.1: Polarizations for several nuclei analyzed in this thesis at different temperatures from 1.2 K (critical liquid helium in our setup), 4.2 K (liquid helium temperature) and 298 K (room temperature) in DNP polarizers with magnetic fields of 3.35 and 6.7 T, and the experimental 9.4 T magnet recently installed in our laboratory. [22]

Hopefully for our hyperpolarized ambitions and to avoid spending severe expenses, Dynamic Nuclear Polarization, dubbed as the "*Brain Force*" method by Abragam, in opposition to the "*Brute Force*" discussed previously, relies mainly on the introduction in the system of paramagnetic species such as free electrons (the most commonly used radicals are Trityl and TEMPO). Therefore the goal of DNP is to play on the difference of the gyromagnetic ratios γ of electrons and nuclei:

$$\frac{\gamma_e}{\gamma_{^1H}} \approx 660 \text{ and } \frac{\gamma_e}{\gamma_{^{13}C}} \approx 2615 \quad (2.11)$$

where γ_e , $\gamma_{^1H}$ and $\gamma_{^{13}C}$ represent the gyromagnetic ratios of the electron, the proton and the carbon respectively.

In Fig 2.4, the polarizations of electrons and carbon-13 nuclei are represented as a function of the temperature in a 6.7 T magnetic field, as implemented in our laboratory. [13, 14] This graph shows that the maximum of the electron polarization of almost $P(e^-) \approx 100\%$ is already reached at 1.2 K, due to a strong rearrangement of the electron populations in the lower state, in comparison with carbon-13, where $P(^{13}C) \approx 0.14\%$ at the same temperature. Therefore an approach considered as "*cerebra*" consisting in the transfer of this optimum electron enhancement to other species that are in lack of polarization needs to be found.

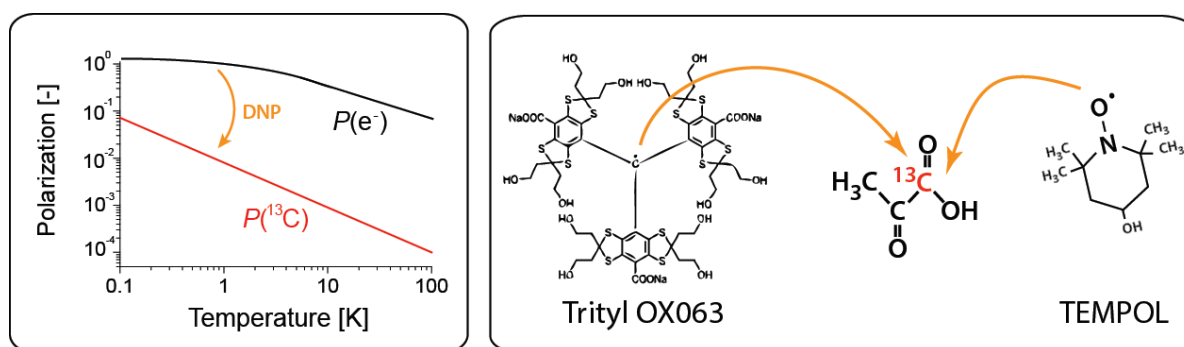


Figure 2.4: Polarizations of electron and carbon-13 spins as a function of temperature in the 6.7 T home-built DNP polarizer operating in our laboratory. [13, 14] The DNP process occurs by applying a microwave irradiation at a specific frequency of the ESR line of the radicals in the system. The most common radicals used are Trityl OX063 (left) or TEMPOL (right), which can both directly polarize the ^{13}C nuclei of organic molecules like pyruvate.

To allow this transfer, a microwave irradiation needs to be applied to establish a communication between the electrons represented by free radicals (usually Trityl OX063 or TEMPOL) and the nuclear species, and to promote a leakage of polarization from the paramagnetic impurities to the initially less polarized species like 1H or ^{13}C nuclei. However, the application of this microwave irradiation has to be precise and will depend on several factors that will be discussed straight away.

2.2.2 Electron Spin Resonance (ESR) line shape

The transfer of polarization from the paramagnetic species present in the system to the nuclei to be polarized depends on several elements. The electron resonance frequency is specific to every radical used and represents the frequency at which the electron absorbs the emitted microwave irradiation. The relaxation time T_{1e} corresponds to the time after which this electron will tend to return to its thermal equilibrium, and finally the shape of the spectrum will define the possibility of the transfer of the hyperpolarization to certain types of nuclei.

With all these factors in hand, it is now possible to predict the polarization transfer by saturating the Electron Spin Resonance lineshape of the radical species at a certain set frequency. In our laboratory, the nitroxide based radicals TEMPO or TEMPOL are the most commonly used in order to perform DNP and are described as "*standard*" paramagnetic species all along this thesis. Fig. 2.5 shows the ^1H NMR signal and the ESR signal of TEMPO at a moderate magnetic field ($B_0 = 6.7$ T) and very low temperature ($T = 1.2$ K). The frequency at which the TEMPO radical is absorbing is higher in energy than the one corresponding to the ratio of 660 for protons observed between their gyromagnetic ratios (see Eq. 2.11).

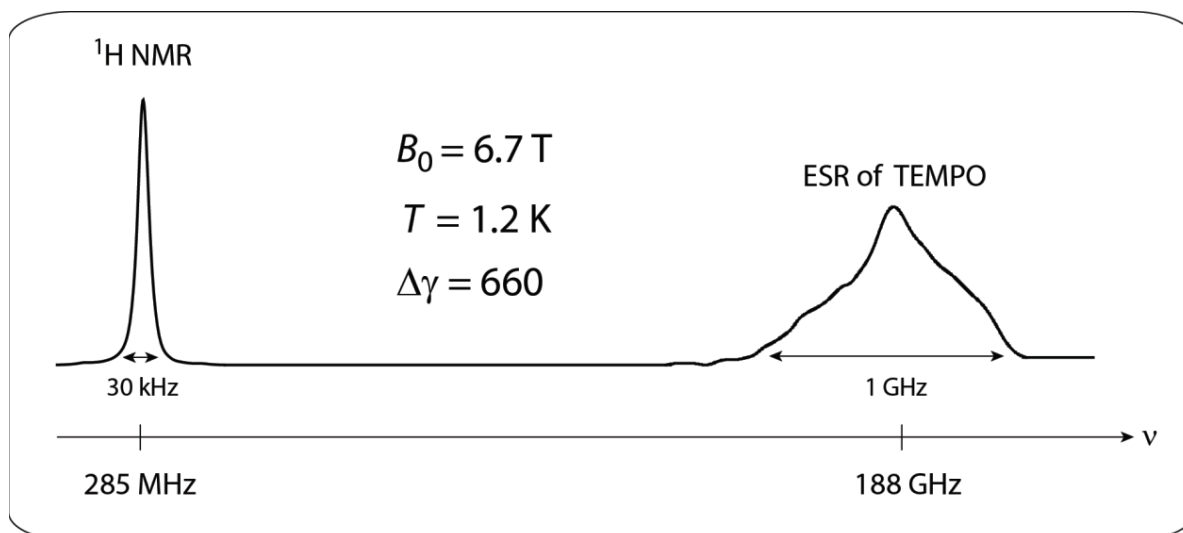


Figure 2.5: Schematic representation of a ^1H NMR spectrum and the ESR spectrum for TEMPO at a moderate magnetic field $B_0 = 6.7$ T and very low temperature $T = 1.2$ K. The difference in frequency of the signals depends principally on the gyromagnetic ratios of the electron and the proton ($\Delta\gamma = 660$), which makes one resonate in the radiowave spectrum and the other in the microwave spectrum.

The large difference in spectral widths between the signals of protons (only 30 kHz broad) and the signals of the TEMPO radicals (1 GHz broad) results mainly from the different orientations of the paramagnetic species in the system. For protons, the spectral width mainly depends on their dipolar interactions that will be affected by the concentration in the sample analyzed; the less protons in the system, the narrower the spectral width will be.

For paramagnetic impurities, other interactions contribute to the line shape depending on the type of radical used. They can be separated in two types of broadening. The three principal properties are shown and described in Fig. 2.6. In TEMPO, a coupling occurs between the electron on the nitroxide group (NO^\bullet) and the ^{14}N which possess a spin $I = 1$, resulting in a triplet signal corresponding to the magnetic moment $m = -1 ; 0 ; +1$. This interaction is called the hyperfine coupling and is part of the so-called inhomogeneous broadening, because the electrons in the system perceive different local magnetic fields. Another example of inhomogeneous broadening is the g-anisotropy. The spectral width will then depend on the random orientations of the radical with respect to an external magnetic field. The sample containing TEMPO should be in a frozen non-crystalline form to allow the different conformations of the radical in order to obtain a broad ESR line. Finally, in a frozen matrix containing the embedded radicals, dipole-dipole couplings between the electrons take place, which are part of the so-called homogeneous broadening, because the dipole-dipole interactions between pairs of nitroxide radicals do not fluctuate. [23]

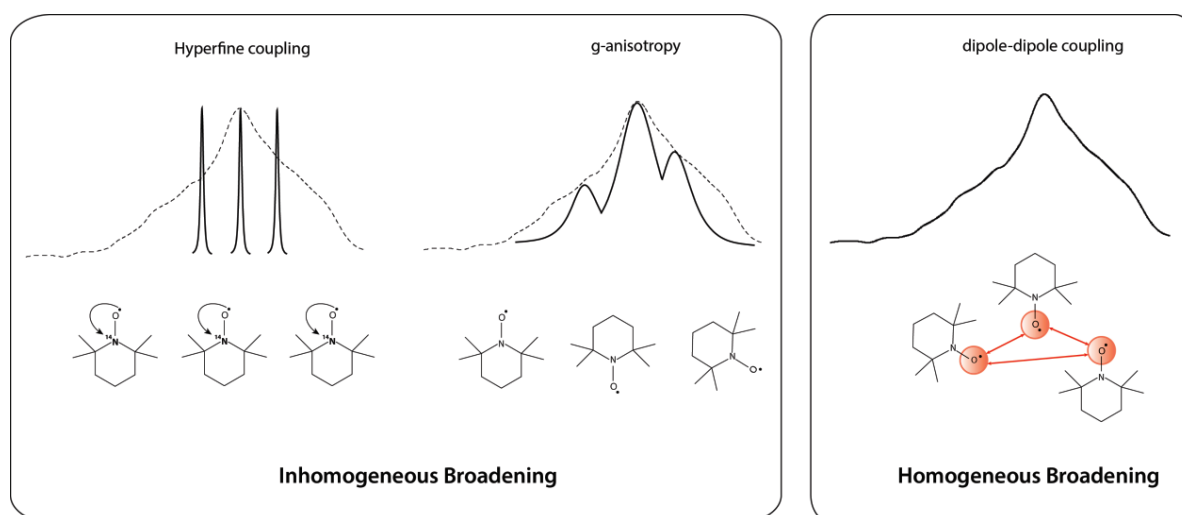


Figure 2.6: Schematic representation of the spectral width of the ESR line shapes of TEMPO radicals affected by inhomogeneous and homogeneous broadening. The hyperfine coupling between ^{14}N and the electron and the g-anisotropy corresponding to the orientations of the radicals lead to inhomogeneous broadening, while dipolar couplings between the electrons cause homogeneous broadening.

2.3 Dynamic Nuclear Polarization Mechanisms

Up to now, several mechanisms have been proposed to explain the transfer of polarization from electron spins to nuclear spins by DNP. These effects, known as Solid Effect (SE), Cross Effect (CE), Thermal Mixing (TM) and Overhauser Effect (OE), are quite different and arise independently or simultaneously under different conditions such as the strength of the magnetic field, the concentration of the electrons, and the temperature of the spin bath. Each of them will be mentioned separately in this chapter and explained briefly using schematic representations to get an idea about the predominant effect as a function of the experimental conditions.

2.3.1 The Solid Effect (SE)

The Solid Effect was described for the first time by Jeffries [7] in 1957 and was experimentally demonstrated in ^6LiF one year later by Abragam. [8] Its principle is one of the simplest to explain in order to understand DNP and relies on the interaction between one electron spin and one nuclear spin as presented in Fig. 2.7.

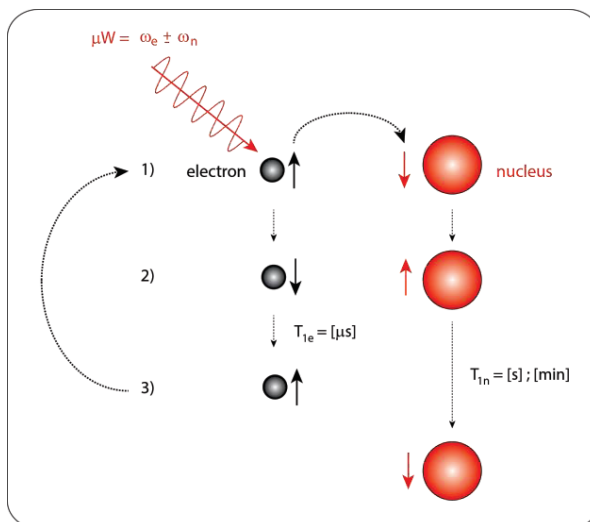


Figure 2.7: Simple representation of the Solid Effect involving an electron spin and a nuclear spin. (1) The hyperpolarized electron can transfer its polarization because a specific microwave irradiation is applied to the system (red arrow). (2) A flip-flop transition occurs and the nucleus is polarized. (3) The relaxation time T_{1e} of the electron is shorter than the relaxation time T_{1n} of the nucleus, bringing back the electron spin to its equilibrium state, allowing the process to start again by polarizing more nuclear spins.

In the first step, a hyperpolarized electron spin in the "up" position ($S = -\frac{1}{2}$ for electron) is irradiated by a specific microwave frequency $\omega_e \pm \omega_n$ (explained in more detail below) and is able to transfer its polarization to a distant nucleus in the "down" position ($I = \frac{1}{2}$ for proton). Second, the nucleus is now polarized in the "up" position and the electron in the "down" position; this process is referenced as a "flip-flop" transition. Then, both spins relax according to their spin-lattice relaxation times, the difference being that the relaxation time of the electron T_{1e} is shorter (microseconds) than the relaxation time T_{1n} of the nucleus (seconds to minutes, even hours at very low temperatures).

Thus the electron spin has enough time to flip back to its steady-state and the process can be repeated to polarize another nucleus (the spin diffusion process will be discussed later in this chapter), leading to the polarization of further nuclear spins.

To allow this transfer of polarization, a precise microwave frequency has to be applied to the system containing the electrons and nuclear species. This frequency has to be set to the difference $\omega_e - \omega_n$ (positive lobe) or to the sum $\omega_e + \omega_n$ (negative lobe) of the resonance frequencies of the electron and the nuclear spins, which will give rise to a DNP signal for the nucleus as explained in Fig. 2.8. If the microwave frequency is set to the resonance frequency of the electron ω_e , no signal will arise in the NMR spectrum through the Solid Effect mechanism.

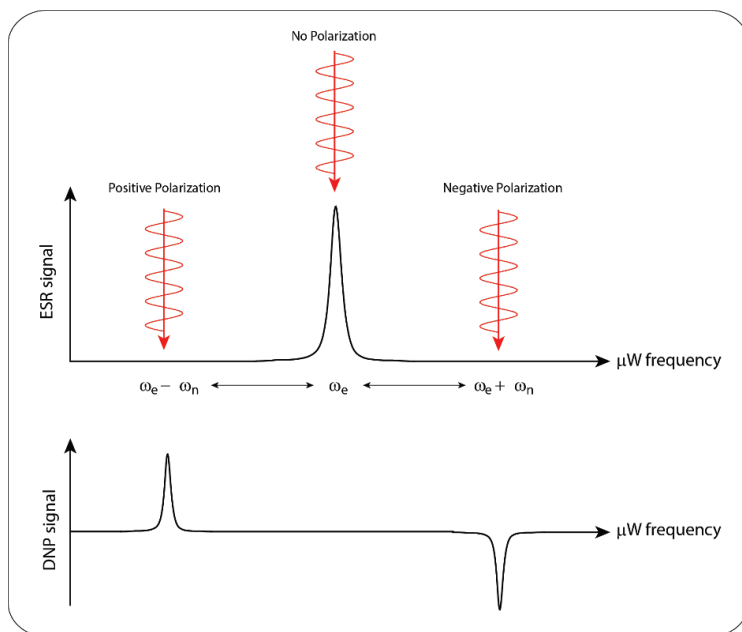


Figure 2.8: ESR signal of a radical with microwave irradiations at different frequencies for positive, central and negative lobes. The DNP signals arise from the Solid Effect when the microwave irradiation hits a precise frequency corresponding to $\omega_e \pm \omega_n$.

A more detailed explanation of the Solid Effect is given in Fig. 2.9. The electron and nuclear spin populations are distributed at equilibrium following the Boltzmann law (Eq. 2.8). The differences in energy levels reflect the resonance frequencies of the electron and the nucleus. When a positive microwave irradiation is applied (i.e., when the applied microwave resonance frequency is equal to $\omega_e - \omega_n$), the polarization can be transferred through the energy levels spaced by this precise frequency, which is defined as an electron-nuclear "flip-flop". The relaxation time of the electron T_{1e} brings the electron spin back to its thermal equilibrium faster than the relaxation time of the nucleus T_{1n} . Then the polarization cycle can start again to populate the lowest energy level and a so-called "positive polarization" builds up by the Solid Effect mechanism. When a microwave frequency equal to the resonance frequency of the electron ω_e is applied to the system, no transfer of polarization can be observed by SE and therefore no DNP signal is created. Finally, the case where a microwave frequency is applied at $\omega_e + \omega_n$ leads to a "negative polarization" as explained for the "positive polarization".

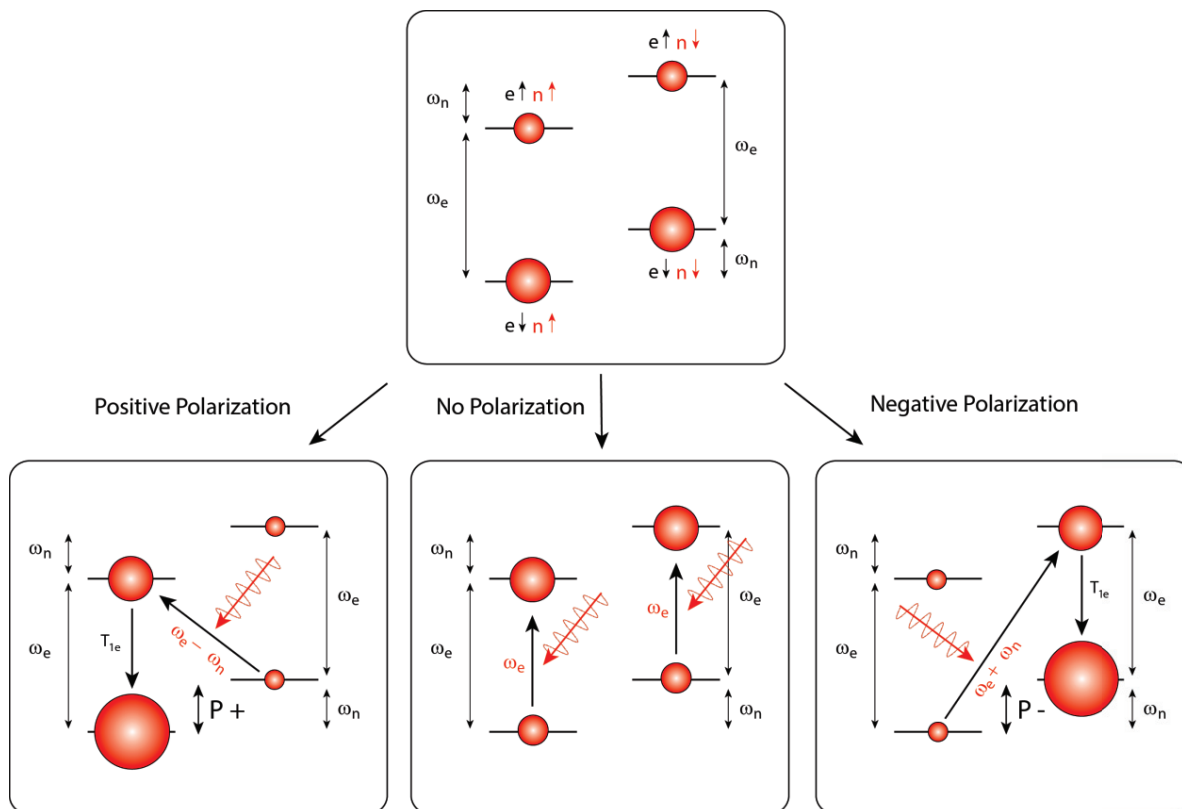


Figure 2.9: Solid Effect mechanism for a system comprising one electron and one nucleus. The different energy levels are represented for the equilibrium state (top), when a positive microwave irradiation (bottom left), a microwave irradiation equal to the resonance frequency of the electron (bottom center) and a negative microwave irradiation (bottom right) are applied to the system. This excitation by microwaves leads to a fast leakage of the populations through the different energy levels and in a slight excess of spins in one of these levels corresponding to a measurable polarization of the system. [24]

In order to be in a Solid Effect regime, different parameters comprising the microwave power, the concentration of the electron and nuclear spins and T_{2e} have to be fulfilled.

First of all, the previously defined "flip-flops" are second-order transitions allowed by dipolar interactions that are referred as "forbidden transitions". Thus, a strong saturation of the ESR line is needed to allow these transitions, which requires the use of a high microwave power input (like a gyrotron with a microwave power up to 15 W in continuous mode). Unfortunately this necessity for high μ -wave power could jeopardize the initial polarization of our system by providing heat to it, leading to a decrease of the optimal polarization that could have been achieved.

The concentration of the electrons in the DNP sample is also a critical factor to determine if we have preferentially a SE mechanism. The electron concentration has to be low, in contrast to the concentration of the nuclear species. Because of this, the relaxation time T_{2e} of the electrons can be long enough to avoid the loss of electron polarization during the transfer to the nuclei.

Furthermore, for the SE mechanism to work efficiently, the ESR linewidth of the radical species should be narrower than the nuclear Larmor frequency of the nucleus, which is, for example, not the case for nitroxide radicals like TEMPO and carbon-13. Another radical known as Trityl OX063 possess a smaller ESR lineshape in comparison with the ^{13}C Larmor frequency, which leads to the possibility of achieving a more efficient DNP enhancement via the Solid Effect mechanism.

Finally, in order to work effectively, "*Spin Diffusion*" (SD) has to occur in the DNP sample. [23] In a frozen state at very low temperatures, the distant nuclei do not have the ability to move near to an electron and do not have a chance to be properly hyperpolarized. Nevertheless, the polarization of the few nuclei that are close to an electron can be carried to the vast numbers of nuclear spins that are further away by a spin diffusion process relying on dipolar interactions.

Other features are specific to the Solid Effect, such as the maximum ideal polarization that can be achieved using a pure SE mechanism with a strong saturation, which is independent of the type of nucleus that is hyperpolarized. This means that the SE mechanism theoretically allows to get the same final polarization for any nuclei such as protons, carbons or nitrogens. However, even if the same level of polarization could be achieved, this does not imply that the nuclei would reach that level in the same build-up time T_{bup} . Furthermore the microwave irradiation has to be set at different frequencies depending on the nature of the nuclear spins to be polarized, which is in total opposition with the Thermal Mixing (TM) mechanism which will be described thereafter.

2.3.2 The Cross Effect (CE)

In comparison with the SE, the Cross Effect mechanism [25, 26, 27] involves two electrons and one nucleus representing a three-spin system. In order to achieve CE, the electron spins have to be dipolar coupled and their difference in spin resonance frequencies ($\omega_{e1} - \omega_{e2}$) should be separated by exactly the nuclear Larmor frequency ω_n . This last condition has to be fulfilled in order to allow the transfer of polarization from the electrons to the nucleus of interest, as illustrated by the red arrow in Fig. 2.10.

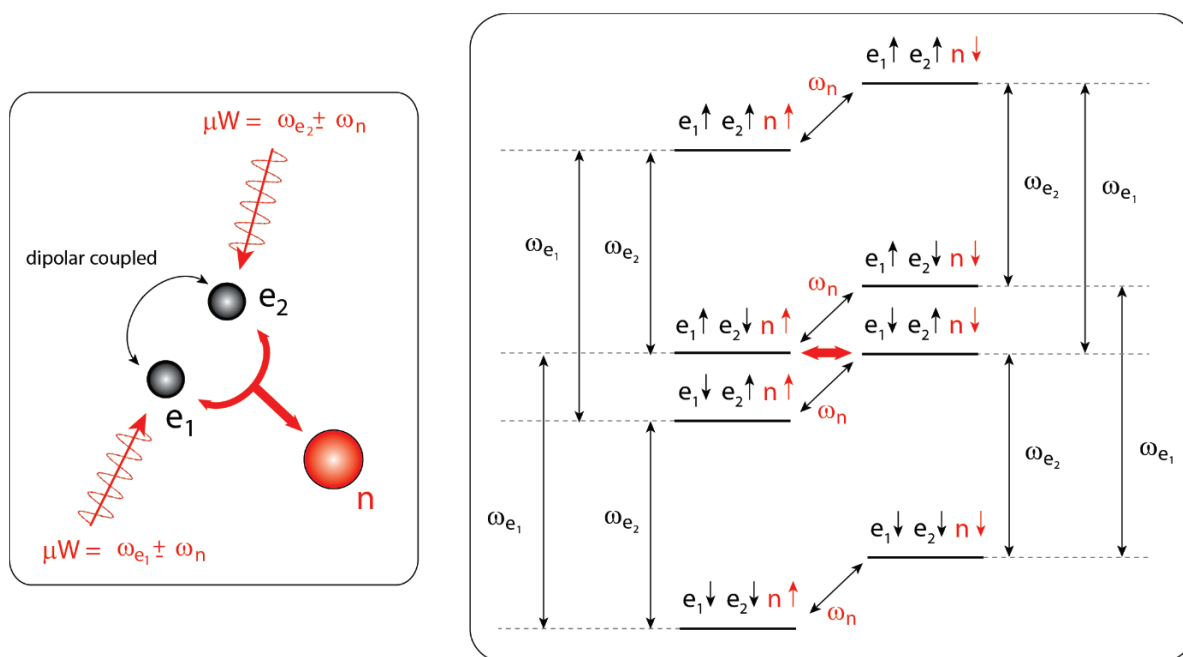


Figure 2.10: (Left) schematic representation of the Cross Effect mechanism involving two dipolar coupled electrons and one nucleus. (Right) Energy-level diagram of the CE involving the electron e_1 , the electron e_2 and the nucleus. The different levels are separated by the electron spin transitions ω_{e1} and ω_{e2} and the Larmor frequency of the nucleus ω_n . The red arrow represents the transfer of polarization, resulting from the "flip-flop" of the electrons that are dipolar coupled to the nucleus.

For the CE mechanism, the "flip-flop" transition occurring between the two electrons is not considered anymore as a forbidden transfer, as it was the case for the SE mechanism. Because of the condition that the difference of the electron spin resonances is equal to the Larmor frequency of the nucleus ($|\omega_{e1} - \omega_{e2}| = \omega_n$), the remaining energy can be transferred to perform a "flip-flop" of the nucleus. Because of this "allowed" transition, the microwave irradiation needed to perform the Cross Effect mechanism for a DNP sample is less demanding in energy than for the Solid Effect (milliwatts instead of a few watts).

Finally, in opposition to SE, CE is more efficient when a radical with an ESR line that is broader than the nuclear NMR Larmor frequency is used. Therefore, nitroxide radicals like TEMPO become the favorite candidate to hyperpolarize protons by the Cross Effect mechanism.

2.3.3 The Thermal Mixing (TM)

Thermal Mixing has first been described by Redfield [10], Provotorov [11] and later demonstrated by Cox and co-workers in 1973 [28], when they observed the evolution of the polarization after having switched off the microwave irradiation. During this experiment, they were polarizing ^{19}F and ^7Li in lithium fluoride at very low temperatures ($T = 0.74\text{ K}$) and low magnetic field ($B_0 = 2.5\text{ T}$) as presented in Fig. 2.11 A. By applying a saturation to ^7Li and by switching off the microwave irradiation, they were able to record the recovery of the polarization of lithium-7, which followed the decay of the polarization of ^{19}F , demonstrating that the two nuclei were able to communicate and to equalize their polarizations (Fig. 2.11 B). Then, after ^7Li has reached a plateau and with the microwaves still off, the entire system relaxed to its thermal equilibrium (Fig 2.11 C).

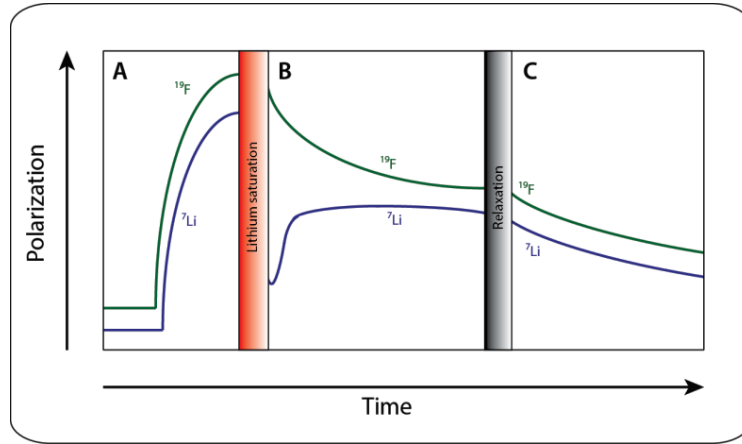


Figure 2.11: Schematic representation inspired by the work of Cox *et al.* [28] showing how Thermal Mixing was observed for the first time experimentally for lithium fluoride. (A) Dynamic Nuclear Polarization of ^7Li and ^{19}F nuclei at low temperature ($T = 0.74\text{ K}$) and low magnetic field ($B_0 = 2.5\text{ T}$). (B) A strong saturation is applied to ^7Li to destroy its polarization and the microwave irradiation is switched off. Through Thermal Mixing, the polarization of lithium recovers while the fluorine polarization decays. (C) After mixing and the equalization of the polarizations, the polarizations of the two nuclei relax to their thermal equilibrium.

In order to understand in more detail and to explain properly the concept of the Thermal Mixing mechanism, we have to introduce new terms like the spin temperature, the lattice reservoir, dynamic cooling and thermal contact.

The spin temperature T_S of a system can be described in analogy to the lattice temperature T_L at thermal equilibrium and can be defined by rearranging Eq. 2.10. It is important to notice that T_S can have positive or negative values.

$$T_S = \frac{\hbar\gamma B_0}{2k \cdot \tanh^{-1}(P_0)} = \frac{\hbar\gamma B_0}{k \cdot \ln\left(\frac{1+P_0}{1-P_0}\right)} \quad (2.12)$$

with $T_S = T_L$ at Boltzmann equilibrium.

However, when the system is not anymore at thermal equilibrium (e.g., when DNP occurs), the spin temperature T_S is not equal to the lattice temperature T_L . This phenomenon takes place when the system reaches another equilibrium by spin diffusion within a time T_{SD} that is smaller than T_{1e} . The advantage of defining the spin temperature instead of the polarization during a Thermal Mixing DNP process is that the different nuclei present in the DNP sample (^1H or ^{13}C) will have the same final value for T_S while their final polarization P will be different.

As mentioned before, the DNP process involving the TM mechanism involves a lattice which can be defined as a "reservoir" with a constant lattice temperature T_L . The overall system is also composed of an electron and a nuclear Zeeman system with different temperatures and an electron broadening system which depends on the electron concentration. [23] These three different reservoirs (i.e., the nuclear Zeeman, electron Zeeman and electron broadening reservoirs) should be in thermal contact as presented in Fig. 2.12.

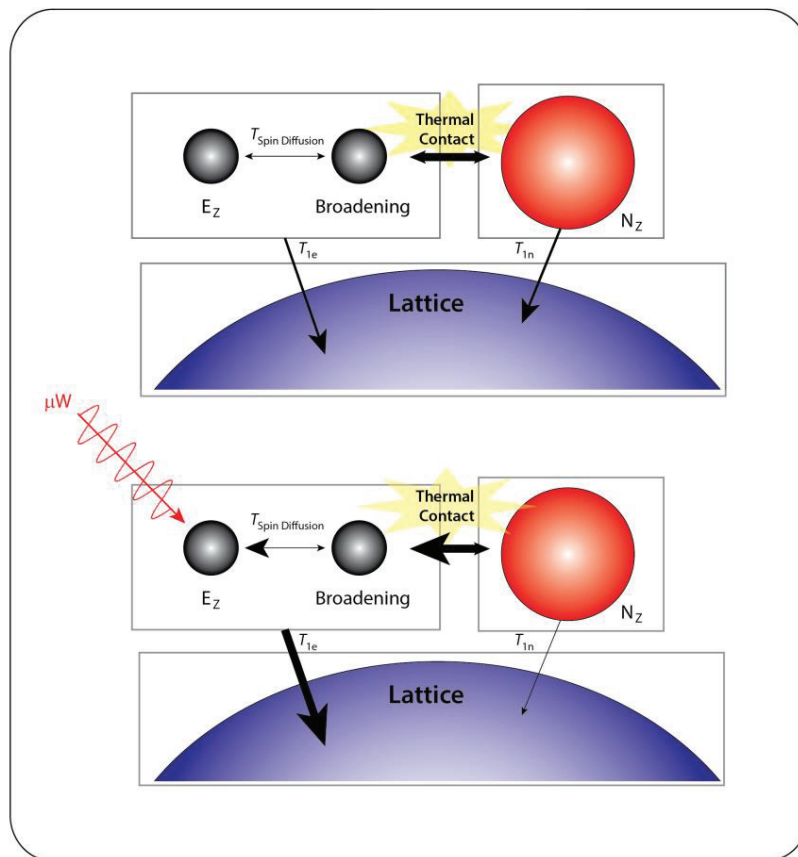


Figure 2.12: Schematic representation of the Thermal Mixing mechanism (adapted from Jannin [24]) showing the system at thermal equilibrium (top) and during the DNP process (bottom), leading to a leakage of order from the nuclear Zeeman system (N_Z) into the electron broadening reservoir by thermal contact. By applying a microwave irradiation and by rapid spin diffusion, the temperature of the electron Zeeman system is increased as it relaxes to the lattice reservoir.

To understand the cooling process of Thermal Mixing in more detail, we have to investigate how these systems interact with each other. In Fig. 2.13, a schematic representation of the electron Zeeman system composed of the two energy levels ($S = -1/2$) is shown as a function of the electron spin population. At thermal equilibrium, the populations are distributed between the two energy levels following Boltzmann's law. These levels are composed of different sub-levels reflecting the dipolar couplings and the g -anisotropy, and are defined as the electron broadening system. As previously said, the spin diffusion time T_{SD} should be smaller than the relaxation time of the electron T_{1e} to allow the electron broadening reservoir to achieve its own spin temperature. Therefore the electron concentration has to be sufficiently high to allow a fast spin diffusion in opposition to the SE mechanism. By applying a microwave irradiation (orange arrow in the figure; either in the positive lobe with $\omega_e - \omega_n$ or the negative lobe with $\omega_e + \omega_n$), the distribution of populations is rearranged as represented by the red curve in Fig. 2.13. This leads to a leakage of spin order of the electron broadening reservoir, which therefore decreases while the spin temperature of the electron Zeeman system increases.

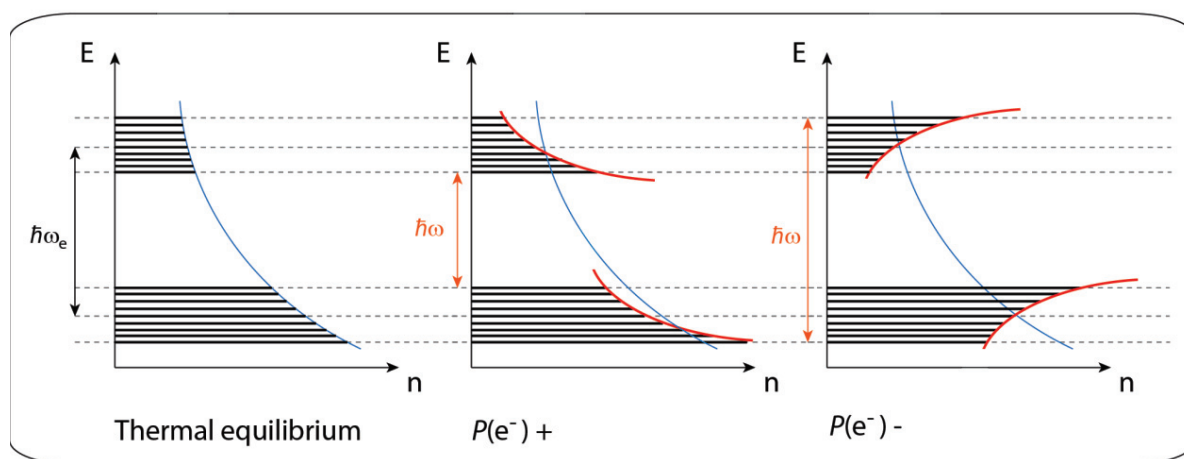


Figure 2.13: Energy level representation of the Thermal Mixing mechanism involving an electron Zeeman system composed of two degenerate energy levels ($S = -1/2$) and the electron broadening system represented by sub-levels. (Left) In thermal equilibrium, the electron spin populations follow a Boltzmann distribution (blue). (Middle) The system has achieved its own spin temperature and can be perturbed by applying a positive microwave irradiation (orange arrow) corresponding to $\omega_e - \omega_n$ which leads to a rearrangement of the populations (red curve). (Right) the opposite effect can occur by applying a negative microwave irradiation $\omega_e + \omega_n$.

Finally, for DNP to occur, a thermal contact between the nuclear Zeeman reservoir (N_Z) and the electron broadening reservoir has to be achieved (Fig. 2.14). This happens because the nuclear Zeeman reservoir tends to equalize its temperature with the one of the electron broadening reservoir. Nevertheless, a condition has to be fulfilled to allow the equalization of temperatures; the ESR line shape of the electrons should be wider than the NMR Larmor frequency of the nucleus. This is why nitroxide radicals like TEMPO are more efficient than Trityl OX063 to polarize protons via Thermal Mixing.

An important point to mention is that this thermal contact does not depend on the amplitude of the microwave irradiation. Therefore, less μ -wave power is required and the optimum μ -wave frequency is identical for all kinds of nuclear spins (^1H , ^{13}C , etc.) Another significant difference between Thermal Mixing and the Solid Effect is that the maximum of polarization achieved with TM is proportional to the gyromagnetic ratio of the nuclear species.

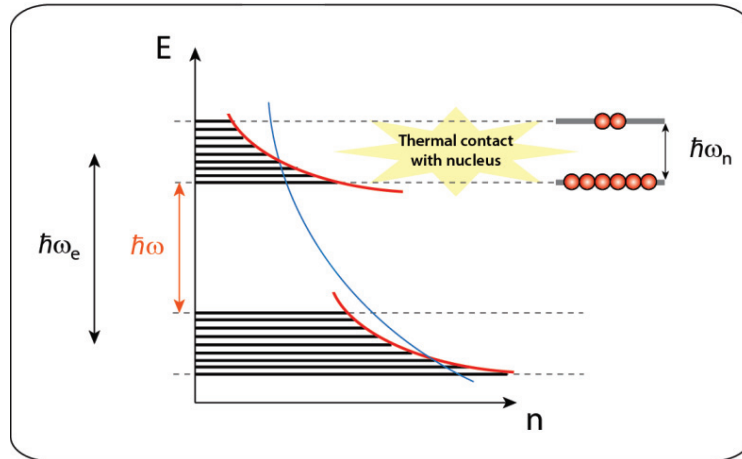


Figure 2.14: Energy level representation of the Thermal Mixing mechanism when irradiating a positive lobe to achieve hyperpolarized. The nuclear Zeeman system is in close contact with the electron broadening system allowing an equalization of their spin temperatures and thus leading to DNP.

2.3.4 The Overhauser Effect (OE)

Even if the Overhauser Effect was the first mechanism ever described for DNP by Overhauser himself [20], it remained, for more than half a century, only observable in conducting solids like metals and at very low field. The OE mainly relies on an imbalance between the rates of the zero quantum (ZQ) and double quantum (DQ) relaxation pathways of the system as shown in Fig. 2.15. In opposition with all the other mechanisms described before, the microwave irradiation applied should correspond to the electron spins resonance $\omega_{\mu W} = \omega_e$.

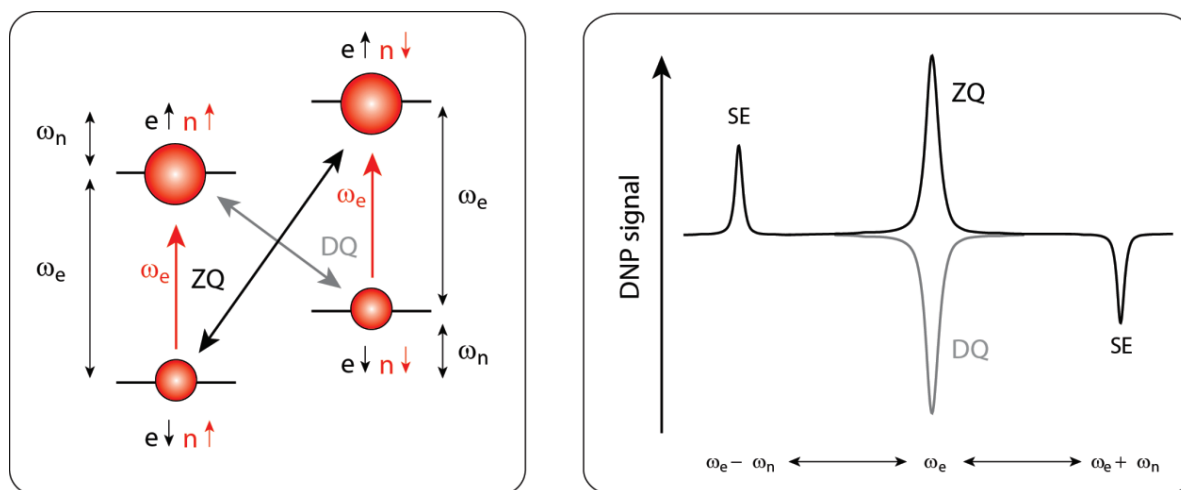


Figure 2.15: (Left) Overhauser Effect (OE) mechanism for a system comprising one electron and one nucleus. The two relaxation pathways are represented by grey and black arrows for Double Quantum (DQ) and Zero Quantum (ZQ) transitions. In order for OE to happen, the microwave frequency irradiation should be applied at the exact electron spin resonance $\omega_{\mu W} = \omega_e$. Then the difference in the relaxation rates across DQ and ZQ transitions allows one to observe a slight excess of the nuclear spins population in one of the energy levels, resulting in an increase in NMR signal. (Right) Schematic representation of the OE mechanism when a microwave irradiation is applied at the exact electron resonance frequency. The DQ is the predominant relaxation pathway for protons in liquids, resulting in a negative DNP enhancement. However, the ZQ becomes the dominant pathway in solid samples, resulting in a positive DNP enhancement. The Solid Effect peaks are represented for positive ($\omega_e - \omega_n$) and negative ($\omega_e + \omega_n$) lobes.

It is only recently that Griffin et al., followed by several other groups, discovered that this effect could be observed in Magic Angle Spinning (MAS) [29] and liquid DNP [30] by using 1,3-bisdiphenylene-2-phenylallyl (BDPA) radicals or Trityl. For protons in liquids, the DQ relaxation pathway is dominant and results in a negative DNP enhancement. In solids studied in our laboratory, the ZQ relaxation pathway seems to be the dominant pathway since a positive DNP enhancement has been observed at 1.2 K and 6.7 T for a static deuterated polystyrene matrix containing BDPA radicals. These results will be discussed in more detail in the thesis of Xiao Ji.

2.3.5 DNP mechanisms that are favored in our laboratory

With all these DNP mechanisms now in hand, we can have a better idea about the predominant effects present under our specific conditions and with our materials. In our laboratory, as explained in the next chapters, we are currently working on a 6.7 T DNP polarizer with an accessible temperature range from 1.2 to 4.2 K. [13, 14] Our DNP samples contain the nitroxide radical TEMPOL with a typical concentration of 50 mM and our microwave source can produce a maximum power of 87.5 mW. In practical experiments, the SE, CE, TM and OE could all be present when we perform DNP. In our case, the microwave power is much lower compared to experiments involving a gyrotron. We observe a saturation of the polarization in the mW range. Therefore, no more μ -wave power is required and we can neglect the Solid Effect mechanism since it relies mainly on forbidden transitions that require a strong microwave irradiation. Since the Overhauser Effect is specific to radicals like BDPA or Trityl, and since no DNP signals have been measured near the central frequency ω_e , the OE can be dismissed as well. Finally, we end up with Thermal Mixing and the Cross Effect. When previous experiments were performed at half the magnetic field that we have presently ($B_0 = 3.35$ T), the Thermal Mixing process was the favored DNP mechanism. By doubling the magnetic field to 6.7 T, we ended up with shorter T_{1e} compared with the diffusion time T_{SD} , which has, as mentioned before, an important impact on the system. At different concentrations of radicals and with the use of frequency modulation of the microwave irradiation (see chapter 3.3), we have been able to determine that the most favored DNP mechanisms under the specific conditions of our laboratory are a combination of the Cross Effect and the Thermal Mixing. More information will be presented in the chapters 3.2 and 3.3.

2.4 Magic Angle Spinning-DNP (MAS-DNP)

At low temperatures (typically between 1 and 100 K), the main problem that emerges with a static DNP sample is the low resolution of the signal recorded due to dipolar couplings, chemical shift anisotropy and quadrupolar effects. Indeed, the different NMR signals obtained are broad and overlap with each other, making it difficult and sometimes even impossible to assign the peaks to different chemical environments and functional groups of the molecules.

To counterbalance this negative effect and to obtain well-resolved spectra, Magic Angle Spinning-DNP (MAS-DNP) was first developed by Vriend *et al.* [31] in 1984 resulting from MAS NMR, which was discovered in 1958 [32] and is nowadays a well-spread technique in the DNP community. [29] In comparison with dissolution-DNP, MAS-DNP is essentially performed at "*moderately low*" temperatures $90 < T_{\text{MAS-DNP}} < 110$ K instead of "*very low*" temperatures $1.2 < T_{\text{d-DNP}} < 4.2$ K. Even if some sacrifices are made by depleting both the electronic polarization and the nuclear polarization due to higher temperatures (see Fig. 2.4), the NMR linewidths become narrower and the overall spectrum is better resolved. In addition, spinning the sample at high frequency (up to $\nu_{\text{rot}} = 40$ kHz [33]) and at the so-called magic angle ($\vartheta_m = 54.74^\circ$) allows one to average the dipolar, the chemical shift anisotropy and quadrupolar interactions, which are orientation-dependent. With these improvements it is now possible to recover useful information and to be able to differentiate signals in the solid-state.

In MAS-DNP, the maximum enhancement possible to achieve corresponds to $\gamma_e / \gamma_{1\text{H}} \approx 660$, which is relatively low compared to the typical enhancements obtained in d-DNP ($100 < \epsilon_{\text{d-DNP}} < 50'000$). Nevertheless, even a small improvement of $\epsilon_{\text{MAS-DNP}} \approx 10$ -100 can lead to considerable time-savings and are therefore not negligible. Nowadays, enhancements over 500 can be obtained by using proper concentration of (bi)radicals like TekPol or AmuPol in a specific glass-forming matrix (glycerol, DMSO, etc.) at moderate magnetic fields ($B_0 = 9.4$ T). [34] Another advantage of MAS-DNP is the possibility of accumulating series of hyperpolarized spectra, which is not feasible for dissolution-DNP because of the fast decay of hyperpolarized signals in liquids, resulting in the loss of signal after only few seconds. Thanks to this advantage, time-consuming experiments like 2D NMR using multiple scans and phase-cycling are compatible with MAS-DNP.

To perform MAS-DNP, a large set of different pieces of equipment is required, most of which are relatively expensive. Just to create sufficient microwave power (about 15 Watts in continuous mode) and to properly saturate the ESR line of the radicals, a gyrotron is needed to perform DNP. In our laboratory, a 400 MHz NMR spectrometer is used for MAS [35], thus the microwave frequency has to be set at 263.7 GHz (see Fig. 2.15). A transmission line allows the microwave irradiation generated by the gyrotron to be transmitted to the NMR MAS probe. Spinning the DNP sample is also quite challenging, because a continuous flow of gaseous nitrogen has to be controlled precisely in order to get the right spinning rate ν_{rot} . In addition to that, nitrogen is also used to cool down the sample to the desired temperature $90 < T_{\text{MAS-DNP}} < 110$ K. These functions are supported and controlled by a "*cooling cabinet*".

Nowadays, MAS-DNP has emerged as a technique of choice for different applications and is widely spread in the DNP community. It is used for example for the characterization of mesoporous materials [36], the study of the structure of proteins [37] and the acquisition of 2D spectra. [38]

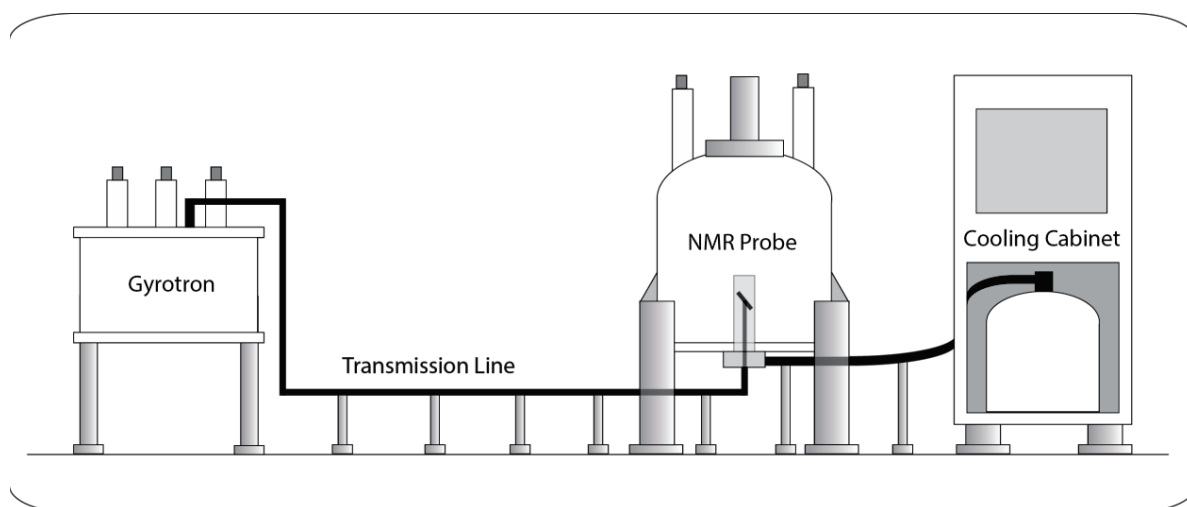


Figure 2.15: MAS-DNP system in our laboratory. A gyrotron operating at 263.7 GHz is connected via a transmission line to a 400 MHz NMR spectrometer. A cooling cabinet allows one to set the temperature in the NMR probe in a range from 90 to 110 K and at the same time the smooth spinning of the rotors at the desired frequency ν_{rot} up to about 12 kHz.

2.5 Dissolution Dynamic Nuclear Polarization (d-DNP)

Even if MAS-DNP can enhance the signals by several orders of magnitude ($\epsilon_{\max} \approx 660$) and is well adapted for the characterization of protein structures, signal acquisition can only be performed in solids at low temperatures. Therefore, MAS-DNP does not allow the observation of several important and interesting mechanisms like real-time chemical reactions or protein-ligand interactions, which occur solely in a liquid state under ambient conditions.

In 2003, a new method dubbed dissolution Dynamic Nuclear Polarization (d-DNP) was first introduced by Ardenkjaer-Larsen *et al.* [12] This technique allows one to separate the DNP system in three important parts; (i) a DNP polarizer where the polarization is built up at very low temperatures, (ii) a fast dissolution process to melt and transfer the DNP sample and (iii) an NMR spectrometer where the hyperpolarized signals are recorded in liquid phase.

Since the desired hyperpolarized signals are not analyzed in the DNP polarizer, the experiments can be run at lower temperatures ($T = 1.2 - 4.2$ K) in a cryostat filled with liquid helium where the polarization of electrons is close to 100 %, thus allowing to achieve higher nuclear polarizations in comparison with MAS-DNP. Furthermore, the microwave power needed to perform DNP can be reduced and relatively cheap available microwave sources can be used instead of gyrotrons.

However a dissolution system has to be built to quickly dissolve the frozen hyperpolarized sample and to transfer the resulting solution to an NMR spectrometer in order to record the desired signals in liquid phase (described in more detail in chapter 2.6). As previously mentioned, great enhancements up to $\epsilon_{\text{d-DNP}} = 50'000$ (see Fig. 2.16) have been achieved after dissolution [39] in comparison with the theoretical maximum of $\epsilon_{\text{MAS-DNP}} \approx 660$ obtained in MAS-DNP.

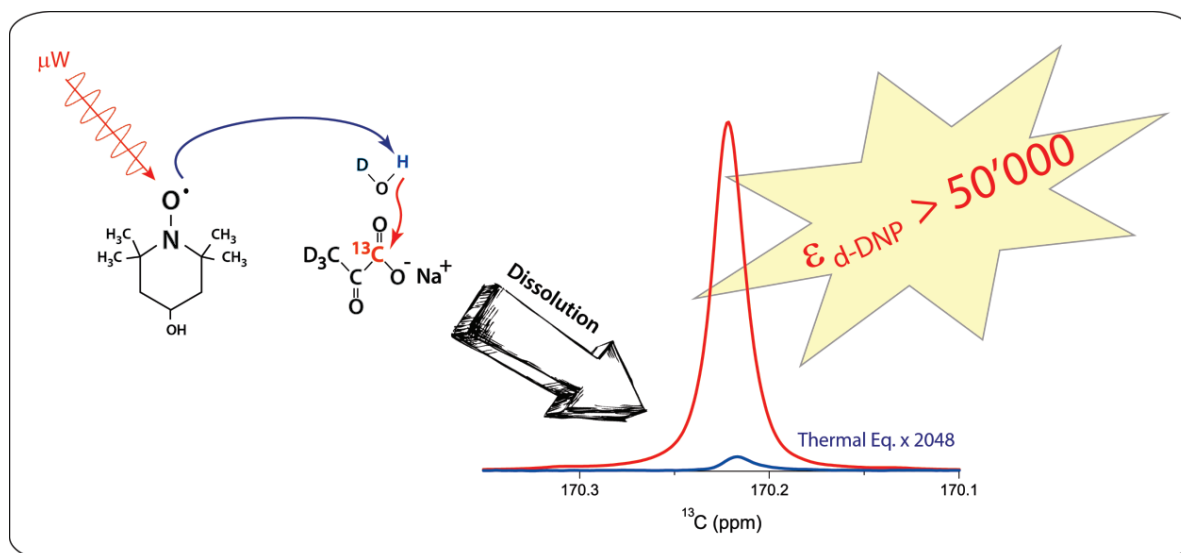


Figure 2.16: Typical representation of a Dissolution DNP experiment performed in our laboratory. TEMPOL radicals are preferentially used with metabolites, like deuterated enriched [$1\text{-}^{13}\text{C}$] sodium pyruvate in this particular case. The DNP sample is hyperpolarized by DNP and dissolved to get enhancement factors higher than 50'000 in liquid state in comparison with their thermal equilibrium (here multiplied by a factor 2048). [39]

Despite the higher polarization values that can be obtained, one of the major problems of d-DNP is the time available for signal acquisition. First of all, dissolution-DNP is considered as a "*one-shot*" experiment, where the high magnetization created in the solid can be only recorded in a single-scan after dissolution and therefore cannot result from a series of signal accumulations as it is the case for MAS-DNP. This is mainly due to the T_1 of molecules in liquid phase which are in the order of few seconds and that is why the high polarizations obtained at low temperatures tend to return rapidly back to their Boltzmann equilibrium under ambient conditions. Thus, the hyperpolarized signals are only detectable during a short time and time-consuming NMR sequences like 2D acquisitions or phase cycling are difficult or even impossible to be applied to dissolution-DNP.

In addition to several NMR experiments that will be discussed in this thesis, dissolution-DNP has also found various applications in the field of *in-vivo* MRI. It has been demonstrated that certain cancer cells are more demanding in energy than healthy ones and that their enzymatic conversion of pyruvate into lactate is thus accelerated. [40, 41] With the use of d-DNP, it was recently made possible in real time imaging, after injection of hyperpolarized pyruvate into a human patient, to detect the change in rate of conversion in a localized area. [42] As an extension of this application, d-DNP was also used to evaluate tumor grades [43] and to monitor the response to treatment of cancer cells [44] using a continuous tracking of living organisms. Because d-DNP is a non-invasive and non-radioactive technique, in contrast to PET-scans or CT-scans, several experiments can be continuously performed without endangering the life of the subjects. Thanks to these discoveries, new horizons are nowadays in sight for the detection of localized tumors and more specifically for prostate cancer.

2.5.1 TEMPOL: a new radical

Dissolution-DNP was initially developed using Trityl radicals (see Fig. 2.17) to polarize directly and efficiently nuclei such as ^{13}C [12, 45], ^{15}N [46], ^{129}Xe [47] or ^{89}Y . [48] The interest of polarizing these kinds of nuclei by DNP is that most of them are insensitive and difficult to observe by standard NMR spectroscopy.

This low sensitivity is mainly due to the low gyromagnetic ratio γ of these nuclei (e.g., $\frac{\gamma_{^1\text{H}}}{\gamma_{^{13}\text{C}}} = 3.97$) and their low natural abundance in comparison with protons (e.g. $^{13}\text{C} = 1.108\%$ in comparison with $^1\text{H} = 99.985\%$). Another great advantage in the use of these low gamma nuclei for d-DNP is their relatively long T_1 in solution under ambient conditions that can even extend to few minutes [49] and can make it possible the record of hyperpolarized signals for a long time after the dissolution process.

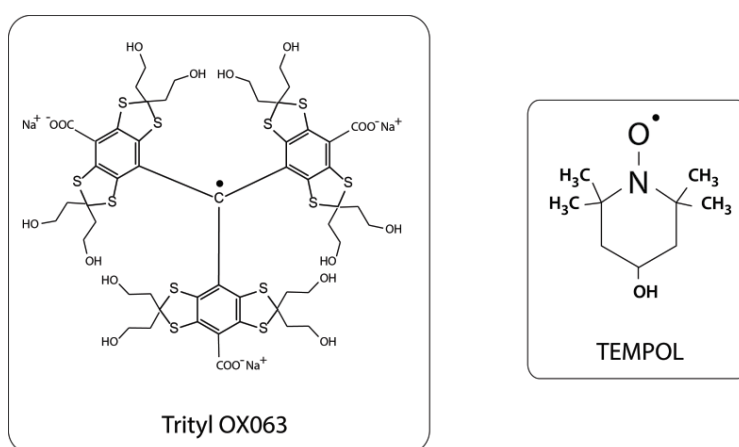


Figure 2.17: The two most common radicals used for dissolution-DNP. Trityl OX063 (left) and 4-hydroxy-2,2,6,6-tetramethylpiperidin-1-oxyl or TEMPOL (right).

Even if the use of Trityl OX063 at an optimum concentration of 15 mM allows an efficient direct polarization of low gamma nuclei (up to $P(^{13}\text{C}) = 36\%$) at a low magnetic field $B_0 = 3.35\text{ T}$ [50], one of the major problems of using this radical with narrow ESR lines is the long polarization build-up time ($T_{\text{bup}} = 2300\text{ s}$) required at 1.2 K (see Fig. 2.18 A). These relatively long build-up times do not allow a rapid succession of d-DNP experiments that is desirable for various *in-vivo* applications, where time is a crucial factor. Another important point to mention is the limited availability and high cost of Trityl OX063 resulting from its complicated synthesis and the protection by a patent [51, 52], which can be inconvenient to afford and can hamper its routine use in the laboratory.

To overcome these two main drawbacks, a generation of stable nitroxide radicals was introduced for d-DNP. The most common structure of these piperidine radicals is 2,2,6,6-tetramethylpiperidin-1-oxyl, more commonly called TEMPO. In our experiments, the TEMPOL radical is used preferably because of its high solubility in water. It is commercially available and differs from TEMPO by inserting a hydroxyl group at C₄ (see Fig. 2.17). This nitroxide radical is relatively cheap and its solubility in water is increased in comparison with Trityl; concentrations up to 200 mM can be obtained, even if 10 - 50 mM correspond to the optimal range to perform DNP in our experiments. Nevertheless, because of their broad ESR lines, nitroxide radicals are poor candidates for the direct hyperpolarization of ¹³C (only $P(^{13}\text{C}) = 10\%$ under the same conditions in Fig. 2.18 B), even if they can reduce the build-up time by a factor 7 ($T_{\text{bup}}(^{13}\text{C}) = 324\text{ s}$). [53] But the wide ESR lines lead to the great advantage that protons can be efficiently polarized by DNP ($P(^1\text{H}) = 40\%$) in a record build-up time of only $T_{\text{bup}} = 70\text{ s}$.

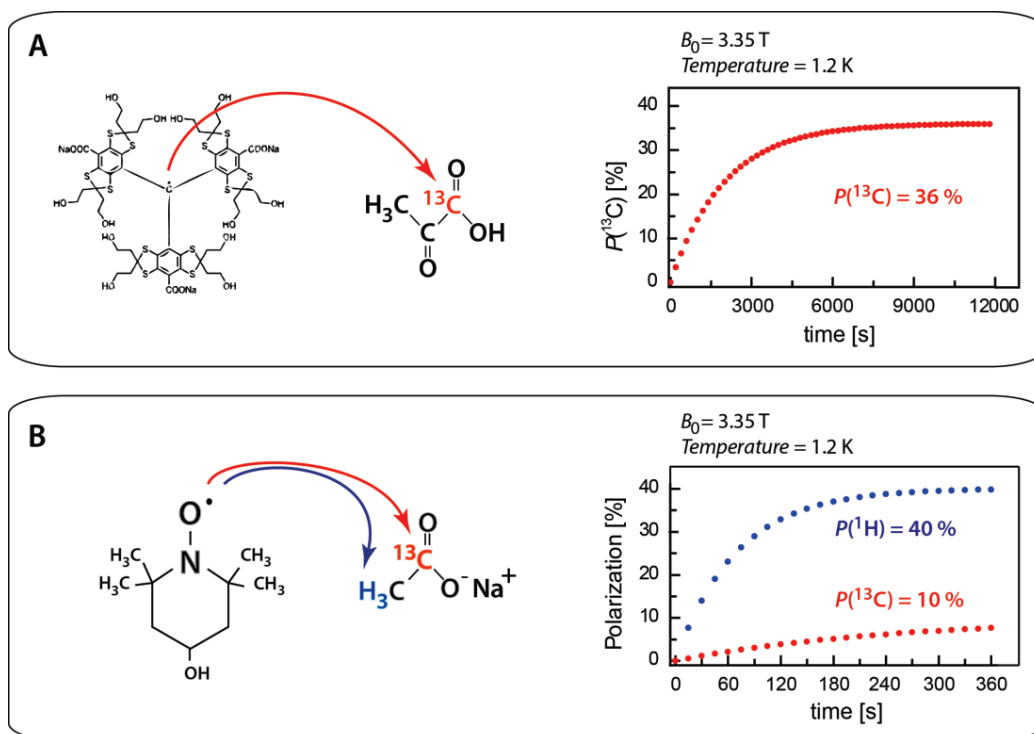


Figure 2.18: Comparison of the polarizations and build-up curves obtained by DNP for the two different radicals Trityl and TEMPOL at low magnetic field $B_0 = 3.35\text{ T}$ and at very low temperature $T = 1.2\text{ K}$. (A) Trityl is used at a concentration of 15 mM with pure $[1-^{13}\text{C}]$ pyruvic acid to achieve a final carbon polarization of $P(^{13}\text{C}) = 36\%$ after a relatively long build-up time of $T_{\text{bup}} = 2300\text{ s}$. (B) TEMPOL is used at a concentration of 30 mM in a mixture of glycerol- d_8 / D_2O (1/1) with 3 M of $[1-^{13}\text{C}]$ sodium acetate to achieve a direct carbon-13 polarization of only $P(^{13}\text{C}) = 10\%$ after $T_{\text{bup}} = 324\text{ s}$. A proton polarization of $P(^1\text{H}) = 40\%$ can also be obtained because of the broad ESR line shape of nitroxide radicals after a very short build-up time $T_{\text{bup}} = 70\text{ s}$.

Another inconvenience resulting from the use of nitroxide radicals is that they are easily reduced by pyruvic acid and therefore only derivative salts like sodium pyruvate or sodium acetate should be used, which diminish the final concentration of the polarized metabolite in the DNP sample, from 14 M for pyruvic acid to 3 M for sodium pyruvate or sodium acetate.

The negative aspects of using TEMPOL instead of Trityl in DNP samples (i.e., lowering the final carbon-13 polarization and reducing the concentration of the analyzed metabolites) can be compensated by a technique known as Cross-Polarization that has emerged. [54, 55] This method can be employed to equilibrate magnetization between two nuclear spin species with different gyromagnetic ratios.

2.5.2 Hartmann-Hahn Cross Polarization

In 1962, Hartmann and Hahn described for the first time the method of Cross-Polarization (CP) between two different nuclei. [54] By applying two strong radiofrequency fields to the system, they showed that it was possible to obtain a transfer when the two nuclear spins (for example ^1H and ^{13}C) have the same Larmor frequencies in their respective rotating frames, as described by Eq. 2.13. Therefore, when this so-called "*Hartmann-Hahn condition*" is fulfilled, one obtains:

$$\gamma_{^1\text{H}} B_1(^1\text{H}) = \gamma_{^{13}\text{C}} B_1(^{13}\text{C}) \quad (2.13)$$

where the different gyromagnetic ratios γ are represented for ^1H and ^{13}C and B_1 corresponds to the radiofrequency intensity applied for each nucleus to match their Larmor frequencies and fulfill the "*Hartmann-Hahn condition*". As a result, the strong magnetization of one of the nuclear spins can be transferred to the other through dipole-dipole couplings.

2.5.3 Cross-Polarization applied to d-DNP

With this concept of CP and the possibility to transfer magnetization through dipolar interactions, it was possible to transfer the high polarization of protons to other nuclei in solids. [55] This method can be adapted to Dynamic Nuclear Polarization at very low temperatures. [53, 56, 57, 58] In our experiments, as described before, the aim of using CP is that the polarization of high gyromagnetic ratio nuclei like ^1H can be used as a reservoir of magnetization that is transferrable to nuclear species like ^{13}C , ^{15}N , ^{31}P or even ^{129}Xe that have lower gyromagnetic ratios. The use of radicals like TEMPO with sufficiently broad ESR lines becomes important to allow the "*reservoir*" of proton polarization to build up efficiently in a very short time. Such a strategy has a great advantages in comparison with Trityl.

Some non-negligible prerequisites need to be taken into account in order to make Cross-Polarization compatible with the conditions that are specific to DNP. First of all, a special DNP probe compatible with dissolution was built in our laboratory following the procedure developed by Dr. Roberto Melzi in collaboration with Bruker. [53] This dissolution-DNP probe allows to operate under low temperatures. It is mainly composed of a set of two saddle coils for ^1H and ^{13}C (presented in more detail in chapter 2.6). A solid-state NMR console has to be connected to the DNP probe in order to generate pulses and acquire signals at very low temperatures. More importantly, this console allows the monitoring and optimization of the CP build-up as a function of time. By generating the correct radiofrequency (*rf*) field to each specific nucleus and thereby matching the "*Hartmann-Hahn condition*" for a pair of nuclear spins, the high proton polarization can be efficiently transferred to the ^{13}C spins that lack magnetization.

This overall process is now implemented in our laboratory in a 6.7 T DNP polarizer and efficiently performed at a temperature of 1.2 K. [59] A simple first-generation representation of the CP-DNP sequence adapted to our d-DNP setup is shown in Fig. 2.19. It is worth noting that the electron microwave frequency is always switched on throughout the Cross-Polarization process. (a) The sequence starts with a strong saturation of ^1H and ^{13}C by applying 90° pulses to both channels to kill any remaining polarization. (b) The ^1H polarization increases during the DNP build-up time, as does the ^{13}C polarization. The timing mostly depends on the time required to build up the proton polarization in order to get the maximum transferrable magnetization of ^1H in the shortest period. (c) Two 90° pulses are applied to both channels to rotate the ^1H and ^{13}C magnetizations in the transverse plane. (d) During the CP contact time, the ^1H and ^{13}C radiofrequency amplitudes have to be optimized in order to match the "*Hartmann-Hahn condition*", which is usually done in our laboratory prior to each DNP experiment. This contact time should be much shorter than the proton DNP build-up time, to avoid relaxation with $T_{1\rho}$ and therefore a de-magnetization of protons in the transverse plane. The high proton polarization can be efficiently transmitted to the ^{13}C nuclei through dipolar interactions. (e) One final critical factor we need to consider for dissolution-DNP is that the final magnetization of ^{13}C should be aligned with the magnetic field B_0 , otherwise the polarization acquired in the frozen state would be completely lost when the sample is melted and transferred for measurements. This is why a $(\pi/2)$ flip-back pulse is applied at the end of the sequence in order to remove the final magnetization from the transverse plane, where it would be lost. The magnetization of ^1H is also flipped back in order to repeat this cycle a desired number of times if necessary until the maximum ^1H polarization has been transferred to ^{13}C . (f) An additional small angle pulse (usually 5°) is applied to the carbon channel to be able to measure and follow a fraction of the hyperpolarized signal transmitted without destroying the overall magnetization.

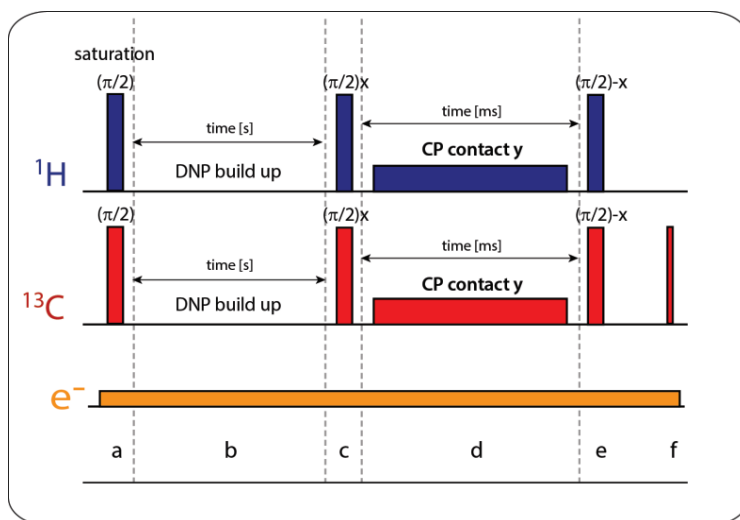


Figure 2.19: The Cross-Polarization sequence used for dissolution-DNP. (a) A strong saturation of both ^1H and ^{13}C channels is applied to start the CP sequence. (b) A short ^1H build-up time allows the polarization of protons to grow. (c) Both magnetizations are flipped into the transverse plane to start the CP process. (d) A CP contact is established between the two nuclei to transfer the polarization from ^1H to ^{13}C via dipole-dipole interactions. (e) The magnetizations are flipped back along B_0 to save the polarization acquired during the CP transfer. (f) A small angle pulse can be applied to ^{13}C in order to measure the proper functioning of the CP sequence.

The major problem resulting from this Cross-Polarization sequence is that under our conditions most of the ^{13}C magnetization is lost when the cycle is repeated to build up the carbon polarization. This is mainly due to $T_{1\rho}$ relaxation when both magnetizations are in the transverse plane during the CP contact. To overcome this hampering effect, the CP sequence was modified by replacing the strong 90° pulses by adiabatic frequency-swept pulses (WURST pulses) [60], inspired by the work of Perez-Linde and Kockenberger. [56]

Both nuclei are now in contact during the first adiabatic full-passage or adiabatic inversion (see Fig. 2.20) and their magnetization vectors that were initially aligned in the $+z$ axis are now aligned along the $-z$ axis. Then, a second adiabatic inversion permits to bring the magnetization vectors back to the $+z$ axis, allowing one to repeat the sequence to build up the ^{13}C polarization. This second passage is important, because it brings the magnetization back, and avoids that the DNP microwave irradiation (switched on during the entire experiment) destroys the nuclear polarization obtained if it is oriented along the $-z$ axis after the first adiabatic inversion.

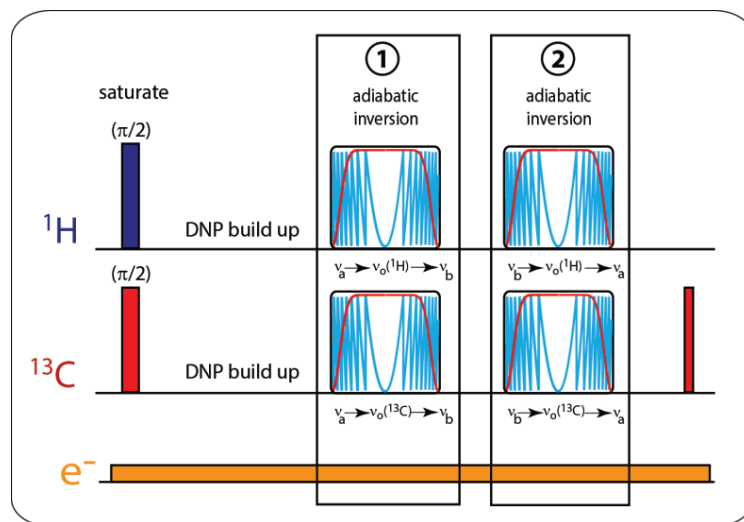


Figure 2.20: Enhanced CP sequence used in our laboratory, similar to the previous sequence of Fig. 2.19. The only difference is that this sequence is composed of two adiabatic inversions instead of the strong 90° pulses, which allows one to better preserve the polarization transferred from ^1H to ^{13}C .

Finally, with this optimized sequence it is possible to record the transfer of polarization and increase the ^{13}C magnetization. In Fig 2.21, a schematic representation of different build-up curves for ^1H and ^{13}C is presented when the CP sequence is applied to the system. Each point corresponds to a measurement by applying a small angle pulse to avoid the destruction of the hyperpolarized signal. The proton build-up curve is shown in blue with a maximum of polarization approaching 90% in the best conditions. [53] The delay between each CP transfer is usually set to be equal to 5 times the build-up time of ^1H in order to leave enough time for the ^1H polarization to build up again instead of being completely destroyed. Therefore a CP transfer (represented by an orange arrow) can be applied after that time and the resulting enhancement of the ^{13}C polarization appears like a "steplike" function. Then, during the time between two consecutive CP transfers, the ^{13}C relaxes with a relaxation time T_{Relax} . Before the complete loss of ^{13}C signal, several CP transfers can be performed in a relatively short amount of time and can lead to a final polarization $P(^{13}\text{C})$ that is higher in comparison with the direct polarization of ^{13}C (dashed red line).

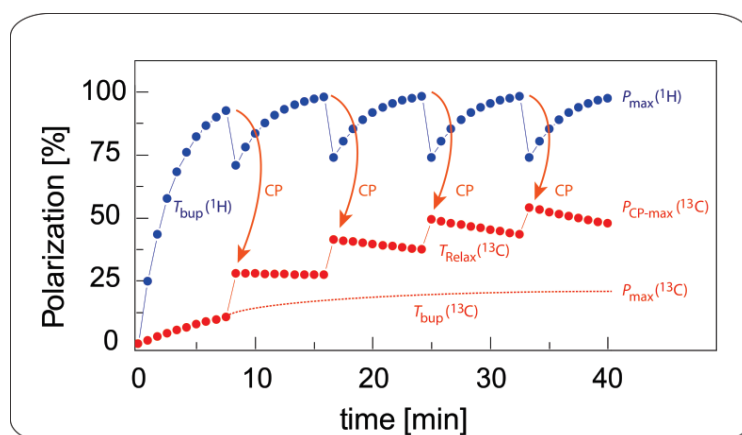


Figure 2.21: Representation of the polarization build-up curves for ^1H and ^{13}C . The proton polarization (blue) is transferred by CP (orange) to ^{13}C (red) resulting in a fast increase of the ^{13}C polarization. Therefore the maximum polarization $P_{\text{CP-max}}(^{13}\text{C})$ obtained with CP is much higher than the maximum polarization $P_{\text{max}}(^{13}\text{C})$ achieved with direct DNP.

2.5.4 Cross-Polarization at 3.35 T

With shorter build-up times and higher ^{13}C polarizations, the Cross-Polarization technique is a well-suited candidate to improve the usual d-DNP experiments using Trityl. Therefore, in our laboratory, the CP-DNP setup was implemented and enhanced results have been measured. [58]

The following Fig. 2.22 can be compared with Fig. 2.18 where direct polarization of ^{13}C was recorded. In this figure, the ^{13}C polarization builds up after each CP at 1.2 K and a maximum of $P(^{13}\text{C}) = 23\%$ is obtained only after a short build-up time $T_{\text{bup}}(^{13}\text{C}) = 170\text{ s}$ for a sample containing $[1\text{-}^{13}\text{C}]$ sodium acetate and 30 mM TEMPOL in a mixture of glycerol- d_8 / D_2O (1/1). Therefore, the ^{13}C polarization is enhanced by a factor $\epsilon_{\text{CP}} = 2.3$ and the build-up time is decreased by a factor 2.6 when Cross-Polarization is used.

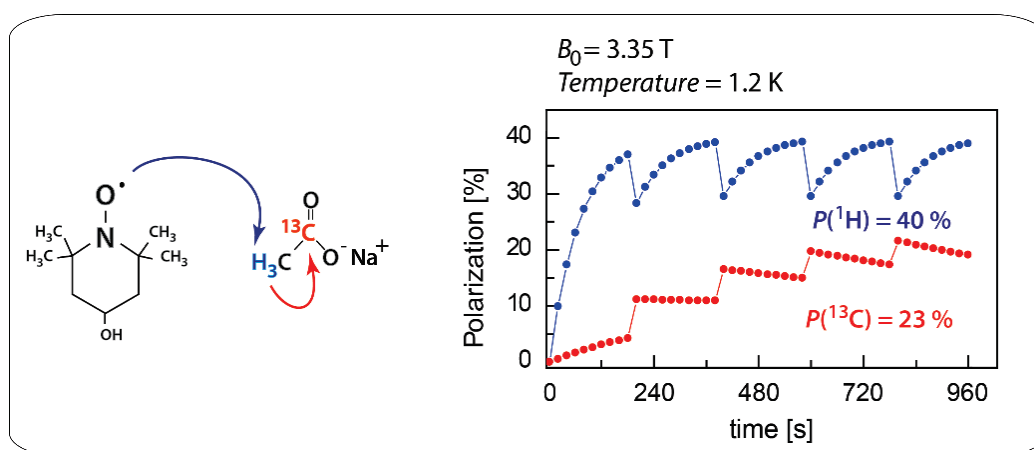


Figure 2.22: TEMPOL is used at a concentration of 30 mM in a mixture of glycerol- d_8 / D_2O (1/1) with 3 M of $[1\text{-}^{13}\text{C}]$ sodium acetate to finally achieve a proton polarization of $P(^1\text{H}) = 40\%$ after a short build-up time $T_{\text{bup}} = 70\text{ s}$. By applying the Cross-Polarization technique, this polarization can be efficiently transferred to the ^{13}C nuclear spins during a short contact. A higher ^{13}C polarization of $P(^{13}\text{C}) = 23\%$ in a shorter build-up time $T_{\text{bup}}(^{13}\text{C}) = 170\text{ s}$ could be achieved in comparison with direct DNP where $P(^{13}\text{C}) = 10\%$ and $T_{\text{bup}}(^{13}\text{C}) = 450\text{ s}$.

Despite the relatively high polarization values achieved in very short build-up times using Cross-Polarization, the results obtained with an optimal DNP solution containing Trityl radicals (see Fig. 2.18) show an even higher polarization $P(^{13}\text{C}) = 36\%$. To be competitive with this standard DNP experiment, it was decided to double the strength of the magnetic field of our DNP polarizer to $B_0 = 6.7\text{ T}$. [13, 14] The electron-spin polarization at this specific magnetic field and at a temperature of 1.2 K should be close to unity, ($P(e^-) = 99.9\%$ (see Table 2.1), and should improve the overall DNP process.

2.5.5 Cross-Polarization at 6.7 T

Encouraging CP-based results were obtained for the same sample containing $[1-^{13}\text{C}]$ sodium acetate and a different optimal concentration of TEMPOL of 50 mM at a higher field. Polarization values as high as $P(^{13}\text{C}) = 40\%$ have been observed at a low temperature of 1.2 K [59], showing that Dynamic Nuclear Polarization benefits from the use of high fields. Moreover, the build-up time $T_{\text{bup}}(^{13}\text{C}) = 810\text{ s}$ has been reduced by a factor 2.8 in comparison with experiments involving Trityl radicals where $T_{\text{bup}}(^{13}\text{C}) = 2300\text{ s}$.

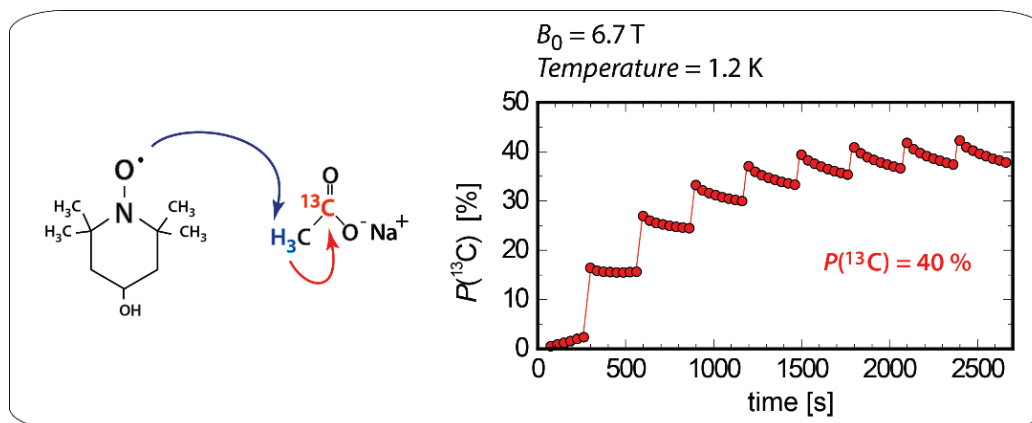


Figure 2.23: When the TEMPOL concentration is increased to 50 mM in a mixture of glycerol- d_8 /D $_2$ O (1/1) with 3 M of $[1-^{13}\text{C}]$ sodium acetate, a carbon-13 polarization of $P(^{13}\text{C}) = 40\%$ is achieved in a short build-up time $T_{\text{bup}}(^{13}\text{C}) = 810\text{ s}$ in comparison with Fig. 2.18 and 2.22.

2.5.6 Cross-Polarization at 9.4 T

To push the limits of DNP to further frontiers, a new DNP polarizer based on a magnet developed by Cryogenic Ltd. [22] was recently implemented in our laboratory with a stronger magnetic field of 9.4 T. Even if the limit of the electron spins polarization was already reached at 6.7 T (see Table 2.1), one of the advantages of increasing the strength of the magnetic field (without taking into account the electron relaxation) is to be able to perform the same experiments with the same efficiency, but at higher temperatures between 2.2 and 4.2 K. The temperature is a critical factor in our DNP experiments, because it requires a high consumption of liquid helium and the use of specific pumps (as described in chapter 2.6) to achieve a temperature of 1.2 K. Therefore, to work instead at 2.2 or 4.2 K is energy- and cost-saving. The electron polarization $P(e^-) = 99.3\%$ at 2.2 K and $P(e^-) = 90.6\%$ at 4.2 K are close to $P(e^-) = 99.9\%$ achieved at 6.7 T and 1.2 K.

2.6 Dissolution-DNP Setup at the EPFL

At the EPFL, the home-built DNP system developed [13, 14] is inspired by the work of Ardenkjaer-Larsen *et al.* [12] As described in Fig. 2.24, it is composed of a DNP polarizer containing a cryostat operating between 1.2 and 4.2 K (built in collaboration with the Paul Scherrer Institute) and a superconducting wide-bore magnet (Oxford Instruments) with a magnetic field $B_0 = 6.7$ T. A dissolution tube surrounded by a magnetic tunnel [61] allows the transfer of the hyperpolarized solution after dissolution to the NMR spectrometer where the signals are recorded in liquid phase.

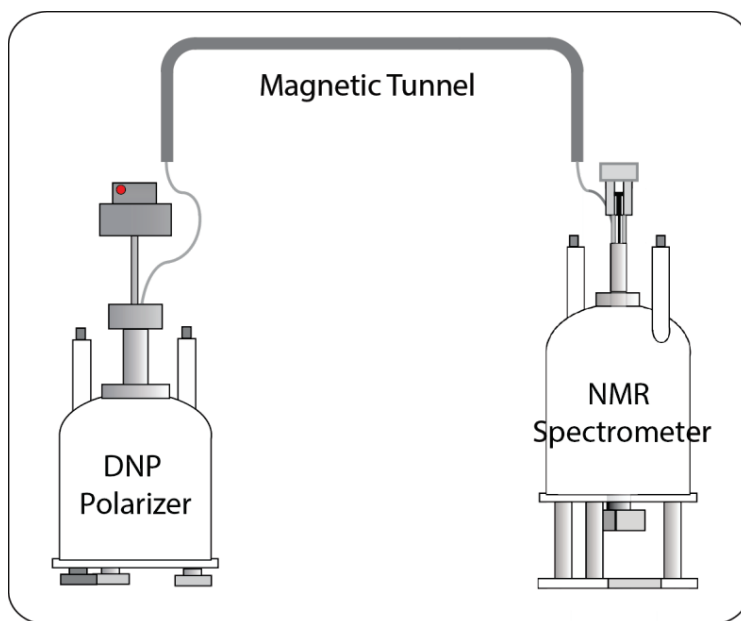


Figure 2.24: Schematic representation of the overall DNP setup at the EPFL composed of a DNP polarizer, a magnetic tunnel and an NMR spectrometer (300 or 500 MHz).

2.6.1 Preparation of DNP samples

Some specific conditions related to the preparation of DNP samples are required to perform DNP efficiently at low temperatures. First of all, paramagnetic impurities or free radicals such as TEMPOL or Trityl should be present in the sample at precise concentrations (typically in our case the optimal concentrations of TEMPOL are situated between 10 and 50 mM), otherwise no transfer of polarization can be achieved. Secondly, the molecules to be polarized (pyruvate, glucose, etc.) should be in large concentration in comparison with the radical species (typically 1 to 3 M). Finally, and probably the most crucial condition, these different species (radicals and molecules) should be distributed in a non-crystalline way in order to achieve the most efficient DNP effect. This is often done by adding a specific volume of a viscous solvent (usually glycerol or DMSO) to our DNP sample in order to get a "glassy matrix" where all species are well-distributed in a homogeneous manner. The ideal preparation of a DNP sample (see Fig. 2.25) can be easily recognized by the formation of a transparent glass-forming matrix in liquid nitrogen, resulting in a homogeneous distribution of all species in the frozen matrix.

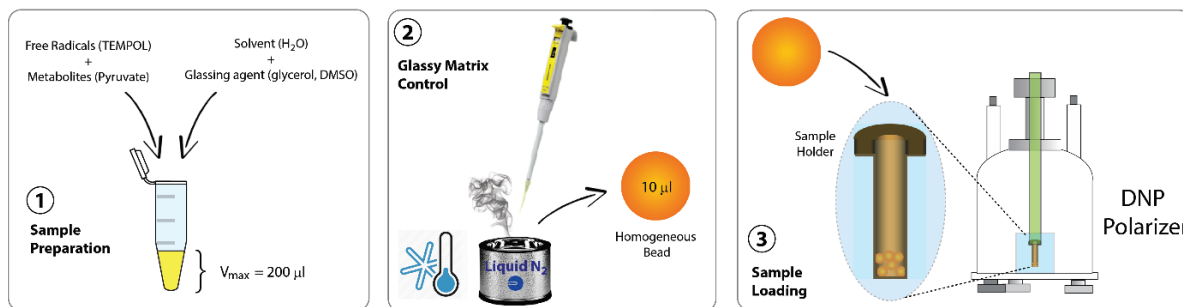


Figure 2.25: The different steps to prepare a suitable DNP sample are described. (1) The metabolites to be hyperpolarized (like pyruvate, glucose, etc.) are mixed together with the free radicals (TEMPOL, Trityl) in a solution usually composed of water and a glassing agent like glycerol or DMSO. (2) The sample is controlled by dropping small beads (10 μ l) into liquid nitrogen to ensure that the components of the DNP sample are homogeneously distributed. (3) The DNP sample is placed in a sample holder which can be put in the DNP polarizer in liquid helium at very low temperatures ($T = 1.2 - 4.2$ K).

2.6.2 DNP polarizer

A more detailed representation of the DNP polarizer operating at 6.7 T is shown in Fig. 2.26. A helium tank is used to cool the system by transferring liquid helium ($T = 4.2$ K) through a line directly into a small chamber inside the cryostat. The flow of helium can be adjusted by a flow sensor and a membrane pump in order to refill the cryostat properly. By manually adjusting the needle valves, we can open this chamber to let the liquid helium go into the cavity where the DNP sample is placed. With a turbo pump allowing the pressure to be reduced down to 10^{-5} bar, the cryostat is put under vacuum to minimize the thermal contact with the magnet and reduce helium consumption. In order to fill the polarizer properly, two rotative pumps controlled by a pressure sensor are used to lower the pressure inside the cryostat. The first one allows us to go down to 800 mbar in order to pump the helium from the reservoir and facilitate its transfer into the cryostat. This pump can go down to 50 mbar in order to decrease the temperature of helium below 4.2 K. In order to go to the lowest temperature possible with our system ($T = 1.2$ K), a second more powerful pump is used to decrease the pressure to 0.8 mbar in the cryostat. A flow sensor is installed and is able to control the flow of helium pumped into the cryostat with the use of a membrane pump. A helium recuperation line is connected to the system to reduce losses and to recollect the helium for further use.

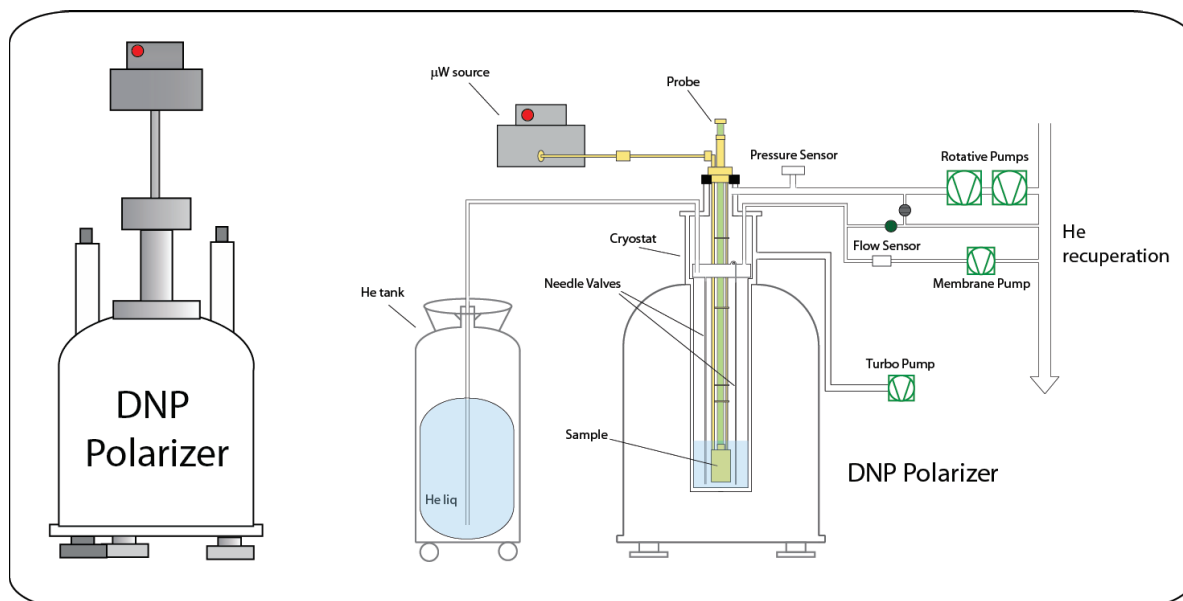


Figure 2.26: The DNP polarizer setup in our laboratory is composed of a cryostat, a magnet operating at $B_0 = 6.7$ T, a liquid helium tank, a microwave source and a home-built DNP probe. [53] By running the different pumps, the polarizer can be filled with liquid helium and the temperature inside can be decreased from 4.2 K to 1.2 K, allowing a more efficient DNP process.

In addition to the DNP polarizer, a microwave source is placed on top of the machine to generate microwave irradiation at a specific frequency in order to allow DNP. The model of the source is a commercially available ELVA VCOM-10/0.5/94/400 operating at a frequency of $f_{\mu W} = 94 \text{ GHz} \pm 250 \text{ MHz}$ at the WR-10 output in the rectangular fundamental TE_{10} mode, delivering a maximum microwave power of $P_{\mu W} = 400 \text{ mW}$. The use of a Voltage Control Oscillator (VOC) allows fast frequency modulation (up to 10 MHz) over a wide bandwidth ($\pm 250 \text{ MHz}$). In order to work efficiently at $B_0 = 6.7 \text{ T}$, a Virginia Diode D200 is used to double the microwave frequency to $f_{\mu W} = 188 \text{ GHz} \pm 500 \text{ MHz}$ at the WR-5 waveguide output in the TE_{10} mode which corresponds to the region of the ESR lines of the radicals that we have used (TEMPOL, BDPA and Trityl). Unfortunately, because of this doubler, the microwave power is decreased by a factor 4, leading to a final maximum power $P_{\mu W} = 100 \text{ mW}$. At the exit of this doubler, a commercial rectangular-to-circular transition device (Quinstar QWC series) was placed, as indicated by its name, to convert the rectangular TE_{10} mode to a circular TE_{10} mode.

To guide the microwave irradiation to the DNP sample placed inside the polarizer (see Fig. 2.26), a home-built DNP probe [53] comprising a stainless steel waveguide with a 4.5 mm inner diameter is used (Fig. 2.27). The upper part is composed of an insert to be able to transfer the sample inside the cavity of the cryostat and a gold-plated miter bend to reflect the microwave irradiation at 90 degrees through the waveguide. In addition, tuning and matching boxes are placed outside the polarizer to avoid to place the capacitors in liquid helium. The bottom part is also composed of a mirror to carry the microwave irradiation to the sample cavity composed of gold-plated reflecting mirrors and to focus the microwave irradiation on the DNP sample. The final microwave power of the irradiation obtained after the transfer through the waveguide is $P_{\mu W} \approx 87.5 \text{ mW}$. To record an NMR signal inside the polarizer at low temperatures, a home-built system composed of two saddle coils tuned for different nuclei ($f(^1\text{H}) = 285.2 \text{ MHz}$ and $f(^{13}\text{C}) = 71.7 \text{ MHz}$, $f(^{15}\text{N}) = 28.9 \text{ MHz}$, $f(^{29}\text{Si}) = 56.7 \text{ MHz}$ in our laboratory) is used to perform Cross-Polarization (CP).

Generally speaking, as described elsewhere [53, 62], this system is composed of an inner coil containing the two saddle coils that are inductively coupled to an external coil to be able to apply radiofrequency irradiation regardless of the nucleus to allow Cross-Polarization. The choice to use saddle coils instead of solenoid coils, in which high ^{13}C polarization values $P(^{13}\text{C}) = 70\%$ were achieved [14], is solely made to be compatible with the dissolution process. Saddle coils allow the insertion of a dissolution stick directly inside the DNP chamber in liquid helium to avoid losses of magnetization as much as possible.

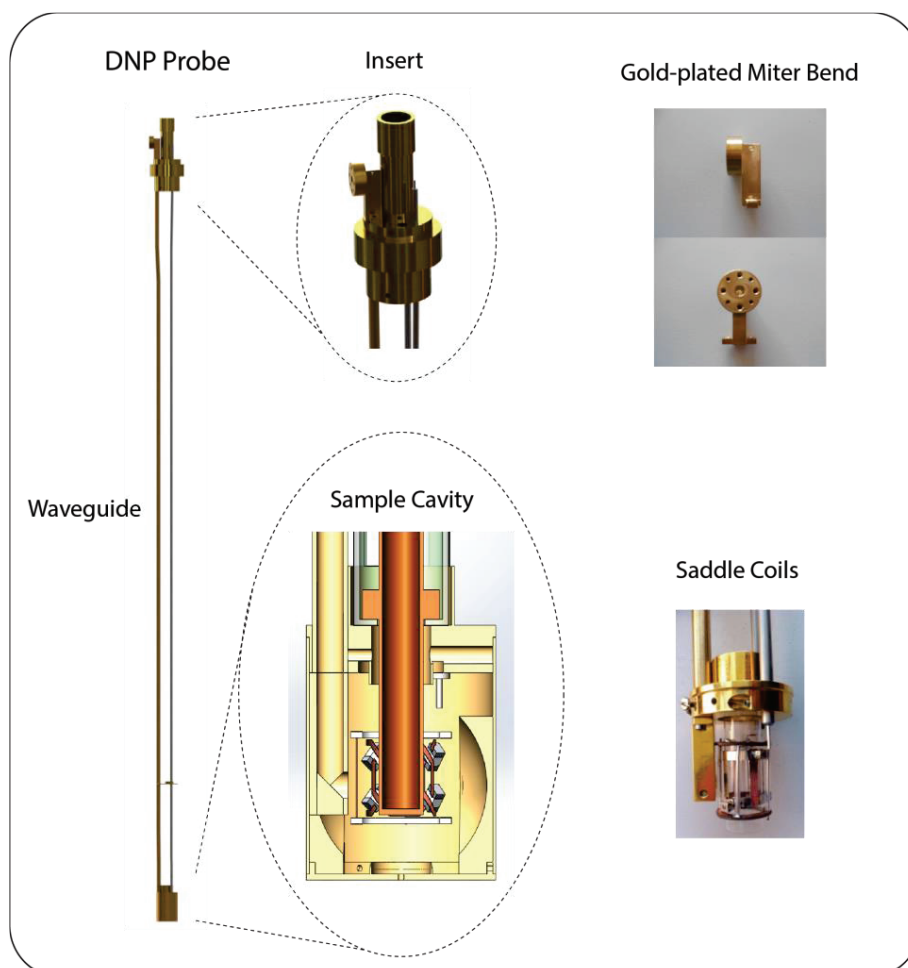


Figure 2.27: Pictures of the different parts of the DNP probe. The upper part is composed of an insert and a gold-plated miter bend and the bottom part comprises a sample cavity with reflecting mirrors and two saddle coils for the measurement of the NMR signal inside the polarizer.

2.6.3 Dissolution stick

The DNP sample sits inside the polarizer in a liquid helium bath and should be dissolved and transferred very rapidly in order to keep most of the polarization acquired at low temperatures. To do so, a dissolution stick was designed and built in our laboratory (Fig. 2.28). The upper part of the dissolution stick is composed of an oven controlled by a pressure transducer and N_2 gas valves where the dissolution solvent can be introduced through the top (green valve) and heated to the desired temperature (for D_2O : $p = 10$ bar and $T = 140$ °C) by increasing the pressure using the helium gas connecting line. When the desired temperature of the solvent is reached, the dissolution stick is rapidly placed inside the DNP polarizer and coupled to a Vespel sample holder containing the hyperpolarized sample. Dissolution is then performed manually by pressing a red button on the stick, which releases the solvent and pushes it through the tube. The superheated solution can quickly melt the frozen solid DNP sample (in ≈ 0.7 s) and, after reaching the top of the stick, can be expelled and transferred to the NMR spectrometer. The overall system is controlled by a LabView software.

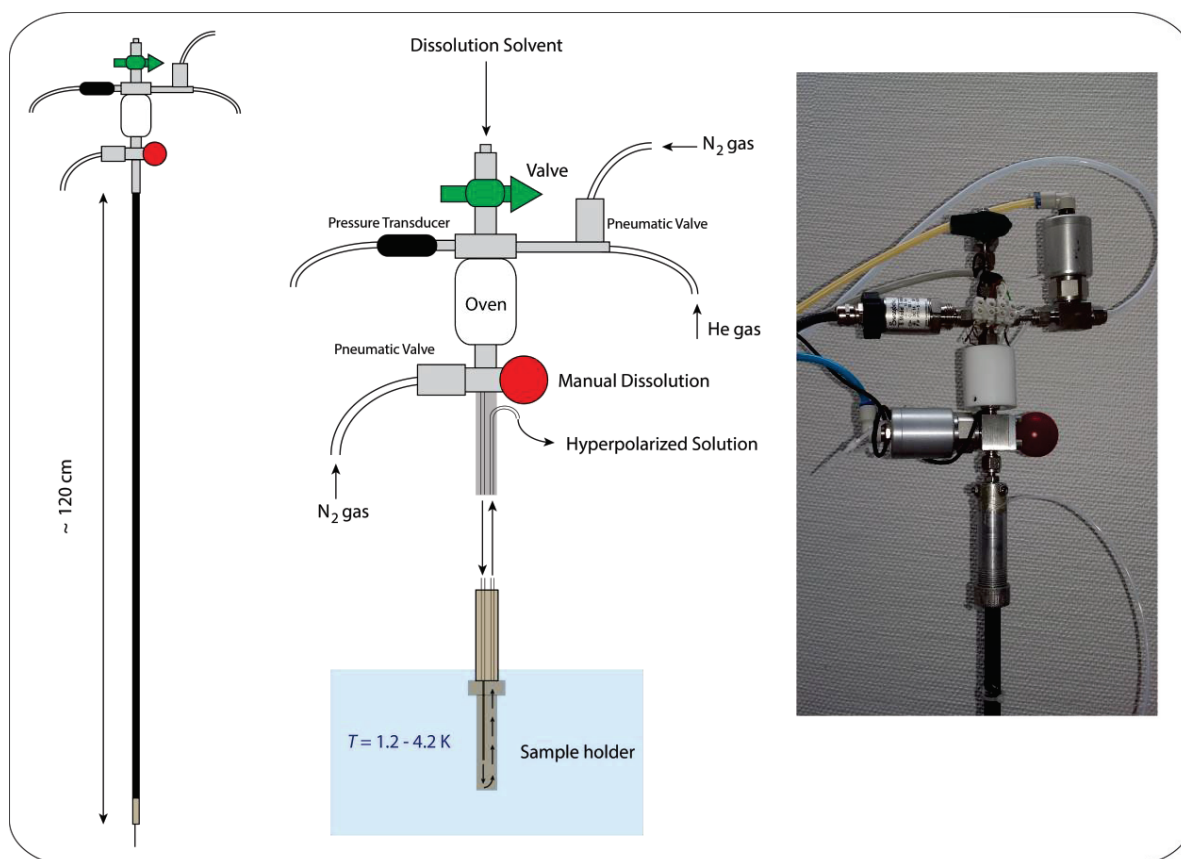


Figure 2.28: Schematic representation and picture of the dissolution stick built in our laboratory to perform dissolution-DNP experiments. Its upper part is composed of an oven chamber that can be filled with the dissolution solvent and heated at the desired temperature. The dissolution is then performed manually by introducing and coupling the cane to the DNP sample inside the DNP polarizer. The hyperpolarized frozen sample is then rapidly melted by the superheated solvent and is pushed back into the stick to be transferred to an NMR spectrometer.

2.6.4 Magnetic tunnel

After being dissolved by a superheated solvent inside the polarizer, the hyperpolarized solution must be transferred to an NMR spectrometer to record the enhanced signal in liquid phase. Usually, this transfer is performed through a polytetrafluoroethylene (PTFE) transfer tube that is directly connected to the outlet of the dissolution stick and to the injector in the NMR spectrometer. In our laboratory, the closest NMR magnets are 300 and 500 MHz NMR spectrometers which are roughly 3 and 5 m from the DNP polarizer. By applying a sufficient pressure of helium inside the transfer tube ($p = 6$ bar), the solution can be pushed in approximately 3.5 s, respectively 5.5 s, to reach the two NMR spectrometers. Despite a relatively fast transfer and quick recording of the NMR signal in the liquid state, several relaxation mechanisms occur in the molecules, like cross-relaxation or simply the fast depletion of polarization due to spin-lattice relaxation with a time constant T_1 , which strongly depends on the magnetic field, and can be very fast at very low field (e.g., in the Earth's magnetic field). This could result in a partial or complete loss of the polarization, thus endangering our hyperpolarized ambitions. To avoid the so-called "*death valley*" [61] during the transfer, we have designed a magnetic tunnel to shelter the hyperpolarized fluids and to keep as much as possible of the enhanced signals.

As previously mentioned, our laboratory is equipped with two different NMR spectrometers (an unshielded 300 MHz and an ultra-shielded 500 MHz NMR spectrometer) close to the 6.7 T DNP polarizer (Fig. 2.29). Therefore, two different magnetic tunnels were built using permanent magnets to transfer the hyperpolarized solutions to the NMR machines.

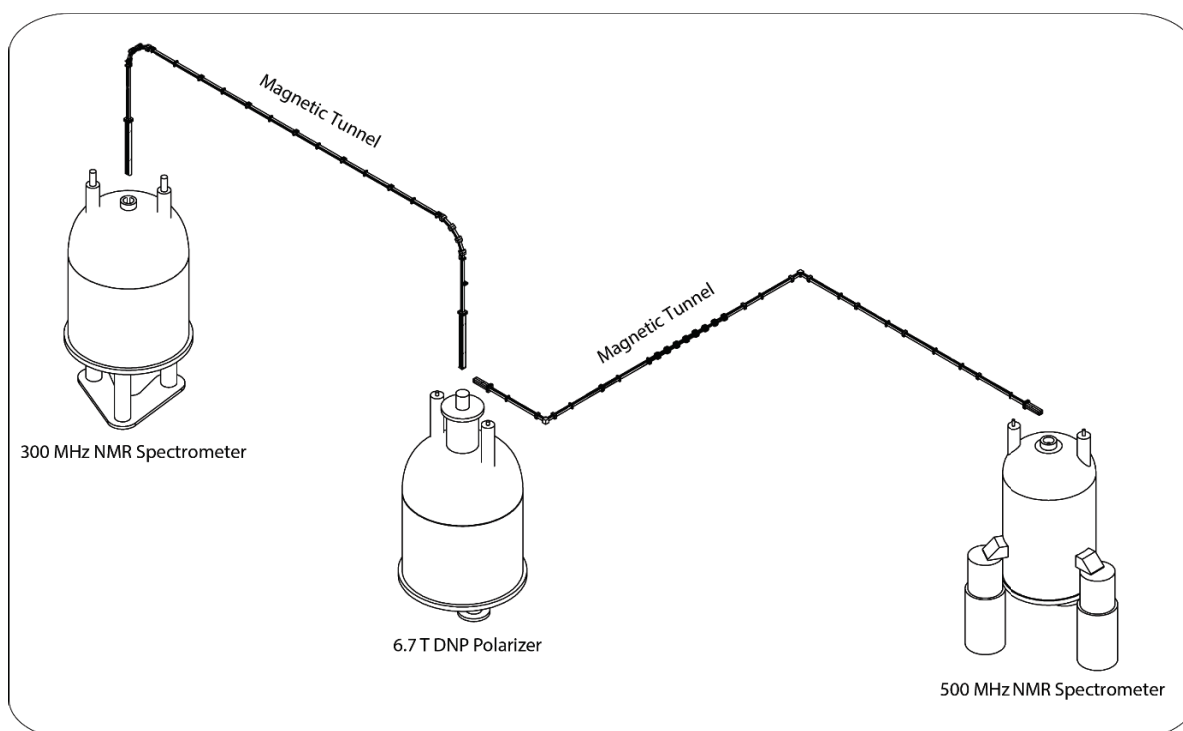


Figure 2.29: DNP equipment in our laboratory is composed of two magnetic tunnels starting at the 6.7 T DNP polarizer and finishing either at the 300 MHz (left) or at the 500 MHz (right) NMR spectrometers. [61]

A small section of the final design of the magnetic tunnel is represented in Fig. 2.30. It is composed of permanent neodymium boron magnets (bought from Supermagnete Webcraft GmbH, 5 x 5 x 100 mm, NdFeB, N52, with Ni-Cu-Ni coating) maintained by a plastic structure printed using a 3D printer, and designed to be placed in a home-built consolidated aluminum structure. The inner PTFE tube can pass through the middle of this structure and the different magnets are positioned according to a Halbach design [63] to maximize the magnetic field in the center of the structure to $B_{\text{tunnel}} > 0.9 \text{ T}$ in order to keep the polarization constant all the way to the NMR spectrometers.

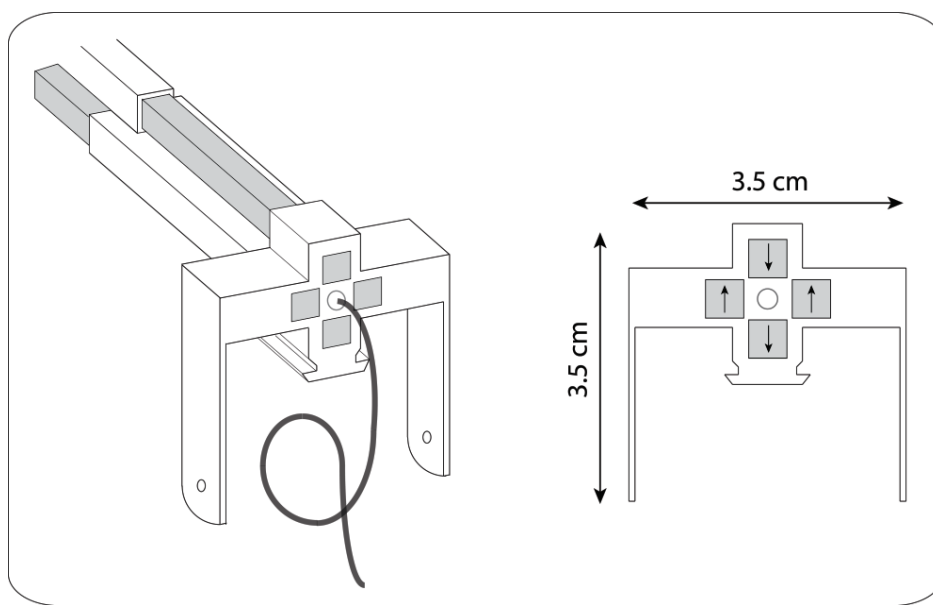


Figure 2.30: Small portion of the structure of the magnetic tunnel built in our laboratory composed of four lines of permanent magnets arranged in a Halbach design to maximize the magnetic field $B_0 > 0.9 \text{ T}$ in its center. The PTFE tube is running through the center to preserve the polarization of the hyperpolarized fluids in the best possible way.

The use of a magnetic tunnel to shelter the polarization during the dissolution and transfer process of the hyperpolarized solutions has led to improvement factors from $1 < \epsilon_{\text{tunnel}} < 25$ for different molecules. These results have been presented in more detail in the thesis of Dr. Jonas Milani and therefore will not be further discussed herein. [61, 62] The effect of keeping the field above 0.9 T all along the transfer is much more pronounced for protons, which are more sensitive to variations of the magnetic field and tend to relax faster in comparison with carbon-13 nuclei. Finally, no negative effects of the magnetic tunnels have been found so far in our systems, so that all our experiments were carried out with magnetic tunnels.

2.6.5 Injector and NMR spectrometer

The final part of the DNP system in our laboratory is composed of an NMR spectrometer to record the hyperpolarized signals in liquid phase and of a home-built injector placed above the probe (Fig. 2.31). When the hyperpolarized solution is expelled from the DNP polarizer by the dissolution solvent and transferred in a few seconds through the magnetic tunnel, it reaches the end of the tube which is situated in the injector chamber. Then the amount of liquid that one wishes to transfer to the NMR tube can be precisely controlled by pushing with a piston connected to a stepper motor controlled by a LabView software. In this manner, precisely controlled volumes from 200 μl to 1 ml of the hyperpolarized solution can be injected, depending on the nature of the experiment.

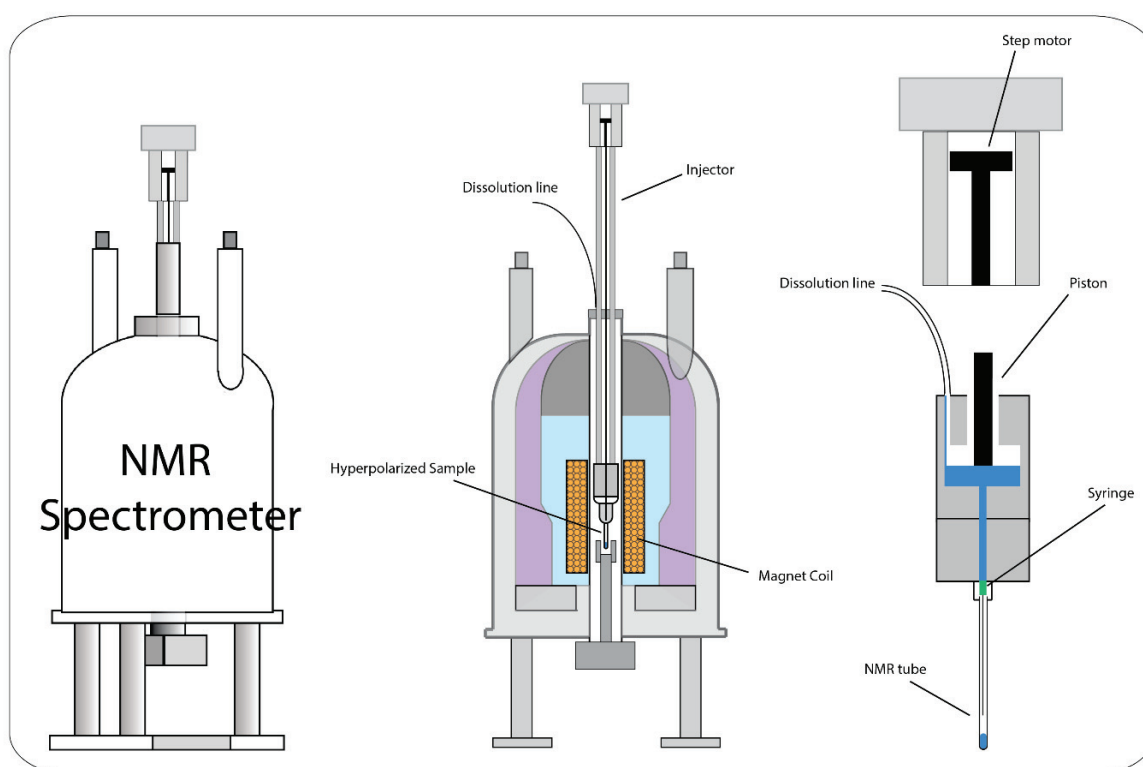


Figure 2.31: Representation of an NMR spectrometer with injector for dissolution-DNP. The injector is placed on top of the magnet and a stepper motor connected to a piston allows one to control with great precision the volume injected into the NMR tube.

References

1. I. Rabi, J. R. Zacharias, S. Millman and P. Kusch, *A new method of measuring nuclear magnetic moment*, 1938, Phys. Rev. 53, 318-318.
2. F. Bloch, *Nuclear Induction*, 1946, Phys. Rev. 70, 460-474.
3. E. M. Purcell, H. C. Torrey and R. V. Pound, *Resonance Absorption by Nuclear Magnetic Moments in a Solid*, 1946, Phys. Rev. 69, 37-38.
4. P. J. Hore, *Nuclear magnetic resonance*, 1995, Oxford University Press, Oxford, New York.
5. M. Abraham, M. A. H. Mccausland and F. N. H. Robinson, *Dynamic Nuclear Polarization*, 1959, Phys. Rev. Lett. 2, 449-451.
6. A. Abragam and M. Goldman, *Principles of Dynamic Nuclear-Polarization*, 1978, Reports on Progress in Physics 41, 395-467.
7. C. D. Jeffries, *Polarization of Nuclei by Resonance Saturation in Paramagnetic Crystals*, 1957, Phys. Rev. 106, 164-165.
8. A. Abragam and W. G. Proctor, *Une nouvelle méthode de polarisation dynamique des noyaux atomiques dans les solides*, 1958, C. R. Acad. Sc. Paris 246, 2253-2256.
9. K. R. Thurber and R. Tycko, *Theory for cross effect dynamic nuclear polarization under magic-angle spinning in solid state nuclear magnetic resonance: The importance of level crossings*, 2012, J. Chem. Phys. 137, 084508.
10. A. G. Redfield, *Nuclear Magnetic Resonance Saturation and Rotary Saturation in Solids*, 1955, Phys. Rev. 98, 1787-1809.
11. B. N. Provotorov, *Magnetic Resonance Saturation in Crystals*, 1962, Sov. Phys. JETP-USSR 14, 1126-1131.
12. J. H. Ardenkjaer-Larsen, B. Fridlund, A. Gram, G. Hansson, L. Hansson, M. H. Lerche, R. Servin, M. Thaning and K. Golman, *Increase in signal-to-noise ratio of > 10,000 times in liquid-state NMR*, 2003, P. Natl. Acad. Sci. USA 100, 10158-10163.
13. A. Comment, B. van den Brandt, K. Uffmann, F. Kurdzesau, S. Jannin, J. A. Konter, P. Hautle, W. T. H. Wenckebach, R. Gruetter and J. J. van der Klink, *Design and performance of a DNP prepolarizer coupled to a rodent MRI scanner*, 2007, Concepts in Magnetic Resonance Part B 31B, 255-269.
14. S. Jannin, A. Bornet, R. Melzi and G. Bodenhausen, *High field dynamic nuclear polarization at 6.7 T: Carbon-13 polarization above 70% within 20 min*, 2012, Chem. Phys. Lett. 549, 99-102.
15. A. Kastler, *Optical Methods of Atomic Orientation and of Magnetic Resonance*, 1957, J. Opt. Soc. Am. 47, 460-465.
16. T. G. Walker and W. Happer, *Spin-exchange optical pumping of noble-gas nuclei*, 1997, Rev. Mod. Phys. 69, 629-642.
17. J. Natterer and J. Bargon, *Parahydrogen induced polarization*, 1997, Prog. Nucl. Mag. Res. Sp. 31, 293-315.
18. M. L. Hirsch, N. Kalechofsky, A. Belzer, M. Rosay and J. G. Kempf, *Brute-Force Hyperpolarization for NMR and MRI*, 2015, J. Am. Chem. Soc. 137, 8428-8434.
19. M. L. Hirsch, B. A. Smith, M. Mattingly, A. G. Goloshevsky, M. Rosay and J. G. Kempf, *Transport and imaging of brute-force C-13 hyperpolarization*, 2015, J. Magn. Reson. 261, 87-94.
20. A. W. Overhauser, *Polarization of Nuclei in Metals*, 1953, Phys. Rev. 91, 476-476.
21. T. R. Carver and C. P. Slichter, *Polarization of Nuclear Spins in Metals*, 1953, Phys. Rev. 92, 212-213.
22. A. Bornet, M. Baudin, B. Vuichoud, S. Jannin, G. Bodenhausen, *Dynamic Nuclear Polarization at 9.4 T*, 2016, in preparation.
23. T. Wenckebach, *Essentials of Dynamic Nuclear Polarization*, 2016, Spindrift Publications, The Netherlands.

24. S. Jannin, *Dynamic Nuclear Polarization for NMR Spectroscopy*, 2013, EPFL course, Switzerland.
25. A. V. Kessenikh, A. A. Manenkov and G. I. Pyatnitskii, *On Explanation of Experimental Data on Dynamic Polarization of Protons in Irradiated Polyethylenes*, 1964, *Sov. Phys-Sol. State* 6, 641-643.
26. C. F. Hwang and D. A. Hill, *New Effect in Dynamic Polarization*, 1967, *Phys. Rev. Lett.* 18, 110-112.
27. D. S. Wollan, *Dynamic Nuclear-Polarization with an Inhomogenesouly Broadened ESR Line. 1. Theory*, 1976, *Phys. Rev. B.* 13, 3761-3685.
28. S. F. J. Cox, V. Bouffard and M. Goldman, *Coupling of two Nuclear Zeeman Reservoirs by Electronic Spin-Spin Reservoir*, 1973, *J. Phys. C Solid State* 6, L100-L103.
29. T. V. Can, Q. Z. Ni and R. G. Griffin, *Mechanisms of dynamic nuclear polarization in insulating solids*, 2015, *J. Magn. Reson.* 253, 23-35.
30. P. J. M. van Bentum, G. H. A. van der Heijden, J. A. Villanueva-Garibay and A. P. M. Kentgens, *Quantitative analysis of high field liquid state dynamic nuclear polarization*, 2011, *Phys. Chem. Chem. Phys.* 13, 17831-17840.
31. R. A. Wind, M. J. Duijvestijn, C. Vanderlugt, A. Manenschijn and J. Vriend, *Applications of Dynamic Nuclear-Polarization in ¹³C NMR in Solids*, 1985, *Prog. Nucl. Mag. Res. Sp.* 17, 33-67.
32. E. R. Andrew, A. Bradbury and R. G. Eades, *Nuclear Magnetic Resonance Spectra from a Crystal Rotated at High Speed*, 1958, *Nature* 182, 1659-1659.
33. S. R. Chaudhari, P. Berruyer, D. Gajan, C. Reiter, F. Engelke, D. L. Silverio, C. Copéret, M. Lelli, A. Lesage and L. Emsley, *Dynamic nuclear polarization at 40 kHz magic angle spinning*, 2016, *Phys. Chem. Chem. Phys.* 18, 10616-10622.
34. D. J. Kubicki, A. J. Rossini, A. Porea, A. Zagdoun, O. Ouari, P. Tordo, F. Engelke, A. Lesage and L. Emsley, *Amplifying Dynamic Nuclear Polarization of Frozen Solutions by Incorporating Dielectric Particles*, 2014, *J. Am. Chem. Soc.* 136, 15711-15718.
35. M. Rosay, L. Tometich, S. Pawsey, R. Bader, R. Schauwecker, M. Blank, P. M. Borchard, S. R. Cauffman, K. L. Felch, R. T. Weber, R. J. Temkin, R. G. Griffin and W. E. Maas, *Solid-state dynamic nuclear polarization at 263 GHz: spectrometer design and experimental results*, 2010, *Phys. Chem. Chem. Phys.* 12, 5850-5860.
36. D. Gajan, M. Schwarzwälder, M. P. Conley, W. R. Grüning, A. J. Rossini, A. Zagdoun, M. Lelli, M. Yulikov, G. Jeschke, C. Sauvee, O. Ouari, P. Tordo, L. Veyre, A. Lesage, C. Thieuleux, L. Emsley and C. Copéret, *Solid-Phase Polarization Matrixes for Dynamic Nuclear Polarization from Homogeneously Distributed Radicals in Mesostuctured Hybrid Silica Materials*, 2013, *J. Am. Chem. Soc.* 135, 15459-15466.
37. A. B. Barnes, B. Corzilius, M. L. Mak-Jurkauskas, L. B. Andreas, V. S. Bajaj, Y. Matsuki, M. L. Belenky, J. Lugtenburg, J. R. Sirigir, R. J. Temkin, J. Herzfeld and R. Griffin, *Resolution and polarization distribution in cryogenic DNP/MAS experiments*, 2010, *Phys. Chem. Chem. Phys.* 12, 5861-5867.
38. T. Maly, L. B. Andreas, A. A. Smith and R. G. Griffin, *²H-DNP-enhanced ²H-¹³C solid-state NMR correlation spectroscopy*, 2010, *Phys. Chem. Chem. Phys.* 12, 5872-5878.
39. B. Vuichoud, J. Milani, A. Bornet, R. Melzi, S. Jannin and G. Bodenhausen, *Hyperpolarization of Deuterated Metabolites via Remote Cross-Polarization and Dissolution Dynamic Nuclear Polarization*, 2014, *J. Phys. Chem. B* 118, 1411-1415.
40. K. Golman, R. in't Zandt and M. Thaning, *Real-time metabolic imaging*, 2006, *P. Natl. Acad. Sci. USA* 103, 11270-11275.
41. K. Golman, R. in't Zandt, M. Lerche, R. Pehrson and J. H. Ardenkjaer-Larsen, *Metabolic imaging by hyperpolarized ¹³C magnetic resonance imaging for in vivo tumor diagnosis*, 2006, *Cancer Res.* 66, 10855-10860.

42. S. J. Nelson, J. Kurhanewicz, D. B. Vigneron, P. E. Z. Larson, A. L. Harzstark, M. Ferrone, M. van Criekinge, J. W. Chang, R. Bok, I. Park, G. Reed, L. Carvajal, E. J. Small, P. Munster, V. K. Weinberg, J. H. Ardenkjaer-Larsen, A. P. Chen, R. E. Hurd, L. I. Odegardstuen, F. J. Robb, J. Tropp and J. A. Murray, *Metabolic Imaging of Patients with Prostate Cancer Using Hyperpolarized [1-¹³C]Pyruvate*, 2013, *Sci. Transl. Med.* 5, 198ra108.
43. F. A. Gallagher, M. I. Kettunen, D. E. Hu, P. R. Jensen, R. in't Zandt, M. Karlsson, A. Gisselsson, S. K. Nelson, T. H. Witney, S. E. Bohndiek, G. Hansson, T. Peitersen, M. H. Lerche and K. M. Brindle, *Production of hyperpolarized [1,4-¹³C₂]malate from [1,4-¹³C₂]fumarate is a marker of cell necrosis and treatment response in tumors*, 2009, *P. Natl. Acad. Sci. USA* 106, 19801- 19806.
44. S. E. Day, M. I. Kettunen, F. A. Gallagher, D. E. Hu, M. Lerche, J. Wolber, K. Golman, J. H. Ardenkjaer-Larsen and K. M. Brindle, *Detecting tumor response to treatment using hyperpolarized ¹³C magnetic resonance imaging and spectroscopy*, 2007, *Nat. Med.* 13, 1382-1387.
45. J. H. Ardenkjaer-Larsen, S. Macholl and H. Johannesson, *Dynamic nuclear polarization with trityls at 1.2 K*, 2008, *Appl. Magn. Reson.* 34, 509-522.
46. C. Gabellieri, S. Reynolds, A. Lavie, G. S. Payne, M. O. Leach and T. R. Eykyn, *Therapeutic target metabolism observed using hyperpolarized ¹⁵N choline*, 2008, *J. Am. Chem. Soc.* 130, 4598-4599.
47. N. N. Kuzma, M. Pourfathi, H. Kara, P. Manasseh, R. K. Ghosh, J. H. Ardenkjaer-Larsen, S. J. Kadlecsek and R. R. Rizi, *Cluster formation restricts dynamic nuclear polarization of xenon in solid mixtures*, 2012, *J. Chem. Phys.* 137, 104508.
48. M. E. Merritt, C. Harrison, Z. Kovacs, P. Kshirsagar, C. R. Malloy and A. D. Sherry, *Hyperpolarized ⁸⁹Y offers the potential of direct imaging of metal ions in biological systems by magnetic resonance*, 2007, *J. Am. Chem. Soc.* 129, 12942-12943.
49. H. Nonaka, R. Hata, T. Doura, T. Nishihara, K. Kumagai, M. Akakabe, M. Tsuda, K. Ichikawa and S. Sando, *A platform for designing hyperpolarized magnetic resonance chemical probes*, 2013, *Nat. Commun.* 4, 2411.
50. J. H. Ardenkjaer-Larsen, A. M. Leach, N. Clarke, J. Urbahn, D. Anderson and T. W. Skloss, *Dynamic Nuclear Polarization Polarizer for Sterile Use Intent*, 2011, *NMR Biomed.* 24, 927-932.
51. I. Dhimitruka, M. Velayutham, A. A. Bobko, V. V. Khramtsov, F. A. Villamena, C. M. Hadad and J. L. Zweier, *Large-scale synthesis of a persistent trityl radical for use in biomedical EPR applications and imaging*, 2007, *Bioorg. Med. Chem. Lett.* 17, 6801-6805.
52. Mikkel Thaning and Rolf Servin, *Method of dynamic nuclear polarisation (DNP) using a trityl radical and a paramagnetic metal ion*, 2006, Patent CA2628539 A1.
53. A. Bornet, R. Melzi, S. Jannin and G. Bodenhausen, *Cross Polarization for Dissolution Dynamic Nuclear Polarization Experiments at Readily Accessible Temperatures 1.2 < T < 4.2 K*, 2012, *Appl. Magn. Reson.* 43, 107-117.
54. S. R. Hartmann and E. L. Hahn, *Nuclear Double Resonance in Rotating Frame*, 1962, *Phys. Rev.* 128, 2042-2053.
55. A. Pines, J. S. Waugh and M. G. Gibby, *Proton-Enhanced Nuclear Induction Spectroscopy - Method for High-Resolution NMR of Dilute Spins in Solids*, 1972, *J. Chem. Phys.* 56, 1776-1777.
56. A. J. Perez Linde, *Application of cross polarisation techniques to dynamic nuclear polarisation dissolution experiments*, 2010, Ph. D. Thesis, University of Nottingham, United Kingdom.
57. S. Jannin, A. Bornet, S. Colombo and G. Bodenhausen, *Low-temperature cross polarization in view of enhancing dissolution Dynamic Nuclear Polarization in NMR*, 2011, *Chem. Phys. Lett.* 517, 234-236.
58. A. Bornet and S. Jannin, *Optimizing dissolution dynamic nuclear polarization*, 2016, *J. Magn. Reson.* 264, 13-21.
59. A. Bornet, R. Melzi, A. J. P. Linde, P. Hautle, B. van den Brandt, S. Jannin and G. Bodenhausen, *Boosting Dissolution Dynamic Nuclear Polarization by Cross Polarization*, 2013, *J. Phys. Chem. Lett.* 4, 111-114.

60. E. Kupce and R. Freeman, *Adiabatic Pulses for Wide-Band Inversion and Broad-Band Decoupling*, 1995, J. Magn. Reson. Ser. A 115, 273-276.
61. J. Milani, B. Vuichoud, A. Bornet, P. Miéville, R. Mottier, S. Jannin and G. Bodenhausen, *A magnetic tunnel to shelter hyperpolarized fluids*, 2015, Rev. Sci. Instrum. 86, 024101.
62. J. Milani, *Novel Instrumentation and Methods for Chemical Applications of Dissolution Dynamic Nuclear Polarization*, 2016, Ph. D. Thesis, EPFL, Switzerland.
63. K. Halbach, *Design of Permanent Multipole Magnets with Oriented Rare-Earth Cobalt Material*, 1980, Nucl. Instrum. Methods 169, 1-10.

Chapter 3: Improvements in Dynamic Nuclear Polarization

3.1 Introduction

In this chapter, the optimization of the preparation of DNP samples to enhance the polarization levels at low temperatures by changing the structure of the nitroxide radical TEMPOL is discussed. The optimum concentration of this radical is determined for our specific conditions at $B_0 = 6.7$ T and $T = 1.2 - 4.2$ K [1] and the results obtained for different nitroxide radicals are presented and compared in chapter 3.2.

Furthermore, the implementation of a recent technique named microwave frequency modulation [2, 3] is described. This useful method is coupled to our DNP setup in order to improve the overall DNP process while allowing a reduction of the radical concentration in the DNP sample. All the advantages resulting from the modulation of the microwave frequency are explained in detail in chapter 3.3.

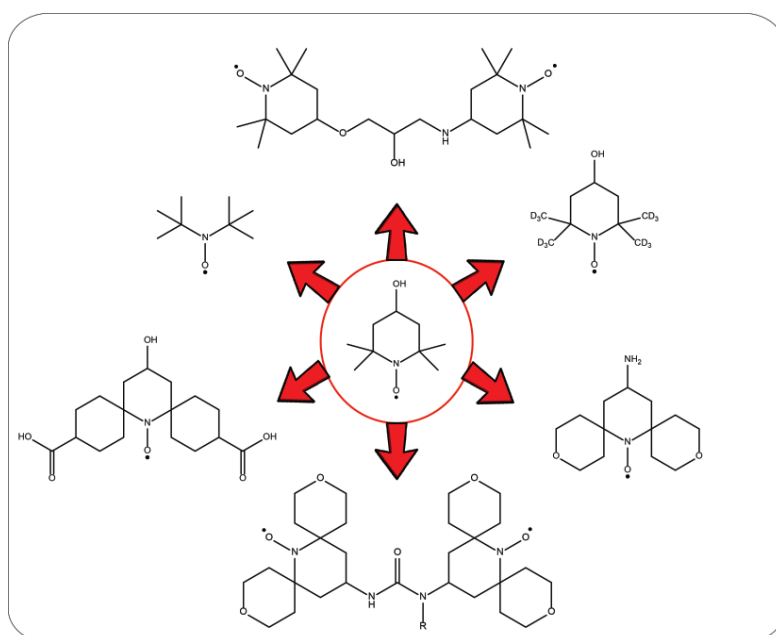
3.2 Optimization of Radicals for Dissolution-DNP

Dissolution-DNP (d-DNP) is usually performed using Trityl radicals [4] for direct ^{13}C polarization at low temperatures ($T = 1.2 - 4.2$ K). Even if this type of radical is commonly used in the DNP community, it remains difficult to obtain (GE patent) [5] and is complicated to synthesize. [6] Furthermore, because of the direct ^{13}C polarization, the DNP build-up times are in general relatively long (a few hours).

Fortunately for our hyperpolarized ambitions, a more affordable radical exists that belongs to the nitroxide radical family. One of the most commonly used radicals in this family is 4-hydroxy-2,2,6,6-tetramethylpiperidin-1-oxyl or TEMPOL, which has a very simple structure and a high solubility in water. Even if nitroxide radicals are less efficient than Trityl for direct ^{13}C polarization under the same conditions, because of their larger ESR linewidths, they are more suitable candidates for the hyperpolarization of protons. [7] With the Hartmann-Hahn Cross-Polarization (CP) technique, we have demonstrated that the high ^1H polarization could be transferred to ^{13}C in an efficient way, leading to a ^{13}C polarization comparable to what can be achieved with Trityl, but in much shorter DNP build-up times (of only few minutes). [8]

As mentioned, TEMPOL is one of the favorite mono-radicals used for CP-DNP at very low-temperatures. However, at higher temperatures ($T \approx 100$ K for MAS-DNP experiments), more suitable bi-nitroxide radicals like TOTAPOL [9] or AMUPOL [10] are to be preferred in order to achieve greater enhancements through the Cross Effect mechanism. In MAS-DNP, the optimization of the structure of biradicals has been a key challenge for achieving greater enhancements. [11] A similar optimization has not yet been performed for d-DNP at $T = 1.2 - 4.2$ K to determine if more efficient nitroxide radicals can be found.

Therefore, new types of nitroxide radicals, which were found to be the most suitable for Dynamic Nuclear Polarization, were selected in order to determine if, by altering their structure, the DNP effect could be enhanced under our conditions. In addition, different concentrations of radicals in the DNP sample were tested to achieve the maxima of the DNP polarization levels.



3.2.1 TEMPOL, TOTAPOL and AMUPOL

The first experiments were carried out using TEMPOL (MW = 172.25 g/mol) , TOTAPOL (MW = 399.58 g/mol) [9] and AMUPOL (MW = 726.91 g/mol) [10] (see Fig. 3.1) in order to observe if the presence of biradicals in the DNP sample has a beneficial effect under our DNP conditions ($B_0 = 6.7$ T and $T = 4.2$ K) as for MAS-DNP experiments. Different concentrations of the radicals were tested in order to find the optima of the polarizations and build-up times for each biradical.

The DNP samples were prepared by dissolving the different nitroxide radicals (with concentrations between 20 – 65 mM) in a mixture of $H_2O/D_2O/glycerol-d_8$ (v/v/v : 10/40/50). The resulting solutions were then inserted in the DNP polarizer at $B_0 = 6.7$ T and $T = 4.2$ K (for more detail, see Supporting Information).

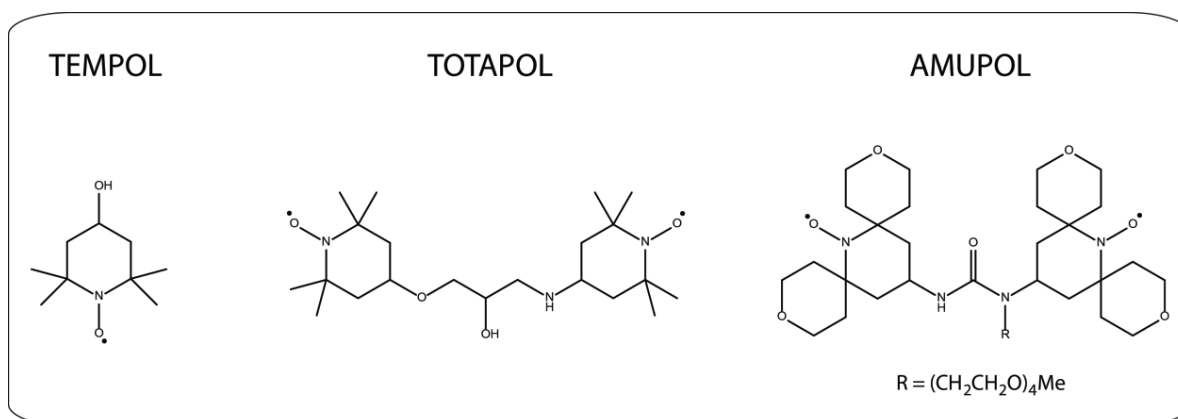


Fig. 3.1: Chemical structures of the three nitroxide radicals that have been tested: TEMPOL, TOTAPOL and AMUPOL.

Dynamic Nuclear Polarization was performed on these samples with a constant microwave irradiation ($P_{\mu W} = 87.5$ mW). The 1H polarizations and DNP build-up times were recorded by applying small angle pulses to each sample at different microwave frequencies ranging from $187.5 < f_{\mu W} < 188.5$ GHz at $T = 4.2$ K (see Fig. 3.2). For TEMPOL, the maximum of 1H polarization $P(^1H) \approx 40\%$ was achieved with a concentration of 35 mM and with a relatively short build-up time $T_{bup}(^1H) = 100$ s. The decrease in TEMPOL concentration to 20 mM led to a dramatic loss in proton polarization and a great extension of the build-up time to $T_{bup}(^1H) = 250$ s. Even when increasing the radical concentration by almost a factor two (65 mM), the 1H polarization remains relatively high, $P(^1H) = 30\%$. For the biradical TOTAPOL, a concentration of 25 mM (representing a total concentration of unpaired electrons of 50 mM) was found to be the optimum for a 1H polarization $P(^1H) = 30\%$ with a short build-up time $T_{bup}(^1H) = 100$ s. For AMUPOL, the concentration was reduced to 17.5 mM (representing 35 mM for the total concentration of unpaired electrons) to achieve a proton polarization of only $P(^1H) = 20\%$, with a very short build-up time $T_{bup}(^1H) < 50$ s. A slight increase of the radical concentration to 25 mM AMUPOL led to a drop in proton polarization, albeit without much affecting the DNP build-up time. By comparing these 3 different samples at $B_0 = 6.7$ T and $T = 4.2$ K, the mono-radical TEMPOL seems therefore to be the best candidate to perform DNP at low temperatures, in comparison with both biradicals TOTAPOL and AMUPOL. The proton polarization achieved by using TEMPOL is well above the ones obtained with the two others radicals and the build-up times achieved at different concentrations is almost comparable to those obtained with AMUPOL. Therefore, the use of biradicals for d-DNP under our specific conditions does not bring a sufficient advantage in terms of a gain in polarization levels and a reduction of the build-up times to justify their use.

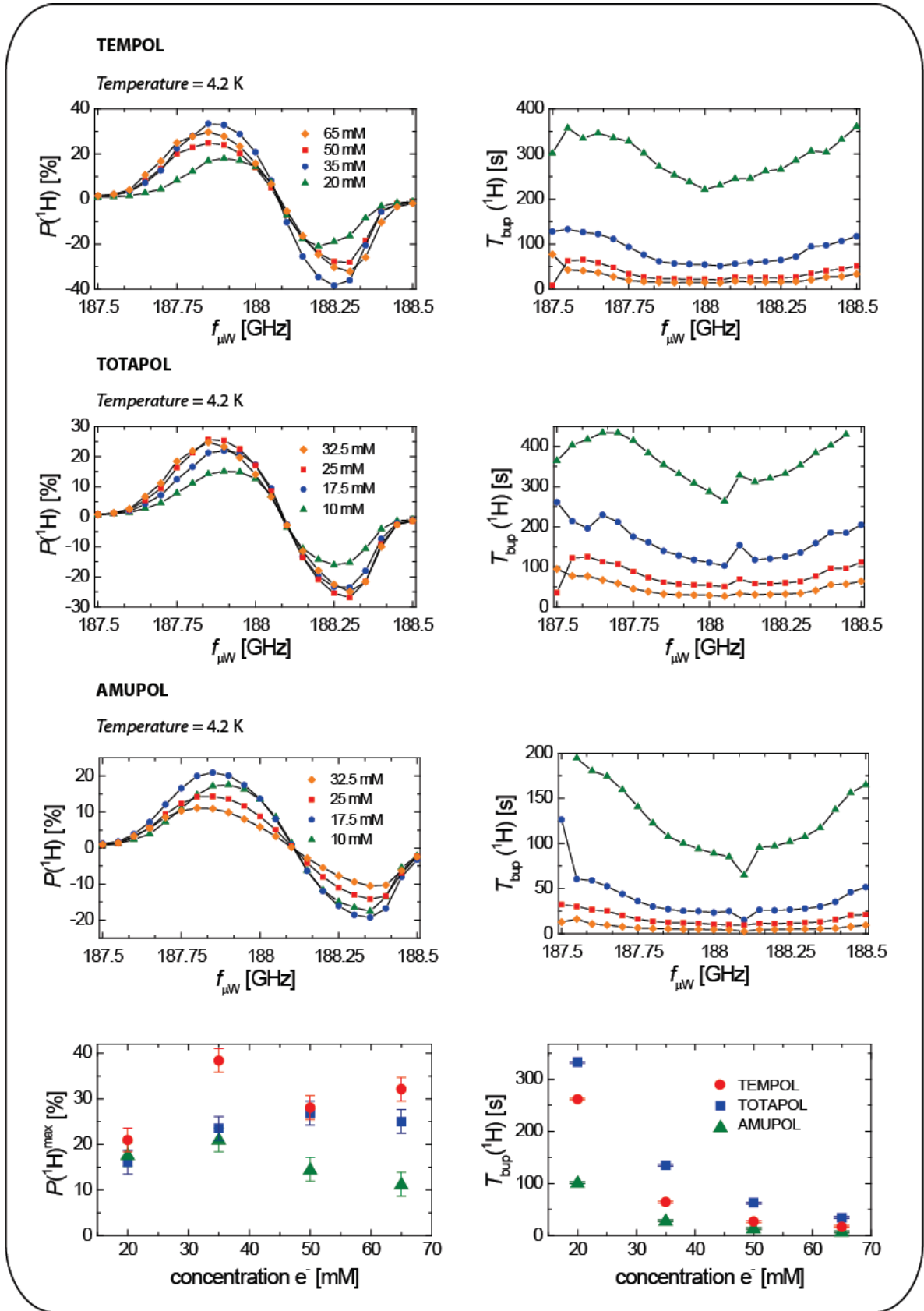


Fig. 3.2: Proton polarizations $P(^1\text{H})$ and DNP build-up times $T_{\text{bup}}(^1\text{H})$ for TEMPOL, TOTAPOL and AMUPOL for different radical concentrations in the range 20 – 65 mM, at different microwave frequencies $187.5 < f_{\mu\text{W}} < 188.5$ GHz, at $B_0 = 6.7$ T and $T = 4.2$ K. The two graphs at the bottom show comparisons of the polarizations and build-up times between the three radicals.

3.2.2 Nitroxide radicals derived from TEMPOL

Since biradicals were rejected for applications to our d-DNP setup because of the lower proton polarizations achieved, we therefore focused on derivatives of TEMPOL in order to enhance our hyperpolarized signals in DNP. In collaboration with the Equipe Structure et Réactivité des Espèces Paramagnétiques (SREP) at Aix-Marseille Université (AMU) which provided us with these radicals, we decided to test fully deuterated TEMPOL (MW = 184.32 g/mol), as well as what we have dubbed ditertbutyl-TEMPO (MW = 144.24 g/mol), PyTEMPAMINE (MW = 255.34 g/mol) (a precursor for the synthesis of PyPOL [10]) and CarbTEMPOL (MW = 340.40 g/mol) (see Fig. 3.3).

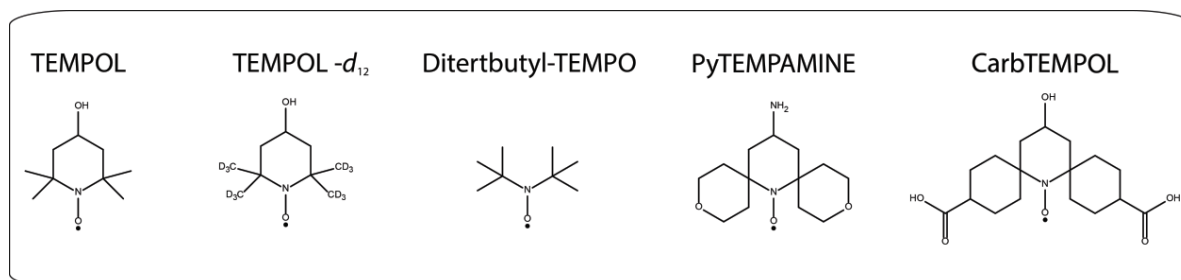


Fig. 3.3: Chemical structures of nitroxide radicals derived from TEMPOL: TEMPOL- d_{12} , ditertbutyl-TEMPO, PyTEMPAMINE and CarbTEMPOL.

The experiments were performed in the same manner for each radical at two different concentrations (1) 25 mM and (2) 40 mM in a mixture of H₂O/D₂O/glycerol- d_8 (v/v/v : 10/40/50), except for ditertbutyl-TEMPO (only 40 mM) and for CarbTEMPOL where the pH of the solution was adjusted to 8-9 in order to properly solubilize the radical in water (see Supporting Information). DNP was performed at both $T = 1.2$ and 4.2 K with frequency-modulated microwave irradiation [3] ($f_{\text{mod}} = 10$ kHz and $\Delta f_{\mu\text{W}} = 100$ MHz; see chapter 3.3) and a microwave power of $P_{\mu\text{W}} = 87.5$ mW. The results obtained for the different nitroxide radicals are described in detail in Table 3.1. For clarity and a better understanding of these results, they are compared with the "standard" TEMPOL radical used in our laboratory.

At first sight, deuteration of TEMPOL seemed to be a good approach to enhance the proton polarization, since the ¹H that are attached to the radical are not observable because of the so-called "bleaching effect" and since protonated methyl groups tend to relax faster longitudinally than their deuterated analogues, thus hampering the DNP build-up. However, the anticipated advantages were not observed when fully deuterated TEMPOL was used. Indeed, for both concentrations of 25 mM and 40 mM at 4.2 K, the proton polarization was lower and the build-up times longer for the deuterated radical. The only advantage of the use of 25 mM TEMPOL- d_{12} is that a ¹H polarization as high as 74 % has been achieved at 1.2 K, compared to 54 % with 25 mM non-deuterated TEMPOL at 1.2 K. Nevertheless, the full deuteration of TEMPOL does not generally lead to a greater enhancement in proton polarization levels as expected. Therefore, we can argue that the mere presence of the protons attached to the methyl groups of the radicals has the desirable effect of improving the transfer of the ¹H polarization throughout the DNP sample.

Because of this unsuccessful attempt, we decided to change the overall structure of the TEMPOL radical. Therefore, the piperidine group was replaced by two tertiary butyl groups attached to the nitroxide residue to obtain ditertbutyl-TEMPO. As expected, the ^1H build-up times for this radical became shorter (an effect that is much more pronounced at 1.2 K), but unfortunately the ^1H polarization at 1.2 K dropped dramatically from $P(^1\text{H}) = 91$ to 50 % with 40 mM ditertbutyl-TEMPO. Thus, the more rigid structure due by the presence of a piperidine group in TEMPOL represents an important factor to get the maximum DNP enhancement.

In a third attempt, PyTEMPAMINE, a precursor in the synthesis of PyPOL, was tested in order to keep the same ring structure as in the piperidine group of TEMPOL, but the methyl groups were replaced by bulkier tetrahydro-2*H*-pyran groups. Because of these heavier functional groups attached near the perimeter of the radical, an interesting effect was observed at 4.2 K with 25 mM PyTEMPAMINE: the ^1H DNP build-up times are slightly shortened to $T_{\text{bup}}(^1\text{H}) = 143$ s compared to $T_{\text{bup}}(^1\text{H}) = 156$ s for 25 mM TEMPOL without hampering the overall polarization. This is not the case with 40 mM PyTEMPAMINE where the build-up times are longer, i.e., $T_{\text{bup}}(^1\text{H}) = 68$ s compared to $T_{\text{bup}}(^1\text{H}) = 40$ s for 40 mM TEMPOL. The same experiments were carried with 25 mM PyTEMPAMINE at a lower temperature of 1.2 K, where the ^1H polarizations were greatly enhanced to $P(^1\text{H}) = 77$ % compared to $P(^1\text{H}) = 51$ % for 25 mM TEMPOL at 1.2 K. Surprisingly, when the concentration of PyTEMPAMINE was increased to 40 mM at 1.2 K, the ^1H polarizations became lower compared for the same radical at a lower concentration of 25 mM, while the build-up times remained almost the same. Therefore, we can argue that the use of PyTEMPAMINE at low concentrations has a beneficial effect in terms of both achievable polarizations levels and build-up times when compared to TEMPOL.

Finally, CarbTEMPOL was selected as a candidate for our DNP experiments, because of its even bulkier groups compared to PyTEMPAMINE. At 4.2 K, this radical shows a slightly better proton polarization than TEMPOL at concentrations of both 25 and 40 mM, but exhibits build-up times that are twice as long. The same inconvenience is observed at 1.2 K for 40 mM CarbTEMPOL, where the proton polarization $P(^1\text{H}) = 87$ % is fairly high compared to $P(^1\text{H}) = 91$ %, but the build-up times $T_{\text{bup}}(^1\text{H}) = 231$ s for CarbTEMPOL are clearly excessive compared to $T_{\text{bup}}(^1\text{H}) = 122$ s for TEMPOL.

3.2.3 Conclusions concerning TEMPOL derivatives

With these preliminary results in hand, it is interesting to notice that TEMPOL remains for the moment the best candidate to perform DNP under our conditions at $B_0 = 6.7$ T and $T = 1.2$ K. The presence of protonated methyl groups in TEMPOL has an important favorable impact on the achievable polarization levels, and its chemical structure has an advantageous effect on the ^1H build-up times. However, the use of PyTEMPAMINE should be interesting if we wish to decrease the radical concentration to 25 mM, since it seems to be a better polarizing agent than TEMPOL for these specific conditions.

For future experiments, it would be interesting to test these radicals and biradicals at a higher magnetic field $B_0 = 9.4$ T in our new DNP polarizer based on a Cryogenics magnet. Indeed, at this magnetic field, the Cross Effect mechanism should be more pronounced and it would perhaps be interesting to test biradicals again, since they should be better-suited candidates for DNP, as well as the previously mentioned derivatives of TEMPOL.

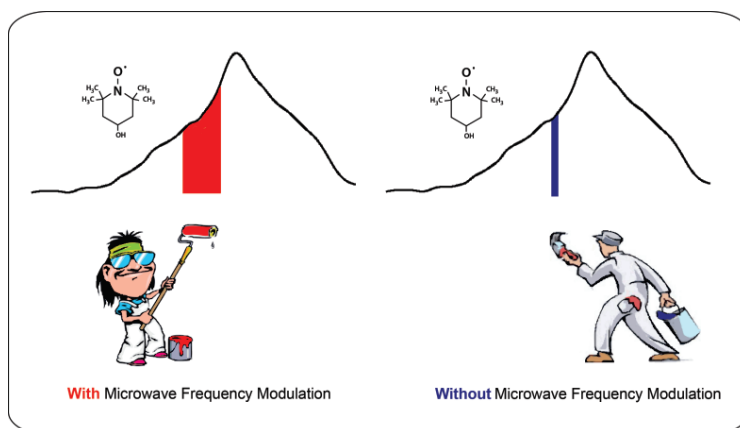
Radical	Temp. [K]	Concentration [mM]	$f_{\mu\text{W}}$ [GHz]	Polarization $P(^1\text{H})$ [%]	$T_{\text{bup}}(^1\text{H})$ [s]	Temp. [K]	Concentration [mM]	$f_{\mu\text{W}}$ [GHz]	Polarization $P(^1\text{H})$ [%]	$T_{\text{bup}}(^1\text{H})$ [s]
TEMPOL	4.2	25	187.9	29 ± 2	156 ± 1	1.2	25	187.9	49 ± 2	273 ± 1
			188.3	30 ± 2	177 ± 1			188.3	54 ± 2	281 ± 1
		40	187.9	32 ± 2	40 ± 1		187.9	76 ± 2	87 ± 2	
			188.3	31 ± 2	48 ± 1		188.3	91 ± 2	122 ± 2	
TEMPOL-d_{12}	4.2	25	187.9	28 ± 2	235 ± 1	1.2	25	187.9	58 ± 2	696 ± 5
			188.2	29 ± 2	252 ± 1			188.3	74 ± 2	643 ± 3
		40	187.8	21 ± 2	50 ± 1		187.8	75 ± 2	174 ± 4	
			188.3	19 ± 2	58 ± 1		188.4	80 ± 2	233 ± 4	
Diterbutyl-TEMPO	4.2	25	187.9	-	-	1.2	25	187.9	-	-
			188.3	-	-			188.3	-	-
		40	187.9	20 ± 2	42 ± 1		187.9	48 ± 2	80 ± 1	
			188.3	18 ± 2	46 ± 1		188.3	50 ± 2	101 ± 1	
PyTEMPAMINE	4.2	25	187.9	31 ± 2	143 ± 1	1.2	25	187.9	70 ± 2	349 ± 1
			188.3	30 ± 2	155 ± 1			188.3	77 ± 2	392 ± 3
		40	187.9	28 ± 2	68 ± 1		187.9	67 ± 2	356 ± 3	
			188.3	29 ± 2	75 ± 1		188.3	70 ± 2	388 ± 2	
CarbTEMPOL	4.2	25	187.9	33 ± 2	315 ± 3	1.2	25	187.9	60 ± 2	868 ± 5
			188.3	32 ± 2	347 ± 4			188.3	73 ± 2	885 ± 10
		40	187.9	37 ± 2	79 ± 1		187.9	71 ± 2	143 ± 2	
			188.3	36 ± 2	96 ± 1		188.3	87 ± 2	231 ± 3	

Table 3.1: Proton polarizations $P(^1\text{H})$ and DNP build-up times $T_{\text{bup}}(^1\text{H})$ for the different radicals TEMPOL, TEMPOL- d_{12} , di-tert-butyl-TEMPO, PyTEMPAMINE and CarbTEMPOL at $B_0 = 6.7$ T and $T = 1.2 - 4.2$ K, with a concentration of 25 and 40 mM, determined at the negative and positive maxima of the microwave irradiation (188.3 and 187.9 GHz respectively). The "best" conditions for each temperature and radical concentration are highlighted in blue.

3.3 Microwave Frequency Modulation for Dissolution Dynamic Nuclear Polarization

Hyperpolarization by Dissolution Dynamic Nuclear Polarization is mainly achieved by using a monochromatic microwave irradiation of the ESR spectrum of the radicals at low temperatures. It was recently demonstrated by Hovav *et al.* [2] that the use of frequency-modulated microwave irradiation could improve DNP at $B_0 = 3.34$ T and at temperatures between 10 and 50 K. Because of these encouraging results [2], we decided to implement a similar frequency modulation to our system under harsher conditions ($B_0 = 6.7$ T and $T = 1.2$ K). Because of this new method, we ended up with several improvements in our DNP experiments for our standard DNP samples: higher polarization levels, faster build-up rates, lower radical concentrations and therefore less paramagnetic broadening, which enabled us to perform a more efficient Cross-Polarization transfer from ^1H to ^{13}C .

These improvements discussed in this chapter are adapted from the publication entitled "*Microwave frequency modulation to enhance Dissolution Dynamic Nuclear Polarization*". [3]



3.3.1 Optimization of microwave frequency modulation

As discussed in previous chapters, several mechanisms like the Solid Effect (SE) [12], the Cross Effect (CE) [13, 14, 15], Thermal Mixing (TM) [16, 17] and the Overhauser Effect (OE) [18] are responsible for the DNP enhancements of the nuclear spins. These enhancements depend on the offset between the microwave frequency and the center of the ESR line.

Even if TM is best performed using a monochromatic microwave irradiation, it was recently shown [2, 19, 20] that for the CE and SE mechanisms, DNP can be greatly improved by using either a field modulation or a frequency-modulated microwave irradiation. In our experimental setup and under our specific conditions, the predominant mechanisms are TM and CE, and the application of a frequency-modulated irradiation should have a significant effect. This is why we decided to use the same approach to observe if we could obtain similar benefits as Hovav *et al.* [2] did at $B_0 = 3.34$ T and temperatures between 10 and 50 K, but here at a higher field $B_0 = 6.7$ T and at temperatures as low as $T = 1.2$ K.

In our experiments, substantial gains in polarization values $P(^1\text{H})$ were achieved by factors up to $\epsilon_{fm} > 3$ by using frequency modulation, in comparison with conventional monochromatic irradiation. Moreover, the DNP build-up times have been reduced by factors up to $\kappa_{fm} \approx 10$, while the concentration of radicals could be reduced by a factor 2. This last advantage results in narrower ^1H NMR linewidths and longer $T_{1\rho}$, so that Cross-Polarization could be significantly improved.

In order to modulate the microwave frequency, we used an Elva VCOM microwave source that is described in more detail in chapter 2.6. To quickly summarize, this microwave source allows one to control the frequency by a voltage-controlled oscillator (VCO) driven either by a constant or by a modulated voltage (Stanford Research Systems DS345). This combination enables a frequency modulation that is fast (up to 10 MHz) and broad (± 500 MHz), which is well-suited to our experimental needs.

Different factors have to be taken into account and should be optimized in order to achieve the maximum possible enhancement. In Fig. 3.4, a scheme illustrating the frequency modulation method is presented. The first parameter that has to be set is the average microwave frequency $f_{\mu\text{W}}$ to allow the DNP process. For the nitroxide radicals used in our laboratory, this frequency corresponds to $f_{\mu\text{W}} = 187.9$ GHz for the positive lobe of the ESR line and $f_{\mu\text{W}} = 188.3$ GHz for the negative one. In order to perform the modulation, the range $\Delta f_{\mu\text{W}}$ of the frequency modulation must be adjusted as well as the modulation frequency f_{mod} so that the microwave frequency varies in sinusoidal fashion:

$$f_{\mu\text{W}}(t) = f_{\mu\text{W}} + \frac{1}{2}\Delta f_{\mu\text{W}} \sin(2\pi f_{\text{mod}} t) \quad (3.1)$$

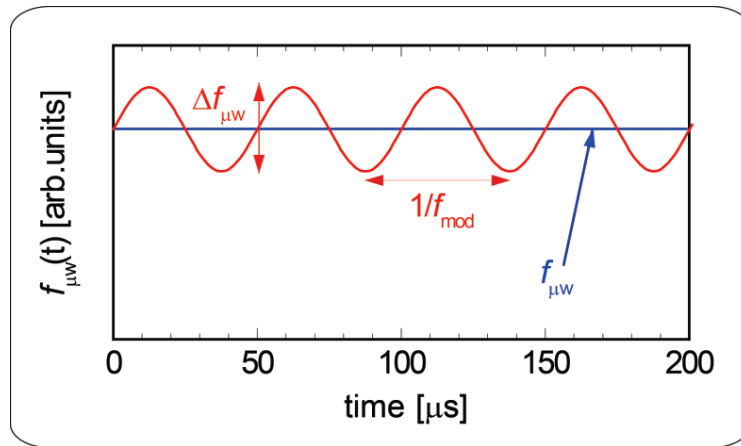


Fig. 3.4: Schematic illustration of the frequency modulation method implemented in our laboratory. The microwave frequency varies in a sinusoidal fashion $f_{\mu\text{W}}(t) = f_{\mu\text{W}} + \frac{1}{2}\Delta f_{\mu\text{W}} \sin(2\pi f_{\text{mod}} t)$.

The two parameters $\Delta f_{\mu\text{W}}$ and f_{mod} have been carefully optimized in order to get the maximum proton polarization $P(^1\text{H})$. This optimization was done on a DNP sample containing 25 mM TEMPOL in a $\text{H}_2\text{O}/\text{D}_2\text{O}/\text{glycerol-}d_8$ (v/v/v : 10/40/50) mixture. The average microwave frequency was set to $f_{\mu\text{W}} = 187.9$ GHz for the positive lobe of the ESR line and the measurements were carried out at $T = 1.2$ K.

The first graph in Fig. 3.5 represents the dependence of the polarization $P(^1\text{H})$ as a function of the modulation frequency f_{mod} , with a constant amplitude of the modulation $\Delta f_{\mu\text{W}} = 100$ MHz. The most striking feature is that the dependence is rather flat with a broad optimum $1 < f_{\text{mod}} < 1000$ kHz. The second graph in Fig. 3.5 shows the dependence of the polarizations $P(^1\text{H})$ as a function of the amplitude $\Delta f_{\mu\text{W}}$ with a constant modulation frequency $f_{\text{mod}} = 10$ kHz. As before, the optimal condition does not change much over a range $20 < \Delta f_{\mu\text{W}} < 100$ MHz. The power was therefore optimized for $f_{\text{mod}} = 10$ kHz and $\Delta f_{\mu\text{W}} = 100$ MHz to yield $P_{\mu\text{W}} = 87.5$ mW at $T = 1.2$ K. As a general rule, the amplitude of the modulation should cover a lobe of the ESR line while having a constructive effect (either positive or negative), while the modulation frequency should be faster than the electron spin-lattice relaxation rate ($f_{\text{mod}} > 1/T_{1e} \approx 10$ Hz since $T_{1e} \approx 100$ ms under our specific conditions).

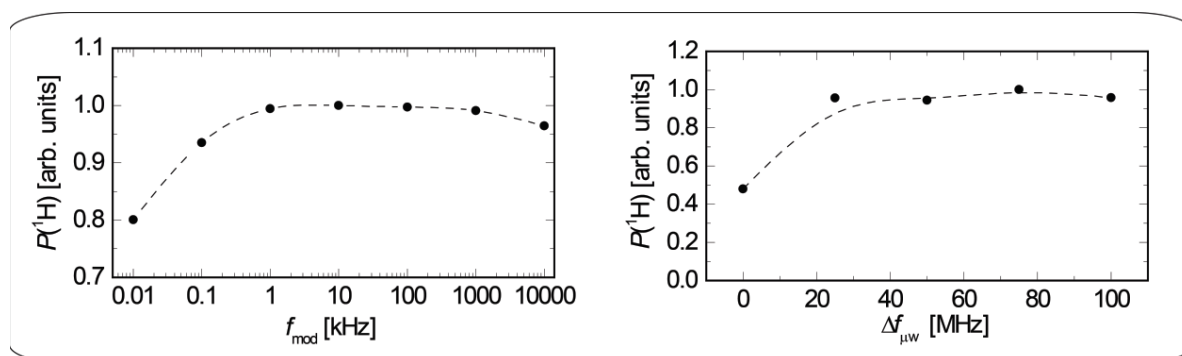


Fig. 3.5: Proton polarization $P(^1\text{H})$ of a DNP sample containing 25 mM TEMPOL as a function of the modulation frequency f_{mod} (left) and as a function of the amplitude of the modulation $\Delta f_{\mu\text{W}}$ (right).

3.3.2 Experimental results for microwave frequency modulation

After the selecting the optimum $\Delta f_{\mu\text{W}}$ and f_{mod} , the polarization $P(^1\text{H})$ of the same DNP sample containing 25 mM TEMPOL in a mixture of $\text{H}_2\text{O}/\text{D}_2\text{O}/\text{glycerol-}d_8$ (v/v/v : 10/40/50) at 1.2 K was compared with and without frequency modulation for both maximum positive and negative lobes of the ESR line ($f_{\mu\text{W}} = 187.9$ GHz and 188.3 GHz respectively) (see Supporting Information for more detail). The results are shown in Fig. 3.6 and in Table 3.2. The first observation resulting from the use of frequency modulation is that the enhancement achieved is higher and the build-up times are faster.

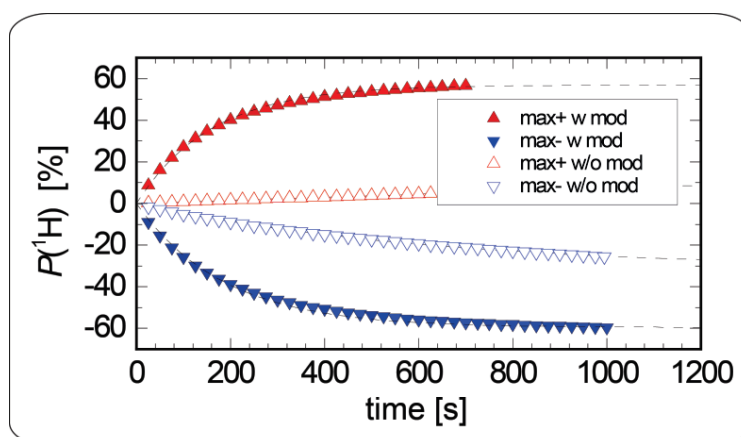


Fig. 3.6: Negative and positive ^1H DNP build-up curves in a DNP sample containing 25 mM of TEMPOL ($\text{H}_2\text{O}/\text{D}_2\text{O}/\text{glycerol-}d_8$ (v/v/v : 10/40/50)) at $T = 1.2$ K. The optimal frequencies $f_{\mu\text{W}} = 187.9$ GHz and 188.3 GHz were set for positive and negative DNP with fixed $\Delta f_{\mu\text{W}} = 100$ MHz, $f_{\text{mod}} = 10$ kHz and $P_{\mu\text{W}} = 87.5$ mW.

The proton polarization $P(^1\text{H})$ and the build-up rates for two other samples with different concentrations of TEMPOL radicals (10 and 50 mM) were also analyzed (Table 3.2) with and without frequency modulation. The results show that the effect of the modulation is less pronounced at a high radical concentration of 50 mM (even if there is still a benefit from using modulation) but that the effect is much more pronounced as the radical concentration is decreased to 10 mM. This could be explained by the fact that at higher radical concentrations, the dipolar couplings between the electrons enable a rapid spectral spin diffusion within the broad inhomogeneous ESR line of TEMPOL. This means that a much larger fraction of the electron spins contribute to the DNP process when the radical concentration approaches 50 mM. At lower concentrations (10 and 25 mM), these dipole-dipole interactions are less important and the Spin Diffusion (SD) process is hampered, leading to a dramatic drop of the enhancement and longer build-up times. The use of frequency modulation can overcome this inconvenience because it can play a similar role as Spin Diffusion [2] by the excitation of more electron packets in the ESR line. Thus, the high 50 mM concentration of radicals is not necessary anymore to achieve high enhancements in short times and the DNP samples can be prepared with half the initial concentration, i.e., only 25 mM TEMPOL.

[PA]/mM	Modulation	$P_+ (^1\text{H})$ [%]	$T_{\text{bup}+} (^1\text{H})$ [s]	$P_- (^1\text{H})$ [%]	$T_{\text{bup}-} (^1\text{H})$ [s]
10	With	14.5*	2600 ± 1000**	-21.1*	2500 ± 1000**
	Without	0.9*	NA***	-1.2*	NA***
25	With	57.3	159 ± 1.8	-60.7	185 ± 2
	Without	9.3*	9000 ± 2000**	-29.5	625 ± 11
50	With	61.3	108 ± 1.6	-63.3	152 ± 2
	Without	21.9	338 ± 7	-43.7	218 ± 4

Table 3.2: Proton polarization $P(^1\text{H})$ and build-up times $T_{\text{bup}}(^1\text{H})$ at $T = 1.2$ K and $B_0 = 6.7$ T for three different radical concentrations (10, 25 and 50 mM TEMPOL) in a mixture of $\text{H}_2\text{O}/\text{D}_2\text{O}/\text{glycerol-}d_8$ (v/v/v : 10/40/50) with and without frequency modulation. (*) The maximum polarization $P(^1\text{H})$ was not reached, and the polarization listed was achieved after 20 min of microwave irradiation. (**) These fits have larger uncertainties because only the first 20 min of the DNP build-up curve were recorded. (***) The estimate of the build-up times are not available due to poor fits.

In Fig. 3.7 (left), the entire DNP microwave spectrum was measured for a sample containing 25 mM TEMPOL, showing the proton polarization $P(^1\text{H})$ achieved at $T = 1.2$ K as a function of the average microwave irradiation $f_{\mu\text{W}}$ with and without frequency modulation. The DNP microwave spectra acquired with and without modulation are contained within the limits of the ESR spectra (the positive and negative lobes achieved with modulation are separated roughly by the ^1H Larmor frequency $f = 285.23$ MHz), suggesting that the Cross Effect or Thermal Mixing are the dominant DNP mechanisms. For the Solid Effect, the "wings" of the DNP spectra would extend well beyond the limits of the ESR line (with modulation, the optima should be separated by twice the ^1H Larmor frequency $2f = 570.46$ MHz). Moreover, the absence of a unique spin temperature for both ^1H and ^{13}C spins under DNP supports the idea that CE is predominant. On the other hand, the DNP microwave spectrum recorded without modulation has a width that has shrunk to ca. 150 MHz which could be explained by the small fraction of the electron spins that contribute to the DNP process, which becomes even smaller when the average microwave frequency is shifted towards the tails of the ESR spectrum. This results in longer DNP build-up times and reduced DNP enhancements.

The Fig. 3.7 (right) represents the proton polarization $P(^1\text{H})$ as a function of the microwave power with and without frequency modulation. With our current setup, the maximum polarization is achieved in this case when frequency modulation is used (a "plateau" can be reached above $P_{\mu\text{W}} = 80$ mW) and therefore there is no need for more microwave power to enhance our DNP signals.

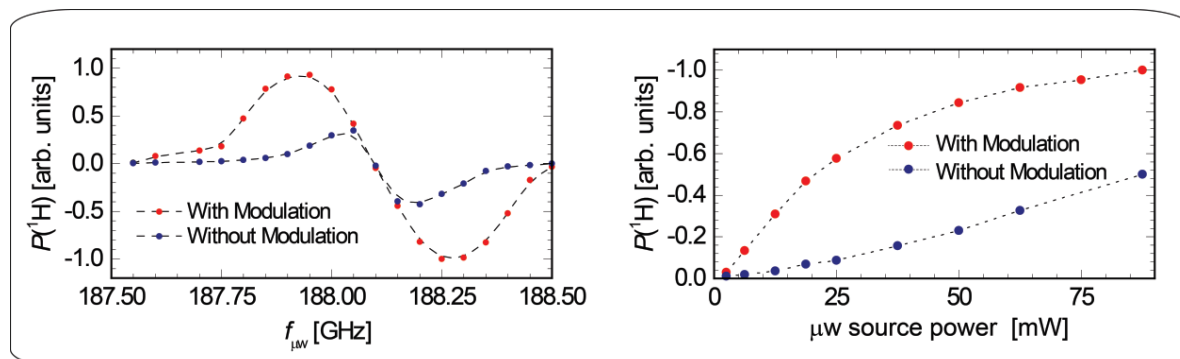


Fig. 3.7: (Left) Proton polarization $P(^1\text{H})$ with and without frequency modulation for a sample containing 25 mM TEMPOL in a mixture of $\text{H}_2\text{O}/\text{D}_2\text{O}/\text{glycerol-}d_8$ (v/v/v : 10/40/50) as a function of the average microwave frequency. (Right) Proton polarization $P(^1\text{H})$ with and without frequency modulation for the same sample as a function of the microwave power.

Finally, frequency modulation was applied to improve Cross-Polarization from ^1H to ^{13}C . One of the advantages of the modulation technique is that it allows, as previously demonstrated, the reduction of the concentration of the radicals by a factor of at least two, which could result in an extension of the nuclear spin-lattice relaxation time both before and after dissolution and therefore improves the preservation of the hyperpolarized magnetization. With such a reduction in radical concentration, we observed that for a sample containing 3 M of $[1-^{13}\text{C}]$ sodium acetate at $T = 1.2$ K, the ^1H line became narrower because of reduction of paramagnetic line broadening (from 35 kHz for 50 mM TEMPOL to 25 kHz for 25 mM TEMPOL). These positive side effects make CP more efficient when frequency modulation is applied. This concept is illustrated in Fig. 3.8, where, even though the proton polarization $P(^1\text{H})$ slightly decreases when the radical concentration is reduced from 50 to 25 mM TEMPOL, the carbon polarization $P(^{13}\text{C})$ after the CP process is increased from $P(^{13}\text{C}) = 42\%$ without modulation to $P(^{13}\text{C}) = 47\%$ with modulation.

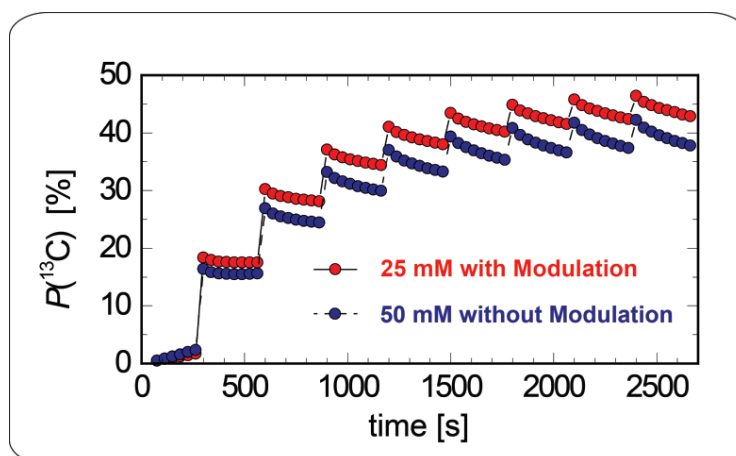


Fig. 3.8: DNP build-up of the ^{13}C polarization measured with multiple CP contacts in a sample containing 3 M $[1-^{13}\text{C}]$ sodium acetate in a mixture of $\text{H}_2\text{O}/\text{D}_2\text{O}/\text{glycerol-}d_8$ (v/v/v : 10/40/50) with 25 mM TEMPOL with microwave frequency modulation (red circles), and with 50 mM TEMPOL without microwave frequency modulation (blue circles).

3.3.3 Conclusions concerning microwave frequency modulation

Different advantages of the use of a frequency-modulated microwave irradiation for dissolution-DNP have been demonstrated: 1) The enhancements achieved for ^1H and ^{13}C are higher at lower temperatures and lower radical concentrations, in comparison with the usual monochromatic irradiation; 2) The DNP build-up times are faster with frequency modulation; 3) The experimental implementation of frequency modulation is straightforward and the parameters can be easily optimized; 4) Cross-Polarization becomes more efficient when radical concentration is reduced; 5) Losses in polarization due to paramagnetic relaxation can therefore be alleviated during the dissolution process.

Since there are no significant inconveniences, frequency modulation has now become a routinely used technique in our laboratory. For future experiments, this method could probably also be applied to other DNP samples containing radicals with narrower ESR line such as Trityl. This would help to reduce the amounts of toxic radicals for *in vivo* imaging for those who still favor the use of direct ^{13}C polarization.

References

1. (a) A. Comment, B. van den Brandt, K. Uffmann, F. Kurdzesau, S. Jannin, J. A. Konter, P. Hautle, W. T. H. Wenckebach, R. Gruetter and J. J. van der Klink, *Design and performance of a DNP prepolarizer coupled to a rodent MRI scanner*, 2007, Concepts in Magnetic Resonance Part B 31B, 255-269. (b) S. Jannin, A. Bornet, R. Melzi and G. Bodenhausen, *High field dynamic nuclear polarization at 6.7 T: Carbon-13 polarization above 70% within 20 min*, 2012, Chem. Phys. Lett. 549, 99-102.
2. Y. Hovav, A. Feintuch, S. Vega and D. Goldfarb, *Dynamic nuclear polarization using frequency modulation at 3.34 T*, 2014, J. Magn. Reson. 238, 94-105.
3. A. Bornet, J. Milani, B. Vuichoud, A. J. Perez Linde, G. Bodenhausen and S. Jannin, *Microwave frequency modulation to enhance Dissolution Dynamic Nuclear Polarization*, 2014, Chem. Phys. Lett. 602, 63-67.
4. J. H. Ardenkjaer-Larsen, S. Macholl and H. Johannesson, *Dynamic nuclear polarization with trityls at 1.2 K*, 2008, Appl. Magn. Reson. 34, 509-522.
5. Mikkel Thaning and Rolf Servin, *Method of dynamic nuclear polarisation (DNP) using a trityl radical and a paramagnetic metal ion*, 2006, Patent CA2628539 A1.
6. I. Dhimitruka, M. Velayutham, A. A. Bobko, V. V. Khramtsov, F. A. Villamena, C. M. Hadad and J. L. Zweier, *Large-scale synthesis of a persistent trityl radical for use in biomedical EPR applications and imaging*, 2007, Bioorg. Med. Chem. Lett. 17, 6801-6805.
7. A. Bornet and S. Jannin, *Optimizing dissolution dynamic nuclear polarization*, 2016, J. Magn. Reson. 264, 13-21.
8. A. Bornet, R. Melzi, S. Jannin and G. Bodenhausen, *Cross Polarization for Dissolution Dynamic Nuclear Polarization Experiments at Readily Accessible Temperatures $1.2 < T < 4.2$ K*, 2012, Appl. Magn. Reson. 43, 107-117.
9. C. Song, K. N. Hu, C. G. Joo, T. M. Swager and R. G. Griffin, *TOTAPOL: A biradical polarizing agent for dynamic nuclear polarization experiments in aqueous media*, 2006, J. Am. Chem. Soc. 128, 11385-11390.
10. C. Sauvee, M. Rosay, G. Casano, F. Aussenac, R. T. Weber, O. Ouari and P. Tordo, *Highly Efficient, Water-Soluble Polarizing Agents for Dynamic Nuclear Polarization at High Frequency*, 2013, Angew. Chem. Int. Edit. 52, 10858-10861.
11. D. J. Kubicki, A. J. Rossini, A. Porea, A. Zagdoun, O. Ouari, P. Tordo, F. Engelke, A. Lesage and L. Emsley, *Amplifying Dynamic Nuclear Polarization of Frozen Solutions by Incorporating Dielectric Particles*, 2014, J. Am. Chem. Soc. 136, 15711-15718.
12. C. D. Jeffries, *Polarization of Nuclei by Resonance Saturation in Paramagnetic Crystals*, 1957, Phys. Rev. 106, 164-165.
13. A. V. Kessenikh, A. A. Manenkov and G. I. Pyatnitskii, *On Explanation of Experimental Data on Dynamic Polarization of Protons in Irradiated Polyethylenes*, 1964, Sov. Phys-Sol. State 6, 641- 643.
14. C. F. Hwang and D. A. Hill, *New Effect in Dynamic Polarization*, 1967, Phys. Rev. Lett. 18, 110-112.
15. D. S. Wollan, *Dynamic Nuclear-Polarization with an Inhomogenesouly Broadened ESR Line. 1. Theory*, 1976, Phys. Rev. B. 13, 3761.3685.
16. B. N. Provotorov, *Magnetic Resonance Saturation in Crystals*, 1962, Sov. Phys. JETP-USSR 14, 1126-1131.
17. M. Goldman and A. Landesman, *Dynamic Polarization by Thermal Mixing between 2 Spin Systems*, 1963, Phys. Rev. 132, 610-620.
18. A. W. Overhauser, *Polarization of Nuclei in Metals*, 1953, Phys. Rev. 91, 476-476.

19. K. R. Thurber, W. M. Yau and R. Tycko, *Low-temperature dynamic nuclear polarization at 9.4 T with a 30 mW microwave source*, 2010, J. Magn. Reson. 204, 303-313.
20. M. C. Cassidy, H. R. Chan, B. D. Ross, P. K. Bhattacharya and C. M. Marcus, *In vivo magnetic resonance imaging of hyperpolarized silicon particles*, 2013, Nat. Nanotechnol. 8, 363-368.

Chapter 4: Improvements in Dissolution Dynamic Nuclear Polarization

4.1 Introduction

In this chapter, several dissolution-DNP experiments that have been performed in the course of this thesis are described in some detail. First of all, a new method to quantify precisely the polarization after dissolution, while obviating the need for the time-consuming determination of the thermal equilibrium, is explained in detail in chapter 4.2 with its advantages and limitations.

In chapter 4.3, we demonstrate that Cross-Polarization [1] can be performed using remote protons present in the "*DNP juice*", allowing the use of fully deuterated molecules that help to extend the lifetimes of hyperpolarization after dissolution.

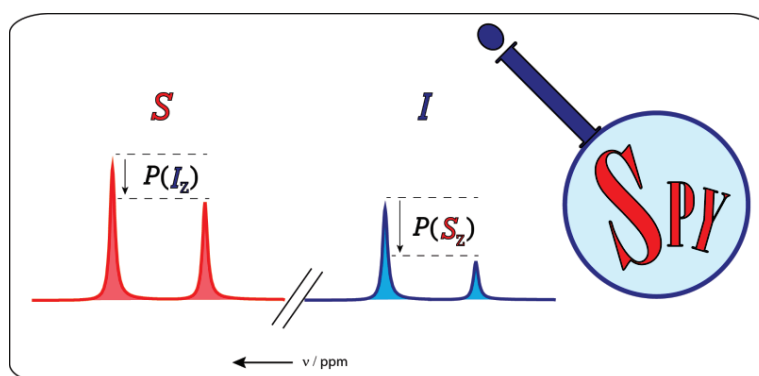
Furthermore, new materials composed of a silica matrix and containing the polarizing agents were synthesized and optimized to produce pure hyperpolarized solutions that are free of any kind of contaminants after dissolution. New applications using these mesoporous matrices are described in chapter 4.4.

Finally, in chapter 4.5, the synthesis of a polymer-based radical is described that allows us to hyperpolarize water efficiently. This can produce pure hyperpolarized water after dissolution, with interesting applications to proteins.

4.2 Spin Polarimetry Magnetic Resonance (SPY-MR)

To obviate the need for time-consuming measurements to determine the thermal equilibrium (TE) polarization of diluted samples, we proposed a new method dubbed *Spin Polarimetry Magnetic Resonance (SPY-MR)* to measure the spin polarizations "on the fly" for a large range of molecules after dissolution-DNP. This technique mainly relies on the asymmetries observed in the multiplets of hyperpolarized molecules, and permits one to calculate the polarization of the system in a single scan acquired just after the d-DNP process.

The following chapter results from a publication entitled "*Measuring Absolute Spin Polarization in Dissolution-DNP by Spin Polarimetry Magnetic Resonance (SPY-MR)*". [2]



4.2.1 Why use SPY-MR

A practical challenge of d-DNP is the accurate determination of the nuclear spin polarization $P(^{13}\text{C})$ or, equivalently, its spin temperature $T(^{13}\text{C})$. This is usually determined by comparing the signals obtained with and without hyperpolarization at low temperatures ($T = 1.2 - 4.2$ K) prior to dissolution. In addition, other measurements to determine the polarization in liquid phase are carried out at room temperature immediately after dissolution and at thermal equilibrium (TE) when the system has completely relaxed. However, this last measurement of the thermal equilibrium is most of the time difficult if not impossible. This is usually the case when the hyperpolarized solution is injected into a living organism for real-time metabolic imaging [3, 4] or when the hyperpolarized substance is too strongly diluted or has undergone irreversible chemical reactions.

Recently, it was demonstrated that after hyperpolarization by d-DNP in the liquid state, a strong polarization of a nuclear spin, denoted $^{13}\text{C}'$ or I for "investigated" spin, leads to an asymmetry A_S of the multiplet of a neighboring spin. [5, 6, 7, 8, 9] With some restrictions and some assumptions discussed below in further detail, this feature can be used for a broad range of molecules and provides an elegant way to measure the spin polarization of a system "on the fly" while avoiding the need of time-consuming experiments to determine the thermal equilibrium polarization. It is worth mentioning that these observations are reminiscent of earlier work performed in solids enhanced by DNP at low temperatures. [10, 11, 12, 13, 14, 15] Moreover, a recent study by Donovan *et al.* [16] has shown that rapid heteronuclear cross-relaxation processes can occur in specific molecules, leading to a fast transfer of magnetization and that limits the usefulness of SPY-MR under these conditions.

We decided to propose a simple and accurate theoretical description of the measurement of the polarization of a system dubbed *Spin Polarimetry Magnetic Resonance (SPY-MR)*. We show that this approach is reliable, but relies on several assumptions and therefore has some limitations. The first assumption is that DNP must lead to a uniform spin temperature in the ^{13}C nuclear spin reservoir in the solid state at low temperature, which is usually the case provided Spin Diffusion (SD) is sufficiently effective. Secondly, the cross-relaxation and cross-correlation rates that describe the coupling between Zeeman polarization and two-spin order should be negligible after dissolution. Finally, the effects of second-order couplings on the intensities of the multiplets, usually known as the "roof effect" should be taken into account properly.

4.2.2 Traditional determination of the polarization

In our DNP setup at the EPFL at $B_0 = 6.7$ T and $T = 1.2 - 4.2$ K, the ^{13}C DNP build-up is measured by applying small nutation angle *rf* pulses ($\beta^{small} = 5^\circ$) at regular time intervals ($\Delta t = 5$ s) to limit the perturbations. To acquire a thermal equilibrium signal at low temperature prior to DNP, the sample must be left for a long interval $t \gg 5T_1(^{13}\text{C})$ in order to let the polarization fully relax to its Boltzmann equilibrium. The resulting signal integral, denoted $I_{TE}(^{13}\text{C})$, can in principle be measured by applying a single *rf* pulse with $\beta = 90^\circ$, but this can lead to errors if the nutation angle β^{small} is not properly calibrated. We therefore prefer to apply the same small nutation angle $\beta^{small} = 5^\circ$ that is used to monitor the DNP build-up, but adding N signals acquired at intervals $\Delta t \ll 5T_1(^{13}\text{C})$. The resulting signal needs to be normalized by dividing by a factor δ to account for the number of scans N and for the gradual depletion of the polarization caused by the train of N pulses:

$$\delta = \sum_{i=1}^N (\cos \beta^{small})^{i-1} \quad (4.1)$$

As described in the previous chapters, the thermal equilibrium ^{13}C polarization is determined by Boltzmann's law:

$$P_{TE}(^{13}\text{C}) = \tanh\left(\frac{\hbar\omega}{2k_B T}\right) \quad (4.2)$$

After switching the microwave irradiation on so that the DNP builds up, the hyperpolarized signal integral $I_{DNP}(^{13}\text{C})$ can be measured using a single pulse with a small nutation angle β^{small} . The enhancement can be calculated with the following equation (which involves the factor δ of Eq. 4.1):

$$\epsilon_{DNP} = \frac{P_{DNP}(^{13}\text{C})}{P_{TE}(^{13}\text{C})} = \delta \cdot \frac{I_{DNP}(^{13}\text{C})}{I_{TE}(^{13}\text{C})} \quad (4.3)$$

After the dissolution process, the polarization levels are measured in a similar way by comparing the hyperpolarized ^{13}C polarization $P_{DNP}(^{13}\text{C})$ with the thermal equilibrium $P_{TE}(^{13}\text{C})$. The acquisition of the TE signal must be done after a prolonged delay of at least $t = 16T_1(^{13}\text{C})$ after dissolution, which allows one to approach the thermal equilibrium within 1% if one starts with an enhancement $\epsilon = 10^5$ since $\exp[-t/T_1(^{13}\text{C})] = e^{-16} = 1.1 \cdot 10^{-7}$. The TE signal can be then measured by applying *rf* pulses $\beta = 90^\circ$ spaced by $5T_1$ (typically every 5 min for ^{13}C nuclei with relatively long T_1).

In order to achieve a sufficient signal-to-noise ratio (*SNR*) at 300 MHz without a cryoprobe, at least 128 scans are mandatory for molecules that are isotopically enriched in ^{13}C with concentrations in the millimolar range. These measurements require about 10 hours, so that the determination of thermal equilibrium $P_{\text{TE}}(^{13}\text{C})$ can require more time than the dissolution DNP experiment itself. For molecules in natural abundance, it is not possible to measure a proper TE signal after dissolution with our equipment.

4.2.3 Asymmetry of doublets for non-equilibrium populations

Energy levels and polarization in a coupled two-spin system

The energy-level diagram of a two-spin system in isotropic solution is shown in Fig 4.1 with a scalar coupling constant $J_{IS} > 0$ and a difference in chemical shifts $\Delta\nu = \nu_I - \nu_S$, where $\nu_I = -\gamma_I(1 - \sigma_I)B_0$ and $\nu_S = -\gamma_S(1 - \sigma_S)B_0$ are the Larmor frequencies of spins *I* and *S*. In this usual notation, both ν_I and ν_S have opposite signs with respect to γ_I and γ_S , so that both frequencies are negative for a pair of ^{13}C nuclei, as in singly labeled sodium pyruvate- d_3 [$\text{CD}_3\text{CO}^{13}\text{COO}^-\text{Na}^+$] and in doubly labeled sodium acetate- d_3 [$^{13}\text{CD}_3^{13}\text{COO}^-\text{Na}^+$].

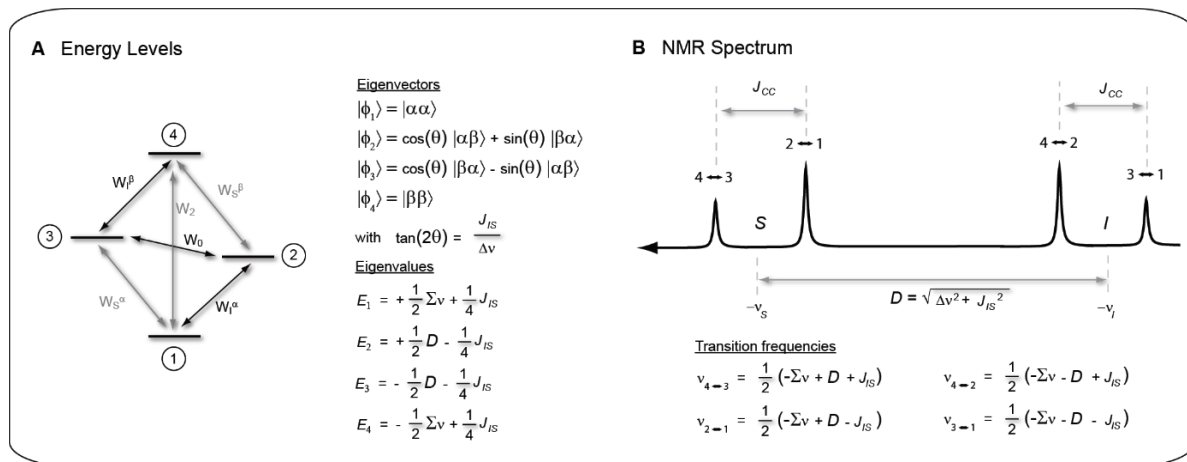


Figure 4.1: (A) Energy-level diagram of a strongly coupled homonuclear two-spin system with γ_I and $\gamma_S > 0$ and $J_{IS} > 0$. (B) Its corresponding NMR spectrum at thermal equilibrium.

4.2.4 Eigenstates of a coupled two-spin system

Some theoretical explanations are necessary to justify the use of the SPY-MR technique instead of the traditional measurement of the polarization. The equations are described in the following subchapters and some examples involving sodium acetate and sodium pyruvate are shown to demonstrate the efficiency of the novel method. Moreover, a few limitations of SPY-MR compared to the conventional measurement of the thermal equilibrium are also discussed, which restrict the use of SPY-MR in unfavorable circumstances.

First of all, the spin Hamiltonian in the rotating frame for a pair of *J*-coupled spins with $I = S = \frac{1}{2}$ is:

$$\mathcal{H} = \nu_I I_z + \nu_S S_z + J_{IS} \mathbf{I} \mathbf{S} \quad (4.4)$$

The matrix representation of this Hamiltonian in the Zeeman product basis $[\alpha\alpha], [\alpha\beta], [\beta\alpha], [\beta\beta]$ is:

$$\mathcal{H} = \frac{1}{2} \begin{pmatrix} \Sigma\nu + \frac{1}{2}J_{IS} & 0 & 0 & 0 \\ 0 & \Delta\nu - \frac{1}{2}J_{IS} & J_{IS} & 0 \\ 0 & J_{IS} & -\Delta\nu - \frac{1}{2}J_{IS} & 0 \\ 0 & 0 & 0 & -\Sigma\nu + \frac{1}{2}J_{IS} \end{pmatrix} \quad (4.5)$$

where $\Sigma\nu = \nu_I + \nu_S$ and $\Delta\nu = \nu_I - \nu_S$ represent the sum and the difference of the Larmor frequencies of I and S in units of Hz. Note that in our example $\Sigma\nu < 0$ since γ_I and $\gamma_S > 0$. The eigenstates of the strongly coupled "AB" two-spin system can be determined by diagonalizing the matrix:

$$\begin{aligned} [\phi_1] &= \begin{pmatrix} 1 \\ 0 \\ 0 \\ 0 \end{pmatrix} \\ [\phi_2] &= \begin{pmatrix} 0 \\ \cos \theta \\ \sin \theta \\ 0 \end{pmatrix} \\ [\phi_3] &= \begin{pmatrix} 0 \\ -\sin \theta \\ \cos \theta \\ 0 \end{pmatrix} \\ [\phi_4] &= \begin{pmatrix} 0 \\ 0 \\ 0 \\ 1 \end{pmatrix} \end{aligned} \quad (4.6)$$

The angle θ expresses the strength of the coupling and leads to the "roof effect":

$$\tan 2\theta = \frac{J_{IS}}{\Delta\nu} \quad (4.7)$$

In general, heteronuclear systems are always weakly coupled (i.e., $\sin 2\theta \approx 0$) in the laboratory frame since $J_{IS} \ll \Delta\nu$. In homonuclear systems where the gyromagnetic ratios are equal $\gamma_I = \gamma_S$, the sign of θ depends on the relative signs of J_{IS} and of $\Delta\nu$.

The associated eigenvalues are:

$$\begin{aligned}
 E_1 &= +\frac{1}{2}\Sigma\nu + \frac{1}{4}J_{IS} \\
 E_2 &= +\frac{1}{2}D - \frac{1}{4}J_{IS} \\
 E_3 &= -\frac{1}{2}D - \frac{1}{4}J_{IS} \\
 E_4 &= -\frac{1}{2}\Sigma\nu + \frac{1}{4}J_{IS}
 \end{aligned} \tag{4.8}$$

where $D = \sqrt{\Delta\nu^2 + J_{IS}^2}$

4.2.5 Transitions frequencies and amplitudes

The transition frequencies of the coupled two-spin system can be determined from the differences between the eigenvalues:

$$\begin{aligned}
 \nu_{4\leftrightarrow 3} &= \frac{1}{2}(-\Sigma\nu + D + J_{IS}) \\
 \nu_{2\leftrightarrow 1} &= \frac{1}{2}(-\Sigma\nu + D - J_{IS}) \\
 \nu_{4\leftrightarrow 2} &= \frac{1}{2}(-\Sigma\nu - D + J_{IS}) \\
 \nu_{3\leftrightarrow 1} &= \frac{1}{2}(-\Sigma\nu - D - J_{IS})
 \end{aligned} \tag{4.9}$$

keeping in mind that $-\Sigma\nu > 0$ in our case of a two-spin system comprising two ^{13}C nuclei. The intensities of the four lines depend on the strength of the coupling and on the populations of the four levels just before the *rf* pulse. If the high-temperature approximation is fulfilled for the nuclear Zeeman interaction, i.e., if $kT \gg \Delta E = \hbar\gamma B_0$, the density operator at thermal equilibrium can be written:

$$\rho_{TE} \propto I_z + S_z \tag{4.10}$$

More specifically, for a two-spin system comprising two ^{13}C nuclei at $T = 300$ K and $B_0 = 7.05$ T:

$$\rho_{TE} = \frac{1}{2} \{ 6.03 \times 10^{-6} \cdot I_z + 6.03 \times 10^{-6} \cdot S_z + 36.36 \times 10^{-12} \cdot 2I_z S_z + 0.5 \cdot \hat{E} \} \tag{4.11}$$

In thermal equilibrium, where the high temperature approximation is fulfilled and where both spins I and S have a common spin temperature, the intensities of the four lines give rise to the so-called "roof effect" (see Fig. 4.1 B), where the inner lines have intensities $a_{4\leftrightarrow 2} = a_{2\leftrightarrow 1}$ that are proportional to $(1 + \sin 2\theta)$, while the intensities of the outer lines $a_{3\leftrightarrow 1} = a_{4\leftrightarrow 3}$ are proportional to $(1 - \sin 2\theta)$.

However, if the four populations are distributed in an arbitrary manner (e.g., the case for hyperpolarized systems where the high temperature approximation is violated), a more general density operator needs to be defined:

$$\rho = n_1|\phi_1\rangle\langle\phi_1| + n_2|\phi_2\rangle\langle\phi_2| + n_3|\phi_3\rangle\langle\phi_3| + n_4|\phi_4\rangle\langle\phi_4| \quad (4.12)$$

where n_1 , n_2 , n_3 , and n_4 represent the populations associated with the four eigenstates $|\phi_1\rangle$, $|\phi_2\rangle$, $|\phi_3\rangle$, and $|\phi_4\rangle$.

4.2.6 Signal amplitudes as a function of the populations

When a pulse with an arbitrary nutation angle β is applied to the system, the signal amplitudes can be calculated in the manner described by Schäublin *et al.* [17]:

$$\begin{aligned} a_{4\leftrightarrow 3} &= -\frac{1}{2}\sin\beta\left(\sin^2\frac{\beta}{2}(1-\sin 2\theta)(n_3-n_1) - \sin^2\frac{\beta}{2}\cos^2 2\theta(n_3-n_2) \right. \\ &\quad \left. + \cos^2\frac{\beta}{2}(1-\sin 2\theta)(n_4-n_3)\right) \\ a_{2\leftrightarrow 1} &= -\frac{1}{2}\sin\beta\left(\cos^2\frac{\beta}{2}(1+\sin 2\theta)(n_2-n_1) - \sin^2\frac{\beta}{2}\cos^2 2\theta(n_3-n_2) \right. \\ &\quad \left. + \sin^2\frac{\beta}{2}(1+\sin 2\theta)(n_4-n_2)\right) \\ a_{4\leftrightarrow 2} &= -\frac{1}{2}\sin\beta\left(\sin^2\frac{\beta}{2}(1+\sin 2\theta)(n_2-n_1) + \sin^2\frac{\beta}{2}\cos^2 2\theta(n_3-n_2) \right. \\ &\quad \left. + \cos^2\frac{\beta}{2}(1+\sin 2\theta)(n_4-n_2)\right) \\ a_{3\leftrightarrow 1} &= -\frac{1}{2}\sin\beta\left(\cos^2\frac{\beta}{2}(1-\sin 2\theta)(n_3-n_1) + \sin^2\frac{\beta}{2}\cos^2 2\theta(n_3-n_2) \right. \\ &\quad \left. + \sin^2\frac{\beta}{2}(1-\sin 2\theta)(n_4-n_3)\right) \end{aligned} \quad (4.13)$$

The two Zeeman polarizations $P(I_z)$ and $P(S_z)$ and the longitudinal two-spin order term $P(2I_zS_z)$ can be defined as a function of the four populations n_1 , n_2 , n_3 , and n_4 :

$$\begin{aligned}
 P(I_z) &= (n_1 - n_4) + (n_2 - n_3) \cos 2\theta \\
 P(S_z) &= (n_1 - n_4) + (n_3 - n_2) \cos 2\theta \\
 P(2I_zS_z) &= (n_1 - n_2) - (n_3 - n_4)
 \end{aligned}
 \tag{4.14}$$

By rewriting these equations, the four populations n_1 , n_2 , n_3 , and n_4 can also be expressed as linear combinations of the two Zeeman polarizations and the longitudinal two-spin order term:

$$\begin{aligned}
 n_1 &= \frac{1}{4}(1 + P(I_z) + P(S_z) + P(2I_zS_z)) \\
 n_2 &= \frac{1}{4}\left(1 - P(2I_zS_z) + (P(I_z) - P(S_z))\frac{1}{\cos 2\theta}\right) \\
 n_3 &= \frac{1}{4}\left(1 - P(2I_zS_z) + (P(S_z) - P(I_z))\frac{1}{\cos 2\theta}\right) \\
 n_4 &= \frac{1}{4}(1 - P(I_z) - P(S_z) + P(2I_zS_z))
 \end{aligned}
 \tag{4.15}$$

Finally, the amplitudes of the four signals can be described in Fig. 4.1 as a function of the two Zeeman polarizations and the longitudinal two-spin order term:

$$\begin{aligned}
a_{4\leftrightarrow 3} &= \frac{1}{8} \sin \beta (1 - \sin 2\theta) \left(2 \frac{P(S_z) \cos \theta - P(I_z) \sin \theta}{\cos \theta - \sin \theta} \right. \\
&\quad \left. - \cos \beta (2P(2I_z S_z) + (P(S_z) - P(I_z)) \tan 2\theta) \right) \\
a_{2\leftrightarrow 1} &= \frac{1}{8} \sin \beta (1 + \sin 2\theta) \left(2 \frac{P(S_z) \cos \theta + P(I_z) \sin \theta}{\cos \theta + \sin \theta} \right. \\
&\quad \left. + \cos \beta (2P(2I_z S_z) + (P(S_z) - P(I_z)) \tan 2\theta) \right) \\
a_{4\leftrightarrow 2} &= \frac{1}{8} \sin \beta (1 + \sin 2\theta) \left(2 \frac{P(I_z) \cos \theta + P(S_z) \sin \theta}{\cos \theta + \sin \theta} \right. \\
&\quad \left. - \cos \beta (2P(2I_z S_z) + (P(S_z) - P(I_z)) \tan 2\theta) \right) \\
a_{3\leftrightarrow 1} &= \frac{1}{8} \sin \beta (1 - \sin 2\theta) \left(2 \frac{P(I_z) \cos \theta - P(S_z) \sin \theta}{\cos \theta - \sin \theta} \right. \\
&\quad \left. + \cos \beta (2P(2I_z S_z) + (P(S_z) - P(I_z)) \tan 2\theta) \right)
\end{aligned} \tag{4.16}$$

In conclusion, the signal amplitudes depend on different factors: the nutation angle β , the parameter θ that describes the strength of the coupling between the two nuclear spins I and S , the two Zeeman polarizations $P(I_z)$, $P(S_z)$, and the longitudinal two-spin order term $P(2I_z S_z)$.

4.2.7 Asymmetry of doublets

Having defined the polarizations, we can now focus on the asymmetries of the peaks observed after dissolution. From a practical point of view, if the violation of the high temperature approximation is significant (if $P(^{13}\text{C}^I) > 5\%$), one can experimentally observe an asymmetry A_S of the doublet of a spy nucleus S that is coupled to the spin I under investigation. This asymmetry can differ dramatically from the "roof effect" that is observed at thermal equilibrium. This asymmetry can be observed in weakly coupled systems ($\theta = 0$), provided that a pulse with a nutation angle $\beta \neq 90^\circ$ is used.

By inspection of Fig. 4.1, the normalized asymmetry A_S can easily be defined by differences of the signal integrals:

$$A_S = \frac{a_{2\leftrightarrow 1} - a_{4\leftrightarrow 3}}{a_{2\leftrightarrow 1} + a_{4\leftrightarrow 3}} \tag{4.17}$$

By combining Eq. 4.16 and Eq. 4.17, the normalized asymmetry A_S can be expressed as follows:

$$A_S = \frac{P(2I_Z S_Z) + \sin 2\theta (a P(S_Z) + b P(I_Z))}{P(S_Z)(c + a) - P(I_Z)(c - b) + P(2I_Z S_Z) \sin 2\theta} \quad (4.18)$$

where $a = (\cos 2\theta + \cos \beta)/(2 \cos \beta \cos 2\theta)$, $b = (\cos 2\theta - \cos \beta)/(2 \cos \beta \cos 2\theta)$, and $c = \cos 2\theta ((1 - \cos \beta)/(2 \cos \beta))$.

Unfortunately, the asymmetry A_S results from a complex mixture of numerous terms. Nevertheless, as pointed out by Lau *et al.* [8], the measured asymmetry "*correlates strongly*" with the polarization $P(I_Z)$. Indeed, some terms in this complicated equation can be simplified.

To start, two simple limits may first be considered: (1) the high-temperature approximation where $P(2I_Z S_Z) = 0$ and $P(I_Z) = P(S_Z)$; and (2) the limit for a weak coupling where $\theta \rightarrow 0$. These approximations lead to greatly simplified equations:

$$\lim_{\Delta E/kT \rightarrow 0} A_S^H = \sin 2\theta \quad (4.19)$$

$$\lim_{\theta \rightarrow 0} A_S = \cos \beta \cdot \frac{P(2I_Z S_Z)}{P(S_Z)} \quad (4.20)$$

Note that θ is negative if $J_{IS} < 0$ or $\Delta v < 0$.

In the following, we will show that with some assumptions related to the DNP process and to nuclear spin-lattice relaxation after dissolution, the asymmetry A_S not only "*correlates strongly*" with the polarization, but in fact "*properly reflects*" the absolute polarization $P(I_Z)$.

4.2.8 Low temperature DNP and uniform spin temperature

As discussed in the previous chapters of this thesis, the polarization in our laboratory generally builds up at very low temperatures $T = 1.2 - 4.2$ K in a moderate magnetic field $B_0 = 6.7$ T. In this particular case, the time constant of the DNP build-up T_{bup} can range from a few minutes to even hours, which is much longer than the time required for Spin Diffusion (SD) to impose a uniform nuclear spin polarization in the DNP sample. Unless the radicals and/or analytes have very low concentrations (i.e., less than 5 mM) or have an unusual inhomogeneous distribution (in a crystalline sample for example), the assumption that the nuclear spin polarization and temperature are uniform is fully justified.

4.2.9 The initial DNP polarizations

If a uniform spin temperature T_{spin} is established by DNP in the solid state, the two spins I and S have the same spin polarizations $P(I_z) = P(S_z) = P_0$, so that we can assume that the distribution of the populations at time $t = 0$ immediately after dissolution can be described by a Boltzmann distribution:

$$\begin{aligned} n_1^{DNP} &= \frac{e^{+\hbar\omega/kT}}{Z} \\ n_2^{DNP} = n_3^{DNP} &= \frac{1}{Z} \\ n_4^{DNP} &= \frac{e^{-\hbar\omega/kT}}{Z} \end{aligned} \tag{4.21}$$

where $Z = e^{-\hbar\omega/kT} + 2 + e^{+\hbar\omega/kT} = \left(e^{-\hbar\omega/2kT} + e^{+\hbar\omega/2kT} \right)^2$

The nuclear spin polarizations of I and S generated by DNP were defined in the first chapters of this thesis:

$$\begin{aligned} P(I_z)_0 = P(S_z)_0 &= \frac{e^{+\hbar\omega/kT} - e^{-\hbar\omega/kT}}{\left(e^{+\hbar\omega/2kT} + e^{-\hbar\omega/2kT} \right)^2} \\ &= \frac{\left(e^{+\hbar\omega/2kT} + e^{-\hbar\omega/2kT} \right) \left(e^{+\hbar\omega/2kT} - e^{-\hbar\omega/2kT} \right)}{\left(e^{+\hbar\omega/2kT} + e^{-\hbar\omega/2kT} \right)^2} \\ &= \frac{\left(e^{+\hbar\omega/2kT} - e^{-\hbar\omega/2kT} \right)}{\left(e^{+\hbar\omega/2kT} + e^{-\hbar\omega/2kT} \right)} = \tanh\left(\hbar\omega/2kT\right) = P_0 \end{aligned} \tag{4.22}$$

$$\begin{aligned} P(2I_z S_z)_0 &= \frac{e^{+\hbar\omega/kT} - 2 + e^{-\hbar\omega/kT}}{\left(e^{+\hbar\omega/2kT} + e^{-\hbar\omega/2kT} \right)^2} \\ &= \frac{\left(e^{+\hbar\omega/kT} - e^{-\hbar\omega/kT} \right)^2}{\left(e^{+\hbar\omega/2kT} + e^{-\hbar\omega/2kT} \right)^2} = \tanh^2\left(\hbar\omega/2kT\right) = P_0^2 \end{aligned} \tag{4.23}$$

4.2.10 Initial asymmetry and polarization immediately after dissolution

If we make the assumption that the polarization achieved by DNP can be entirely preserved during the dissolution process, the transfer and the injection into the sample tube that is waiting in the NMR or MRI system, we can readily express the initial asymmetry $A_{S,0}$:

$$A_{S,0} = P_0 \cos \beta \frac{1 + \sin 2\theta / (P_0 \cos \beta)}{1 + \sin 2\theta \cdot P_0 \cos \beta} \quad (4.24)$$

which can be reorganized as follows:

$$P_0 = \frac{A_{S,0}}{\cos \beta} \cdot \frac{1 - \sin 2\theta / A_{S,0}}{1 - \sin 2\theta \cdot A_{S,0}} \quad (4.25)$$

Thus, for an ideal system where relaxation mechanisms can be neglected, the polarization of the nuclear spins I and S can be determined from the initial asymmetry provided the nutation angle β and the angle θ that describes the strength and sign of the coupling are known.

4.2.11 Relaxation after dissolution

Unfortunately, the dissolution process and the transfer from the polarizer to the NMR or MRI magnet may take several seconds (typically from 5 to 10 s). In this relatively short interval, the sample may be exposed to a time-dependent magnetic field $B_0(t)$, although its fluctuations may be smoothed out by using our "magnetic tunnel". [18] During the transfer, the decay and partial interconversion of the two-spin order and the Zeeman terms are determined by coupled relaxation [19]:

$$\frac{d}{dt} \begin{bmatrix} \Delta\langle I_z \rangle \\ \Delta\langle S_z \rangle \\ \Delta\langle 2I_z S_z \rangle \end{bmatrix} = - \begin{bmatrix} \rho_I & \sigma_{SI} & \delta_{ISI} \\ \sigma_{IS} & \rho_S & \delta_{ISS} \\ \delta_{ISI} & \delta_{ISS} & \rho_{IS} \end{bmatrix} \cdot \begin{bmatrix} \Delta\langle I_z \rangle \\ \Delta\langle S_z \rangle \\ \Delta\langle 2I_z S_z \rangle \end{bmatrix} \quad (4.26)$$

where $\Delta\langle I_z \rangle$, $\Delta\langle S_z \rangle$, and $\Delta\langle 2I_z S_z \rangle$ represent deviations from thermal equilibrium, ρ_I , ρ_S , and ρ_{IS} represent the decay rates of the two Zeeman order terms (with $\rho_I = 1/T_1^{(I)}$ and $\rho_S = 1/T_1^{(S)}$) and of the longitudinal two-spin order term, while $\sigma_{SI} = \sigma_{IS}$ represent the coupling between the Zeeman terms (the cross-relaxation rates that can give rise to Overhauser effects), and δ_{ISI} and δ_{ISS} represent the "cross-correlation rates" that couple the Zeeman terms with the longitudinal two-spin order term. These rates can be expressed as follows:

$$\begin{aligned}
\rho_I &= W_2 + W_0 + W_I^\alpha + W_I^\beta \\
\rho_S &= W_2 + W_0 + W_S^\alpha + W_S^\beta \\
\rho_{IS} &= W_I^\alpha + W_I^\beta + W_S^\alpha + W_S^\beta \\
\sigma_{IS} &= \sigma_{SI} = W_2 - W_0 \\
\delta_{ISI} &= W_I^\alpha - W_I^\beta \\
\delta_{ISS} &= W_S^\alpha - W_S^\beta
\end{aligned} \tag{4.27}$$

In general, relaxation pathways due to cross-relaxation and cross-correlation will tend to drive the asymmetry A_S towards values that may significantly differ from $P(I_z)$. If they could be neglected, we would end up with a diagonal relaxation matrix:

$$\frac{d}{dt} \begin{bmatrix} \Delta\langle I_z \rangle \\ \Delta\langle S_z \rangle \\ \Delta\langle 2I_z S_z \rangle \end{bmatrix} \cong - \begin{bmatrix} \rho_I & 0 & 0 \\ 0 & \rho_S & 0 \\ 0 & 0 & \rho_I + \rho_S \end{bmatrix} \cdot \begin{bmatrix} \Delta\langle I_z \rangle \\ \Delta\langle S_z \rangle \\ \Delta\langle 2I_z S_z \rangle \end{bmatrix} \tag{4.28}$$

For the approximation of a diagonal matrix to hold, the following conditions must be fulfilled:

$$\begin{aligned}
W_I^\alpha &\approx W_I^\beta \\
W_S^\alpha &\approx W_S^\beta \\
W_2, W_0 &\ll W_I^\alpha, W_S^\alpha
\end{aligned} \tag{4.29}$$

In other words, the single-quantum relaxation rates across parallel transitions must be equal, and both double- and zero-quantum relaxation rates must be negligible compared to the single-quantum relaxation rates. In an ideal case where all these conditions are fulfilled, the asymmetry A_S perfectly reflects the polarization $P(I_z)$ even after dissolution, transfer, injection, and partial relaxation in the NMR or MRI magnet. These conditions hold for ^{13}C spin pairs, especially when relaxation is driven by intramolecular dipole-dipole interactions with nearby protons, or by external fluctuating fields which are usually due to the solvent, radicals, dissolved triplet oxygen, or paramagnetic impurities.

In order to justify these assumptions, the relaxation matrix for the pair of ^{13}C spins of the carboxyl and carbonyl nuclei in pyruvate was determined as follows: (i) the crystal structure of sodium pyruvate was obtained from the Cambridge Structural Database, (ii) the CSA tensor was predicted with CASTEP [20], and (iii) the relaxation was calculated using the SpinDynamica [21] code for Mathematica (see Supporting Information). This allowed us to determine the following elements of the relaxation matrix:

$$\begin{bmatrix} \rho_I & \sigma_{SI} & \delta_{ISI} \\ \sigma_{IS} & \rho_S & \delta_{ISS} \\ \delta_{ISI} & \delta_{ISS} & \rho_{IS} \end{bmatrix} \cong -10^{-4} \begin{bmatrix} \mathbf{146} & 2.05 & -1.10 \\ 2.05 & \mathbf{211} & 0.44 \\ -1.10 & 0.44 & \mathbf{352} \end{bmatrix} \tag{4.30}$$

The first observation is that the double- and zero-quantum relaxation rates are significantly lower than the single-quantum rates ρ_I and ρ_S , typically by nearly two orders of magnitude. As a result, the relaxation matrix is approximately diagonal, and $\rho_{IS} \approx \rho_I + \rho_S$, so that $\Delta\langle 2I_z S_z \rangle$ decays almost twice as fast as $\Delta\langle I_z \rangle$ and $\Delta\langle S_z \rangle$. Therefore, the SPY-MR method can safely be applied to the ^{13}C spin pair in pyruvate. We shall assume this is also valid for the ^{13}C spin pairs in sodium acetate.

4.2.12 Asymmetry after dissolution

In order to determine the polarization of a system from the asymmetry after the dissolution process, using the assumptions made above, one can rearrange the equations with $\rho_{IS} = \rho_I + \rho_S$, so that after an arbitrary time t , the two-spin order polarization is represented by:

$$P(2I_z S_z) = P_0^2 \cdot e^{-t(\rho_I + \rho_S)} = (P_0 \cdot e^{-t \cdot \rho_I})(P_0 \cdot e^{-t \cdot \rho_S}) = P(I_z) \cdot P(S_z) \quad (4.31)$$

By inserting this expression into Eq. 4.24, the asymmetry can be rewritten:

$$A_S = \frac{P(I_z) \cdot P(S_z) + \sin 2\theta (a P(S_z) + b P(I_z))}{P(S_z)(c + a) - P(I_z)(c - b) + P(I_z) \cdot P(S_z) \sin 2\theta} \quad (4.32)$$

Again two limiting cases can be considered:

$$\lim_{\Delta E/kT \rightarrow 0} A_S = \sin 2\theta \quad (4.33)$$

$$\lim_{\theta \rightarrow 0} A_S = \cos \beta \cdot P(I_z) \quad (4.34)$$

The asymmetry A_S obtained from Eq. 4.32 can be further simplified without loss of generality (with an error below 2%) by assuming that:

- (1) The two nuclear spin polarizations $P(I_z)$ and $P(S_z)$ lie in the ranges $1\% \leq |P(I_z)| \leq 50\%$ and $1\% \leq |P(S_z)| \leq 50\%$. In practice, the polarization achieved after dissolution lies in the range between 10% and 20% in most published studies, which is well above the lower limit of 1%. On the other hand, the upper limit $|P(S_z)| = 50\%$ corresponds to the highest ^{13}C polarization that has been achieved so far in d-DNP.
- (2) The strength of the coupling between the two nuclear spins is relatively weak with $-1^\circ \leq \theta \leq 1^\circ$, or equivalently $-0.035 \leq \sin 2\theta \leq 0.035$, which is valid for most ^{13}C spin pairs in high fields.
- (3) The nutation angle β of the pulse that is applied to record the hyperpolarized signal is between $-5^\circ \leq \beta \leq 5^\circ$, as typically used for the signal acquisition of our hyperpolarized metabolites.

When these conditions are fulfilled, the asymmetry can be approximated by a simple relation:

$$A_S \approx P(I_z) + \sin 2\theta \quad (4.35)$$

So that the absolute nuclear spin polarization $P(I_z)$ of the spin I under investigation is:

$$P(I_z) \approx A_S - \sin 2\theta \quad (4.36)$$

4.2.13 Asymmetry in arbitrary two-spin systems

Now that we have determined the polarization $P(I_z)$ of a spin I in a coupled two-spin system with $\gamma_I > 0$, $\gamma_S > 0$, $J_{IS} > 0$, and $|v_S| > |v_I|$ from the asymmetry A_S , we can extend the definition of the asymmetry A_S to all possible cases (there are no less than $2^4 = 16$ different possibilities!) where γ_I , γ_S , and J_{IS} may have arbitrary signs, while one may have $|v_S| < |v_I|$, and the polarization $P(I_z)$ induced by DNP may be either positive or negative. To generalize the formula, we can define the asymmetry A_S as a function of the intensities of the high- and low-frequency signals (a_{HF} and a_{LF}) (see Fig. 4.2) of the spy spin S , regardless of its position (i.e., regardless of whether the chemical shift of spin S is shielded or de-shielded) with respect to the investigated spin I):

$$A_S = \frac{a_{LF} - a_{HF}}{a_{LF} + a_{HF}} \quad (4.37)$$

The asymmetry can be approximated in the same manner to obtain a general equation that depends only on the signs of γ_I , γ_S , J_{IS} and of the polarization $P(I_z)$. Note that the sign of Δv is now simply contained in θ , which results in a remarkably simple equation:

$$A_S \approx s \cdot P(I_z) + \sin 2\theta \quad (4.38)$$

with

$$s = \frac{J_{IS} \gamma_I \gamma_S}{|J_{IS} \gamma_I \gamma_S|} \quad (4.39)$$

Thus, $P(I_z)$ can be expressed in a simple manner as:

$$P(I_z) \approx s \cdot (A_S - \sin 2\theta) \quad (4.40)$$

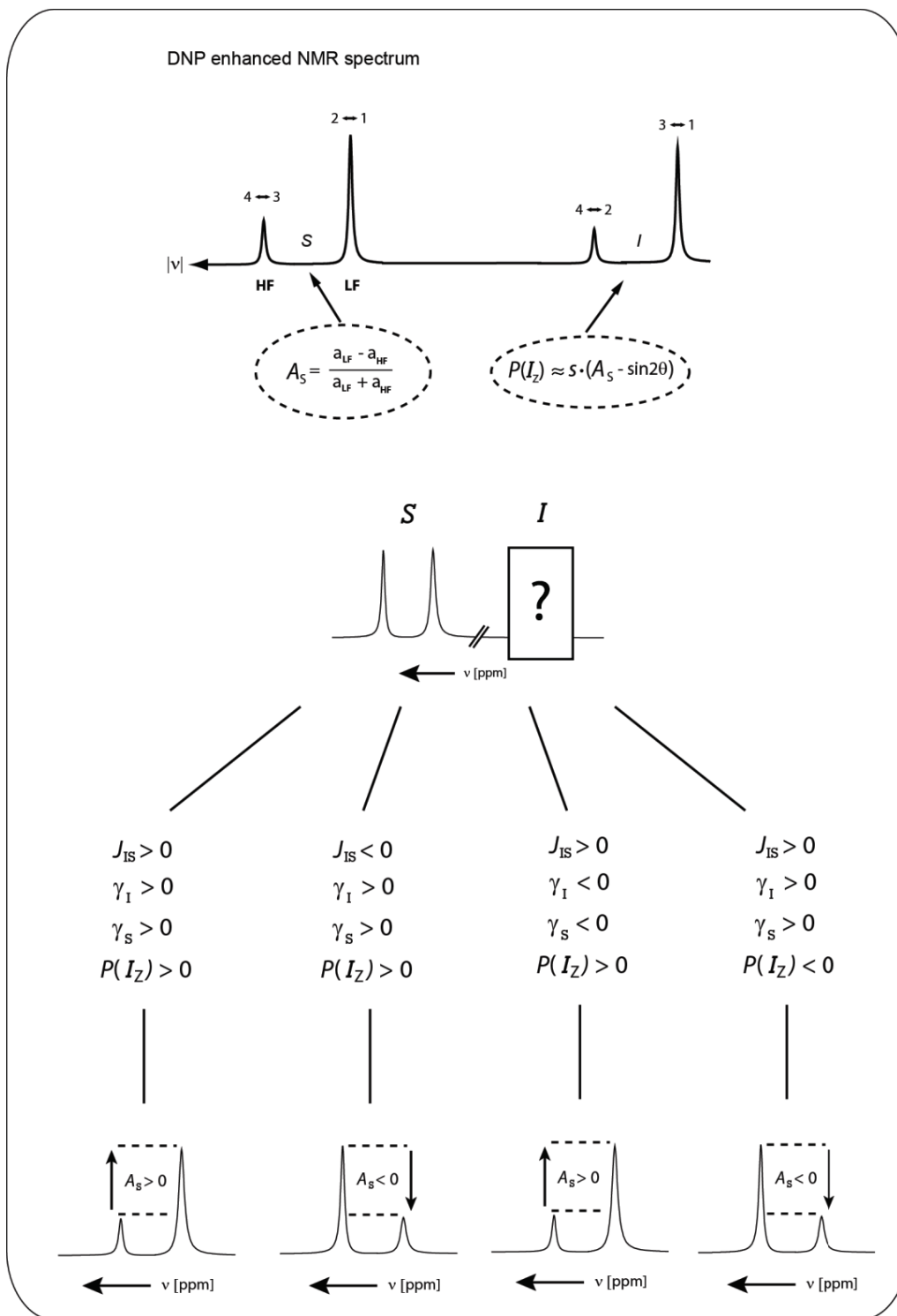


Figure 4.2: Schematic representation of a nNMR spectrum of an arbitrary pair of coupled spins I and S enhanced by d-DNP. Four examples of the 2^4 possibilities for a coupled two-spin system are shown with their respective asymmetries. The absolute sign of J_{IS} can be readily determined provided one knows the signs of the gyromagnetic ratios and the sign of the polarization of the system.

4.2.14 Experimental results of SPY-MR

To confirm the efficiency of the new SPY-MR method, experimental studies were carried out for two different molecules: singly-enriched [$1\text{-}^{13}\text{C}$] sodium pyruvate- d_3 and doubly-enriched [$1,2\text{-}^{13}\text{C}_2$] sodium acetate- d_3 . The aim of using these metabolites is that enriched ^{13}C sites can readily be used as spies S for the determination of the polarization of coupled spins I , even if the latter are in natural abundance. Unfortunately with our equipment, naturally abundant ^{13}C sites could only be used as spies S if the sites I are enriched. Even if we can achieve a high sensitivity enhancement with d-DNP, signals of pairs of coupled spins I and S in natural abundance could not be measured in our laboratory, due to the low probability of about 10^{-4} of obtaining two coupled ^{13}C .

Two different examples are shown in Fig 4.3 and in Fig. 4.4: deuterated [$1\text{-}^{13}\text{C}$] sodium pyruvate and deuterated [$1,2\text{-}^{13}\text{C}_2$] sodium acetate. The preparation of these DNP samples was made according to the standard procedure used in our laboratory, which is described in the previous chapters. A sample containing 1.5 M [$1\text{-}^{13}\text{C}$] sodium pyruvate- d_3 or 1.5 M [$1,2\text{-}^{13}\text{C}_2$] sodium acetate- d_3 in a glass-forming solvent mixture $\text{H}_2\text{O}/\text{D}_2\text{O}/\text{glycerol-}d_8$ (v/v/v : 10/40/50) was doped with 50 mM TEMPOL. Five drops of 10 μl each were inserted into the DNP polarizer at $T = 1.2$ K, and five frozen drops of 10 μl each of 3 M ascorbate were added on top to scavenge radicals during the dissolution process. This composite sample was irradiated at a microwave frequency $f_{\mu\text{w}} = 188.3$ GHz with $P_{\mu\text{w}} = 87.5$ mW to induce a negative polarization. Cross-Polarization was performed to achieve the maximum of ^{13}C polarization and the sample was then quickly dissolved, transferred to a 300 MHz NMR spectrometer and injected into an NMR tube containing 250 μl of D_2O for field-frequency locking in $t_{\text{total}} = 6.2$ s. The hyperpolarized signals were finally acquired at ambient temperature by applying pulses with a small angle $\beta = 5^\circ$ at intervals of 5 s.

The graphs represent the different hyperpolarized signals obtained immediately after the injection of the solution into a sample tube that was waiting in the NMR spectrometer. In all cases, one can clearly observe marked asymmetries A_S that allow one to determine the polarization $P(I_z)$ of the coupled spins. The experimental spectra were fitted using Matlab software. The polarizations $P(I_z)$ determined using SPY-MR were systematically deduced from the asymmetries A_S and compared with the conventional method using the thermal equilibrium signals after complete relaxation as shown in Table 4.1.

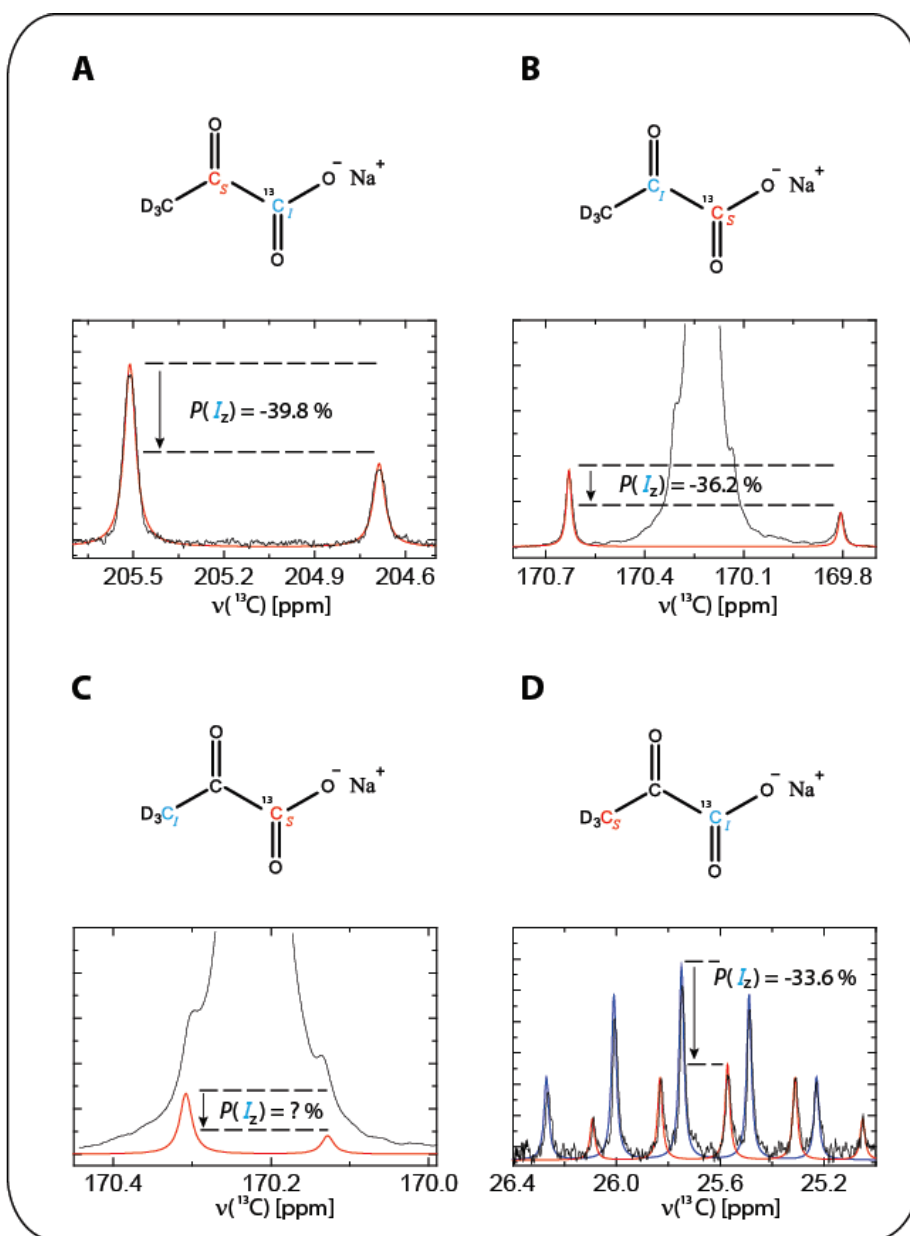


Figure 4.3: Asymmetric doublets observed after dissolution-DNP in singly enriched $[1-^{13}\text{C}]$ pyruvate- d_3 using various spy spins S of the molecule. The graphs of $[1-^{13}\text{C}]$ pyruvate- d_3 highlight which spins are used as a spies C_S (red), and which spins C_I are used as investigated spins (blue). All asymmetries $A_S < 0$ are negative since the high-frequency (left-hand) doublet components are more intense, corresponding to negative polarizations of the investigated spins $P(I_z) < 0$. The following spin pairs I and S are shown: (A) $S = ^{13}\text{CO}$ and $I = ^{13}\text{COO}^-$ with $P(^{13}\text{COO}^-) = -39.8 \pm 1\%$ ($J = 64$ Hz, $\sin 2\theta = 0.024$), (B) $S = ^{13}\text{COO}^-$ and $I = ^{13}\text{CO}$ with $P(^{13}\text{CO}) = -36.2 \pm 2\%$ (with the same $J = 64$ Hz, $\sin 2\theta = -0.024$), (C) $S = ^{13}\text{COO}^-$ and $I = ^{13}\text{CD}_3$ with $P(^{13}\text{CD}_3)$ that could not be determined by SPY-MR ($J = 15$ Hz, $\sin 2\theta = 0.0014$) and (D) $S = ^{13}\text{CD}_3$ and $I = ^{13}\text{COO}^-$ with $P(^{13}\text{COO}^-) = -33.6 \pm 4\%$ (with the same $J = 15$ Hz, $\sin 2\theta = -0.0014$).

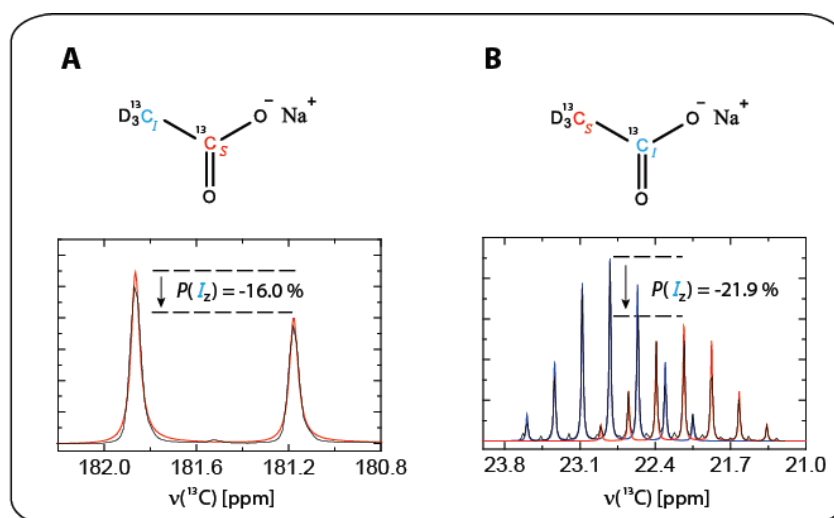


Figure 4.4: Asymmetric doublets observed after dissolution-DNP in doubly-enriched $[1,2-^{13}\text{C}_2]$ acetate- d_3 using the same conventions as in Fig. 4.3. Both asymmetries and polarizations are again negative $A_S < 0$ since $P(I_z) < 0$. The following spin pairs I and S are shown: (A) $S = ^{13}\text{COO}^-$ and $I = ^{13}\text{CD}_3$ with $P(^{13}\text{CD}_3) = -21.9 \pm 1\%$ ($J = 53$ Hz, $\sin 2\theta = -0.0045$) and (B) $S = ^{13}\text{CD}_3$ and $I = ^{13}\text{COO}^-$ with $P(^{13}\text{COO}^-) = -16.0 \pm 1\%$ (with the same $J = 53$ Hz, $\sin 2\theta = 0.0045$).

The main advantage of SPY-MR is that it can provide a rapid measurement of the nuclear spin polarizations, even if the reliability of the method needs to be evaluated on a case-by-case basis. In Table 4.1, we show that the determination of the two ^{13}C polarizations for doubly enriched $[1,2-^{13}\text{C}_2]$ acetate- d_3 by SPY-MR is more accurate when using the traditional comparison with thermal equilibrium measurements, even when the latter were measured over *ca.* 12 hours. The standard deviation could be improved by a factor 10. On the other hand, the use of SPY-MR for singly enriched $[1-^{13}\text{C}]$ pyruvate- d_3 is clearly not justified for all combinations of the pairs S and I . The polarization could be accurately measured for $S = ^{13}\text{CO}$ and $I = ^{13}\text{COO}^-$ with a polarization $P(^{13}\text{COO}^-) = -39.8 \pm 1\%$. However, for all others pairs of spins S and I , the SPY-MR technique gave less precise results than the conventional thermal equilibrium approach.

Investigated ^{13}C site I	$P(I_z)$ [%] <i>from equilibrium</i>	Spy ^{13}C site S	A_S Asymmetry	$\sin 2\theta$ Roof effect	$P(I_z)$ [%] <i>from asymmetry</i>
Pyruvate					
COO	-32 ± 5	CO	-0.374 ± 0.01	+0.024	-39.8 ± 1
		CD ₃	-0.337 ± 0.04	-0.0014	-33.6 ± 4
CO	-31 ± 5	COO	-0.386 ± 0.02	-0.024	-36.2 ± 2
		CD ₃	N.A.	N.A.	N.A.
CD₃	-23 ± 5	COO	?	+0.0014	?
		CO	N.A.	N.A.	N.A.
Acetate					
COO	-16 ± 5	CD ₃	-0.223 ± 0.01	-0.0045	-21.9 ± 1
CD₃	-12 ± 5	COO	-0.155 ± 0.01	+0.0045	-16.0 ± 1

Table 4.1: Absolute polarization $P(I_z)$ of various investigated nuclear spins I in hyperpolarized singly enriched $[1-^{13}\text{C}]$ pyruvate- d_3 and in doubly enriched $[1,2-^{13}\text{C}_2]$ acetate- d_3 . The polarizations were determined in solution at $B_0 = 7.05$ T (300 MHz for protons) and $T = 298$ K immediately after dissolution, either by a conventional comparison with the corresponding thermal equilibrium signals measured after complete relaxation, or by SPY-MR through the asymmetry A_S of a coupled spy spin.

With these limitations of the SPY-MR method, some empirical rules resulting from our experimental studies can be summarized as follows:

- 1) When both nuclear spin S and I are in natural abundance, for example the ^{13}CO and $^{13}\text{CD}_3$ spin pair in deuterated pyruvate, their respective polarizations could not be estimated with our instrument due to a lack of sensitivity. Using the traditional measurement with the thermal equilibrium approach, the polarizations could be estimated to be $P(^{13}\text{CO}) = -30.9\%$ and $P(^{13}\text{CD}_3) = -22.6\%$, albeit with a limited accuracy of $\pm 5\%$.
- 2) The polarizations of the spins $I = ^{13}\text{CO}$ and $I = ^{13}\text{CD}_3$ in natural abundance could be investigated *via* the enriched $S = ^{13}\text{COO}^-$. The only limitation to this rule arises if the "satellite" doublet lines severely overlap with the more intense central line. For example, this overlap is not so severe for $I = ^{13}\text{CO}$ for pyruvate in Fig. 4.3 B allowing a reliable estimate of the polarization $P(^{13}\text{CO}) = -36.2 \pm 2\%$. However for $I = ^{13}\text{CD}_3$, this overlap is more severe (see Fig. 4.3 C) so that it is not possible to determine the polarization $P(^{13}\text{CD}_3)$ by SPY-MR. Using a proper deconvolution, we can see the satellite lines that are hidden under the central peak, but poor shimming or phase errors during the measurements may have detrimental effects on the determination of the I spin polarization.
- 3) It is possible to determine the polarization of an investigated spin I *via* a distant spy S that is a more than one bond away. For example, the polarization of the isotopically enriched $I = ^{13}\text{COO}^-$ spins could be investigated by observing the naturally abundant $S = ^{13}\text{CD}_3$ spins in deuterated pyruvate, despite the complex pattern arising from couplings to three deuterons (see Fig. 4.4). Nevertheless, the estimate $P(^{13}\text{COO}^-) = -33.6 \pm 4\%$ resulting from the observation by the spy $S = ^{13}\text{CD}_3$ is less accurate than $P(^{13}\text{COO}^-) = -38.9 \pm 1\%$ that could be determined by using the nearby spy $S = ^{13}\text{CO}$. To overcome this problem and obtain more accurate values, deuterium decoupling could emerge as an idea to reduce the overlap.

As a general condition, even when using state-of-the-art instrumentation, SPY-MR requires at least one of the two sites I or S to be enriched. Three possible scenarios can occur:

(a) Both sites are enriched. Either site can be used as the spy S , and the determination of the polarization of the other site is straightforward. This scenario offers the most accurate measurement by SPY-MR.

(b) Only the investigated spin I is enriched. In this case, the spy spin S in natural abundance gives rise to a doublet (albeit with a nearly 100-fold reduced sensitivity) with an asymmetry A_S that allows one to determine the polarization $P(I_z)$.

(c) The investigated I spin is in natural abundance and the spectrum of the enriched spy S features two weak satellite peaks owing to the 1.1% abundance of ^{13}C of the site I . If they can be resolved, their asymmetry allows one to determine the polarization $P(I_z)$. However, depending on the line-widths and scalar coupling constants, the intense central peak can overlap with the satellite peaks and affect the accuracy of the SPY-MR approach (see Fig. 4.3 C).

Finally, it is worth mentioning that the measurement of the polarization by SPY-MR is more accurate immediately after dissolution of the hyperpolarized sample than after letting the system relax for a certain amount of time. Fig. 4.5 shows a comparison of the decay of the hyperpolarization of the deuterated methyl group $^{13}\text{CD}_3$ estimated by conventional means (Δ) and by SPY-MR, based on the asymmetry A_s of the neighboring COO^- group in acetate (∇). The asymmetry reliably reflects the absolute polarization over a range highlighted in green ($t \sim 50$ s). After that, the two curves obviously diverge from each other. This can be mainly attributed to small cross-relaxation and cross-correlation rates that have significant effects on a timescale longer than T_1 and that are therefore not negligible anymore. Moreover, the asymmetry of the COO^- peaks becomes increasingly difficult to determine when the signal-to-noise ratio decreases in the course of the decay.

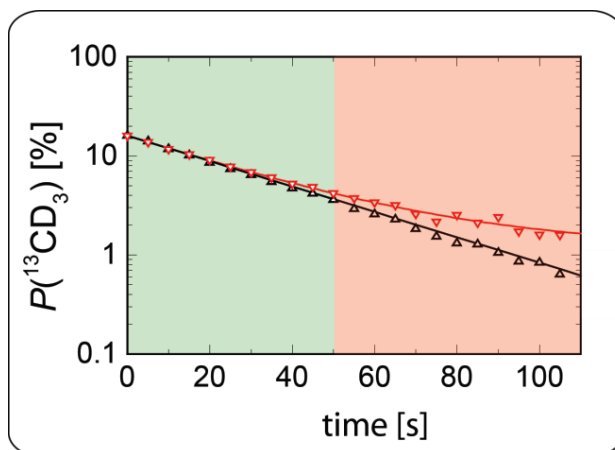


Fig. 4.5: Hyperpolarized decay of $^{13}\text{CD}_3$ in $[1,2-^{13}\text{C}_2]$ acetate- d_3 (Δ) obtained from T_1 relaxation measured with 5° nutation angle pulses, and (∇) derived from the asymmetry A_s of the neighboring COO^- group. The range where SPY-MR is a reliable technique to determine the polarization is highlighted in green. After a certain point (beyond the T_1 of the molecule), cross-relaxation and cross-correlation mechanisms have an important effect on the system and the determination of the polarization by SPY-MR becomes more and more hazardous (highlighted in red).

4.2.15 Conclusions concerning SPY-MR

In this chapter, we demonstrated a novel technique called SPY-MR that is applicable to a broad variety of coupled nuclear spins. This method can provide an alternative to the traditional thermal equilibrium measurements to estimate the absolute polarization of ^{13}C spins after dissolution-DNP. This simple and accurate technique obviates the need for recording a reference signal at thermal equilibrium, which requires in most of the cases laborious measurements that can last more than 12 hours. This study was essentially based on homonuclear examples (^{13}C of pyruvate and acetate), but could also be addressed to heteronuclear cases (^1H and ^{13}C for example) with appropriate cross-relaxation and cross-correlation terms. Finally, in addition to the benefit of reducing the time requirements and to measure the polarization more accurately, SPY-MR can also provide a way to measure the absolute sign of the coupling constant J_{IS} by inspection of the multiplet asymmetry.

4.3 Remote Cross-Polarization for Deuterated Metabolites

The main inconvenience of NMR being its low sensitivity, it can nevertheless be overcome by the use of dissolution-DNP as previously described, which unfortunately suffers from another important obstacle: the very short lifetime of the polarization. Indeed, our hyperpolarized ambitions in liquids are often hampered by the fast relaxation of the highly polarized metabolites.

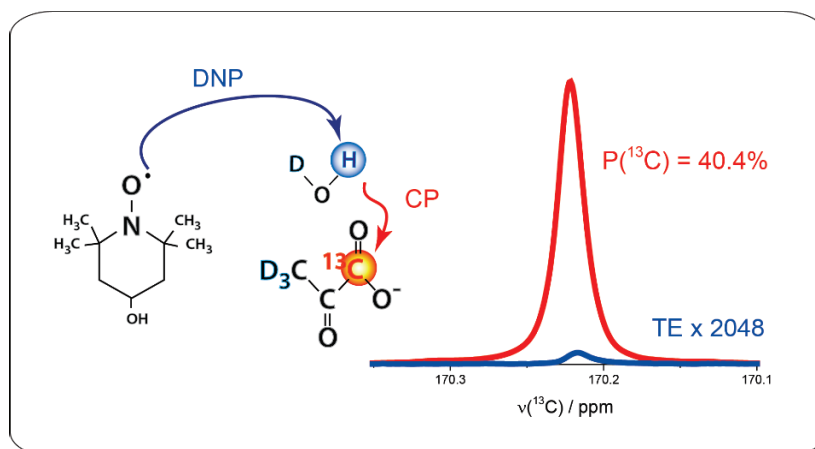
These relaxation processes are accentuated by the compulsory presence of radicals in the DNP sample before and after dissolution, and the fluctuations in the magnetic field during the transfer. Even if several methods have been developed recently to thwart these problems, such as the use of ascorbate to scavenge the radical species [22] or the use of a magnetic tunnel to safely transfer our hyperpolarized solutions [18], the observation by d-DNP of functional groups that naturally relax fast like methyl groups is difficult or sometimes impossible.

It is a well-known effect that deuteration increases the relaxation time T_1 of other spins in a molecule. For example, by simply replacing the protons by deuterium makes it possible to extend the hyperpolarized lifetimes of ^{13}C -enriched metabolites after dissolution.

However, in our particular case, the use of deuterated metabolites would greatly affect our DNP experiments. Indeed, the presence of protons in our samples is mandatory since Cross-Polarization from ^1H to ^{13}C is performed routinely in our laboratory. Thus, a remote source of protons should be present in addition to the fully deuterated molecules. Fortunately, this source can be found in the DNP solvent provided it contains some H_2O in addition to D_2O and glycerol- d_8 .

Thanks to the use of deuterated metabolites in the DNP samples, the lifetimes $T_1(^{13}\text{C})$ of specific functional groups in metabolites such as $[1-^{13}\text{C}]$ sodium pyruvate- d_3 or $[1,2-^{13}\text{C}_2]$ sodium acetate- d_3 can be extended, avoiding the nearly complete loss of the hyperpolarized signals of methyl groups during the transfer process.

The improvements discussed below were described in a publication entitled: "*Hyperpolarization of Deuterated Metabolites via Remote Cross-Polarization and Dissolution Dynamic Nuclear Polarization*". [23]



4.3.1 Extending the lifetimes by deuteration

As previously mentioned, applications of d-DNP are inexorably limited by the lifetime of the hyperpolarized magnetization which is determined by the relaxation time T_1 of the molecules. Considerable efforts have been deployed to dramatically reduce the polarization losses after the dissolution process and during the transfer of the hyperpolarized solutions in order to provide access to slower and subtler chemical transformations such as slow metabolic processes. Indeed, in the context of *in-vivo* experiments, the time required after the dissolution, transfer, filtration, pH adjustment and quality control prior to injection is more than a minute. [4]

Among these methods designed to extend the short-lived fate of spin polarization, the use of ascorbate or Vitamin C was demonstrated to scavenge the radicals and therefore suppress the paramagnetic contributions of the polarizing agents (PAs), which are inevitably present in the dissolved solution. [22] Another technique relies on the storage of hyperpolarized longitudinal magnetization in the form of long-lived states (LLS) [24], which usually involves pairs of inequivalent spins and can exhibit lifetimes up to 13 min [25] or 5 min [26] in suitably tailored molecules.

Whatever paths are chosen for extending the lifetimes of hyperpolarization, in many cases the mere presence of protons in the molecules may impose a severe erosion of the polarization. Indeed, nuclear spin-lattice relaxation driven by intramolecular dipolar interactions, in particular between ^{13}C spin and ^1H spins (even when distant by two or more bonds), may offer efficient relaxation pathways. A simple solution to this problem consists in the partial or complete deuteration of the molecule of interest, such as the amine group in ^{15}N -glutamine [27] or in ^{15}N -trimethylglutamine [28] or even the methyl groups in [$3\text{-}^{13}\text{C}$] pyruvate. [29] More recently, N-trimethylphenylammonium- d_9 has been shown to exhibit an extremely long relaxation time $T_1(^{15}\text{N}) > 800$ s in solution. [30] The ^{13}C or ^{15}N polarization of such deuterated molecular probes can be efficiently performed in a direct manner without Cross-Polarization by using narrow ESR lines radicals like Trityl. However, deuteration may lead to a decrease in DNP efficiency by as much as 40 % [31] when deuterons are fully abundant in the solvent.

To keep sufficiently high polarization levels in the solid phase, and at the same time to extend the lifetime of our hyperpolarized solutions, we proposed to combine the Cross-Polarization technique from diluted remote ^1H of the solvent to ^{13}C in fully deuterated metabolites.

4.3.2 Hyperpolarization of deuterated metabolites

In order to compare "*Remote CP*" with "*Standard CP*", different DNP batches were prepared. For the standard DNP sample, two batches, one containing 1.5 M [$1\text{-}^{13}\text{C}$] sodium pyruvate and the other containing 1.5 M [$1\text{-}^{13}\text{C}$] sodium acetate, were doped with 50 mM TEMPOL in a mixture of $\text{D}_2\text{O}/\text{glycerol-}d_8$ (1/1) in such a way that the only protons are present on the methyl groups of the molecules. For the second two samples, this time using deuterated metabolites, 1.5 M [$1\text{-}^{13}\text{C}$] sodium pyruvate- d_3 and 1.5 M [$1\text{-}^{13}\text{C}$] sodium acetate- d_3 were again doped with 50 mM TEMPOL in a mixture of $\text{H}_2\text{O}/\text{D}_2\text{O}/\text{glycerol-}d_8$ (v/v/v : 10/40/50) to have protons present in the DNP solvent. These samples were inserted in our DNP polarizer operating at $B_0 = 6.7$ T at a temperature $T = 1.2$ K. [32, 33, 34] A microwave irradiation $f_{\mu\text{W}} = 188.3$ GHz (on the negative lobe) was applied to these batches with $P_{\mu\text{W}} = 87.5$ mW (see Supporting Information).

In Fig. 4.6, the ^{13}C polarization was enhanced stepwise by multiple CP contacts [33] every 5 min in the sample containing deuterated pyruvate (**A**) and non-deuterated pyruvate (**B**). The polarization build-up for deuterated pyruvate $T_{\text{bup}}(^1\text{H} \rightarrow ^{13}\text{C}) = 950 \pm 23$ s is comparable to the one observed with non-deuterated pyruvate $T_{\text{bup}}(^1\text{H} \rightarrow ^{13}\text{C}) = 990 \pm 30$ s under the same conditions. Both samples were dissolved after the same duration of the build-up of the polarization and transferred in both cases through a magnetic tunnel [18], to be finally injected into a sample tube that was awaiting in a 300 MHz NMR spectrometer ($t_{\text{overall}} \approx 10$ s). The $[1\text{-}^{13}\text{C}]$ polarization recorded in liquid phase in deuterated pyruvate is slightly higher ($P(^{13}\text{C}) = 40.4\%$) than in its non-deuterated counterpart ($P(^{13}\text{C}) = 37.9\%$) (see Table 4.2). However, the relaxation time $T_1(^{13}\text{C})$ of $[1\text{-}^{13}\text{C}]$ is almost identical for both samples containing pyruvate. On the other hand, the naturally abundant $[2\text{-}^{13}\text{C}]$ and $[3\text{-}^{13}\text{C}]$ show a significant extension of $T_1(^{13}\text{C})$ upon deuteration by factors 1.15 and 9.75 respectively. The reason of this extension is obvious: the heteronuclear $^1\text{H} - ^{13}\text{C}$ dipolar relaxation is negligible in the deuterated molecule. In addition to this remarkable extension of the relaxation time $T_1(^{13}\text{C})$ in $[3\text{-}^{13}\text{C}]$, a significant improvement in the nuclear polarization measured 10 s after dissolution was achieved. The $[3\text{-}^{13}\text{C}]$ polarization was improved by a factor 3 in deuterated pyruvate after dissolution, simply because of the fact that the polarization was better preserved.

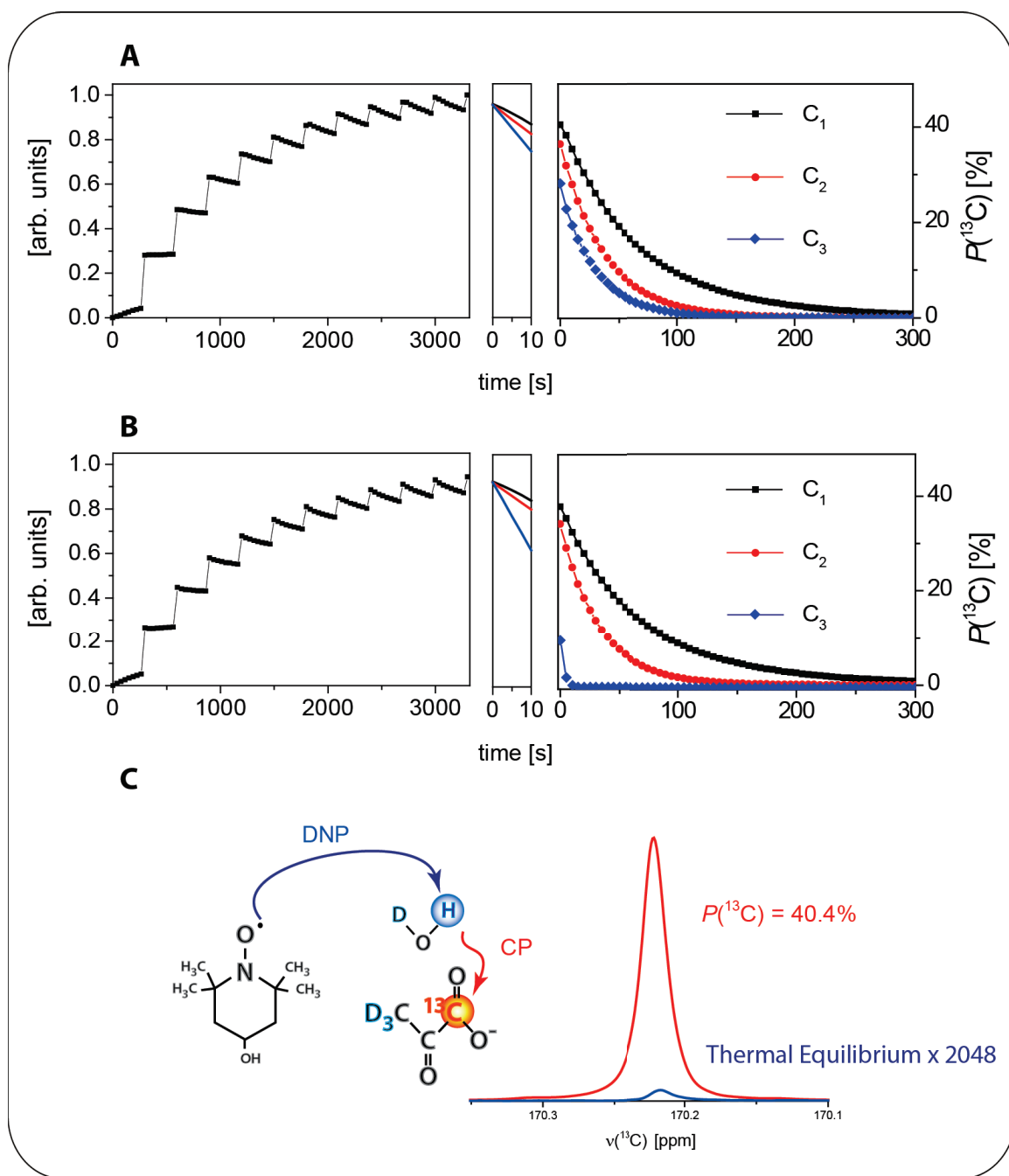


Fig. 4.6: Hartmann-Hahn Cross-Polarization (CP) performed on two samples containing (A) deuterated and (B) non-deuterated $[1-^{13}\text{C}]$ sodium pyruvate. The left panels show the build-up of $P(^{13}\text{C})$ at low temperatures ($T = 1.2$ K) with signals measured every 37.5 s using pulses with 5° nutation angles. Multiple adiabatic CP contacts are established every 5 min, leading to nearly vertical jumps of the ^{13}C signals. The middle panels represent the relaxation during dissolution and transfer through a magnetic tunnel to the 300 MHz NMR spectrometer in approximately 10 s. [18] The right panels show the decay of the polarization $P(^{13}\text{C})$ of carboxyl (C_1), carbonyl (C_2) and methyl (C_3) groups after dissolution. These signals were measured by applying 5° nutation pulses at 5 s intervals. (C) Hyperpolarized spectrum of $[1-^{13}\text{C}]$ pyruvate- d_3 measured directly after dissolution with a single 5° pulse, resulting in $P(^{13}\text{C}) = 40.4\%$ (red) and compared to its thermal equilibrium acquired after complete relaxation of the system with 128 calibrated 90° pulses, and rescaled by a factor 2048 (blue).

Metabolites	site	$P(^{13}\text{C})$ [%]	$T_1(^{13}\text{C})$ [s]
[1-^{13}C] pyruvate	C ₁	37.9 ± 0.8	69.3 ± 0.6
	C ₂	34.2 ± 0.7	41.7 ± 1.0
	C ₃	9.4 ± 0.2	4 ± 2
[1-^{13}C] pyruvate-d_3	C ₁	40.4 ± 0.4	68.0 ± 0.5
	C ₂	36.4 ± 0.4	47.5 ± 0.8
	C ₃	28.2 ± 0.3	39 ± 2
[1,2-$^{13}\text{C}_2$] acetate	C ₁	24.1 ± 1.8	66.7 ± 1.5
	C ₂	5.7 ± 0.3	11.0 ± 0.3
[1,2-$^{13}\text{C}_2$] acetate-d_3	C ₁	19.6 ± 1.7	78.5 ± 0.5
	C ₂	14.5 ± 2.9	35.4 ± 0.4

Table 4.2: Polarizations $P(^{13}\text{C})$ and spin-lattice relaxation times T_1 after dissolution-DNP in non-deuterated and deuterated [1- ^{13}C] pyruvate and [1,2- $^{13}\text{C}_2$] acetate at $B_0 = 7.05$ T and $T = 298$ K.

The same experiments were carried out for non-deuterated and deuterated [1,2- $^{13}\text{C}_2$] acetate and resulted in similar improvements for the spin-lattice relaxation times of the enriched carbons in both cases. Note that even the remote carboxylic group of deuterated acetate shows a longer $T_1(^{13}\text{C})$ in comparison with the protonated one, despite the weaker effect of deuteration due to a greater distance between the methyl and carboxyl groups. In Fig. 4.7, the hyperpolarized decay of both enriched carbons in [1,2- $^{13}\text{C}_2$] acetate- d_3 is represented after dissolution.

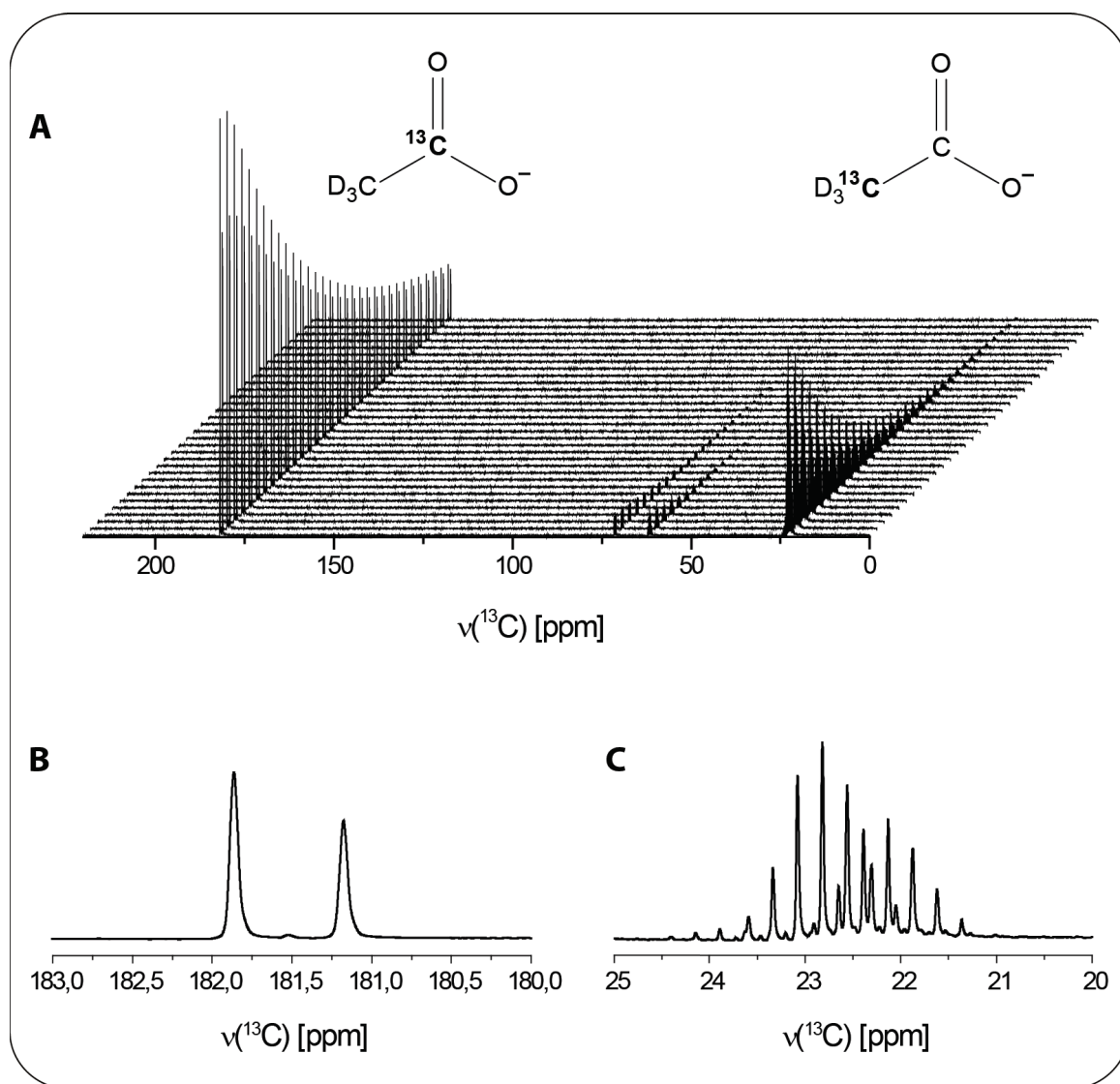


Fig. 4.7: (A) Hyperpolarized ^{13}C NMR spectra of $[1,2-^{13}\text{C}_2]$ acetate- d_3 recorded every 5 s after dissolution by applying 5° nutation angle pulses showing the effects of longitudinal relaxation $T_1(^{13}\text{C})$ at $B_0 = 7.05$ T and $T = 298$ K. The peaks present near 60 and 75 ppm represent the naturally abundant ^{13}C of glycerol- d_8 used as glass-forming matrix during our d-DNP experiments. (B) NMR signals of the carboxyl C_1 and (C) of the methyl C_2 , revealing asymmetries that are characteristic of very low spin temperatures (see Chapter 4.2).

4.3.3 Conclusions concerning remote hyperpolarization

Cross-Polarization can be applied in dissolution-Dynamic Nuclear Polarization of deuterated molecules by using remote ^1H spins present in the DNP solvent. This leads to an unhampered transfer of polarization from ^1H to ^{13}C . This scheme can obviously be applied to a broad range of molecules whose specific functional groups are not suitable to be recorded by d-DNP, because of their short spin-lattice relaxation times. This method can also be applied to molecules that do not possess any proton spins. The main objective of this method is that it relies on the deuteration of molecules which exhibit longer relaxation times and therefore allow a better preservation of the polarization during the dissolution, the transfer and the injection processes. Based on the same principles, the enhanced polarization after dissolution is available over longer time intervals. Finally, this approach can be applied to other nuclei such as ^{15}N in certain molecules that do not contain any protons. [35]

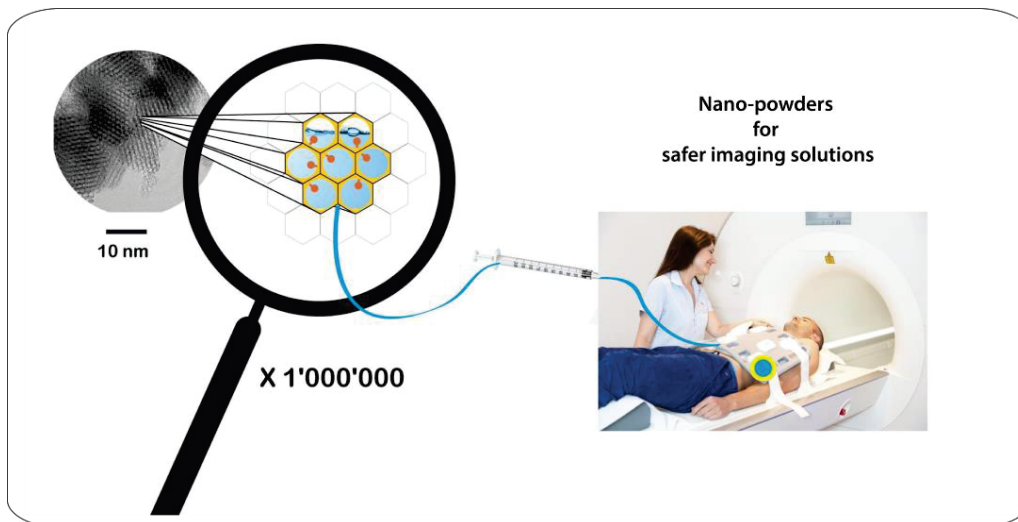
4.4 HYper Polarizing Solids (HYPSO)

A new class of polarizing agents called HYPSO (HYper Polarizing Solids) were synthesized at the CRMN in Lyon and at ETH in Zürich to perform dissolution-DNP without any traces of contaminants after the dissolution process. This HYPSO family is composed of a well-defined mesoporous silica compound with grafted radicals attached to its surface, enabling the DNP process.

The main problem encountered during our dissolution experiments is that the dissolved samples usually contain traces of contaminants such as glass-forming solvents (glycerol or DMSO) or free radical species (like TEMPOL or Trityl), which can perturb *in vivo* MRI applications. However, their presence and homogenous distribution is mandatory at low temperatures in order to allow the DNP process to occur.

HYPSO is a novel class of meso-structured silica material containing TEMPO radicals that are homogeneously distributed and covalently attached in the pore channels, thus avoiding a contamination by their release during the dissolution process. Moreover, the need of a glassy matrix is not mandatory anymore since HYPSO can be directly impregnated by the solution to be hyperpolarized. This new approach can be applied to a broad range of substrates, including metabolites and peptides. Finally, HYPSO can be retained by filtration and only the pure hyperpolarized solution can be collected and analyzed.

The following chapter is essentially based on three different publications entitled "*Hybrid polarizing solids for pure hyperpolarized liquids through dissolution dynamic nuclear polarization*" [36], "*Cubic Three-Dimensional Hybrid Silica Solids for Nuclear Hyperpolarization*" [37] and "*Phenylazide Hybrid-Silica : Polarization Platform for Dynamic Nuclear Polarization at Cryogenic Temperatures*". [38]



4.4.1 The HYP SO family

Throughout the dissolution-DNP processes (heating, dissolution, transfer, injection and recording of NMR signals in an NMR or MRI spectrometer), longitudinal relaxation leads to the erosion of hyperpolarization. The relaxations mechanisms are accelerated by remaining paramagnetic impurities like polarizing agents (PAs) that no longer have any function after dissolution and therefore need to be eliminated to preserve the hyperpolarized signals. [22]

As mentioned in the previous chapters, several techniques have recently emerged to get rid of free radicals in solution. For Trityl, the separation can be achieved by solvent extraction [39] or by precipitation after a pH jump followed by mechanical filtration through a stack of polyethylene filters. [40, 41] The same principle of precipitation could be used for 1,3 bisdiphenylene-2-phenylallyl radicals (BDPA) and 2,2 diphenyl-1-picrylhydrazyl radicals (DPPH). [42, 43] As discussed previously, for TEMPO and its derivatives including biradicals [44, 45, 46, 47, 48, 49, 50], sodium ascorbate (Vitamin C) is a well suited candidate to scavenge chemically the PAs by converting the nitroxide radicals into diamagnetic species through reduction. [22] However, for rapid and effective quenching of the radicals, sodium ascorbate should be used in excess and the remaining ascorbate in solution may affect the analyte or sensitive components present in the system such as enzymes. [51, 52, 53]

Recently, a promising method was proposed by Eichhorn *et al.* [54] to produce hyperpolarized pyruvate solutions without free radicals. This technique simply consists in performing d-DNP on pure [$1\text{-}^{13}\text{C}$] pyruvic acid, in which photo-induced radicals have been generated by intense UV radiation. The main inconvenience is that d-DNP should encompass a wide variety of metabolites and should not be limited to pyruvate. Moreover, the UV irradiation process creates paramagnetic impurities which can be degraded to yield [$1\text{-}^{13}\text{C}$] acetate. Even if acetate is considered as a non-toxic metabolite for *in-vivo* studies, it should nevertheless be considered to be a contaminant and can interfere with the system.

One approach to obtain pure hyperpolarized solutions is to use a polarizing matrix that can be easily separated by filtration. Recently, silica gels or thermoresponsive polymers [55, 56, 57] have been used for Overhauser DNP in liquid water at room temperature, leading to relatively small enhancements. More recently, DNP was shown to produce only modest enhancements ($\epsilon \approx 2$ at $T = 4.2$ K) by exploiting electron spins of dangling bonds on the surface of silicon particles. [58]

We therefore introduced the HYper Polarizing SOLids (HYP SO) family, composed of hybrid organosilica materials in which the PAs are covalently linked to the pore channels and homogeneously distributed in the mesostructured silica matrix. This class of mesoporous nano-powders was proposed for dissolution-DNP because enhancement factors up to $\epsilon = 36$ were reported under MAS-DNP conditions at $T = 100$ K and $B_0 = 9.4$ T. [59] In Fig. 4.8, the first generation of HYP SO-1 material is shown that contains homogeneously distributed TEMPO radicals covalently bound to the silica surface through a propylamide linker [$\text{O}_{1.5}\text{Si}(\text{CH}_2)_3\text{-NHCO-TEMPO}$]. This material has large pore volumes that permit the impregnation of 1.8 mL of solution to be polarized per 1 g of material through the complete filling of both the pores (1.0 mL/g) and the intergrain volumes (0.8 mL/g). After the impregnation of HYP SO-1 with the solution to be polarized, routine DNP can be performed by microwave irradiation. The important point is that the covalent linkage between the TEMPO radicals and the silica matrix avoids the contamination of the expelled hyperpolarized solution during the dissolution process and the filtration of the material. Indeed, this hyperpolarized solution is cleared out of HYP SO-1 by injecting hot water and the silica material can be retained by a cellulose filter placed at the bottom of the dissolution stick.

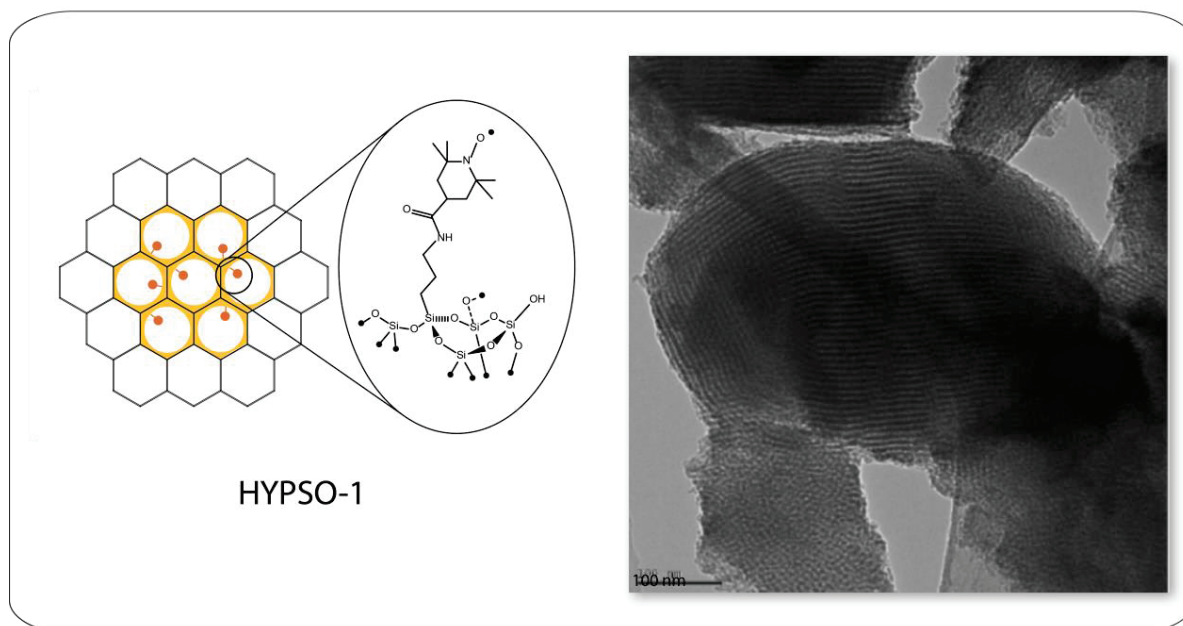


Fig. 4.8: (Left) Schematic representation of HYP SO-1 containing TEMPO radicals covalently attached to its surface. (Right) Transmission Electron Microscopy (TEM) image of mesoporous HYP SO 1.0 taken with a Philips CM30 TEM operating at 300 kV. [59]

4.4.2 Hyperpolarization of [1-¹³C] sodium pyruvate using HYP SO-1

In Fig. 4.9 A, the DNP sample is composed of 20 mg of HYP SO-1 material which contains 88 μmol radical per gram (the optimum concentration for this material, which roughly corresponds to a concentration of 49 mM electrons inside the pores) impregnated with 36 μl of a 3 M solution of [1-¹³C] sodium pyruvate in D₂O. After proper impregnation of HYP SO, the sample is inserted in our DNP polarizer at $B_0 = 6.7$ T [32, 33, 34] and Cross-Polarization contacts between ¹H and ¹³C are performed every 3 min at $T = 1.2$ K with a microwave irradiation $f_{\mu\text{W}} = 188.3$ GHz (negative lobe). After only 20 min, the maximum polarization $P(^{13}\text{C}) > 20\%$ is reached (Fig. 4.9 B). Dissolution is realized as usual by injecting 5 ml superheated D₂O and the entire hyperpolarized solution is expelled from the pores of the material, while the PAs remain attached to the surface of HYP SO (Fig. 4.9 C). After transfer and injection ($t_{\text{overall}} = 10.2$ s) into a sample tube waiting in a 300 MHz NMR spectrometer, the hyperpolarized [1-¹³C] pyruvate signal can be recorded with an enhancement of $\epsilon = 32'500$ compared with its thermal equilibrium, which corresponds to a polarization $P(^{13}\text{C}) = 25.3\%$. Furthermore, the filtration of HYP SO was complete since no free radicals were present in the solution after dissolution, which is confirmed by a long $T_1(^{13}\text{C}) \approx 50$ s.

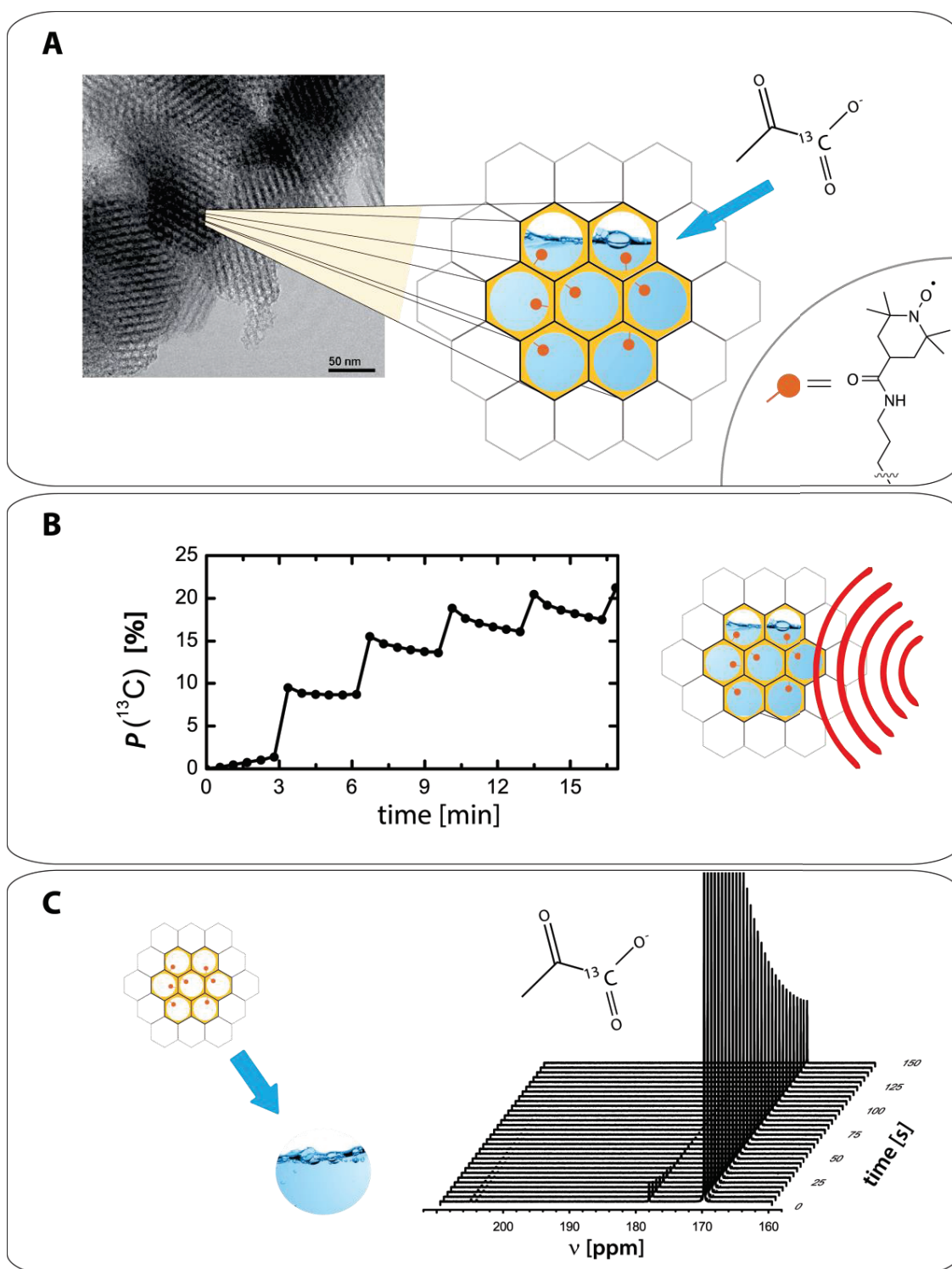


Fig. 4.9: Overall process of hyperpolarization by d-DNP performed with HYPSO. (A) The material HYPSO-1 is impregnated with 36 μl of a solution to be hyperpolarized of 3 M $[1\text{-}^{13}\text{C}]$ sodium pyruvate in D_2O without the need of any glass-forming agents. The Transmission Electron Microscopy (TEM) image was taken with a Philips CM30 TEM operating at 300 kV. This shows the mesoporous structure of the material. In this illustration, the red dots represent the polarizing agents grafted onto the surface of HYPSO. (B) Proton DNP is performed and a build-up time of $T_{\text{bup}}(^1\text{H}) = 119 \pm 1.5$ s is observed. The proton polarization can be transferred by Cross-Polarization from ^1H to ^{13}C in order to reach a final $P(^{13}\text{C}) = 20\%$ after only 17 min. (C) The DNP solution is dissolved and expelled from the pores of HYPSO-1 by injecting 5 ml superheated D_2O ($T = 413$ K and $p = 10$ bar) and is transferred to a 300 MHz NMR spectrometer. A series of ^{13}C NMR spectra of $[1\text{-}^{13}\text{C}]$ sodium pyruvate is recorded every 5 s. The final polarization achieved for this metabolite is $P(^{13}\text{C}) = 25.3\%$ ($\epsilon = 32'500$) and decays with $T_1(^{13}\text{C}) = 49.4 \pm 0.4$ s, which corresponds to a pure D_2O solution of pyruvate without any traces of free radicals.

4.4.3 Hyperpolarization of metabolites with HYPSO-1

The main interest of the use of d-DNP for *in-vivo* applications is the possibility to hyperpolarize a range of various metabolites. In order to justify the use of HYPSO materials for these applications, we performed the same d-DNP experiments with [1-¹³C] sodium acetate, sodium fumarate and the dipeptide L-Alanine-Glycine. The ¹³C polarizations obtained for these different molecules are shown in Fig. 4.10 with $P(^{13}\text{C}) = 16.5\%$ for [1-¹³C] sodium acetate, $P(^{13}\text{C}) = 19.9\%$ for both carboxyl groups at natural abundance in fumarate, and finally $P(^{13}\text{C}) = 15.0\%$ and $P(^{13}\text{C}) = 13.6\%$ for the naturally abundant ¹³C carbonyl groups in Alanine and Glycine of the peptide Ala-Gly.

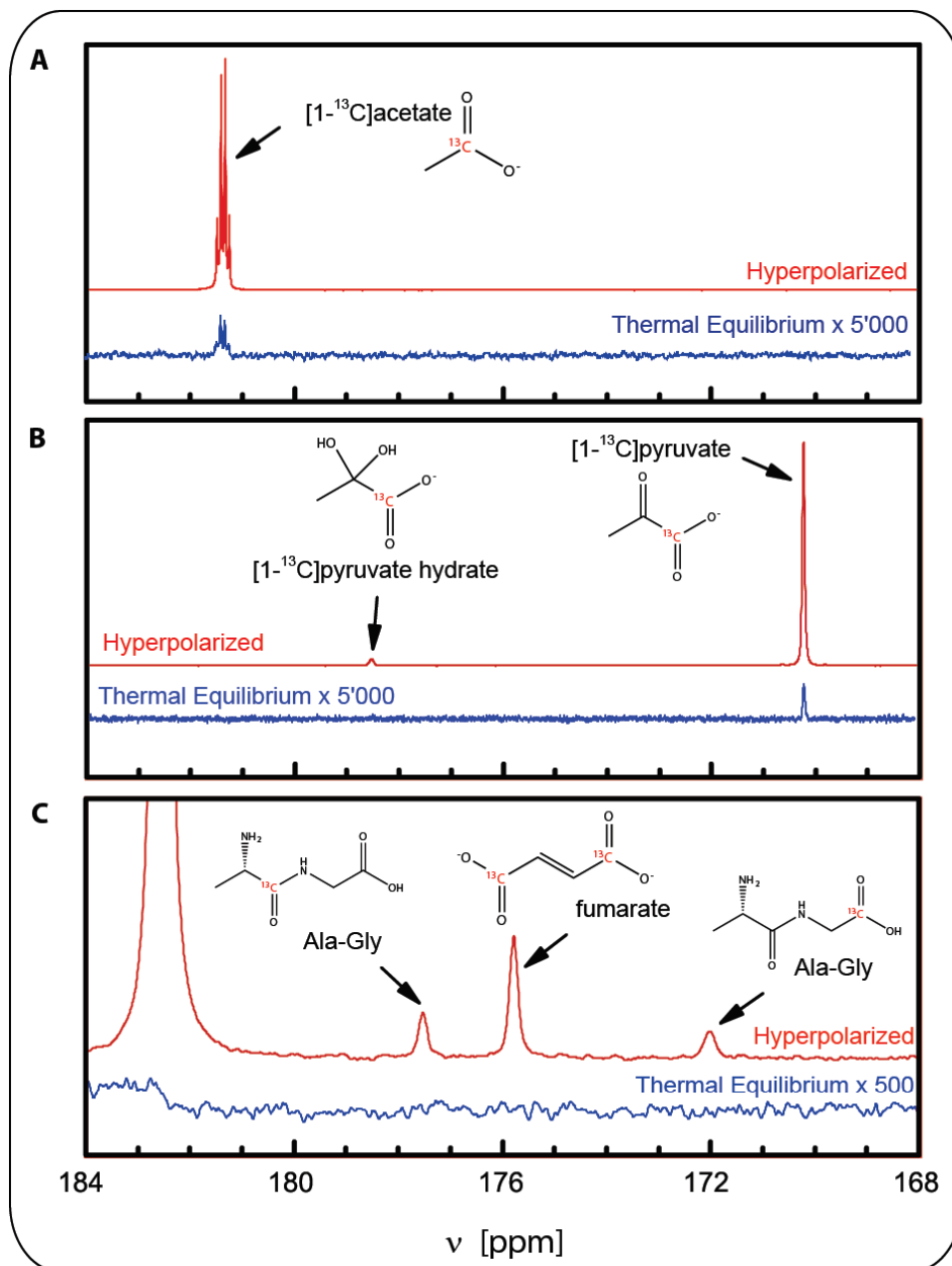


Fig. 4.10: Hyperpolarized ¹³C NMR spectra of (A) [1-¹³C] acetate, (B) [1-¹³C] pyruvate, (C) fumarate and L-Alanine-Glycine with their respective thermal equilibrium spectra. The ¹³C hyperpolarization was boosted by using Cross-Polarization from ¹H to ¹³C. The hyperpolarized signals were acquired with 5° nutation angle pulses, whereas the thermal equilibrium (scaled by a factor 5000 or 500) were measured with 27, 128 and 512 scans for [1-¹³C] acetate, [1-¹³C] pyruvate and fumarate and L-Alanine-Glycine respectively by using 90° nutation angle pulses applied every 300 s.

4.4.4 Optimization of HYP SO materials

We have now demonstrated that the new class of silica matrix HYP SO is well suited for the hyperpolarization of a great variety of metabolites, but the main inconvenience that remains so far is that the ^{13}C polarization achieved is far below our record of $P(^{13}\text{C}) = 40\%$ obtained using glass-forming agents. [33] To overcome this drawback, new classes of porous silica materials were synthesized by changing either the structure of the mesoporous system, the linker connecting the radical species to the surface, or the radical itself.

Thus, the TEMPO radical was replaced by Trityl (Fig. 4.11). A polarization of $P(^{13}\text{C}) = 15\%$ was achieved after 2 h, which could increase to $P(^{13}\text{C}) = 25\%$ at the plateau. Clearly, the use of HYP SO-1 is not limited to a single type of radical. Direct ^{13}C polarization without CP is also possible with this silica matrix.

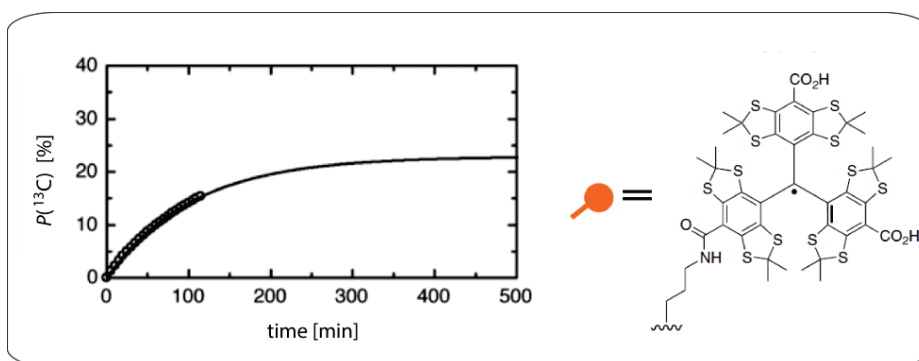


Fig. 4.11: Cross-Polarization from ^1H to ^{13}C DNP performed on 20 mg of HYP SO-1-Trityl (16 $\mu\text{mol/g}$) impregnated with 36 μl of a 3 M solution of $[1-^{13}\text{C}]$ sodium pyruvate in D_2O . A polarization $P(^{13}\text{C}) = 15\%$ is reached after 2 h with $T_{\text{bup}} = 104.6 \pm 2.4$ min.

The second generation of this material dubbed HYP SO-2 was prepared using a different linker for the radical moieties. This synthesis allows one to increase the yield of incorporation and results in a polarization $P(^{13}\text{C}) = 36\%$ in $[1-^{13}\text{C}]$ pyruvate (Fig. 4.12).

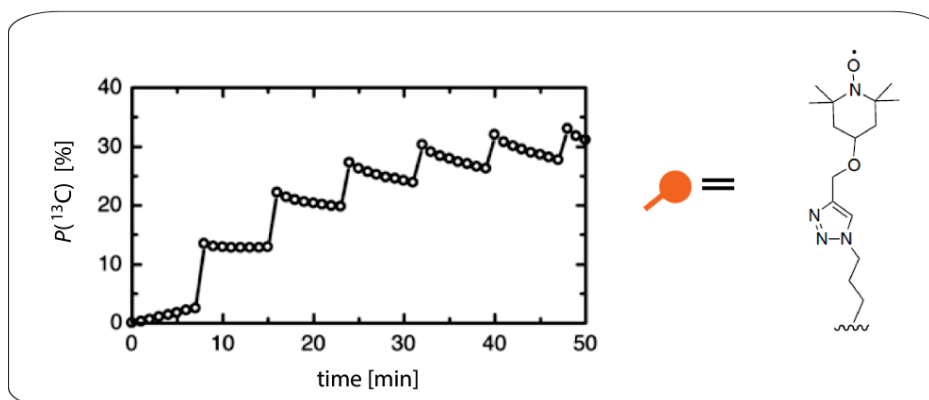


Fig. 4.12: Cross Polarization (CP) from ^1H to ^{13}C DNP was performed on 20 mg of HYP SO-2 (41 $\mu\text{mol/g}$) impregnated with 36 μl of a 3 M solution of $[1-^{13}\text{C}]$ sodium pyruvate in D_2O . A high polarization $P(^{13}\text{C}) = 36\%$ is reached in 32 min with a CP transfer every 7.5 min.

A third and more complex generation of this silica matrix dubbed HYP SO-3 (see Fig. 4.13) was obtained by changing the overall structure of the pores, therefore passing from a two-dimensional tubular conformation to a three-dimensional network of interconnected pores, which is hypothesized to be better for ^1H - ^1H spin diffusion. [37]

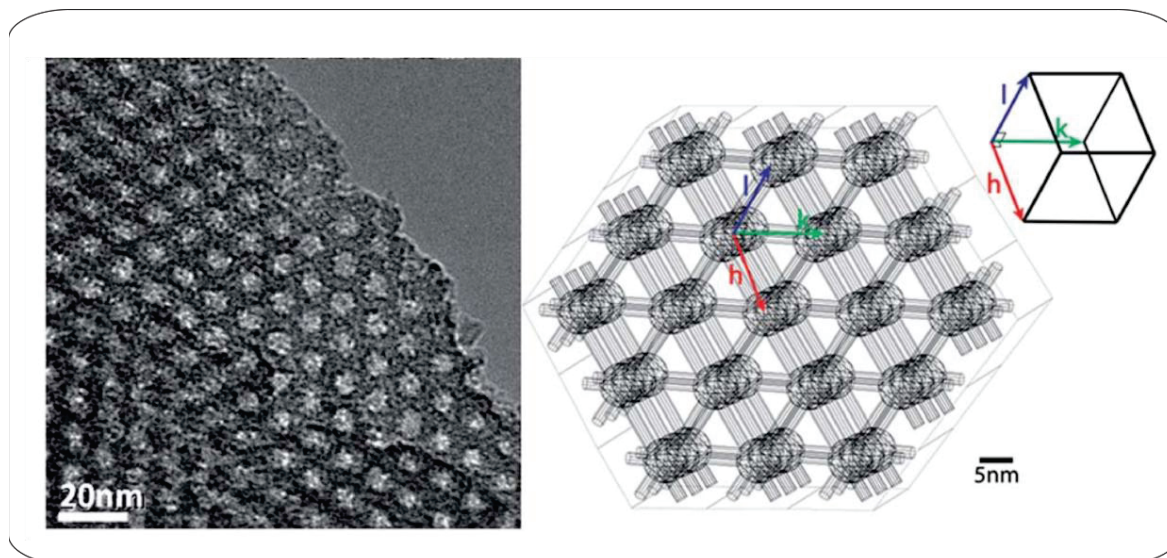


Fig. 4.13: (Left) Transmission electron microscopy (TEM) image of the cubic HYP SO-3 lattice. (Right) Schematic representation of the 3D pore structure with radicals distributed uniformly over the surfaces of the pores.

The well-designed structure of HYP SO-3 comprises a series of connections between the pores that allows one to achieve a proton polarization $P(^1\text{H}) = 63\%$ that is higher than what could be achieved with earlier generations of HYP SO-1 and HYP SO-2. Nevertheless, it was not possible to achieve a higher ^{13}C polarization with this material.

Finally, we recently introduced a fourth generation of HYP SO-4 with a rigid linker constituted of a phenylazide ring that attaches the TEMPO radical to the surface of the material. [38] However, this change did not translate directly into a higher proton polarization in our dissolution-DNP experiments at very low temperatures (see Fig. 4.14).

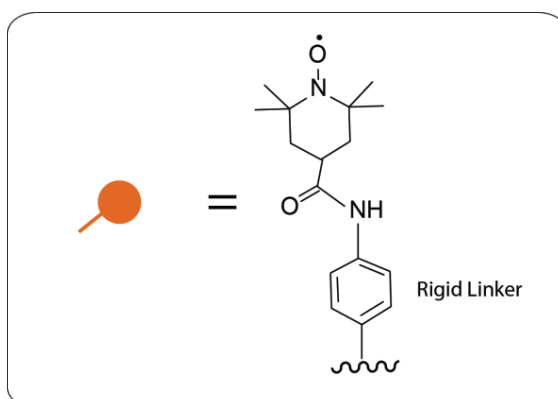


Fig. 4.14: Representation of a polarizing agent (PA) attached via a rigid linker to HYP SO-4.

4.4.5 Conclusions concerning HYP SO

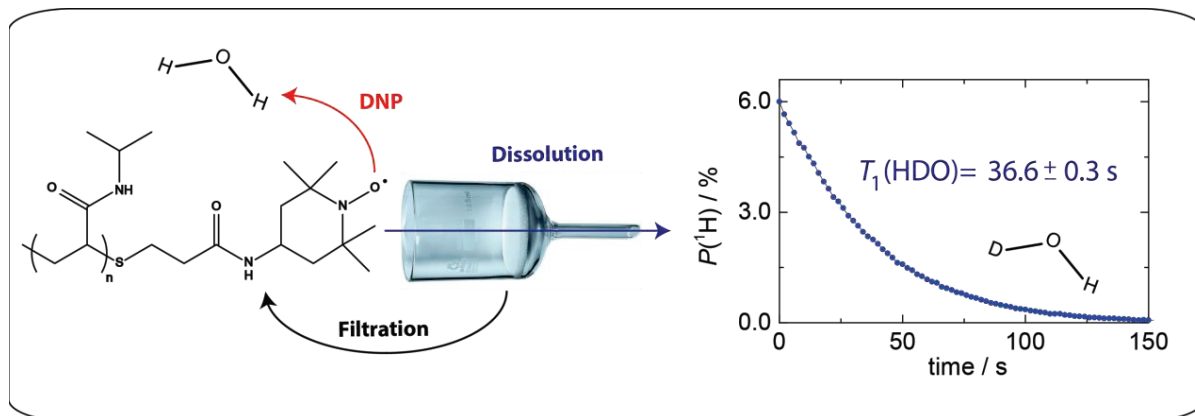
One of the principal advantages of using HYP SO materials is that glass-forming agents such as glycerol or DMSO, which are often not compatible with *in-vivo* experiments, can be avoided in the preparation of DNP samples. Indeed, the silica matrix can play a similar role as the glass-forming agents by preventing the crystallization of the solution to be polarized and thus allowing the DNP process to occur properly. Furthermore, these materials are not limited exclusively to TEMPO functionalities and thus allow access to a broad range of solid polarizing matrices. Several metabolites such as pyruvate, acetate, fumarate and Alanine-Glycine can be efficiently polarized with HYP SO, resulting in pure hyperpolarized solutions after filtration of the silica matrix. Finally, promising new generations of HYP SOs were synthesized at the CRMN in Lyon and at ETH Zürich (HYP SO-5, HYP SO-6 and HYP SO-7). These are currently tested in our laboratory at the EPFL.

4.5 Filterable Labeled Agents for Polarization (FLAP)

The use of glass-forming solvents like glycerol or DMSO in d-DNP, as described previously, has been mandatory to achieve a homogeneous distribution of the radicals and metabolites throughout the sample. Without a glassy matrix, the transfer of the polarization from electrons to nuclear spins is not effective. Even if the use of glycerol or DMSO as a glass-forming matrix is widely spread in the dissolution-DNP community, their main inconvenience is due to the presence as contaminants after the dissolution process. Furthermore, the glassy solvent is intimately mixed with the nitroxide radicals and, even at natural abundance, can be hyperpolarized at the same time as the metabolites, leading to a possible overlaps with the signals of interest after dissolution. Another inconvenience of this conventional method is the presence of radicals during the transfer process, which leads to paramagnetic relaxation and can destroy the polarization of sensitive nuclei like protons.

To overcome these two side effects, a novel generation of polymer-based polarizing agents dubbed FLAP for Filterable Labeled Agents for Polarization was synthesized. It simply consists of a well-known thermo-sensitive polymer *poly(N-isopropylacrylamide)*, also called *pNiPAM-COOH*, with covalently attached nitroxide radicals. By impregnation of this polymer with a solution that does not contain any glass-forming solvents, it is possible to achieve high enhancements by DNP of various metabolites of interest. The dissolution process is then followed by a simple filtration of the polymer, leading to hyperpolarized solutions that are free from any contaminants.

The filterable polymer FLAP described in this chapter is inspired by our work "*Filterable Agents for Hyperpolarization of Water, Metabolites, and Proteins*". [60]



4.5.1 Traditional DNP samples versus FLAP samples

In traditional DNP samples, as mentioned in the first part of this thesis, the use of glass-forming solvents as well as polarizing agents (PAs) such as nitroxide radicals are mandatory to perform DNP. Unfortunately, such PAs lead to a rapid nuclear spin relaxation during the dissolution process and the transfer to NMR or MRI systems. Indeed, protons are very sensitive to paramagnetic relaxation compared to low gamma nuclei such as carbon-13 or nitrogen-15. This is why hyperpolarization of H₂O or HDO remains a particular challenge, because even very low concentrations of free radicals may cause fast relaxation of the protons during the dissolution process. The use of hyperpolarized water has recently become interesting because it allows one to detect ligand binding to macromolecules with DNP-enhanced Water-LOGSY (Water-Ligand Observed via Gradient Spectroscopy). [61] Hyperpolarized water can also be used as a contrast agent in angiography. [62] These applications are hampered by the short $T_1(^1\text{H})$ of HDO resulting from the presence of free radicals in solution. A disappointingly short $T_1(^1\text{H}) = 9.8$ s in HDO after dissolution was determined at 500 MHz in previous studies using DNP-enhanced Water-LOGSY [61], whereas $T_1(^1\text{H})$ is 37 s in degassed and pure H₂O at pH 7. [62] As discussed previously, different strategies have recently been proposed for neutralizing the PAs, for example, via precipitation or filtration [42], solvent extraction [63], or scavenging. [22] Nevertheless, all of these methods have an inconvenience in common: they require a few seconds to be carried out, which implies losses due to relaxation, and may introduce unwanted co-solutes. More recently, a class of HYPISO (HYper Polarizing SOLids) [36, 37, 38] composed of mesoporous silica matrices with free radicals anchored on their surface was introduced. Although these PAs seemed to be particularly suitable for ¹³C hyperpolarization, the proton polarization $P(^1\text{H})$ suffered considerable losses during the dissolution process, presumably because the protons are subject to rapid paramagnetic relaxation before being expelled from the porous network. Because of this inconvenience, the use of HYPISO did not allow us to match the best hyperpolarized signals of HDO after dissolution.

Recently, water hyperpolarization has been demonstrated using thermoresponsive hydrogels [64] via Overhauser DNP, showing modest enhancements $\epsilon(^1\text{H}) = -27$ at $B_0 = 0.345$ T. [56] More recently, these hydrogels were used in d-DNP to generate a polarization $P(^{13}\text{C}) = 2.1$ % in *tert*-butanol. [65] The sudden interest in this class of polymer [66] is due to the fact that they are very soluble in water under ambient conditions, yet precipitate when the temperature increases beyond 32 °C (see Fig. 4.15). This last point is of great interest for d-DNP since the polymer can be extracted during the dissolution process, after superheated D₂O is injected to melt the DNP sample.

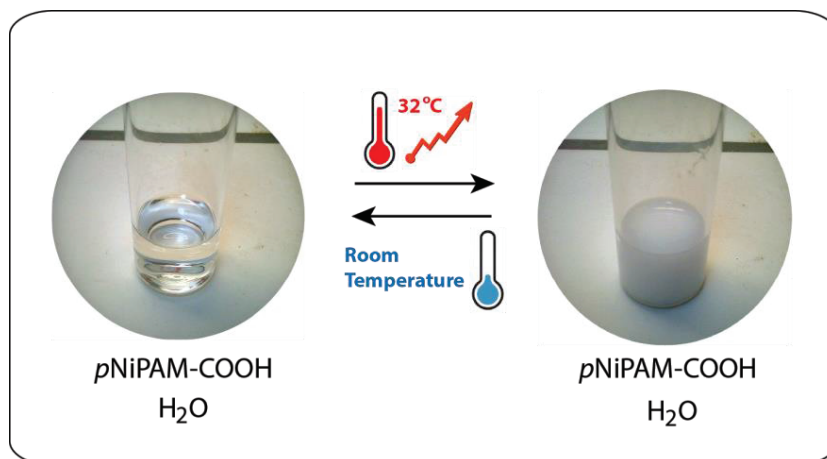


Fig. 4.15: Solution of water containing the polymer $pNiPAM-COOH$ at different temperatures. When the sample is heated above $32\text{ }^{\circ}C$, the polymer precipitates and a white suspension is observed.

Because of this last property, it appears of interest to use this class of polymer for our dissolution experiments by attaching radicals to it. The polymer dubbed FLAP (Filterable Labeled Agents for Polarization) was synthesized using $poly(N\text{-isopropylacrilamide})\text{-COOH}$ ($pNiPAM\text{-COOH}$) with an average molecular mass of 10 kDa [66] and 4-amino-2,2,6,6-tetramethylpiperidin-1-oxyl (4-amino TEMPO) (Fig. 4.16 A). The synthesis of FLAP is described in more detail in the Supporting Information at the end of this thesis. The resulting polymer containing the radicals is dissolved in water, shock frozen, and subsequently cryo-liophilized. The final result is a very fine powder with a uniform distribution of PAs attached to the polymer that resembles the statistical distribution in the dissolved phase. The powder can then be impregnated at room temperature with H_2O , with solvents, or with aqueous solutions containing the metabolites to be polarized (see Fig. 4.16 B). The addition of 1 M NaCl is mandatory to ensure that the polymer remains in suspension and prevents it from dissolving below $32\text{ }^{\circ}C$. Typically, 500 mg of FLAP are used for 1 mL of solution. Prior to freezing, the suspension is centrifuged for 30 s to ensure a homogeneous impregnation of FLAP with the solution. Then, the impregnated powder is shock-frozen to 4.2 K in the liquid helium bath of the polarizer, and further cooled down to 1.2 K for DNP measurements. After the usual optimizations of $P(^1H)$ and CP, superheated D_2O rapidly melts the frozen suspension and FLAP can be quantitatively filtered in-line with a cellulose filter and recollected for further use. After the dissolution process, the only remaining additive is NaCl at concentration of 20 mM, which is lower than in most buffer media that are routinely used for *in vitro* and *in vivo* studies.

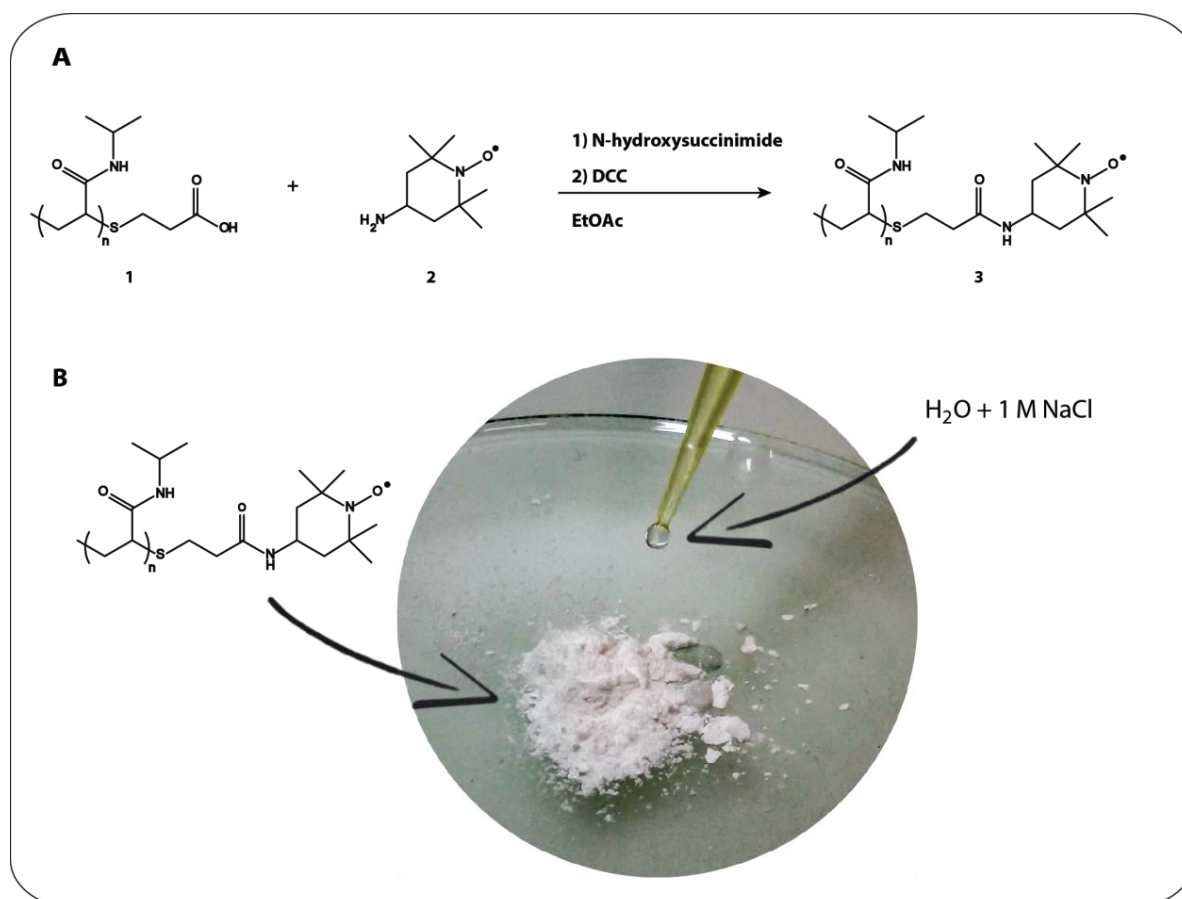


Fig. 4.16: (A) Synthesis of FLAP with an amino-TEMPO unit covalently attached to the carboxylic acid of the terminal residue of *p*NiPAM-COOH (with $n = 60-100$) (see Supporting Information). (B) Preparation of the DNP sample composed of FLAP impregnated with 1 M solution of NaCl in pure H_2O .

4.5.2 Hyperpolarization of water

One of the most challenging d-DNP experiments is the observation of hyperpolarized signals of liquid water. Indeed, protons are much more sensitive than ^{13}C to paramagnetic impurities (free radicals), fluctuations of the magnetic field and fast exchange, so that the hyperpolarized signals of 1H in liquid water tend to relax quickly. [61] FLAP was synthesized in order to extend the lifetime of hyperpolarized HDO after dissolution, because FLAP precipitates at temperatures above 32 °C, which are usually reached during dissolution ($T = 140$ °C in our case), making in-line filtration straightforward.

The DNP sample used for this specific experiment was composed of 50 mg of 25 % spin-labeled solid FLAP intimately mixed with 75 % solid *p*NiPAM-COOH to ensure a good distribution and concentration of the radical species. The resulting powder was impregnated with 100 μ l of a 1 M solution of NaCl in H_2O and shock-frozen in our DNP polarizer at $B_0 = 6.7$ T. [32, 33, 34] The sample was then irradiated at $f_{\mu W} = 187.9$ GHz (maximum of the positive polarization lobe) using modulated microwave frequency modulation, as described in previous chapters. [67]

Fig. 4.17 represents the comparison between the proton DNP build-up curves of a standard DNP sample (25 mM TEMPOL in a mixture of H₂O/glycerol-*d*₈ (v/v : 1/1)) and the FLAP sample. The first observation is that the build-up time for FLAP is much longer ($T_{\text{bup}} = 788 \pm 7$ s) than for the standard sample ($T_{\text{bup}} = 453 \pm 4$ s). In addition, the maximum of ¹H polarization achievable by using FLAP is $P(^1\text{H}) = 63.3\%$ in comparison with standard samples where $P(^1\text{H}) \approx 90\%$ has been recorded. The ¹H NMR spectra of both samples were measured after the DNP build-up curves have reached their plateau. An asymmetry in the FLAP sample (composed only of H₂O) is observable and arises from the high nuclear spin polarization.

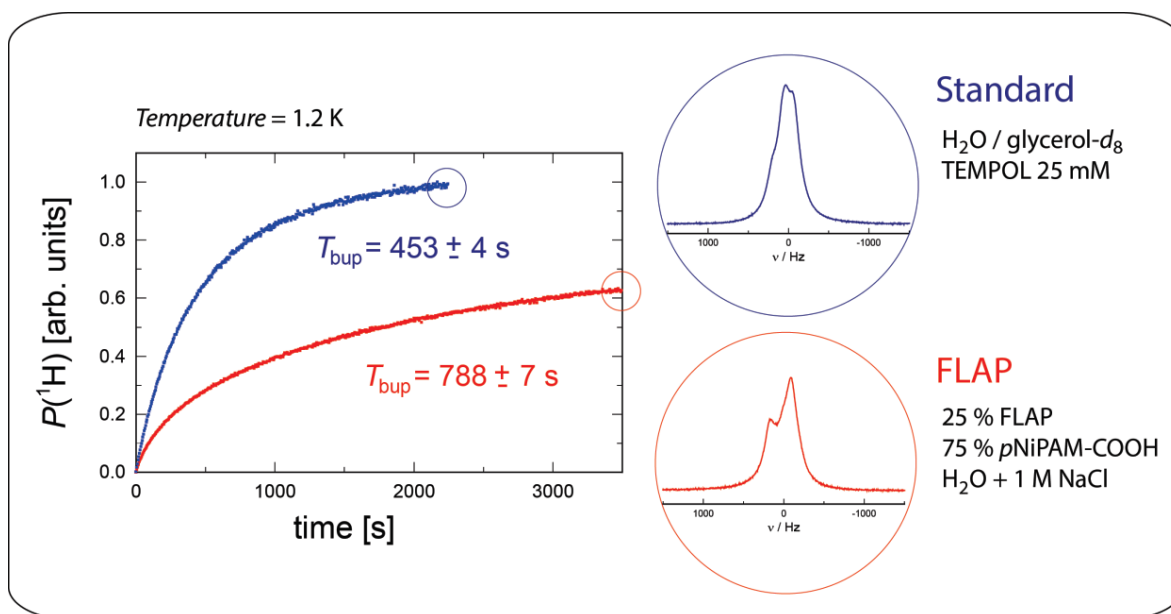


Fig. 4.17: Build-up curves of the proton polarization $P(^1\text{H})$ measured at $T = 1.2$ K for a standard DNP sample (25 mM TEMPOL with H₂O/glycerol-*d*₈ (v/v : 1/1)) and a FLAP sample (25 % FLAP + 75 % pNiPAM-COOH with 1 M NaCl in H₂O). The ¹H NMR spectra were acquired in both cases by applying 0.3° pulses at intervals of 5 s. Their build-up times were $T_{\text{bup}} = 453 \pm 4$ s and $T_{\text{bup}} = 788 \pm 7$ s respectively. The ¹H NMR spectrum of the FLAP sample shows an asymmetry after 3500 s, resulting from the high polarization of $P(^1\text{H}) = 63.3\%$.

This last sample containing FLAP was then quickly dissolved by superheated D₂O at 140 °C following the normal procedure in our laboratory, with a transfer in about 10 s through a magnetic tunnel [18] and an injection into a 500 MHz NMR spectrometer. The polymer was retained by using a small cellulose filter placed at the bottom of the dissolution stick. As shown in Fig. 4.18, FLAP was fully retained in the filter during this process. For a ratio [D₂O] : [H₂O] = 50 : 1, the ¹H NMR spectrum essentially shows HDO, while the final NaCl concentration is about 20 mM. The proton NMR spectra were measured at intervals of 2 s with 0.1° pulses to prevent saturating the receiver and destroying the polarization. In Fig. 4.18 A, a series of ten spectra taken at 40 s intervals is shown. The intense signal in the first spectrum leads to massive radiation damping with a linewidth exceeding 1500 Hz (blue). [68] The lines then become narrower as the polarization decays towards thermal equilibrium (red). Once FLAP has been completely removed by filtration, the longitudinal relaxation time $T_1(\text{HDO}) = 36.6 \pm 0.3$ s of the hyperpolarized HDO is shown in Fig. 4.18 B. A proton polarization of $P(^1\text{H}) = 6\%$ was achieved.

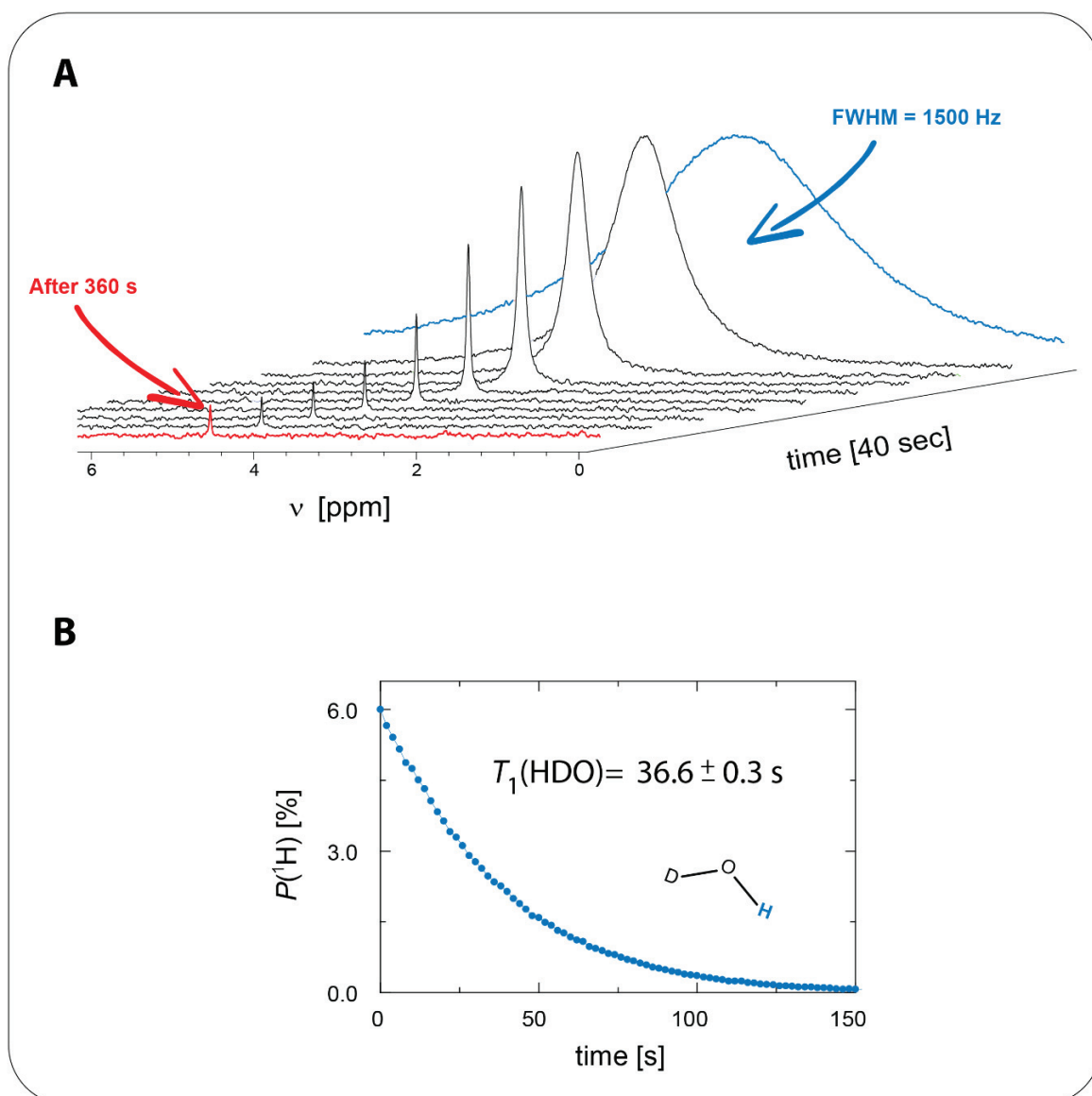


Fig. 4.18: (A) Proton spectra of hyperpolarized HDO observed at 500 MHz after FLAP was completely removed by filtration. A set of ten spectra was measured with 0.1° pulses at intervals of 40 s. The first hyperpolarized ^1H spectrum acquired immediately after injection has a width at half height (FWHM) of 1.5 kHz due to radiation damping. (B) Longitudinal relaxation of hyperpolarized HDO obtained with FLAP with $P(^1\text{H}) = 6\%$ and $T_1(\text{HDO}) = 36.6 \pm 0.3\text{ s}$, indicating that the polymer was efficiently removed by filtration.

In order to prove the utility FLAP for the hyperpolarization of water by d-DNP, we have still to compare the hyperpolarized signals obtained either with traditional DNP samples or with FLAP. In Fig. 4.19, the signals for both samples are compared after hyperpolarization and dissolution. For the standard sample, 5 frozen beads of $10\ \mu\text{l}$ each of 3 M sodium ascorbate in D_2O were added prior to dissolution in order to scavenge the radicals after the dissolution. [22] In addition to a larger FWHM = 1500 Hz and longer relaxation time $T_1 = 36.6\text{ s}$ for the FLAP sample in comparison with the standard one (FWHM = 915 Hz and $T_1 = 18.9\text{ s}$), the ^1H NMR spectrum does not show any traces of contaminants, which is not the case for the standard DNP sample where some antiphase peaks due to glycerol- d_8 are visible.

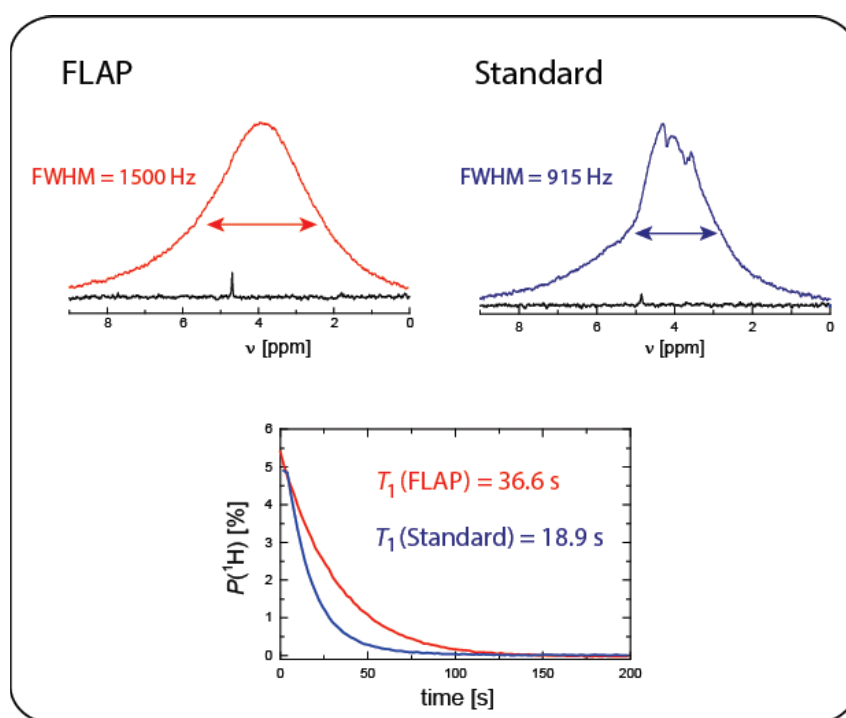


Fig. 4.19: Hyperpolarized proton spectra after dissolution-DNP of a sample containing FLAP mixed with 1 M NaCl in H₂O and a standard DNP sample containing 25 mM TEMPOL in H₂O/glycerol-*d*₈ (v/v : 1/1) with addition of frozen beads of ascorbate to scavenge the radicals. The FLAP sample shows a FWHM = 1500 Hz with a relatively long $T_1 = 36.6$ s after dissolution, which confirms the absence of contaminants like free radicals and the efficiency of the filtration of the polymer. The Standard sample shows signals in antiphase that are due to the presence of glycerol-*d*₈ in the sample. The resulting $T_1 = 18.9$ s is shorter than the one obtained with FLAP because of the presence of free radicals in solution (the scavenging process with ascorbate is not instantaneous).

4.5.3 Hyperpolarization of metabolites

After the successful hyperpolarization and dissolution of water, it was of interest to test FLAP for the ¹³C hyperpolarization of different metabolites. As before, a DNP sample of 50 mg was prepared with 25 % spin-labeled FLAP and 75 % *p*NiPAM-COOH. This powder was then impregnated with a mixture of 0.5 M [1-¹³C] sodium pyruvate, 0.5 M [1-¹³C] sodium acetate and 0.1 M [1-¹³C] alanine in 100 μl H₂O/D₂O (10:90). This sample was irradiated at $f_{\mu W} = 188.3$ GHz (maximum negative proton polarization) using microwave frequency modulation. [67]

In Fig. 4.20, the build-up of $P(^{13}\text{C})$ in [1-¹³C] metabolites is shown. Cross-Polarization from ¹H to ¹³C was used at $T = 1.2$ K at intervals of 600 s (10 min). [33] The discrete steps arise from the ¹H - ¹³C CP transfers resulting in a rapid increase of the carbon polarization within a few milliseconds. After reaching the maximum ¹³C polarization, the sample was quickly dissolved and FLAP was retained as before in a cellulose filter. The pure hyperpolarized solution was transferred and injected into an NMR tube awaiting in a 500 MHz NMR spectrometer. The first spectrum was recorded immediately after dissolution and corresponds to $P(^{13}\text{C}) = 8.3$ % for pyruvate, $P(^{13}\text{C}) = 7.6$ % for acetate, and $P(^{13}\text{C}) = 5.9$ % for alanine. These levels of polarization are relatively low in comparison with the results obtained with standard DNP samples or even with HYPISO. [36] This could be explained by the fact that the polymer is impregnated with the solution, which results in a less homogeneous distribution of the metabolites in the sample which hampers the performance of the Cross-Polarization process.

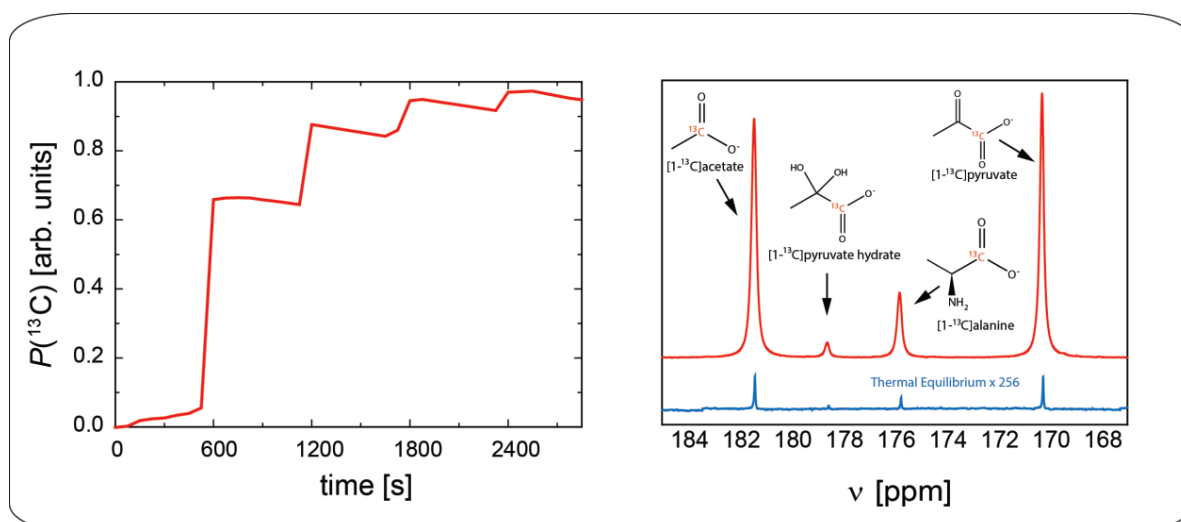


Fig. 4.20: (Left) Stepwise build-up of $P(^{13}\text{C})$ achieved by CP in a mixture of $[^{1-13}\text{C}]$ sodium pyruvate, $[^{1-13}\text{C}]$ sodium acetate, and $[^{1-13}\text{C}]$ alanine in 100 μL $\text{H}_2\text{O}/\text{D}_2\text{O}$ (10:90) with 50 mg of 25 % spin-labeled FLAP and 75 % $p\text{NiPAM-COOH}$. An adiabatic CP was performed every 10 min at $T = 1.2$ K. (Right) Hyperpolarized ^{13}C spectrum acquired immediately after dissolution, and compared with its thermal equilibrium (enlarged 256 times). The polarization was found to be $P(^{13}\text{C}) = 8.3\%$ for pyruvate, $P(^{13}\text{C}) = 7.6\%$ for acetate and $P(^{13}\text{C}) = 5.9\%$ for alanine.

4.5.4 Hyperpolarization of proteins

Finally, based on the positive results for the hyperpolarization of HDO, we decided to transfer the polarization to the protein Osteopontin (OPN220, composed of 220 amino acids) by chemical exchange and/or Overhauser effects. We used the same DNP sample as before, composed of FLAP with 100 μL H_2O and 1 M NaCl with a frequency-modulated microwave irradiation of the positive lobe at $f_{\mu\text{W}} = 187.9$ GHz. The OPN protein was dissolved in a buffer at pH = 6.5, and 150 μL were placed in an NMR tube in a 500 MHz NMR spectrometer and 750 μL of the hyperpolarized HDO was injected.

In the following Fig. 4.21, the proton signals of OPN are presented immediately after injection of the hyperpolarized HDO (red) and after the signal has relaxed back to its thermal equilibrium (blue). The ^1H NMR signal of Osteopontin is also shown as a function of time by applying selective 90° pulses while preserving the hyperpolarized signal.

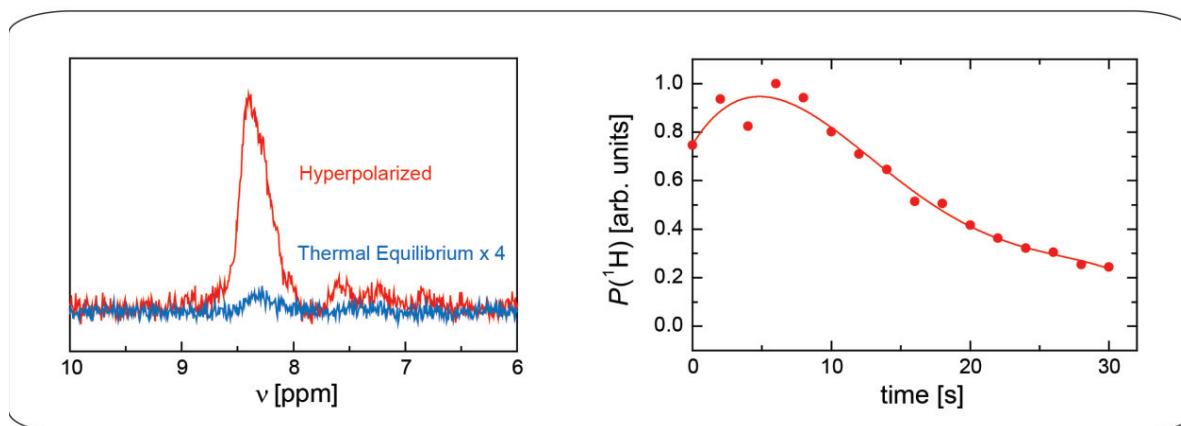


Fig. 4.21: (Left) Proton NMR spectrum of hyperpolarized Osteopontin (OPN) protein recorded 8s after mixing (red) compared to its thermal equilibrium (blue, amplified by a factor 4). (Right) Proton polarization of the OPN signal near 8.2 ppm as a function of time, monitored by applying 90° pulses.

The hyperpolarized signal of OPN shows a maximum enhancement factor $\epsilon = 35$ (8 s after mixing) with respect to its thermal equilibrium. This hyperpolarization lasts for several tens of seconds, apparently following the slow relaxation of HDO.

In addition to this measurement, a SOFAST-HMQC sequence [69] has been applied to Osteopontin. [63] The concentration of OPN was 1.5 mM in 150 μl PBS buffer prior to injection of 750 μl of hyperpolarized HDO. Fig. 4.22 shows the SOFAST-HMQC of OPN after dissolution-DNP. In this experiment, it is worth noticing that the enhancements are not uniform across the protein.

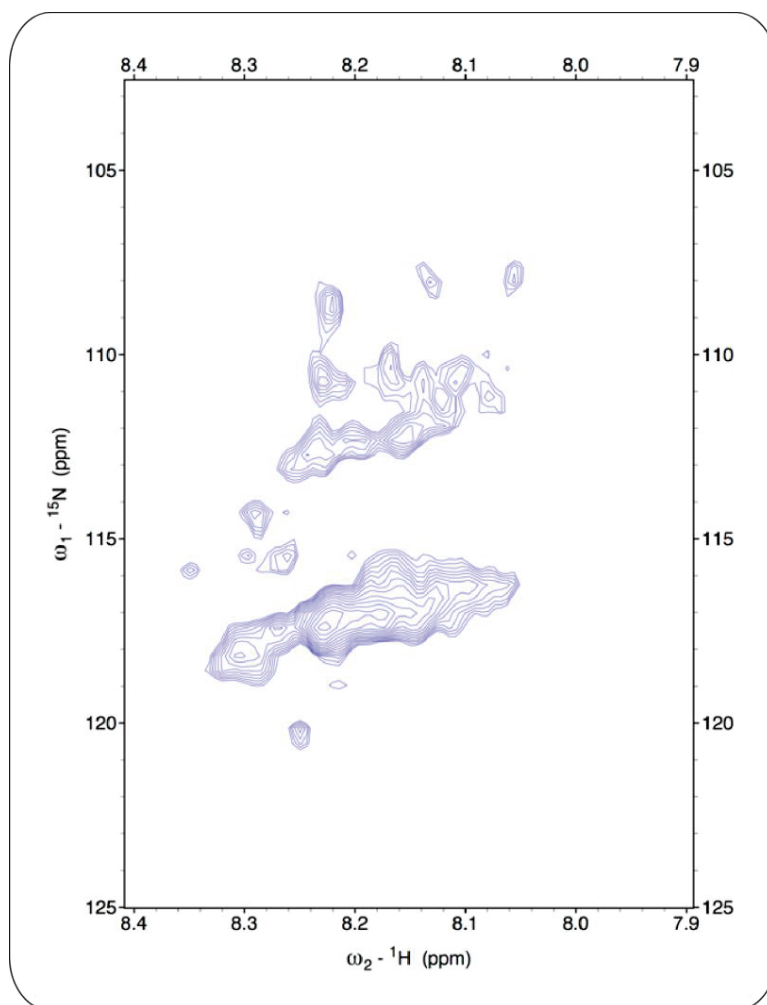


Fig. 4.22: SOFAST-HMQC spectrum of an approximately five-fold diluted 1.5 mM solution of the protein osteopontin (OPN) at pH 6.5 and 300 K in a 500 MHz NMR spectrometer enhanced by polarization transfer from HDO through a combination of intermolecular proton transfer and Overhauser effects.

4.5.5 Stability of FLAP

One important point to mention is the stability of FLAP under ambient conditions. FLAP should be preferably stored as a dry powder to avoid the degradation of the TEMPO radicals, which are sensitive. However, FLAP impregnated with water and NaCl also showed a reasonable stability at room temperature, even after several weeks of storage. In Fig. 4.23, the DNP build-up curves of three identical samples are shown for different room-temperature storage periods. After two weeks, DNP yielded a proton polarization $P(^1\text{H}) > 50\%$, which confirms its relatively good stability.

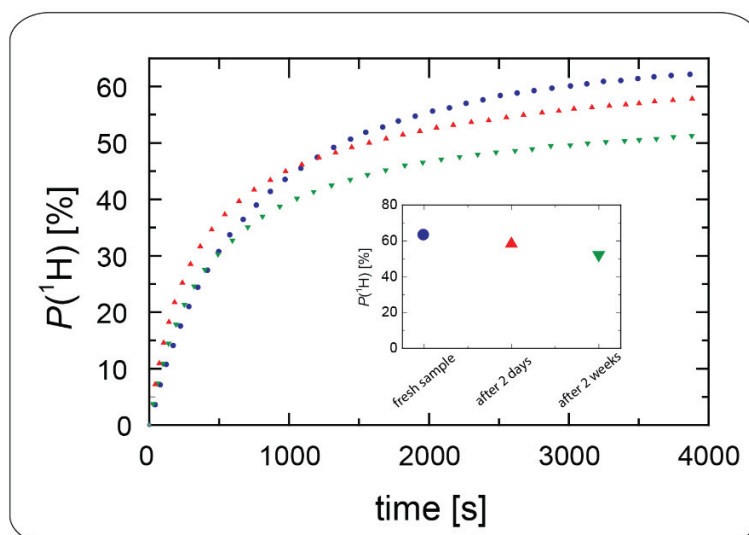


Fig.4.23: Comparison of the build-up of $P(^1\text{H})$ in H_2O at 1.2 K and 6.7 T for three similar samples, all consisting of 25 mg FLAP impregnated with 50 mL H_2O with 1 M NaCl, measured: 1) directly after preparation (blue circles, build-up with a single time constant $T_{\text{bup}} = 788 \pm 7$ s); 2) after storing the impregnated polymer for two days at room temperature (red triangles, showing two time constants $T_{\text{bup1}} = 214 \pm 2$ s and $T_{\text{bup2}} = 1412 \pm 10$ s); and 3) after storing for two weeks at room temperature (green triangles, with two time constants $T_{\text{bup1}} = 273 \pm 3$ s and $T_{\text{bup2}} = 1469 \pm 11$ s).

4.5.6 Conclusions concerning FLAP

In this chapter, a new class of spin-labeled polymers dubbed FLAP were synthesized for dissolution-DNP. The particularity of these polarizing agents is that they do not require any glassing agents, therefore no contaminants such as glycerol are present after the dissolution process. Moreover, they can be simply impregnated with a solution or solvent that one wishes to polarize containing 1 M NaCl or other sodium salts, including metabolites with Na⁺ as counterions, like sodium pyruvate or sodium acetate. The resulting FLAP suspension can then be quantitatively separated by filtration during dissolution, leading to 20 mM NaCl, which is far below the range of physiological NaCl concentrations. High proton polarization levels $P(^1\text{H}) = 63.3\%$ were achieved in 4500 s (75 min) for H₂O impregnated in FLAP and a pure hyperpolarized solution was produced after filtration of the polymer. For hyperpolarized HDO, we have determined $T_1(^1\text{H}) = 36.6 \pm 0.3$ s, which confirms that FLAP was fully retained during the dissolution process. In addition, Cross-Polarization was used in combination with FLAP for different metabolites (pyruvate, acetate and alanine). Finally, these PAs may be stored at room temperature for a long period without significant degradation.

This family of filterable spin-labeled polymers should find various applications in d-DNP experiments, in particular for drug discovery [70, 71] and metabolomics [72], where the use of FLAP makes it possible to obtain pure hyperpolarized solutions without any traces of contaminants, with longer relaxation times T_1 that allow one to follow chemical reactions on extended period.

References

1. S. R. Hartmann and E. L. Hahn, *Nuclear Double Resonance in Rotating Frame*, 1962, Phys. Rev. 128, 2042-2053.
2. B. Vuichoud, J. Milani, Q. Chappuis, A. Bornet, G. Bodenhausen and S. Jannin, *Measuring absolute spin polarization in dissolution-DNP by Spin Polarimetry Magnetic Resonance (SPY-MR)*, 2015, J. Magn. Reson. 260, 127-135.
3. K. Golman, R. in't Zandt, M. Lerche, R. Pehrson and J. H. Ardenkjaer-Larsen, *Metabolic imaging by hyperpolarized ^{13}C magnetic resonance imaging for in vivo tumor diagnosis*, 2006, Cancer Res. 66, 10855-10860.
4. S. J. Nelson, J. Kurhanewicz, D. B. Vigneron, P. E. Z. Larson, A. L. Harzstark, M. Ferrone, M. van Criekinge, J. W. Chang, R. Bok, I. Park, G. Reed, L. Carvajal, E. J. Small, P. Munster, V. K. Weinberg, J. H. Ardenkjaer-Larsen, A. P. Chen, R. E. Hurd, L. I. Odegardstuen, F. J. Robb, J. Tropp and J. A. Murray, *Metabolic Imaging of Patients with Prostate Cancer Using Hyperpolarized $[1-^{13}\text{C}]$ Pyruvate*, 2013, Sci. Transl. Med. 5, 198ra108.
5. M. E. Merritt, C. Harrison, W. Mander, C. R. Malloy and A. D. Sherry, *Dipolar cross-relaxation modulates signal amplitudes in the ^1H NMR spectrum of hyperpolarized $[^{13}\text{C}]$ formate*, 2007, J. Magn. Reson. 189, 280-285.
6. J. Tropp, *Multiplet asymmetry and multi-spin order in liquid-state NMR spectra of hyperpolarized compounds*, 2010, Proc. Intl. Soc. Mag. Reson. Med. 18, 1026.
7. M. C. D. Tayler, I. Marco-Rius, M. I. Kettunen, K. M. Brindle, M. H. Levitt and G. Pileio, *Direct Enhancement of Nuclear Singlet Order by Dynamic Nuclear Polarization*, 2012, J. Am. Chem. Soc. 134, 7668-7671.
8. J. Y. C. Lau, A. P. Chen, Y. P. Gu and C. H. Cunningham, *A calibration-based approach to real-time in vivo monitoring pyruvate C_1 and C_2 polarization using the J_{CC} spectral asymmetry*, 2013, NMR Biomed. 26, 1233-1241.
9. I. Marco-Rius and K.M. Brindle, *Measuring polarization by J_{CC} doublets asymmetry in hyperpolarized $[1,2-^{13}\text{C}_2]$ pyruvate may be distorted by singlet order*, 2014, in 55th ENC conference, Boston.
10. J. S. Waugh, O. Gonen and P. Kuhns, *Fourier-Transform NMR at Low-Temperatures*, 1987, J. Chem. Phys. 86, 3816-3818.
11. N. S. Sullivan and R. V. Pound, *Nuclear-Spin-Lattice Relaxation of Solid Hydrogen at Low-Temperatures*, 1972, Phys. Rev. A 6, 1102-1107.
12. C. M. Edwards, D. Zhou and N. S. Sullivan, *Unusual Low-Temperature Effects on the NMR Line-Shapes in Solid Hydrogen*, 1986, Phys. Rev. B 34, 6540-6542.
13. P. Kuhns, O. Gonen and J. S. Waugh, *Proton Spin-Spin and Spin-Lattice Relaxation in $\text{CaSO}_4 \cdot x\text{H}_2\text{O}$ Below 1 K*, 1989, J. Magn. Reson. 82, 231-237.
14. A. Abragam, M. Chapellier, J. F. Jacquinet and M. Goldman, *Absorption Lineshape of Highly Polarized Nuclear Spin Systems*, 1973, J. Magn. Reson. 10, 322-346.
15. N. N. Kuzma, P. Hakansson, M. Pourfathi, R. K. Ghosh, H. Kara, S. J. Kadlecsek, G. Pileio, M. H. Levitt and R. R. Rizi, *Lineshape-based polarimetry of dynamically-polarized $^{15}\text{N}_2\text{O}$ in solid-state mixtures*, 2013, J. Magn. Reson. 234, 90-94.
16. K. J. Donovan, A. Lupulescu and L. Frydman, *Heteronuclear Cross-Relaxation Effects in the NMR Spectroscopy of Hyperpolarized Targets*, 2014, Chemphyschem 15, 436-443.
17. S. Schaublin, A. Hohener and R. R. Ernst, *Fourier Spectroscopy of Nonequilibrium States, Application to CIDNP, Overhauser Experiments and Relaxation-Time Measurements*, 1974, J. Magn. Reson. 13, 196-216.
18. J. Milani, B. Vuichoud, A. Bornet, P. Miéville, R. Mottier, S. Jannin and G. Bodenhausen, *A magnetic tunnel to shelter hyperpolarized fluids*, 2015, Rev. Sci. Instrum. 86, 024101.

19. C. Dalvit and G. Bodenhausen, *Proton Chemical-Shift Anisotropy: Detection of Cross-Correlation with Dipole-Dipole Interactions by Double-Quantum Filtered Two-Dimensional NMR Exchange Spectroscopy*, 1989, Chem. Phys. Lett. 161, 554-560.
20. S. J. Clark, M. D. Segall, C. J. Pickard, P. J. Hasnip, M. J. Probert, K. Refson and M. C. Payne, *First principles methods using CASTEP*, 2005, Z. Kristallogr. 220, 567-570.
21. SpinDynamica code for Mathematica, programmed by Malcolm H. Levitt, with contributions from Jyrki Rantaharju, Andreas Brinkmann, and Soumya Singha Roy, available at www.SpinDynamica.soton.ac.uk
22. P. Miéville, P. Ahuja, R. Sarkar, S. Jannin, P. R. Vasos, S. Gerber-Lemaire, M. Mishkovsky, A. Comment, R. Gruetter, O. Ouari, P. Tordo and G. Bodenhausen, *Scavenging Free Radicals To Preserve Enhancement and Extend Relaxation Times in NMR using Dynamic Nuclear Polarization*, 2010, Angew. Chem. Int. Edit. 49, 7834-7834.
23. B. Vuichoud, J. Milani, A. Bornet, R. Melzi, S. Jannin and G. Bodenhausen, *Hyperpolarization of Deuterated Metabolites via Remote Cross-Polarization and Dissolution Dynamic Nuclear Polarization*, 2014, J. Phys. Chem. B 118, 1411-1415.
24. M. Carravetta, O. G. Johannessen and M. H. Levitt, *Beyond the T_1 limit: Singlet nuclear spin states in low magnetic fields*, 2004, Phys. Rev. Lett. 92, 153003.
25. G. Pileio, S. Bowen, C. Laustsen, M. C. D. Tayler, J. T. Hill-Cousins, L. J. Brown, R. C. D. Brown, J. H. Ardenkjaer-Larsen and M. H. Levitt, *Recycling and Imaging of Nuclear Singlet Hyperpolarization*, 2013, J. Am. Chem. Soc. 135, 5084-5088.
26. Y. S. Feng, T. Theis, X. F. Liang, Q. Wang, P. Zhou and W. S. Warren, *Storage of Hydrogen Spin Polarization in Long-Lived $^{13}\text{C}_2$ Singlet Order and Implications for Hyperpolarized Magnetic Resonance Imaging*, 2013, J. Am. Chem. Soc. 135, 9632-9635.
27. A. W. Barb, S. K. Hekmatyar, J. N. Glushka and J. H. Prestegard, *Exchange facilitated indirect detection of hyperpolarized $^{15}\text{ND}_2$ -amido-glutamine*, 2013, J. Magn. Reson. 228, 59-65.
28. E. Chiavazza, A. Viale, M. Karlsson and S. Aime, *^{15}N -Permethylated amino acids as efficient probes for MRI-DNP applications*, 2013, Contrast Media Mol. 8, 417-421.
29. A. W. Barb, S. K. Hekmatyar, J. N. Glushka and J. H. Prestegard, *Probing alanine transaminase catalysis with hyperpolarized $^{13}\text{CD}_3$ -pyruvate*, 2011, J. Magn. Reson. 212, 304-310.
30. H. Nonaka, R. Hata, T. Doura, T. Nishihara, K. Kumagai, M. Akakabe, M. Tsuda, K. Ichikawa and S. Sando, *A platform for designing hyperpolarized magnetic resonance chemical probes*, 2013, Nat. Commun. 4, 2411.
31. L. Lumata, M. E. Merritt and Z. Kovacs, *Influence of deuteration in the glassing matrix on ^{13}C dynamic nuclear polarization*, 2013, Phys. Chem. Chem. Phys. 15, 7032-7035.
32. S. Jannin, A. Bornet, R. Melzi and G. Bodenhausen, *High field dynamic nuclear polarization at 6.7 T: Carbon-13 polarization above 70% within 20 min*, 2012, Chem. Phys. Lett. 549, 99-102.
33. A. Bornet, R. Melzi, A. J. P. Linde, P. Hautle, B. van den Brandt, S. Jannin and G. Bodenhausen, *Boosting Dissolution Dynamic Nuclear Polarization by Cross Polarization*, 2013, J. Phys. Chem. Lett. 4, 111-114.
34. A. Comment, B. van den Brandt, K. Uffmann, F. Kurdzesau, S. Jannin, J. A. Konter, P. Hautle, W. T. H. Wenckebach, R. Gruetter and J. J. van der Klink, *Design and performance of a DNP prepolarizer coupled to a rodent MRI scanner*, 2007, Concept. Magn. Reson. B 31B, 255-269.
35. J. Milani, B. Vuichoud, A. Bornet, R. Melzi, S. Jannin and G. Bodenhausen, *Hyperpolarization of Nitrogen-15 Nuclei by Cross Polarization and Dissolution Dynamic Nuclear Polarization*, 2016, Rev. Sci. Instrum., submitted.
36. D. Gajan, A. Bornet, B. Vuichoud, J. Milani, R. Melzi, H. A. van Kalker, L. Veyre, C. Thieuleux, M. P. Conley, W. R. Grüning, M. Schwarzwälder, A. Lesage, C. Copéret, G. Bodenhausen, L. Emsley and S. Jannin, *Hybrid polarizing solids for pure hyperpolarized liquids through dissolution dynamic nuclear polarization*, 2014, P. Natl. Acad. Sci. USA 111, 14693-14697.

37. D. Baudouin, H. A. van Kalker, A. Bornet, B. Vuichoud, L. Veyre, M. Cavailles, M. Schwarzwälder, W.-C. Liao, D. Gajan, G. Bodenhausen, L. Emsley, A. Lesage, S. Jannin, C. Copéret and C. Thieuleux, *Cubic Three-Dimensional Hybrid Silica Solids for Nuclear Hyperpolarization*, 2016, Chem. Sci., DOI: 10.1039/C6SC02055K.
38. W. R. Grüning, H. Bieringer, M. Schwarzwälder, D. Gajan, A. Bornet, B. Vuichoud, J. Milani, D. Baudouin, L. Veyre, A. Lesage, S. Jannin, G. Bodenhausen, C. Thieuleux and C. Copéret, *Phenylazide Hybrid-Silica – Polarization Platform for Dynamic Nuclear Polarization at Cryogenic Temperatures*, 2016, Helv. Chim. Acta, DOI: 10.1002/hlca.201600122.
39. T. Harris, C. Bretschneider and L. Frydman, *Dissolution DNP NMR with solvent mixtures: Substrate concentration and radical extraction*, 2011, J. Magn. Reson. 211, 96-100.
40. J. H. Ardenkjaer-Larsen, A. M. Leach, N. Clarke, J. Urbahn, D. Anderson and T. W. Skloss, *Dynamic Nuclear Polarization Polarizer for Sterile Use Intent*, 2011, NMR Biomed 24, 927-932.
41. D. B. Whitt, A. M. Leach, P. Miller and E. Telfeyan, *Method and apparatus for the dissolution and filtration of a hyperpolarized agent with a neutral dissolution media*, 2009, US Patent US2009263325-A1
42. L. Lumata, S. J. Ratnakar, A. Jindal, M. Merritt, A. Comment, C. Malloy, A. D. Sherry and Z. Kovacs, *BDPA: An Efficient Polarizing Agent for Fast Dissolution Dynamic Nuclear Polarization NMR Spectroscopy*, 2011, Chem. Eur. J. 17, 10825-10827
43. L. Lumata, M. Merritt, C. Khemtong, S. J. Ratnakar, J. van Tol, L. Yu, L. K. Song and Z. Kovacs, *The efficiency of DPPH as a polarising agent for DNP-NMR spectroscopy*, 2012, Rsc. Adv. 2, 12812-12817.
44. C. S. Song, K. N. Hu, C. G. Joo, T. M. Swager and R. G. Griffin, *TOTAPOL: A biradical polarizing agent for dynamic nuclear polarization experiments in aqueous media*, 2006, J. Am. Chem. Soc. 128, 11385-11390.
45. K. N. Hu, C. Song, H. H. Yu, T. M. Swager and R. G. Griffin, *High-frequency dynamic nuclear polarization using biradicals: A multifrequency EPR lineshape analysis*, 2008, J. Chem. Phys. 128, 052302.
46. E. L. Dane, B. Corzilius, E. Rizzato, P. Stocker, T. Maly, A. A. Smith, R. G. Griffin, O. Ouari, P. Tordo and T. M. Swager, *Rigid Orthogonal Bis-TEMPO Biradicals with Improved Solubility for Dynamic Nuclear Polarization*, 2012, J. Org. Chem. 77, 1789-1797.
47. A. Zagdoun, G. Casano, O. Ouari, G. Lapadula, A. J. Rossini, M. Lelli, M. Baffert, D. Gajan, L. Veyre, W. E. Maas, M. Rosay, R. T. Weber, C. Thieuleux, C. Copéret, A. Lesage, P. Tordo and L. Emsley, *A Slowly Relaxing Rigid Biradical for Efficient Dynamic Nuclear Polarization Surface-Enhanced NMR Spectroscopy: Expedient Characterization of Functional Group Manipulation in Hybrid Materials*, 2012, J. Am. Chem. Soc. 134, 2284-2291.
48. M. K. Kiesewetter, B. Corzilius, A. A. Smith, R. G. Griffin and T. M. Swager, *Dynamic Nuclear Polarization with a Water-Soluble Rigid Biradical*, 2012, J. Am. Chem. Soc. 134, 4537-4540.
49. A. Zagdoun, G. Casano, O. Ouari, M. Schwarzwälder, A. J. Rossini, F. Aussenac, M. Yulikov, G. Jeschke, C. Copéret, A. Lesage, P. Tordo and L. Emsley, *Large Molecular Weight Nitroxide Biradicals Providing Efficient Dynamic Nuclear Polarization at Temperatures up to 200 K*, 2013, J. Am. Chem. Soc. 135, 12790-12797.
50. C. Sauvée, M. Rosay, G. Casano, F. Aussenac, R. T. Weber, O. Ouari and P. Tordo, *Highly efficient, water-soluble polarizing agents for dynamic nuclear polarization at high frequency*, 2013, Ange. Chem. Int. Ed. 125, 11058-11061.
51. Y. Lee, G. S. Heo, H. F. Zeng, K. L. Wooley and C. Hilty, *Detection of Living Anionic Species in Polymerization Reactions Using Hyperpolarized NMR*, 2013, J. Am. Chem. Soc. 135, 4636-4639.
52. Y. Lee, H. F. Zeng, S. Ruedisser, A. D. Gossert and C. Hilty, *Nuclear Magnetic Resonance of Hyperpolarized Fluorine for Characterization of Protein-Ligand Interactions*, 2012, J. Am. Chem. Soc. 134, 17448-17451.
53. Y. Lee, H. Zeng, A. Mazur, M. Wegstroth, T. Carlomagno, M. Reese, D. Lee, S. Becker, C. Griesinger and C. Hilty, *Hyperpolarized binding pocket nuclear Overhauser effect for determination of competitive ligand binding*, 2012, Ange. Chem. Int. Ed. 51, 5179-5182.

54. T. R. Eichhorn, Y. Takado, N. Salameh, A. Capozzi, T. Cheng, J. N. Hyacinthe, M. Mishkovsky, C. Roussel and A. Comment, *Hyperpolarization without persistent radicals for in vivo real-time metabolic imaging*, 2013, P. Natl. Acad. Sci. USA 110, 18064-18069.
55. R. Gitti, C. Wild, C. Tsiao, K. Zimmer, T. E. Glass and H. C. Dorn, *Solid/Liquid Intermolecular Transfer of Dynamic Nuclear-Polarization. Enhanced Flowing Fluid ¹H NMR Signals Via Immobilized Spin Labels*, 1988, J. Am. Chem. Soc. 110, 2294-2296.
56. B. C. Dollmann, M. J. N. Junk, M. Drechsler, H. W. Spiess, D. Hinderberger and K. Munnemann, *Thermoresponsive, spin-labeled hydrogels as separable DNP polarizing agents*, 2010, Phys. Chem. Chem. Phys. 12, 5879-5882.
57. E. R. McCarney and S. Han, *Spin-labeled gel for the production of radical-free dynamic nuclear polarization enhanced molecules for NMR spectroscopy and imaging*, 2008, J. Magn. Reson. 190, 307-315.
58. M. C. Cassidy, C. Ramanathan, D. G. Cory, J. W. Ager and C. M. Marcus, *Radical-free dynamic nuclear polarization using electronic defects in silicon*, 2013, Phys. Rev. B 87, 161306.
59. D. Gajan, M. Schwarzwälder, M. P. Conley, W. R. Grüning, A. J. Rossini, A. Zagdoun, M. Lelli, M. Yulikov, G. Jeschke, C. Sauvée, O. Ouari, P. Tordo, L. Veyre, A. Lesage, C. Thieuleux, L. Emsley and C. Copéret, *Solid-Phase Polarization Matrixes for Dynamic Nuclear Polarization from Homogeneously Distributed Radicals in Mesostuctured Hybrid Silica Materials*, 2013, J. Am. Chem. Soc. 135, 15459-15466.
60. B. Vuichoud, A. Bornet, F. de Nanteuil, J. Milani, E. Canet, X. Ji, P. Miéville, E. Weber, D. Kurzbach, A. Flamm, R. Konrat, A. D. Gossert, S. Jannin and G. Bodenhausen, *Filterable Labeled Agents for Hyperpolarization of Water, Metabolites and Proteins*, 2016, Chem. Eur. J., DOI: 10.1002/chem.201602506.
61. Q. Chappuis, J. Milani, B. Vuichoud, A. Bornet, A. D. Gossert, G. Bodenhausen and S. Jannin, *Hyperpolarized Water to Study Protein-Ligand Interactions*, 2015, J. Phys. Chem. Lett. 6, 1674-1678.
62. J. H. Ardenkjaer-Larsen, C. Laustsen, S. Bowen and R. Rizi, *Hyperpolarized H₂O MR Angiography*, 2014, Magn. Reson. Med. 71, 50-56.
63. G. Olsen, E. Markhasin, O. Szekely, C. Bretschneider and L. Frydman, *Optimizing water hyperpolarization and dissolution for sensitivity-enhanced 2D biomolecular NMR*, 2016, J. Magn. Reson. 264, 49-58.
64. F. M. Winnik, M. F. Ottaviani, S. H. Bossmann, M. Garciagaribay and N. J. Turro, *Conosolvency of Poly(N-Isopropylacrylamide) in Mixed Water-Methanol Solutions: A Look at Spin-Labeled Polymers*, 1992, Macromolecules 25, 6007-6017.
65. T. Cheng, M. Mishkovsky, M. J. N. Junk, K. Munnemann and A. Comment, *Producing Radical-Free Hyperpolarized Perfusion Agents for In Vivo Magnetic Resonance Using Spin-Labeled Thermoresponsive Hydrogel*, 2016, Macromol. Rapid. Comm. 37, 1074-1078.
66. H. G. Schild, *Poly (N-Isopropylacrylamide): Experiment, Theory and Application*, 1992, Prog. Polym. Sci. 17, 163-249.
67. A. Bornet, J. Milani, B. Vuichoud, A. J. P. Linde, G. Bodenhausen and S. Jannin, *Microwave frequency modulation to enhance Dissolution Dynamic Nuclear Polarization*, 2014, Chem. Phys. Lett. 602, 63-67.
68. J. Jeener, *Dipolar Field and Radiation Damping: Collective Effects in Liquid-State NMR*, 2007, eMagRes, DOI: 10.1002/9780470034590.emrstm0124.
69. P. Schanda, E. Kupce and B. Brutscher, *SOFAS-HMQC experiments for recording two-dimensional heteronuclear correlation spectra of proteins within a few seconds*, 2005, J. Biomol. NMR 33, 199-211.
70. D. Mammoli, N. Salvi, J. Milani, R. Buratto, A. Bornet, A. A. Sehgal, E. Canet, P. Pelupessy, D. Carnevale, S. Jannin and G. Bodenhausen, *Challenges in preparing, preserving and detecting para-water in bulk: overcoming proton exchange and other hurdles*, 2015, Phys. Chem. Chem. Phys. 17, 26819-26827.

71. R. Buratto, A. Bornet, J. Milani, D. Mammoli, B. Vuichoud, N. Salvi, M. Singh, A. Laguerre, S. Passemard, S. Gerber-Lemaire, S. Jannin and G. Bodenhausen, *Drug Screening Boosted by Hyperpolarized Long-Lived States in NMR*, 2014, *Chemmedchem* 9, 2509-2515.
72. J. N. Dumez, J. Milani, B. Vuichoud, A. Bornet, J. Lalande-Martin, I. Tea, M. Yon, M. Maucourt, C. Deborde, A. Moing, L. Frydman, G. Bodenhausen, S. Jannin and P. Giraudeau, *Hyperpolarized NMR of plant and cancer cell extracts at natural abundance*, 2015, *Analyst* 140, 5860-5863.

Chapter 5: Future Developments of Dissolution Dynamic Nuclear Polarization

5.1 Introduction

In this last chapter, preliminary results and several promising applications involving dissolution-DNP are treated, ranging from the hyperpolarization of hydrocarbon gases to the real-time observation of metabolic pathways in living cells.

These preliminary results open the way for different future developments for applications to metabolomics and catalytic chemistry using the d-DNP technique.

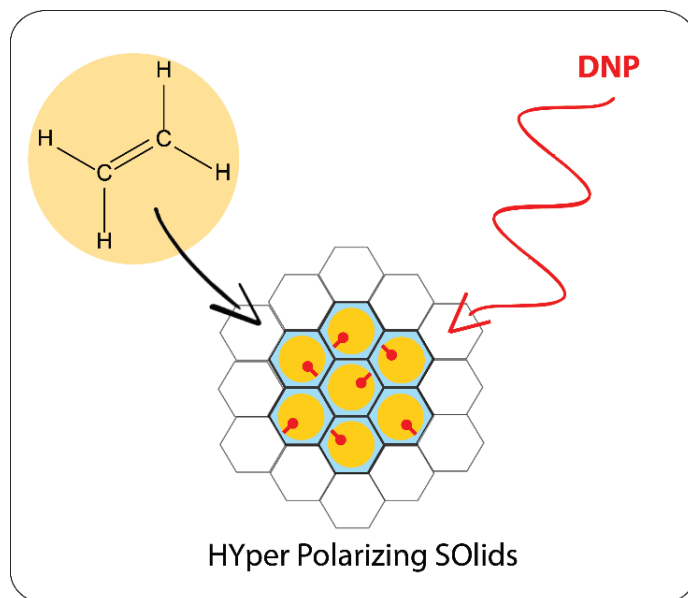
5.2 Hyperpolarization of Frozen Hydrocarbon Gases

Until now, dissolution-DNP was essentially performed on metabolites in solution such as pyruvate or acetate in water/glycerol mixtures and only few experiments were carried out to polarize gaseous molecules such as ^{129}Xe [1, 2, 3] and $^{15}\text{N}_2\text{O}$. [4] The main reason for this limited use of d-DNP for the hyperpolarization of gases is that optical pumping [5, 6] is nowadays the preferred technique for the polarization of noble gases. An inconvenience resulting from the use of d-DNP is that the sample preparation is often a critical step, and a co-solvent has to be added to ensure a good homogeneity of the solution to be polarized, which can lead to a contamination of the solution after dissolution, and reduces the amount of hyperpolarized gases present in the DNP sample.

In order to compete with such a deep-rooted method as optical pumping, a good riposte would be to design a general d-DNP method that can be applied to any kind of gases (either noble or hydrocarbon gases) to obtain hyperpolarized gas molecules that are free of contaminants and that can be prepared in sufficient amounts for a single dissolution shot.

Therefore, we focused our research on a recently synthesized silica matrix HYPISO [7] used for d-DNP, which obviates the need of any co-solvent or any glassing agent, to produce pure hyperpolarized gas molecules. A mixture of *n*-butane, isopropane and propane, or pure ethylene were chosen as hydrocarbon gases to be polarized and to prove the efficiency of this method. Furthermore, we designed and built a system to impregnate the HYPISO material with any kind of gas for routine use.

The work related in this thesis was published in the following issue entitled "*Hyperpolarization of Frozen Hydrocarbon Gases by Dynamic Nuclear Polarization at 1.2 K*". [8]



5.2.1 Dissolution-DNP to hyperpolarize gases

As briefly mentioned before, optical pumping [5, 6] is a well-established method for the hyperpolarization of noble gases such as ^{129}Xe and ^3He [9, 10] and can offer sufficient polarization levels, albeit with limited throughputs (a maximum of 6 L/h for ^{129}Xe with a polarization of $P(^{129}\text{Xe}) = 22\%$). [11] This technique has nowadays found various applications from material science to biomedical research and more particularly to lung imaging by MRI. [12, 13] However, it is restricted to a few noble gases, and molecular gases such as ethylene have not been yet hyperpolarized by optical-pumping.

To overcome this restriction, the para-hydrogen method can be employed to hydrogenate molecules with double or triple carbon-carbon bonds by heterogeneous catalysis in order to produce hyperpolarized gaseous reaction products. [14, 15, 16] Nevertheless, the polarization levels achieved with this technique are well below 1 %.

Even if d-DNP requires more complex instrumentation (cryostats and superconducting magnets) compared to optical pumping and para-hydrogen, it seems well suited to overcome their respective inconveniences. Indeed, hyperpolarization of gases by d-DNP should not be restricted to noble gases, since a broad range of small metabolites can already be efficiently polarized by this technique and the levels of polarization achieved are relatively high, e.g., $P(^{13}\text{C}) = 78\%$. [17] In addition, the use of dissolution-DNP has already been demonstrated to polarize ^{129}Xe [1, 2, 3] and $^{15}\text{N}_2\text{O}$ [4] and it is of great interest to extend its use by proposing a general method applicable to virtually any condensed gas.

The critical step for d-DNP still is the preparation of the sample, which must be inspected before polarization. As discussed in the preceding chapters, the polarizing agents (PAs) and the metabolites to be polarized should be distributed homogeneously in the sample. To ensure this condition and avoid the aggregation of the PAs, glass-forming agents such as glycerol are used, leading to a transparent glass upon freezing. For the hyperpolarization of ^{129}Xe [1], the condensed gas can be mixed with a co-solvent, such as isobutanol, doped with TEMPO under a relatively high pressure ($P \approx 10$ bar) at low temperatures ($T \approx 200$ K) to liquefy xenon and obtain a homogeneous solution of the two compounds. This mixture can then be rapidly frozen in liquid nitrogen to get a homogeneous glassy matrix suitable for DNP experiments. However, even with a careful preparation, it remains difficult to obtain an ideal DNP sample in a reproducible manner because of the possible formation of Xe clusters [3], which would hamper the DNP process. Furthermore, this method cannot be generalized to other gases and other co-solvents. Indeed, we attempted to use this approach for ethylene with ethanol and TEMPO, but this mixture did not produce a homogeneous glass upon freezing as expected. The frozen sample was characterized by a non-uniform color distribution, which clearly indicates a segregation of the components so that ^1H DNP was not feasible.

Thus, an alternative route for polarizing condensed gases was proposed by porous silica materials dubbed HYper Polarizing SOLids (HYPSO) that have been fully described in the previous chapter 4.4. [7, 18, 19] The materials HYPSO-1 [7] and HYPSO-3 [18] were chosen in order to polarize a mixture of *n*-butane, isobutane and propane, and ethylene by impregnation of these silica matrices without the need for any co-solvents or glassing agents (see Fig. 5.1 A).

5.2.2 Hyperpolarization of ethylene and butane

In order to properly impregnate the HYP SO material, a specific system was designed and built at the EPFL (see Fig. 5.1 B). It is composed of several valves that allow the filling of the overall system with an organic gas and its cleaning by means of a vacuum line. The gas is simply released by opening the canister and a manometer allows to read the pressure in the system. Then, its volume can be precisely measured by filling the syringe and injecting the corresponding amount into the HYP SO material contained in a flask.

The first experiment was performed with 50 mL (127 mg) of a mixture of *n*-butane, isobutane, and propane from a gas canister. This mixture was condensed with 10.2 mg of HYP SO-1, corresponding to only 11 mg of the liquefied gas inside the pores, the loading capacity of this material being 1.8 mL/g. This sample was then rapidly frozen in the DNP polarizer [20, 21] at 4.2 K before the temperature was lowered to 1.2 K. A similar procedure was applied for 50 mL (59 mg) of ethylene with 22.5 mg of HYP SO-3 precooled in a bath of liquid ethanol at $T = 159$ K. The loading capacity of HYP SO-3 being 0.47 mL/g, only 5.9 mg of liquid ethylene was expected to enter the pores of the material (Fig. 5.1 C).

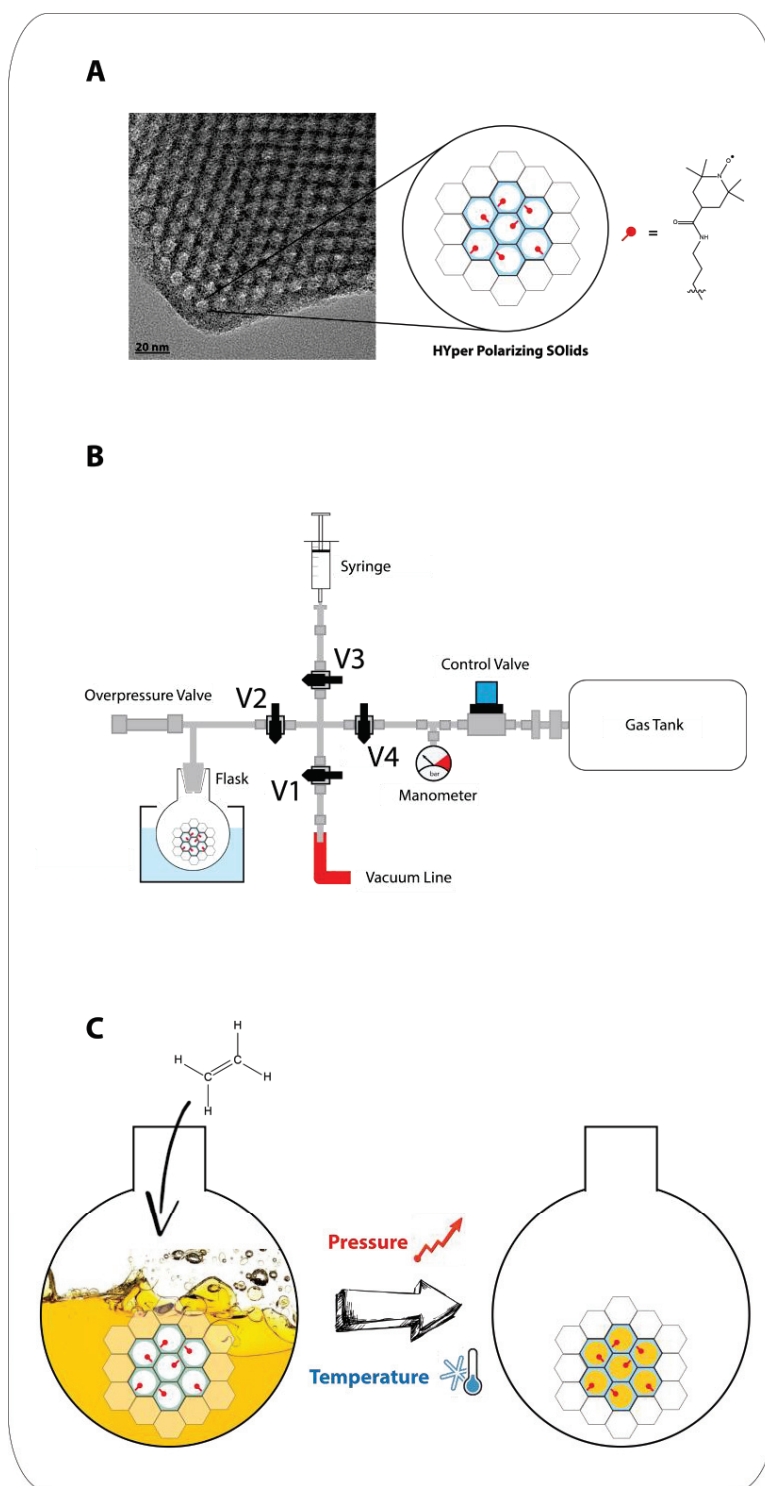


Fig. 4.15: (A) Transmission electron microscopy image of mesoporous HYPSO-1 taken with a Philips CM30 TEM operating at 300 kV. In the schematic representation of the HYPSO structure, the red dots indicate the polarizing agent derived from TEMPO. (B) System designed and built in our laboratory to impregnate HYPSO materials with condensed gases. It is equipped with a flask containing the HYPSO material that can be cooled in an ethanol-liquid N_2 bath ($T = 159$ K). A vacuum can be established in the entire system by opening the valves V1, V2, V3 and V4 and pumping with a rotary pump connected to the vacuum line. A manometer allows one to monitor the pressure. With valves V1 and V2 closed, valves V3 and V4 are opened and the control valve is opened gently to let a desired volume of gas escape from the gas tank and fill the syringe. Finally, V4 is closed and V2 is opened to impregnate the HYPSO powder with the gas. In addition, an overpressure valve ensures safety. (C) By decreasing the temperature to $T = 159$ K using an ethanol-liquid N_2 bath and increasing the pressure, the gas is forced to enter into the mesoporous structure of HYPSO, resulting in a color change of HYPSO from transparent to yellow.

DNP was performed on both samples at 1.2 K with negative microwave irradiation at an average frequency $f_{\mu W} = 188.3$ GHz using microwave frequency modulation [22] as described in chapter 3.3. The ^1H build-up was monitored with 1° pulses applied every 5 s. Furthermore, Cross-Polarization from ^1H to ^{13}C was performed with multiple adiabatic contacts [23] by applying 5° pulses every 37.5 s for the mixture of *n*-butane, isobutane, and propane and every 75 s for ethylene.

In Fig. 5.2, the ^1H polarization build-up curve is shown for the mixture of *n*-butane, isobutane, and propane at $T = 1.2$ K in HYPISO-1. A remarkable $P(^1\text{H}) = 53\%$ has been achieved in 1000 s with a build-up time $T_{\text{bup}}(^1\text{H}) = 228 \pm 4$ s, showing the efficiency of the method to hyperpolarize gases. Cross-Polarization was then performed every 5 min to boost the carbon polarization by transferring the enhancement from ^1H to ^{13}C . Although no proper optimization was performed on this sample, an average polarization of $P(^{13}\text{C}) = 9\%$ was achieved after 20 min. Indeed, this measurement was done only to prove the possibility of applying the method to organic gases. More optimizations were performed on a more interesting molecule: ethylene.

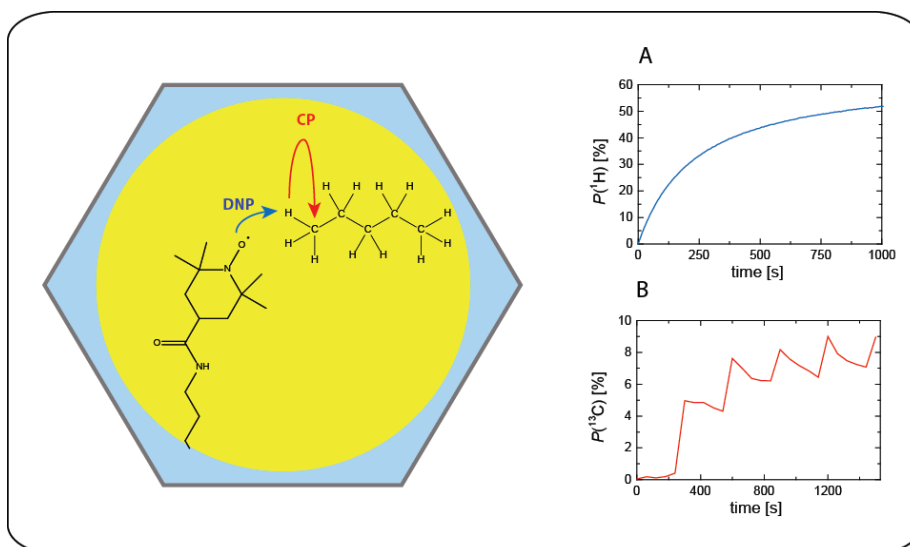


Fig. 5.2: Schematic representation of HYPISO-1 with TEMPO covalently attached to its surface inside the pores and filled with a mixture of *n*-butane, isobutane, and propane (for clarity only *n*-butane is represented). This allows the DNP process to occur and CP can be performed from ^1H to ^{13}C . (A) Proton polarization build-up to $P(^1\text{H}) = 53\%$ recorded at $T = 1.2$ K with a build-up time $T_{\text{bup}}(^1\text{H}) = 228 \pm 4$ s. (B) Carbon build-up to $P(^{13}\text{C}) = 9\%$ after 20 min with CP applied every 5 min at $T = 1.2$ K.

The same experiment was performed and optimized for ethylene (see Fig. 5.3). This time, a higher polarization $P(^1\text{H}) = 70\%$ was achieved after more than 4500 s with a longer build-up time $T_{\text{bup}}(^1\text{H}) = 1384 \pm 13$ s. Two Cross-Polarization contacts were performed, as before, after 10 and 20 min to transfer the polarization from ^1H to ^{13}C . After optimizing the CP step, a polarization $P(^{13}\text{C}) = 27\%$ was achieved after only 20 min for ethylene, which corresponds to a relatively high ^{13}C enhancement if we take into account that the DNP sample only comprises pure ethylene and HYPISO.

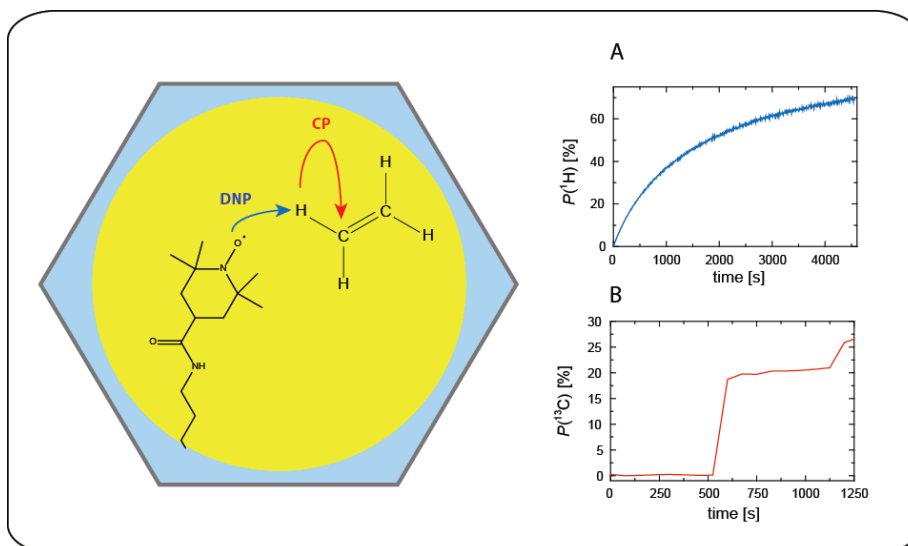


Fig. 5.3: Schematic representation of HYPISO-3 with TEMPO covalently attached to its surface inside the pores and filled with ethylene. As presented in the previous figure, CP can be performed from ^1H to ^{13}C . (A) Proton polarization build-up to $P(^1\text{H}) = 70\%$ recorded at $T = 1.2\text{ K}$ with a build-up time $T_{\text{bup}}(^1\text{H}) = 1384 \pm 13\text{ s}$. (B) Carbon build-up to $P(^{13}\text{C}) = 27\%$ after 20 min with two CP contacts applied after 10 and 20 min at $T = 1.2\text{ K}$.

5.2.3 Dissolution-DNP attempt of hyperpolarized ethylene

Based on these encouraging results, we decided to perform a dissolution-DNP experiment on a sample containing ethylene in order to monitor its epoxidation into ethylene oxide. This molecule is part of an important industrial process and is used as a chemical intermediate for the synthesis of ethylene glycol (antifreeze) or other products like plastics and polyesters. [24, 25] Even if this chemical reaction is used worldwide, the mechanism observed for heterogeneous catalysis that leads to the formation of the corresponding epoxide still remains difficult to understand. Several mechanisms involving different intermediates have therefore been proposed. [25] With the use of d-DNP and the high levels of polarization achieved for ethylene ($P(^{13}\text{C}) = 27\%$), it appears interesting to monitor this oxidation, in the hope of observing the intermediates of the reaction.

As a first test, a setup for homogeneous catalysis with d-DNP was designed to monitor the epoxidation of ethylene. The DNP sample was prepared as mentioned before and the dissolution setup was carefully optimized. Toluene- d_8 was used as dissolution solvent, because it is the best candidate among a broad range of different solvents in which ethylene is soluble, it is one of the least toxic solvents, and at the same time it is not too volatile, unlike diethyl ether. The main idea was to rapidly dissolve hyperpolarized ethylene, transfer it, and inject 700 μl of this mixture into an NMR tube awaiting in the NMR spectrometer. In this NMR tube, 200 μl of a solution containing 30% H_2O_2 in toluene- d_8 with 2 mg of the catalyst Methyltrioxorhenium (MTO) were placed to catalyze the epoxidation of ethylene. [26] It should then be possible to monitor the reaction by recording the decay of hyperpolarized ethylene and the formation of hyperpolarized ethylene oxide (see Fig. 5.4).

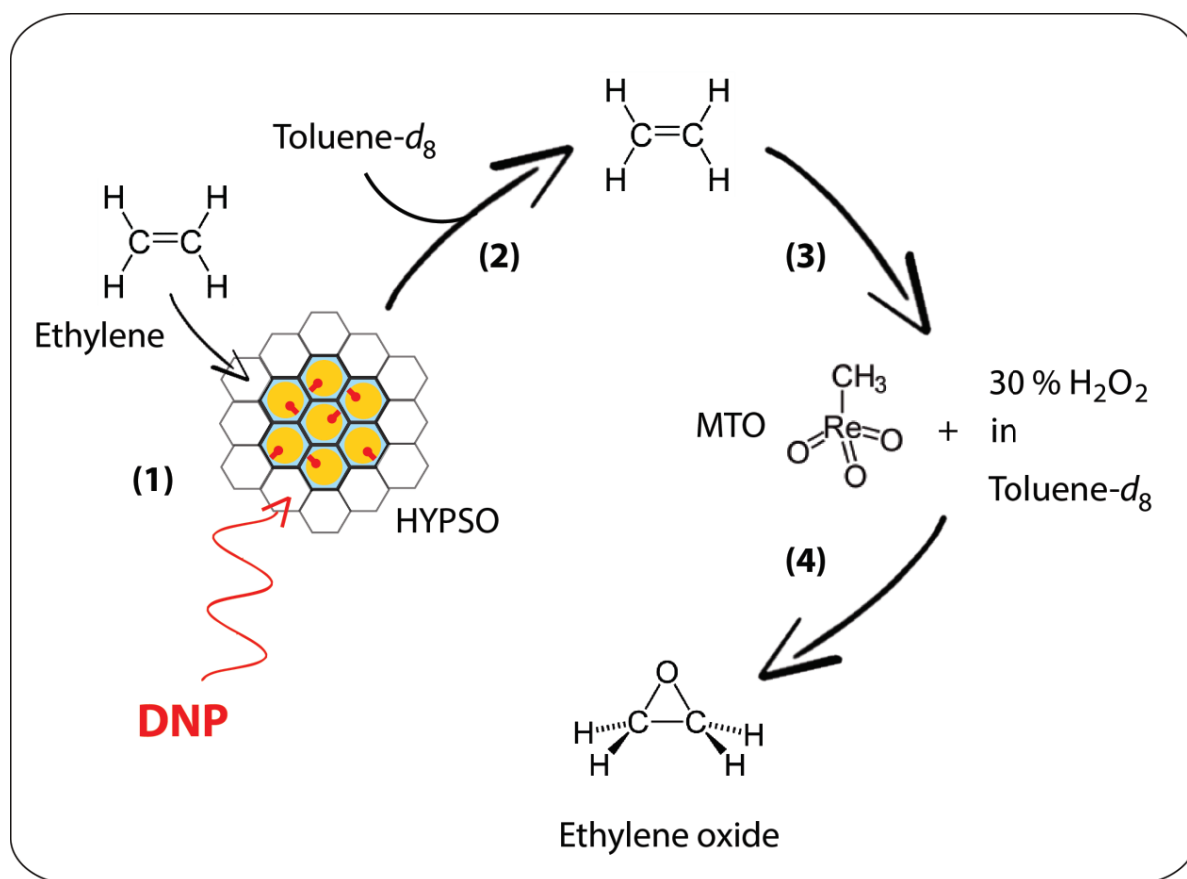


Fig. 5.4: Dissolution-DNP experiment for the epoxidation of hyperpolarized ethylene. (1) The DNP sample is prepared as previously by impregnating pure ethylene in HYPSON material. (2) It is then rapidly dissolved by 5 mL of superheated toluene- d_8 ($T = 353$ K), transferred to the 500 MHz NMR spectrometer, where 700 μl of this hyperpolarized mixture are injected into an NMR tube. (3) In this NMR tube, 200 μl of a solution containing 2 mg of Methyltrioxorhenium (MTO) and 30% H_2O_2 in toluene- d_8 are awaiting for the injection of hyperpolarized ethylene which (4) should be epoxidized catalytically to form ethylene oxide.

Unfortunately, despite our multiple attempts to dissolve ethylene properly, so far no trace of this gaseous molecule could be recorded after dissolution. This could be explained by the poor design of our dissolution setup. Indeed, the dissolution line is not completely closed at its end, where the injector is placed, which could result in a fast degassing of the hyperpolarized ethylene prior to its injection into the NMR tube. To overcome this problem, we have built and are currently testing a hermetically closed dissolution system, inspired by Hilty and co-workers [27], which should be able to resist sufficient high pressures of helium ($P = 20$ bar instead of 6 bar), therefore allowing a fast transfer ($t_{\text{overall}} \approx 2$ s instead of 7 s) and a closed transfer line from which ethylene can in principle not evaporate. [28]

Another alternative to the d-DNP method would be to produce pure hyperpolarized liquid ethylene by rapidly melting the frozen gas with an IR laser [29], which would obviate the need of a dissolution solvent. Several other techniques could be applied to this specific experiment, like collecting the sample in a frozen state while preserving its hyperpolarization and transferring it to the NMR spectrometer where it could be melted. This list of techniques is not exhaustive and the acquisition of hyperpolarized signals of ethylene should in principle be only a matter of time.

5.2.4 Preliminary conclusions concerning the hyperpolarization of ethylene

This initial study demonstrated that hydrocarbon gases such as butane and ethylene can be condensed inside HYPPO materials and polarized by Dynamic Nuclear Polarization at low temperatures. Even if the attempts at dissolution were not yet successful, we are currently developing new strategies to collect the hyperpolarized gases. Indeed, molecular gases represent a unique challenge compared to liquids since the predominance of the spin-rotation relaxation mechanism in gases may lead to fairly short T_1 values. [30, 31, 32, 33, 34] This is why it is preferable to liquefy these gases in order to extend the lifetimes of the polarization. [35] Another method to extend these lifetimes would be to use long-lived spin states (LLS) [36, 37, 38, 39], that have already shown interesting results with $T_{LLS} \approx 1000$ s for ethylene gas. [32]

With the ability to create hyperpolarized gases with lifetimes as long as 10 – 1000 s, new applications such as catalytic transformations could emerge. Indeed, such reactions are of primary importance in modern chemical industry. [40] Thus, novel advanced methods and instrumental techniques like d-DNP could help to understand the mechanisms of heterogeneous catalysis, where other hyperpolarized techniques like para-hydrogen are currently facing some major limitations and are restricted to reactions that involve H_2 . [14, 15, 16]

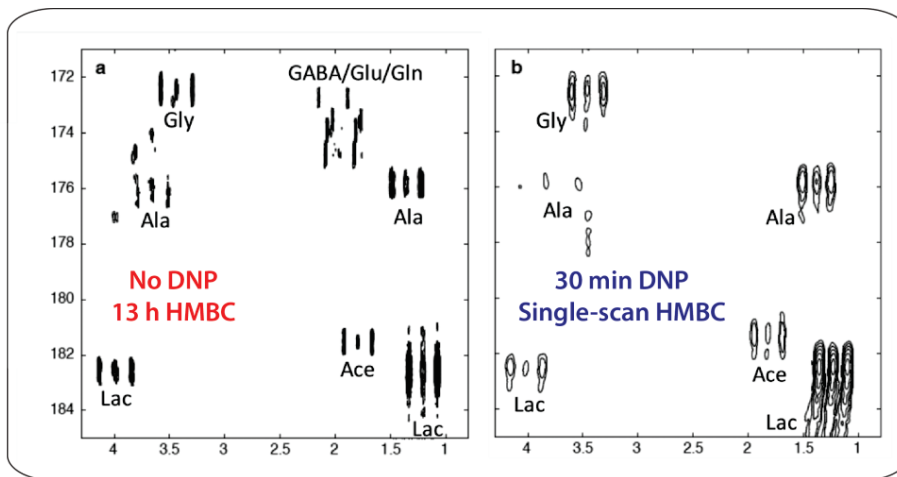
5.3 Hyperpolarization of biological extracts

In the last decade, there has been a growing interest in being able to map metabolic pathways, to identify biomarkers and to follow metabolic fluxes. [41, 42] The use of NMR in the field of metabolomics is a well-spread analytical technique and permits the identification of various metabolic pathways and the determination of time-dependent metabolite concentrations in various extracts and tissues.

However, proton NMR spectra, because of the narrow range of their chemical shifts, tend to suffer from overlapping of signals. Therefore, a reliable and precise identification of the molecules and their corresponding metabolites by proton NMR remains difficult. The use of ^{13}C NMR spectra represents a good alternative to this problem, since they benefit from a much larger chemical shift dispersion. Nevertheless, because of the low natural abundance of ^{13}C , the acquisition of NMR spectra remains time-consuming to achieve a sufficient signal-to-noise ratio, so that this method is not routinely used in metabolomics studies.

Dissolution-DNP represents an efficient way to overcome this lack of sensitivity, and its popularity should be boosted in the metabolomics community. We demonstrated that hyperpolarization by d-DNP of ^{13}C at natural abundance makes it possible to record ^{13}C NMR spectra of metabolites in plant and cancer cell extracts in a single scan.

The work described in this chapter was published in the following article entitled "*Hyperpolarized NMR of plant and cancer cell extracts at natural abundance*". [43]



5.3.1 Dissolution-DNP for metabolomics

As mentioned throughout this thesis, the acquisition of ^{13}C NMR spectra suffers from a lack of sensitivity due to the low natural abundance of carbon-13, which complicates measurements of very diluted samples. Isotopic enrichment [44] is a manner to overcome this low sensitivity, but can result in an enhanced complexity of the NMR spectra due to ^{13}C - ^{13}C couplings. Because of these disadvantages, ^{13}C NMR is not yet a method of choice for metabolomic studies.

However, by introducing d-DNP, we showed that the hyperpolarization of ^{13}C spin nuclei is possible, leading to enhancements in excess of 50'000. [45] Nowadays, dissolution-DNP is mostly restricted to small molecules like pyruvate or acetate [46, 47, 48, 49] rather than to complex mixtures of metabolites. Nonetheless, we demonstrate in the following chapter that, with the use of Cross-Polarization [23] combined with d-DNP, a high ^{13}C polarization can be rapidly achieved in complex samples, even at natural abundance.

5.3.2 Experimental results for tomato and cancer cells extracts

The experiments were carried out on two different types of DNP samples: **(1)** Tomato extracts and **(2)** Cancer cell extracts. The first sample **(1)** was composed of extracts of tomato pericarp of 4-5 different fruits harvested from different plants. These pericarps were immediately frozen, ground in liquid nitrogen and stored at -80°C until freeze-drying. For our DNP measurements, each sample was prepared from extracts of lyophilized tomato powder (see Supporting Information) which were dissolved in 200 μl of $\text{H}_2\text{O}/\text{D}_2\text{O}/\text{glycerol-}d_8$ (v/v/v : 20/30/50) with 25 mM TEMPOL and were inserted in our DNP polarizer. [20, 21] Frequency modulation was used as described before [22] with $f_{\mu\text{W}} = 188.3$ GHz, $f_{\text{mod}} = 10$ kHz and $\Delta f_{\mu\text{W}} = 100$ MHz at $T = 1.2$ K. Cross-Polarization (CP) $^1\text{H} - ^{13}\text{C}$ was performed every 5 min during a total of 30 min, followed by dissolution using superheated D_2O ($T = 140^\circ\text{C}$) and the transfer to a 500 MHz NMR spectrometer (see Fig. 5.5). In Fig 5.5 (right), the ^{13}C NMR spectra focus on the quaternary carbons where the enhancements are best preserved due to their long T_1 . The gain in sensitivity can be easily observed between the two samples with and without DNP and the single-scan ^{13}C DNP shows more peaks than the thermal equilibrium spectrum recorded in *ca.* 12 h with 1024 scans at intervals of 41 s.

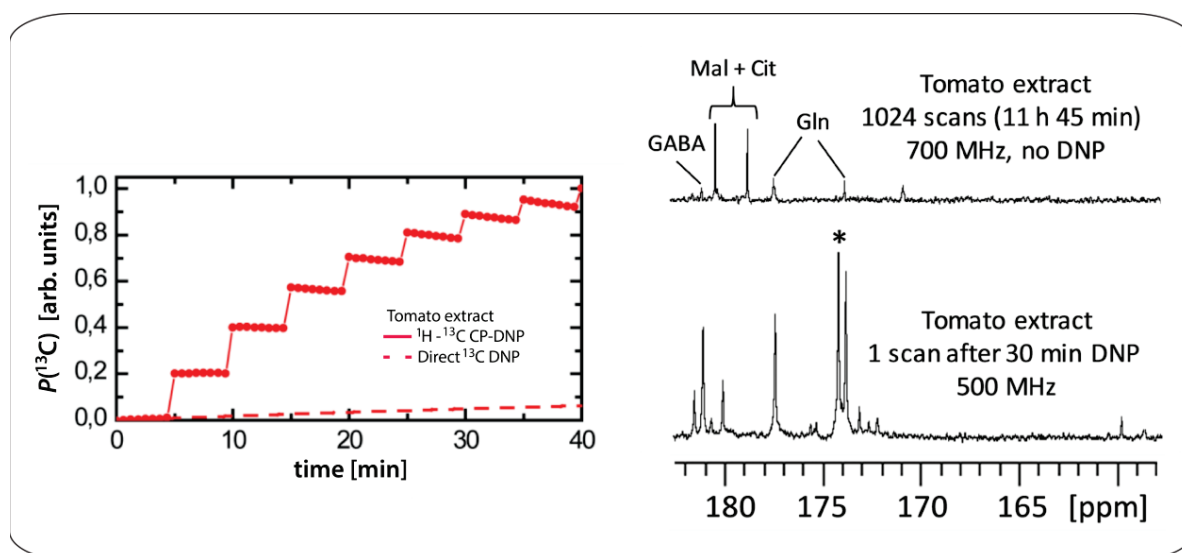


Fig. 5.5: (Left) Cross-Polarization build-up of the ^{13}C polarization of a tomato extract, composed of lyophilized powder in 200 μl of $\text{H}_2\text{O}/\text{D}_2\text{O}/\text{glycerol-}d_8$ (v/v/v : 20/30/50) and 25 mM TEMPOL, with adiabatic CP contacts applied every 5 min. The dashed line represents the extrapolated ^{13}C polarization obtained with direct ^{13}C DNP. (Right) ^{13}C NMR spectra of the tomato extract at thermal equilibrium with 1024 scans acquired over a period of ca. 12 h (top) and after being hyperpolarized by DNP during 30 min in a single scan (bottom). * indicates a signal of $[1-^{13}\text{C}]$ sodium pyruvate, an impurity from the d-DNP setup.

It is worth noticing that two major limitations arise in this experiment. First of all, only quaternary carbons are clearly defined in the NMR spectra, because of their long $T_1(^{13}\text{C})$ relaxation times. Indeed, and from what has been discussed in the previous chapters, protonated carbon nuclei possess a very short T_1 and tend to lose their polarization more rapidly during the transfer from the polarizer to the NMR spectrometer. A second important drawback is the difficulty of assigning the peaks in this 1D ^{13}C NMR spectrum, since the metabolites present in the tomato extract are not well known beforehand and the assignment of the peaks is mainly based on previous experiments with similar samples at thermal equilibrium.

To overcome possible overlaps of different peaks, single-scan 2D NMR (also known as Ultrafast 2D NMR) [50] and more precisely HMBC-type experiments allow one to assign the quaternary carbons. [48] This strategy was therefore applied to our second DNP sample obtained from human breast cancer cell lines, either at natural abundance or with partial isotopic enrichment.

Two different DNP samples containing the cancer cell extracts were prepared (see Supporting Information), either at natural abundance or partially enriched. They were mixed with 200 μl of $\text{H}_2\text{O}/\text{D}_2\text{O}/\text{glycerol-}d_8$ (v/v/v : 20/30/50) with 25 mM TEMPOL and inserted into our DNP Polarizer. In Fig. 5.6, Cross-Polarization was performed as before with adiabatic contacts every 5 min. A conventional HMBC $^1\text{H} - ^{13}\text{C}$ 2D NMR spectrum of an enriched ^{13}C cell extract is presented in (a) and is compared with (b) a single-scan HMBC (inspired by Frydman *et al.* [48]) of the same sample recorded after d-DNP. Because of T_1 losses, the GABA/Glu/Gln region has disappeared, but all other peaks remain present after being hyperpolarized by DNP during 30 min and transferred to a 500 MHz NMR spectrometer. This result confirms the time-saving of d-DNP measurements, since only 30 min were needed in comparison with the conventional measurement which needs ca. 14 h. In (c), a similar approach was carried out for DNP sample containing cell extracts at natural ^{13}C abundance, where NMR signals are still present after the dissolution process, which would not have been the case for a conventional HMBC measurement, where a tremendous experimental time would have been required.

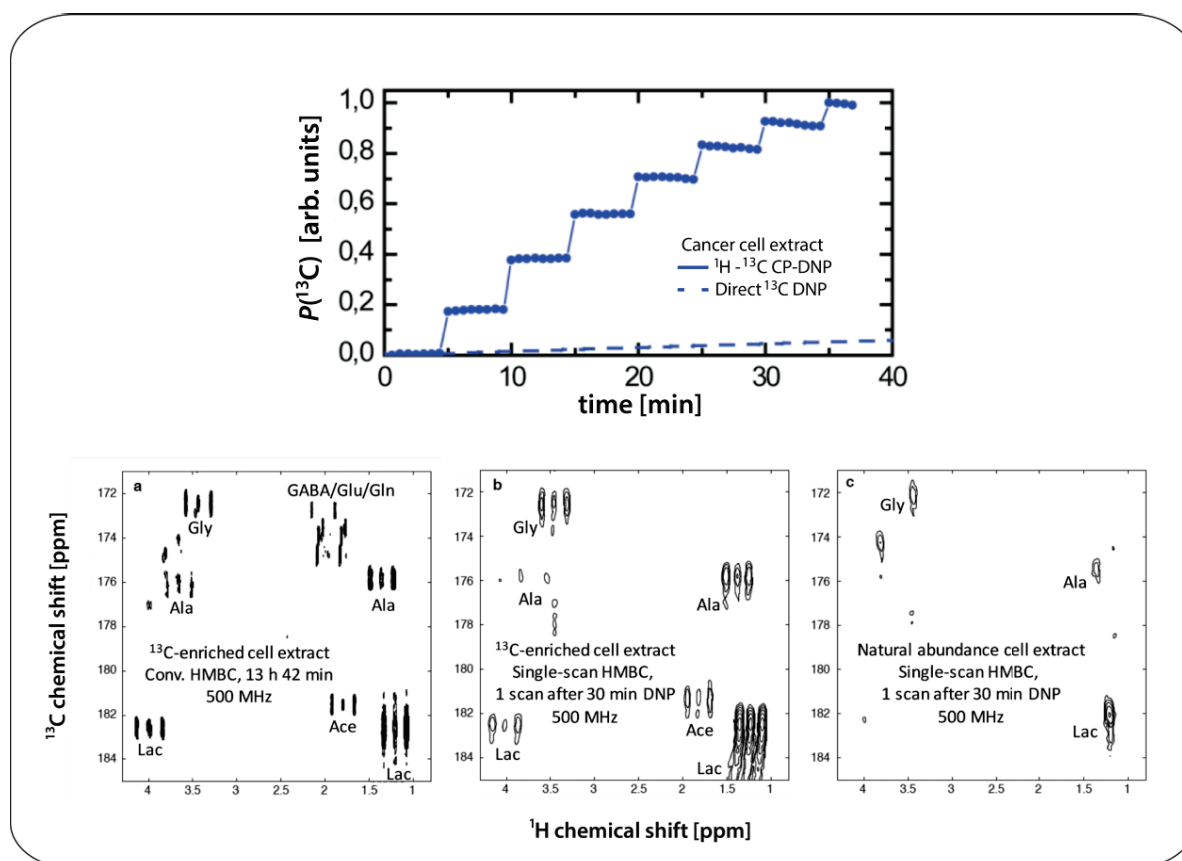


Fig. 5.6: (Top) Cross-Polarization build-up of the cancer cell extract in 200 μl of $\text{H}_2\text{O}/\text{D}_2\text{O}/\text{glycerol-}d_8$ (v/v/v : 20/30/50) and 25 mM TEMPOL, with adiabatic CP contacts applied every 5 min. The dashed line represents the extrapolated ^{13}C polarization obtained with direct ^{13}C DNP. (a) Conventional $^1\text{H} - ^{13}\text{C}$ HMBC spectrum of partially enriched cancer cells extracts in 700 μl D_2O recorded after *ca.* 14 h at 500 MHz. (b) Single-scan HMBC performed on the hyperpolarized sample containing the enriched cell extracts after being hyperpolarized during 30 min. (c) Same as (b) but with natural abundant cell extracts. Ace: acetate; Lac: lactate; Ala: alanine; Gly: glycine; GABA: γ -aminobutyrate; Glu: glutamate; Gln: glutamine.

5.3.3 Conclusions concerning d-DNP for metabolomics

Thanks to Cross-Polarization combined with dissolution-DNP, information on the metabolites of our two biological samples derived from tomato and breast cancer cell extracts have been recorded via the detection of 1D and 2D ^{13}C spectra. Even at natural abundance, it was possible to measure a 2D HMBC $^{13}\text{C} - ^1\text{H}$ spectrum in a single scan after only 30 min of DNP hyperpolarization.

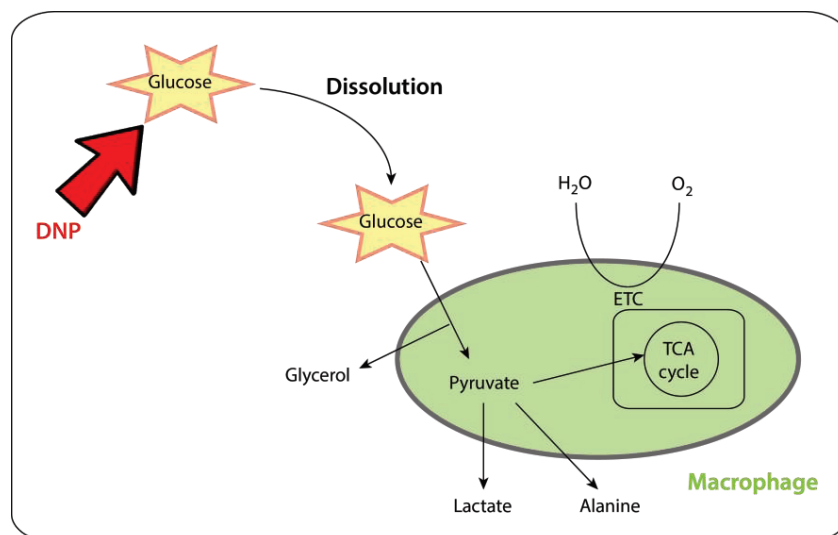
Furthermore, this application is not sample specific and should be applicable to a wide range of metabolites and extracts. With such a gain in time (*ca.* 1 h in total, in comparison with *ca.* 14 h) and sensitivity, d-DNP offers a promising perspective for metabolomics studies.

5.4 In-Cell Dissolution Dynamic Nuclear Polarization

So far, dissolution-DNP has been principally used for the hyperpolarization of small metabolites and, as previously discussed, for the hyperpolarization of more complex mixtures of metabolites. Another application of this method is the possibility of monitoring molecules in real time in living cells, including *E. coli* (prokaryotic cells) [51, 52] and *S. cerevisiae* (eukaryotic cells) [53], to characterize the glycolytic pathways and the TCA cycle.

Even if preliminary studies involving hyperpolarization of metabolites by d-DNP were performed on bacteria and yeasts, no experiments had been recorded so far on living mammalian cells, where the metabolic processes are much slower. Therefore, [$1\text{-}^{13}\text{C}$] sodium pyruvate and [$U\text{-}^2\text{H}$, ^{13}C] glucose were hyperpolarized by d-DNP and injected in a medium containing living mammalian macrophages to monitor the slow cellular metabolic pathways.

The results obtained are described in more detail in the thesis of Dr. Morgane Callon [54] and are in preparation for publication as "*Real-Time Observation by NMR of Slow Metabolic Events in Living Mammalian Macrophages by Dissolution Dynamic Nuclear Polarization*". [55]



5.4.1 D-DNP for macrophages

By using d-DNP, one can overcome the problem of low sensitivity of NMR for diluted concentrations of metabolites in cells, which normally limits the use of NMR to favorable cell lines that produce sufficiently concentrated materials. The choice for our application was focused on a precise type of cells, i.e., on macrophages.

These macrophages (see Supporting Information) are phagocytic cells of the immune system, which are mainly responsible of the elimination of pathogens and the clearing of dead cells. [56] The interest in studying these particular white blood cells is that their metabolic pathways depend on stimuli to which they are exposed. [57, 58] After a bacterial or an anti-inflammatory activation, the metabolism of macrophages is characterized either by a fast consumption of glucose [59, 60] or by an increase of mitochondrial oxidation. [61] Dissolution-DNP is a good candidate to quantify the metabolic response to different stimuli and to better understand the role of the metabolism.

5.4.2 Experimental results for d-DNP on macrophages

To be able to monitor metabolic processes by d-DNP, two different DNP samples were prepared with **(1)** 867 mM of [U - ^2H , ^{13}C] glucose in $\text{H}_2\text{O}/\text{D}_2\text{O}/\text{glycerol-}d_8$ (v/v/v : 10/40/50) with 50 mM TEMPOL, and **(2)** 1.5 M [1 - ^{13}C] sodium pyruvate in $\text{D}_2\text{O}/\text{glycerol-}d_8$ (v/v : 1/1) with 25 mM TEMPOL. These samples were inserted in our DNP polarizer at $T = 1.2$ K. [20, 21] Direct ^{13}C polarization was used for sample **(1)**, while Cross-Polarization was performed every 5 minutes to build up the carbon-13 polarization for sample **(2)**. Frequency modulation [22] was also used with $f_{\mu\text{W}} = 188.3$ GHz, $f_{\text{mod}} = 10$ kHz and $\Delta f_{\mu\text{W}} = 50$ MHz. The samples were dissolved by superheated D_2O ($T = 140$ °C and $P = 10$ bar), pushed in 10 s through a magnetic tunnel [62] and injected in a 500 MHz NMR spectrometer containing 400 μl of a suspension in D_2O of 80 million macrophages at 37° C.

Preliminary results were performed on these macrophages and showed that glucose is efficiently metabolized into lactate at a rate of 1-3 nmol/min per million cells. This would represent a conversion of 1.3 - 4 nmol/s for our d-DNP experiments. These results are explained in more detail in the thesis of Dr. Morgane Callon. [54]

The sample containing deuterated glucose ([U - ^2H , ^{13}C] glucose) was favored, because initial experiments involving non-deuterated glucose ([U - ^{13}C] glucose) did not allow the observation of any hyperpolarized signals after dissolution, which must be due to the short $T_1(^{13}\text{C}) < 1$ s of the molecule, while its deuterated isotopologue has $T_1(^{13}\text{C}) = 12$ s. In Fig. 5.7 A, the decay of hyperpolarized ^{13}C in deuterated glucose was recorded by applying 10° pulses at intervals of 6 s. These spectra also show an accumulation of glycerol resulting from the metabolic conversion of glucose in the macrophages. The thermal equilibrium (Fig. 5.7 B) of this suspension was recorded 30 min after dissolution during a total of 30 min. The presence of lactate and alanine was confirmed after complete relaxation.

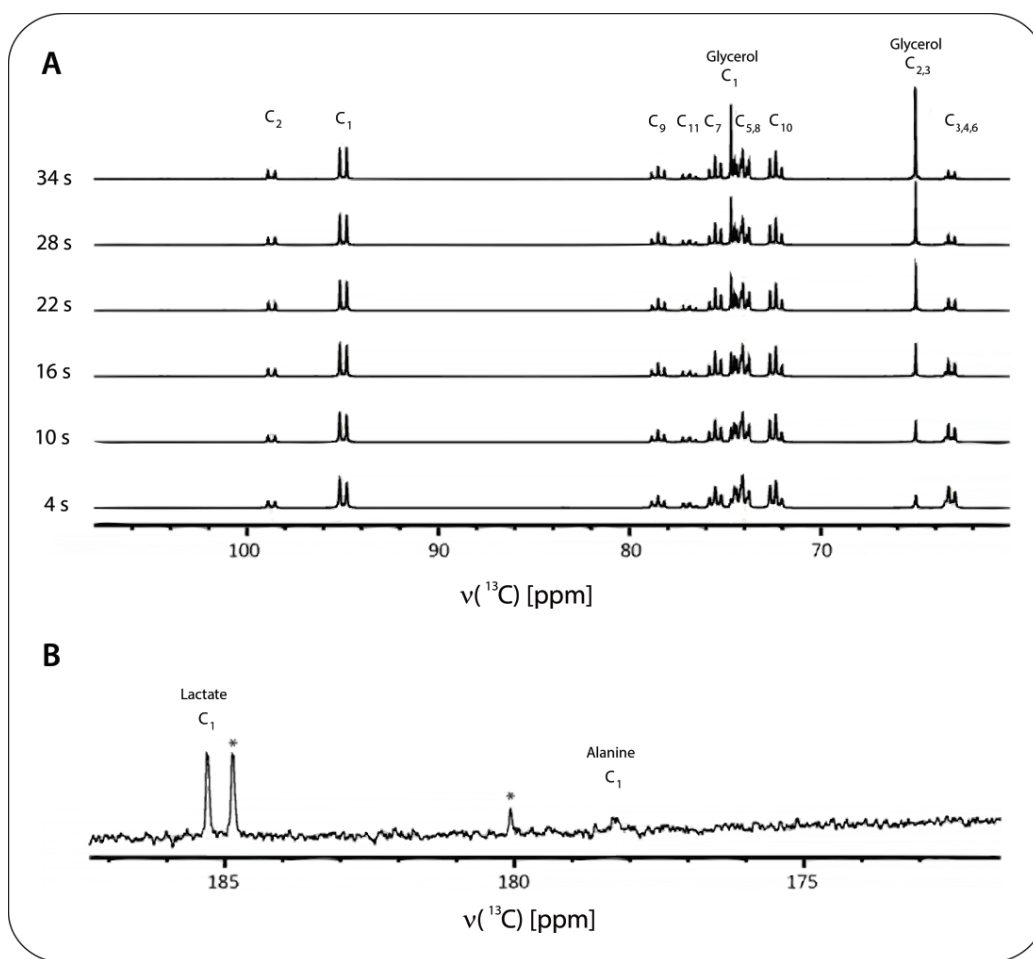


Fig. 5.7: (A) ^{13}C NMR spectra of macrophages fed with hyperpolarized [$U\text{-}^2\text{H}$, ^{13}C] glucose enhanced by d-DNP. The NMR spectra were recorded at intervals of 6 s by applying 10° pulses and show the decay of hyperpolarized deuterated glucose ($\text{C}_1 - \text{C}_{11}$) and the accumulation of extracellular glycerol. (B) Thermal equilibrium spectrum of the same sample acquired 30 min after dissolution during 30 min, showing the presence of lactate and alanine in the medium. Impurities are labeled with *.

Unfortunately in this experiment, no intermediates of the glycolytic pathway could be observed by NMR, as expected. The main reason is that the concentrations of these intermediate metabolites were probably too low, because, although they are constantly produced, they are also directly metabolized, which was not the case for glycerol, which is an end-product and therefore accumulates. Note that lactate was not observed by d-DNP, which shows that the conversion of glucose into lactate is less efficient than into glycerol.

Therefore, we decided to change the hyperpolarized metabolite from deuterated glucose to $[1-^{13}\text{C}]$ sodium pyruvate for two main reasons: (1) The relaxation time of pyruvate $T_1(^{13}\text{C}) = 70$ s is 6 times longer than for deuterated glucose and (2) a single reaction, involving lactate dehydrogenase, allows the conversion of pyruvate into lactate.

The Fig. 5.8 represents the ^{13}C NMR spectra acquired after dissolution of hyperpolarized $[1-^{13}\text{C}]$ sodium pyruvate every 30 s. After 45 s, we can clearly observe the conversion of pyruvate into lactate and alanine.

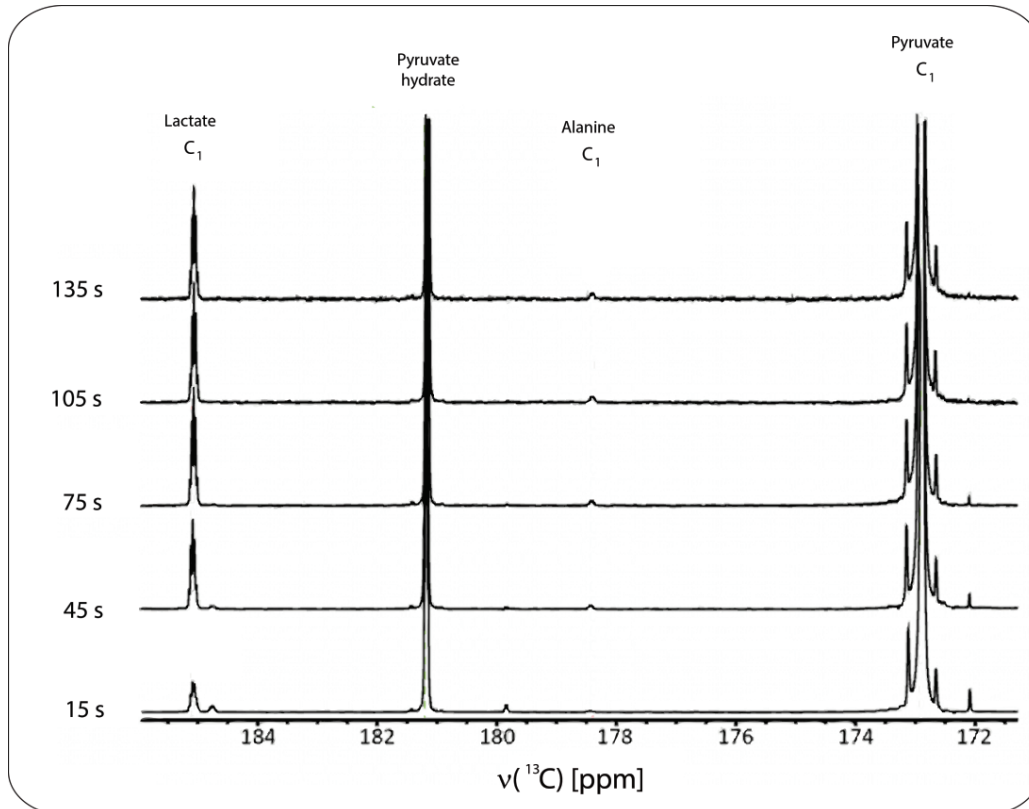


Fig. 5.8: ^{13}C NMR spectra of macrophages fed with hyperpolarized $[1-^{13}\text{C}]$ sodium pyruvate after d-DNP. The NMR spectra were recorded at intervals of 30 s by applying 10° pulses and show the conversion of pyruvate into lactate and alanine.

5.4.3 Conclusions concerning metabolism in cells

By feeding macrophages with two different metabolites, $[U-^2\text{H}, ^{13}\text{C}]$ glucose and $[1-^{13}\text{C}]$ sodium pyruvate, we have been able to observe in real time their conversion into their corresponding metabolites (glycerol, alanine and lactate). Future interesting applications of d-DNP could be the observation of changes in metabolic pathways of macrophages by applying different stimuli to the cells.

References

1. A. Comment, S. Jannin, J. N. Hyacinthe, P. Miéville, R. Sarkar, P. Ahuja, P. R. Vasos, X. Montet, F. Lazeyras, J. P. Vallee, P. Hautle, J. A. Konter, B. van den Brandt, J. P. Ansermet, R. Grütter and G. Bodenhausen, *Hyperpolarizing Gases via Dynamic Nuclear Polarization and Sublimation*, 2010, Phys. Rev. Lett. 105, 018104.
2. A. Capozzi, C. Roussel, A. Comment and J. N. Hyacinthe, *Optimal Glass-Forming Solvent Brings Sublimation Dynamic Nuclear Polarization to ^{129}Xe Hyperpolarization Biomedical Imaging Standards*, 2015, J. Phys. Chem. C 119, 5020-5025.
3. N. N. Kuzma, M. Pourfathi, H. Kara, P. Manasseh, R. K. Ghosh, J. H. Ardenkjaer-Larsen, S. J. Kadlecsek and R. R. Rizi, *Cluster formation restricts dynamic nuclear polarization of xenon in solid mixtures*, 2012, J. Chem. Phys. 137, 104508.
4. R. K. Ghosh, N. N. Kuzma, S. J. Kadlecsek and R. R. Rizi, *Versatile Pulse Sequence Device to Conserve Hyperpolarization for NMR and MRI Studies*, 2016, Magn. Reson. Med. 75, 1822-1830.
5. A. Kastler, *Optical Methods of Atomic Orientation and of Magnetic Resonance*, 1957, J. Opt. Soc. Am. 47, 460-465.
6. T. G. Walker and W. Happer, *Spin-exchange optical pumping of noble-gas nuclei*, 1997, Rev. Mod. Phys. 69, 629-642.
7. D. Gajan, A. Bornet, B. Vuichoud, J. Milani, R. Melzi, H. A. van Kalkeren, L. Veyre, C. Thieuleux, M. P. Conley, W. R. Grüning, M. Schwarzwälder, A. Lesage, C. Copéret, G. Bodenhausen, L. Emsley and S. Jannin, *Hybrid polarizing solids for pure hyperpolarized liquids through dissolution dynamic nuclear polarization*, 2014, P. Natl. Acad. Sci. USA 111, 14693-14697.
8. B. Vuichoud, E. Canet, J. Milani, A. Bornet, D. Baudouin, L. Veyre, D. Gajan, L. Emsley, A. Lesage, C. Copéret, C. Thieuleux, G. Bodenhausen, I. Koptuyug and S. Jannin, *Hyperpolarization of Frozen Hydrocarbon Gases by Dynamic Nuclear Polarization at 1.2 K*, 2016, J. Phys. Chem. Lett. 7, 3235-3239.
9. D. Raftery, H. Long, T. Meersmann, P. J. Grandinetti, L. Reven and A. Pines, *High-Field NMR of Adsorbed Xenon Polarized by Laser Pumping*, 1991, Phys. Rev. Lett. 66, 584-587.
10. F. D. Colegrove and P. A. Franken, *Optical Pumping of Helium in the $^3\text{S}_1$ Metastable State*, 1960, Phys. Rev. 119, 680-690.
11. I. C. Ruset, S. Ketel and F. W. Hersman, *Optical pumping system design for large production of hyperpolarized ^{129}Xe* , 2006, Phys. Rev. Lett. 96, 053002.
12. T. Meersmann and E. Brunner, *Hyperpolarized ^{129}Xe Magnetic Resonance: Concepts, Production, Techniques and Applications*, 2015, RSC Publishing, Cambridge, U.K.
13. A. Cherubini and A. Bifone, *Hyperpolarised xenon in biology*, 2003, Prog. Nucl. Mag. Res. Sp. 42, 1-30.
14. K. V. Kovtunov, V. V. Zhivonitko, I. V. Skovpin, D. A. Barskiy and I.V. Koptuyug, *Parahydrogen-induce polarization in heterogeneous catalytic processes*, 2012, Top. Curr. Chem. 338, 123-180.
15. K. V. Kovtunov, D. A. Barskiy, A. M. Coffey, M. L. Truong, O. G. Salnikov, A. K. Khudorozhkov, E. A. Inozemtseva, I. P. Prosvirin, V. I. Bukhtiyarov, K. W. Waddell, E. Y. Chekmenev and I. V. Koptuyug, *High-resolution 3D proton MRI of hyperpolarized gas enabled by parahydrogen and Rh/TiO₂ heterogeneous catalyst*, 2014, Chemistry 20, 11636-11639.
16. V. V. Zhivonitko, V. V. Telkki and I. V. Koptuyug, *Characterization of microfluidic gas reactors using remote-detection MRI and parahydrogen-induced polarization*, 2012, Angew. Chem. Int. Ed. 51, 8054-8058.

17. A. Bornet, A. Pinon, A. Jhajharia, M. Baudin, X. Ji, L. Emsley G. Bodenhausen, J. H. Ardenkjaer-Larsen and S. Jannin, *Microwave-Gated Dynamic Nuclear Polarization*, 2016, Phys. Chem. Chem. Phys., in press.
18. D. Baudouin, H. A. van Kalkeren, A. Bornet, B. Vuichoud, L. Veyre, M. Cavailles, M. Schwarzwälder, W.-C. Liao, D. Gajan, G. Bodenhausen, L. Emsley, A. Lesage, S. Jannin, C. Copéret and C. Thieuleux, *Cubic Three-Dimensional Hybrid Silica Solids for Nuclear Hyperpolarization*, 2016, Chem. Sci., DOI: 10.1039/C6SC02055K.
19. W. R. Grüning, H. Bieringer, M. Schwarzwälder, D. Gajan, A. Bornet, B. Vuichoud, J. Milani, D. Baudouin, L. Veyre, A. Lesage, S. Jannin, G. Bodenhausen, C. Thieuleux and C. Copéret, *Phenylazide Hybrid-Silica – Polarization Platform for Dynamic Nuclear Polarization at Cryogenic Temperatures*, 2016, Helv. Chim. Acta, DOI: 10.1002/hlca.201600122.
20. A. Comment, B. van den Brandt, K. Uffmann, F. Kurdzesau, S. Jannin, J. A. Konter, P. Hautle, W. T. H. Wenckebach, R. Gruetter and J. J. van der Klink, *Design and performance of a DNP prepolarizer coupled to a rodent MRI scanner*, 2007, Concept. Magn. Reson. B 31B, 255-269.
21. S. Jannin, A. Bornet, R. Melzi and G. Bodenhausen, *High field dynamic nuclear polarization at 6.7 T: Carbon-13 polarization above 70% within 20 min*, 2012, Chem. Phys. Lett. 549, 99-102.
22. A. Bornet, J. Milani, B. Vuichoud, A. J. P. Linde, G. Bodenhausen and S. Jannin, *Microwave frequency modulation to enhance Dissolution Dynamic Nuclear Polarization*, 2014, Chem. Phys. Lett. 602, 63-67.
23. A. Bornet, R. Melzi, A. J. P. Linde, P. Hautle, B. van den Brandt, S. Jannin and G. Bodenhausen, *Boosting Dissolution Dynamic Nuclear Polarization by Cross Polarization*, 2013, J. Phys. Chem. Lett. 4, 111-114.
24. T.E Lefort, *Process for the production of ethylene oxide*, 1935, Patent US1998878 A.
25. M. O. Ozbek and R. A. van Santen, *The Mechanism of Ethylene Epoxidation Catalysis*, 2013, Catal. Lett. 143, 131-141.
26. J. Rudolph, K. L. Reddy, J. P. Chiang and K. B. Sharpless, *Highly efficient epoxidation of olefins using aqueous H₂O₂ and catalytic methyltrioxorhenium/pyridine: Pyridine-mediated ligand acceleration*, 1997, J. Am. Chem. Soc. 119, 6189-6190.
27. S. Bowen and C. Hilty, *Rapid sample injection for hyperpolarized NMR spectroscopy*, 2010, Phys. Chem. Chem. Phys. 12, 5766-5770.
28. J. Milani, *Novel Instrumentation and Methods for Chemical Applications of Dissolution Dynamic Nuclear Polarization*, 2016, Ph. D. Thesis, EPFL, Switzerland.
29. C. G. Joo, K. N. Hu, J. A. Bryant and R. G. Griffin, *In situ temperature jump high-frequency dynamic nuclear polarization experiments: Enhanced sensitivity in liquid-state NMR spectroscopy*, 2006, J. Am. Chem. Soc. 128, 9428-9432.
30. M. Bloom, M. Lipsicas and B. H. Müller, *Proton spin-lattice relaxation in polyatomic gases*, 1961, Can. J. Phys. 39, 1093-1109.
31. C. J. J. Jameson, A. K. Jameson, N. C. Smith, J. K. Hwang and T. Zia, *Carbon-13 and proton spin relaxation in methane in the gas phase*, 1991, J. Phys. Chem. 95, 1092-1098.
32. V. V. Zhivonitko, K. V. Kovtunov, P. L. Chapovsky and I. V. Koptug, *Nuclear spin isomers of ethylene: enrichment by chemical synthesis and application for NMR signal enhancement*, 2013, Angew. Chem. Int. Ed. 52, 13251-13255.
33. G. J. Hirasaki, S. W. Lo and Y. Zhang, *NMR properties of petroleum reservoir fluids*, 2003, Magn. Reson. Imaging 21, 269-277.
34. K. Jackowski and M. Jaszunski, *Gas-Phase NMR*, 2016, Royal Society of Chemistry, Cambridge, U.K.
35. N. J. L. Trappeniers and F. A. S. Ligthart, *Proton spin relaxation in ethylene. A new high pressure phase*, 1973, Chem. Phys. Lett. 19, 465-470.
36. R. Buratto, A. Bornet, J. Milani, D. Mammoli, B. Vuichoud, N. Salvi, M. Singh, A. Laguerre, S. Passemard, S. Gerber-Lemaire, S. Jannin and G. Bodenhausen, *Drug Screening Boosted by Hyperpolarized Long-Lived States in NMR*, 2014, Chemmedchem 9, 2509-2515.

37. G. Stevanato, J. T. Hill-Cousins, P. Hakansson, S. S. Roy, L. J. Brown, R. C. Brown, G. Pileio and M. H. Levitt, *A Nuclear Singlet Lifetime of More than One Hour in Room-Temperature Solution*, 2015, *Angew. Chem. Int. Ed.* 127, 3811-3814.
38. G. Stevanato, S. S. Roy, J. Hill-Cousins, I. Kuprov, L. J. Brown, R. C. Brown, G. Pileio and M. H. Levitt, *Long-lived nuclear spin states far from magnetic equivalence*, 2015, *Phys. Chem. Chem. Phys.* 17, 5913-5922.
39. P. R. Vasos, A. Comment, R. Sarkar, P. Ahuja, S. Jannin, J. P. Ansermet, J. A. Konter, P. Hautle, B. van den Brandt and G. Bodenhausen, *Long-lived states to sustain hyperpolarized magnetization*, 2009, *P. Natl. Acad. Sci. USA* 106, 18469-18473.
40. *Ullmann's Encyclopedia of Industrial Chemistry*, 2012, Wiley-VCH, Verlag GmbH & Co. KGaA.
41. W. J. Griffiths, *Metabolomics, Metabonomics and Metabolite Profiling*, 2008, Cambridge RSC Publishing.
42. O. Jones, *Metabolomics and Systems Biology in Human Health and Medicine*, 2014, RMIT University, Australia.
43. J. N. Dumez, J. Milani, B. Vuichoud, A. Bornet, J. Lalande-Martin, I. Tea, M. Yon, M. Maucourt, C. Deborde, A. Moing, L. Frydman, G. Bodenhausen, S. Jannin and P. Giraudeau, *Hyperpolarized NMR of plant and cancer cell extracts at natural abundance*, 2015, *Analyst* 140, 5860-5863.
44. R. Peyraud, P. Kiefer, P. Christen, S. Massou, J. C. Portais and J. A. Vorholt, *Demonstration of the ethylmalonyl-CoA pathway by using ¹³C metabolomics*, 2009, *P. Natl. Acad. Sci. USA* 106, 4846-4851.
45. B. Vuichoud, J. Milani, A. Bornet, R. Melzi, S. Jannin and G. Bodenhausen, *Hyperpolarization of deuterated metabolites via remote cross-polarization and dissolution dynamic nuclear polarization*, 2014, *J. Phys. Chem. B* 118, 1411-1415.
46. D. M. Wilson, K. R. Keshari, P. E. Larson, A. P. Chen, S. Hu, M. Van Criekinge, R. Bok, S. J. Nelson, J. M. Macdonald, D. B. Vigneron and J. Kurhanewicz, *Multi-compound polarization by DNP allows simultaneous assessment of multiple enzymatic activities in vivo*, 2010, *J. Magn. Reson.* 205, 141-147.
47. C. Ludwig, I. Marin-Montesinos, M. G. Saunders, A. H. Emwas, Z. Pikramenou, S. P. Hammond and U. L. Günther, *Application of ex situ dynamic nuclear polarization in studying small molecules*, 2010, *Phys. Chem. Chem. Phys.* 12, 5868-5871.
48. M. Mishkovsky and L. Frydman, *Progress in hyperpolarized ultrafast 2D NMR spectroscopy*, 2008, *ChemPhysChem* 9, 2340-2348.
49. P. Giraudeau, Y. Shrot and L. Frydman, *Multiple ultrafast, broadband 2D NMR spectra of hyperpolarized natural products*, 2009, *J. Am. Chem. Soc.* 131, 13902-13903.
50. L. Frydman, T. Scherf and A. Lupulescu, *The acquisition of multidimensional NMR spectra within a single scan*, 2002, *P. Natl. Acad. Sci. USA* 99, 15858-15862.
51. S. Meier, P. R. Jensen and J. O. Duus, *Direct Observation of Metabolic Differences in Living Escherichia Coli Strains K-12 and BL21*, 2012, *Chembiochem* 13, 308-310.
52. S. Meier, P. R. Jensen and J. O. Duus, *Real-time detection of central carbon metabolism in living Escherichia coli and its response to perturbations*, 2011, *Febs. Lett.* 585, 3133-3138.
53. S. Meier, M. Karlsson, P. R. Jensen, M. H. Lerche and J. O. Duus, *Metabolic pathway visualization in living yeast by DNP-NMR*, 2011, *Mol. Biosyst.* 7, 2834-2836.
54. M. Callon, *NMR experiments to characterize cellular and molecular mechanisms : from metabolomics to protein biogenesis*, 2016, Ph. D. Thesis, University of Basel, Switzerland.
55. M. Callon, B. Vuichoud, M. Rosas-Ballina, A. Bornet, L. He, J. Milani, M. Baudin, G. Bodenhausen, D. Bumann, S. Jannin and S. Hiller, *Real-Time Observation by NMR of Slow Metabolic Events in Living Mammalian Macrophages by Dissolution Dynamic Nuclear Polarization*, 2016, in preparation.
56. D. A. Ovchinnikov, *Macrophages in the embryo and beyond: Much more than just giant phagocytes*, 2008, *Genesis* 46, 447-462.
57. B. Ghesquiere, B. W. Wong, A. Kuchnio and P. Carmeliet, *Metabolism of stromal and immune cells in health and disease*, 2014, *Nature* 511, 167-176.

58. S. Galvan-Pena and L. A. J. O'Neill, *Metabolic reprogramming in macrophage polarization*, 2014, *Front. Immunol.* 5, 420.
59. P. Newsholme, R. Curi, S. Gordon and E. A. Newsholme, *Metabolism of Glucose, Glutamine, Long-Chain Fatty-Acids and Ketone-Bodies by Murine Macrophages*, 1986, *Biochem. J.* 239, 121-125.
60. G. C. Hard, *Some biochemical aspects of the immune macrophage*, 1970, *Br. J. Exp. Pathol.* 51, 97-105.
61. S. E. Calvano, W. Z. Xiao, D. R. Richards, R. M. Felciano, H. V. Baker, R. J. Cho, R. O. Chen, B. H. Brownstein, J. P. Cobb, S. K. Tschoeke, C. Miller-Graziano, L. L. Moldawer, M. N. Mindrinos, R. W. Davis, R. G. Tompkins and S. F. Lowry, *Inflammation Host Response Injury, A network-based analysis of systemic inflammation in humans*, 2005, *Nature* 437, 1032-1037.
62. J. Milani, B. Vuichoud, A. Bornet, P. Miéville, R. Mottier, S. Jannin and G. Bodenhausen, *A magnetic tunnel to shelter hyperpolarized fluids*, 2015, *Rev. Sci. Instrum.* 86, 024101.

Conclusions

In this thesis, several improvements have been made in order to achieve large enhancements in liquid phase after dissolution-DNP.

We have shown the benefits of using frequency-modulated microwave irradiation to increase the hyperpolarized signals in the solid state, while lowering by a factor of two the radical concentrations in DNP samples, which leads to more persistent hyperpolarized solutions after dissolution. Furthermore, we have tested different mono- and bi-radicals under our specific conditions ($B_0 = 6.7$ T and $T = 1.2 - 4.2$ K) to observe the effects on the ^1H polarization of small changes in the structures of these molecules that contain unpaired electrons.

We have demonstrated that Cross-Polarization can be performed by starting from remote protons that are present in the "*DNP juice*", so that it was possible to fully deuterate the metabolites to be polarized in order to extend their hyperpolarized lifetimes after dissolution. In order to obtain pure and persistent hyperpolarized solutions, a novel generation of materials dubbed HYPISO for d-DNP was tested in our laboratory, and gave relatively good results for the ^{13}C polarization of metabolites. To obtain similar results for pure and persistent hyperpolarized water, a new class of filterable polymers containing radicals, called FLAP, was also synthesized and tested in our laboratory.

Finally, a wide variety of applications that can benefit from dissolution-DNP were presented, ranging from metabolomic studies to the real-time observation of metabolic pathways in cells. This list is not exhaustive and, in the next few years, the popularity of d-DNP is likely to extend to other domains.

Supporting Information

6.1 Annexes

Herein are described the preparation of various DNP samples, the synthesis of different polarizing agents, and the specifications of the DNP methods used for each experiment. These annexes are summarized for each chapter of this thesis in the order where they appear.

6.1.1 Optimization of radicals for dissolution-DNP

Sample preparation:

TEMPOL (Sigma Aldrich), TOTAPOL (provided by the SREP, Institut de Chimie Radicalaire, Aix-Marseille Université) and AMUPOL (also provided by the SREP) were dissolved at concentrations varying from 20 – 65 mM in a mixture of H₂O/D₂O/glycerol-*d*₈ (v/v/v : 10/40/50). The resulting solutions were rapidly inserted in the DNP polarizer at $T = 4.2$ K. DNP was performed using continuous microwave irradiation at frequencies $187.5 < f_{\mu\text{W}} < 188.5$ GHz with a maximum power $P_{\mu\text{W}} = 87.5$ mW at the top of the DNP insert.

TEMPOL (Sigma Aldrich), TEMPOL-*d*₁₂, ditertbutyl-TEMPO, PyTEMPAMINE and CarbTEMPOL (all provided by the SREP, Institut de Chimie Radicalaire, Aix-Marseille Université) were dissolved at concentrations of 25 and 40 mM in a mixture of H₂O/D₂O/glycerol-*d*₈ (v/v/v : 10/40/50) and shock-frozen in the DNP polarizer at 4.2 K. For CarbTEMPOL, the pH was adjusted to 8-9 in order to properly solubilize the radicals. The temperature was cooled down to 1.2 K before starting the measurements. DNP was performed using frequency-modulated microwave irradiation at $f_{\mu\text{W}} = 187.9$ and 188.3 GHz (modulation frequency 10 kHz and modulation amplitude ± 100 MHz) [1] with a maximum power $P_{\mu\text{W}} = 87.5$ mW at the top of the DNP insert.

6.1.2 Microwave frequency modulation for dissolution Dynamic Nuclear Polarization

Sample preparation:

TEMPOL (purchased from Sigma Aldrich) was dissolved in H₂O/D₂O/glycerol-*d*₈ (v/v/v : 10/40/50). To verify the efficiency of ¹H – ¹³C Cross-Polarization, 3M [¹³C] sodium acetate (Cambridge Isotopes) was added to the mixture. For each sample, 10 pellets of 10 μl each (i.e., a total of 100 μl) were frozen at 70 K in liquid nitrogen, visually inspected to ensure a good homogeneity by checking that the beads remained translucent and glassy, and then transferred to the DNP polarizer at 4.2 K.

Cross-Polarization:

Cross-Polarization experiments from ¹H to ¹³C were accomplished during DNP by applying radio-frequency modulated WURST pulses simultaneously to both channels, with durations optimized to 2 ms for samples containing 25 mM of TEMPOL and 1 ms for samples containing 50 mM of TEMPOL, with frequency sweeps of 100 kHz, and amplitudes $\gamma B_1 / (2\pi) = 20$ kHz on both channels to match the Hartmann-Hahn condition.

Microwave irradiation:

DNP was performed using microwave irradiation at frequencies $187.5 < f_{\mu\text{W}} < 188.5$ GHz with a maximum power $P_{\mu\text{W}} = 87.5$ mW at the top of the DNP insert. The frequency was controlled by a voltage control oscillator (VCO) with either a constant or a modulated voltage, thus allowing a fast and broad frequency modulation up to 10 MHz over a range of ± 500 MHz.

NMR measurements:

The polarization was carefully calibrated at $T = 4.2$ K and $B_0 = 6.7$ T by applying 32 pulses with 1° nutation angles for ¹H, and 16 pulses with 5° nutation angles for ¹³C. The depletion of the polarization caused by these pulses (0.999 for ¹H and 0.95 for ¹³C) was taken into account. The exact same pulses were used during the measurement of the DNP-enhanced spectra.

6.1.3 Spin Polarimetry Magnetic Resonance (SPY-MR)

Sample preparation:

A precise amount of 111 mg (1 mmol) of [1-¹³C] sodium pyruvate (purchased from Cambridge Isotopes) was added to 20 ml D₂O 99.9 % (Cambridge Isotopes). The pH of this solution was adjusted to pH 10 by addition of 10 μl 1 M NaOD (Sigma Aldrich). The overall mixture was then stirred for 1 day at room temperature and the reaction was stopped by adding 1 M DCl (Sigma Aldrich) to make the pH neutral. The resulting solution of [1-¹³C] sodium pyruvate-*d*₃ was lyophilized in order to remove D₂O and a white powder was obtained as final product. Two solutions, one containing 1.5 M [1-¹³C] sodium pyruvate-*d*₃, and the other 1.5 M [1,2-¹³C₂] sodium acetate-*d*₃ (Cambridge Isotopes), were prepared in a glass-forming solvent mixture H₂O/D₂O/glycerol-*d*₈ (v/v/v : 10/40/50) doped with 50 mM of TEMPOL.

Dissolution-DNP experiments:

Of each sample, 5 droplets of 10 μl were frozen in liquid nitrogen and inserted in the DNP polarizer. Five frozen drops of 10 μl each containing 3 M ascorbate in D₂O were also inserted in the polarizer in order to scavenge the radicals after dissolution. [2] DNP was performed by monochromatic microwave irradiation at $f_{\mu\text{W}} = 188.3$ GHz with $P_{\mu\text{W}} = 87.5$ mW and combined with ¹H – ¹³C CP contacts every 5 min. Dissolution was performed in 700 ms with 5 ml superheated D₂O ($T = 413$ K and $p = 10$ bar). The dissolved sample was pushed by helium gas at 6 bar in 3.5 s to a 7.05 T Bruker magnet through a 1.5 mm inner diameter polytetrafluoroethylene (PTFE) tube running through a 0.9 T magnetic tunnel [3] leading to a home-built injector placed just above a 5 mm sample tube containing 250 μl of D₂O for field-frequency locking; the sample was then injected in 2 s. The overall sequence of dissolution, transfer and injection took place in $t_{\text{overall}} = 6.2$ s and 5° pulses were applied to the ¹³C nuclei at intervals of 5 s.

Relaxation Matrix:

For sodium pyruvate, the relaxation matrix was determined as follows: (1) the crystal structure of sodium pyruvate was obtained from the Cambridge Structural Database, (2) the CSA tensor was predicted with CASTEP [4], and the relaxation was calculated using the SpinDynamica code for Mathematica. [5]

Constants

```

γCI = 6.728 × 107;
γCS = 6.728 × 107 * (1 + 30 × 10-6);
h = 1.05457173 × 10-34;
kB = 1.3806488 × 10-23;
τc = 4 × 10-12;
B0 = 7.05;
σCI = 70 × 10-6;
σCS = 90 × 10-6;
φ = 0;
r = 1.54 × 10-10;

```

Spectral densities

```

JII[γCI_, γCS_, σCI_, σCS_, φ_, r_, τc_, B0_, ω_] :=  $\frac{1}{30} \gamma_{CI}^2 B0^2 \sigma_{CI}^2 \frac{\tau c}{1 + (\omega \tau c)^2}$ ;
JISI[γCI_, γCS_, σCI_, σCS_, φ_, r_, τc_, B0_, ω_] :=  $\frac{1}{10} (10^{-7}) \gamma_{CI}^2 \gamma_{CS} h (r^{-3}) B0 \sigma_{CI} \frac{\tau c}{1 + (\omega \tau c)^2} \frac{1}{2} (3 \text{Cos}[\phi \text{Degree}]^2 - 1)$ ;
JISIS[γCI_, γCS_, σCI_, σCS_, φ_, r_, τc_, B0_, ω_] :=  $\frac{3}{10} (10^{-7})^2 \gamma_{CI}^2 \gamma_{CS}^2 h^2 (r^{-3})^2 \frac{\tau c}{1 + (\omega \tau c)^2}$ ;
JIS[γCI_, γCS_, σCI_, σCS_, φ_, r_, τc_, B0_, ω_] :=  $\frac{1}{30} \gamma_{CS}^2 B0^2 \sigma_{CS}^2 \frac{\tau c}{1 + (\omega \tau c)^2}$ ;
JISS[γCI_, γCS_, σCI_, σCS_, φ_, r_, τc_, B0_, ω_] :=  $\frac{1}{10} (10^{-7}) \gamma_{CS}^2 \gamma_{CI} h (r^{-3}) B0 \sigma_{CS} \frac{\tau c}{1 + (\omega \tau c)^2} \frac{1}{2} (3 \text{Cos}[\phi \text{Degree}]^2 - 1)$ ;

JII[γCI, γCS, σCI, σCS, φ, r, τc, B0, γCI B0]
JISI[γCI, γCS, σCI, σCS, φ, r, τc, B0, γCI B0]
JISIS[γCI, γCS, σCI, σCS, φ, r, τc, B0, γCI B0]
JIS[γCI, γCS, σCI, σCS, φ, r, τc, B0, γCS B0]
JISS[γCI, γCS, σCI, σCS, φ, r, τc, B0, γCS B0]

```

Transitions

```

WIIaint[γCI_, γCS_, σCI_, σCS_, φ_, r_, τc_, B0_] :=  $\frac{1}{2} J_{ISIS}[\gamma_{CI}, \gamma_{CS}, \sigma_{CI}, \sigma_{CS}, \phi, r, \tau c, B0, \gamma_{CI} B0] + 2 J_{II}[\gamma_{CI}, \gamma_{CS}, \sigma_{CI}, \sigma_{CS}, \phi, r, \tau c, B0, \gamma_{CI} B0] - 2 J_{ISI}[\gamma_{CI}, \gamma_{CS}, \sigma_{CI}, \sigma_{CS}, \phi, r, \tau c, B0, \gamma_{CI} B0]$ ;
WIIβint[γCI_, γCS_, σCI_, σCS_, φ_, r_, τc_, B0_] :=  $\frac{1}{2} J_{ISIS}[\gamma_{CI}, \gamma_{CS}, \sigma_{CI}, \sigma_{CS}, \phi, r, \tau c, B0, \gamma_{CI} B0] + 2 J_{II}[\gamma_{CI}, \gamma_{CS}, \sigma_{CI}, \sigma_{CS}, \phi, r, \tau c, B0, \gamma_{CI} B0] + 2 J_{ISI}[\gamma_{CI}, \gamma_{CS}, \sigma_{CI}, \sigma_{CS}, \phi, r, \tau c, B0, \gamma_{CI} B0]$ ;
WISaint[γCI_, γCS_, σCI_, σCS_, φ_, r_, τc_, B0_] :=  $\frac{1}{2} J_{ISIS}[\gamma_{CI}, \gamma_{CS}, \sigma_{CI}, \sigma_{CS}, \phi, r, \tau c, B0, \gamma_{CS} B0] + 2 J_{IS}[\gamma_{CI}, \gamma_{CS}, \sigma_{CI}, \sigma_{CS}, \phi, r, \tau c, B0, \gamma_{CS} B0] - 2 J_{ISS}[\gamma_{CI}, \gamma_{CS}, \sigma_{CI}, \sigma_{CS}, \phi, r, \tau c, B0, \gamma_{CS} B0]$ ;
WISβint[γCI_, γCS_, σCI_, σCS_, φ_, r_, τc_, B0_] :=  $\frac{1}{2} J_{ISIS}[\gamma_{CI}, \gamma_{CS}, \sigma_{CI}, \sigma_{CS}, \phi, r, \tau c, B0, \gamma_{CS} B0] + 2 J_{IS}[\gamma_{CI}, \gamma_{CS}, \sigma_{CI}, \sigma_{CS}, \phi, r, \tau c, B0, \gamma_{CS} B0] + 2 J_{ISS}[\gamma_{CI}, \gamma_{CS}, \sigma_{CI}, \sigma_{CS}, \phi, r, \tau c, B0, \gamma_{CS} B0]$ ;
W2[γCI_, γCS_, σCI_, σCS_, φ_, r_, τc_, B0_] :=  $2 J_{ISIS}[\gamma_{CI}, \gamma_{CS}, \sigma_{CI}, \sigma_{CS}, \phi, r, \tau c, B0, (\gamma_{CI} + \gamma_{CS}) B0]$ ;
W0[γCI_, γCS_, σCI_, σCS_, φ_, r_, τc_, B0_] :=  $-\frac{1}{3} J_{ISIS}[\gamma_{CI}, \gamma_{CS}, \sigma_{CI}, \sigma_{CS}, \phi, r, \tau c, B0, (\gamma_{CI} - \gamma_{CS}) B0]$ ;

WIIaint[γCI, γCS, σCI, σCS, φ, r, τc, B0]
WIIβint[γCI, γCS, σCI, σCS, φ, r, τc, B0]
WISaint[γCI, γCS, σCI, σCS, φ, r, τc, B0]
WISβint[γCI, γCS, σCI, σCS, φ, r, τc, B0]
W2[γCI, γCS, σCI, σCS, φ, r, τc, B0]
W0[γCI, γCS, σCI, σCS, φ, r, τc, B0]

```

Values

```

ρItotint = W2[γCI, γCS, σCI, σCS, φ, r, τc, B0] + W0[γCI, γCS, σCI, σCS, φ, r, τc, B0] + WIIaint[γCI, γCS, σCI, σCS, φ, r, τc, B0] + WIIβint[γCI, γCS, σCI, σCS, φ, r, τc, B0]
TIItotint = 1 / ρItotint
ρStotint = W2[γCI, γCS, σCI, σCS, φ, r, τc, B0] + W0[γCI, γCS, σCI, σCS, φ, r, τc, B0] + WISaint[γCI, γCS, σCI, σCS, φ, r, τc, B0] + WISβint[γCI, γCS, σCI, σCS, φ, r, τc, B0]
TISStotint = 1 / ρStotint

TIExp = 68
ρIExp = 1 / 68 // N
|valeur numérique

JextI =  $\frac{1}{2} (\rho_{IExp} - \rho_{Itotint})$ 

TISExp = 47.5
ρSExp = 1 / 47.5 // N
|valeur numérique

JextS =  $\frac{1}{2} (\rho_{SExp} - \rho_{Stotint})$ 

ρIS = WIIaint[γCI, γCS, σCI, σCS, φ, r, τc, B0] + WIIβint[γCI, γCS, σCI, σCS, φ, r, τc, B0] + WISaint[γCI, γCS, σCI, σCS, φ, r, τc, B0] + WISβint[γCI, γCS, σCI, σCS, φ, r, τc, B0]
σI = W2[γCI, γCS, σCI, σCS, φ, r, τc, B0] - W0[γCI, γCS, σCI, σCS, φ, r, τc, B0]
δI = WIIaint[γCI, γCS, σCI, σCS, φ, r, τc, B0] - WIIβint[γCI, γCS, σCI, σCS, φ, r, τc, B0]
δS = WISaint[γCI, γCS, σCI, σCS, φ, r, τc, B0] - WISβint[γCI, γCS, σCI, σCS, φ, r, τc, B0]

```

6.1.4 Remote Cross-Polarization for deuterated metabolites

Sample preparation:

[1-¹³C] sodium pyruvate (purchased from Cambridge Isotopes, 111 mg, 1 mmol) was added to 20 ml D₂O 99.9 % (Cambridge Isotopes). The solution was adjusted to pH 10 by adding 10 µl of 1 M NaOD (Sigma Aldrich) and the solution was stirred for 1 day at room temperature. The reaction was stopped by adding 1 M DCl (Sigma Aldrich) to lower the pH to 7. The reaction produces [1-¹³C] sodium pyruvate-*d*₃ with a yield > 90 %. The side product [1,6-¹³C] parapyruvate-*d*₆ was produced with a yield < 10 %. The solution was then lyophilized in order to remove D₂O and a white powder was obtained.

Solutions of 1.5 M [1-¹³C] sodium pyruvate-*d*₃ and [1,2-¹³C₂] sodium acetate-*d*₃ (Cambridge Isotope) in D₂O/glycerol-*d*₈ (1/1) were doped with 50 mM TEMPOL (Sigma Aldrich). Solutions of 1.5 M [1-¹³C] sodium pyruvate-*d*₃ and [1,2-¹³C₂] sodium acetate-*d*₃ in H₂O/D₂O/glycerol-*d*₈ (v/v/v : 10/40/50) were also doped with 50 mM TEMPOL (Sigma Aldrich).

Dissolution-DNP experiments:

DNP was performed by applying CW microwave irradiation at $f_{\mu\text{W}} = 188.3$ GHz and $P_{\mu\text{W}} = 87.5$ mW. Adiabatic CP contacts were established at intervals of 5 min with 30 W applied to the ¹H and 45 W to the ¹³C channels (radio-frequency amplitudes of 40 kHz on both channels). Five frozen beads of 10 µl each of the DNP sample were mixed with 5 frozen beads of 10 µl each containing 3 M ascorbate in D₂O. They were dissolved together with 5 ml of superheated D₂O ($T = 413$ K and $p = 10$ bar) and intimately mixed in 700 ms, transferred in 3.5 s to a 7.05 T Bruker magnet through a 1.5 mm diameter PTFE tube in a 0.9 T magnetic tunnel [3], pressurized with helium gas at 6 bar. After a fast injection in 0.5 s into a 5 mm NMR tube containing 250 µl of D₂O to allow field-frequency locking, 5° detection pulses were applied every 5 s to record the decay of the hyperpolarized ¹³C signal.

6.1.5 HYperPolarizing Solids (HYPSO)

Sample preparation:

Three different solutions were prepared: **(1)** 3 M [^{13}C] sodium pyruvate (Cambridge Isotopes) in $\text{H}_2\text{O}/\text{D}_2\text{O}$ (v/v : 1/9) with a $\text{NaH}_2\text{PO}_4/\text{Na}_2\text{HPO}_4$ buffer at pH 7.5-8, **(2)** 3 M [^{13}C] sodium acetate (Cambridge Isotopes) in $\text{H}_2\text{O}/\text{D}_2\text{O}$ (v/v : 1/9), **(3)** a mixture of 1 M sodium fumarate in natural abundance, 1 M alanine-glycine in natural abundance [$\text{CH}_3\text{CH}(\text{NH}_2)^{13}\text{CONHCH}_2^{13}\text{COOH}$] and 1 M [^{13}C] enriched sodium acetate (Cambridge Isotopes) in $\text{H}_2\text{O}/\text{D}_2\text{O}$ (v/v : 1/9). Typically 20 mg of HYPSO materials are impregnated with 36 μl solution; the wetted solid is placed in the DNP polarizer.

Synthesis of HYPSO:

HYPSO-1 (formerly called MatTEMPO 1/X), HYPSO-1 containing trityl and HYPSO-2 were synthesized at the CRMN in Lyon and at ETH in Zürich according to the literature. [6]

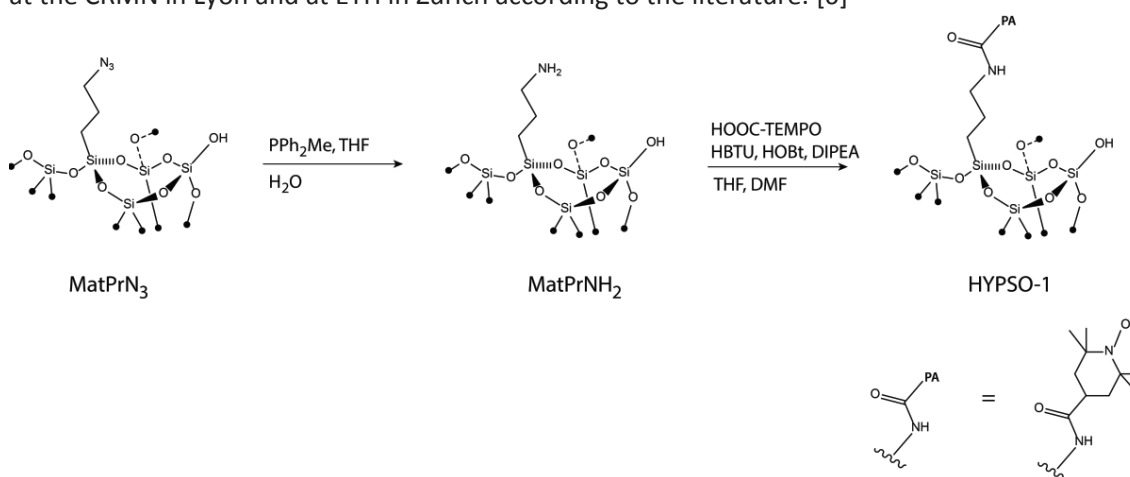


Fig. 6.1: Synthesis of HYPSO-1.

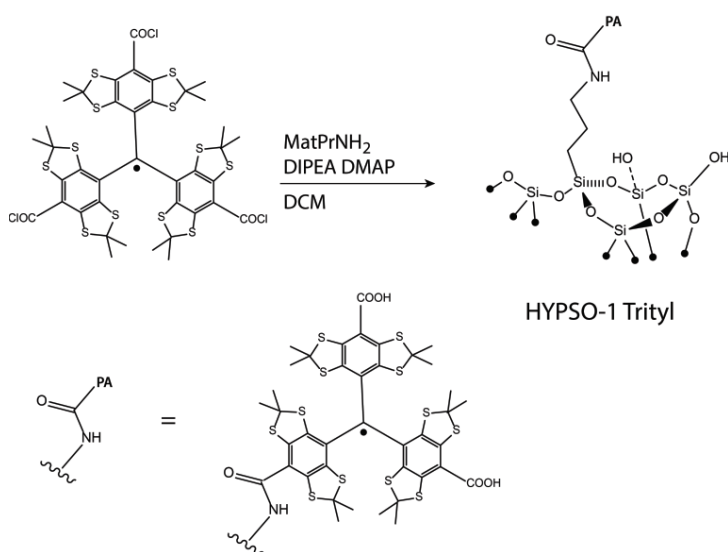


Fig. 6.2: Synthesis of HYPSO-1 with trityl radicals.

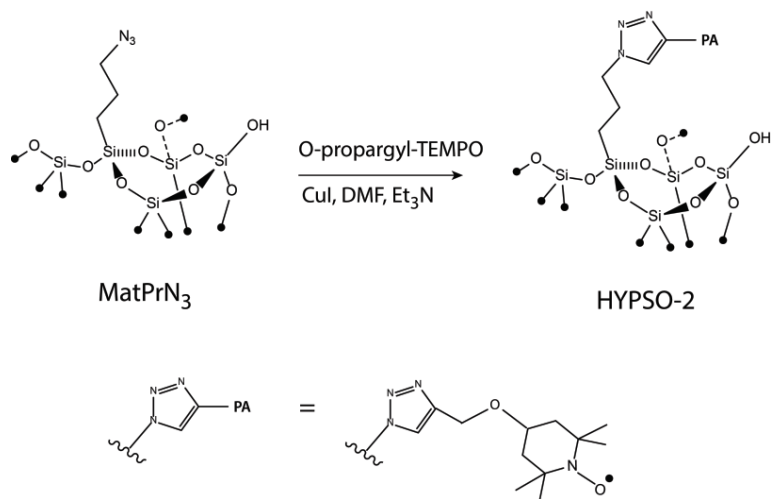


Fig. 6.3: Synthesis of HYPSO-2.

6.1.6 Filterable Labeled Agents for Polarization (FLAP)

Sample preparation:

*p*NiPAM-COOH (2.00 g, 0.2 mmol, 1 equiv.) with an average mass of approximately 10 kDa (from 7500 to 12'500 by GPC), terminated by a carboxylic acid (Sigma Aldrich), was dissolved in 25 mL dry EtOAc under N₂ in a 100 mL flask. *N*-hydroxy succinimide (58 mg, 0.5 mmol, 2.5 equiv.) and *N,N'*-dicyclohexylcarbodiimide (DCC, 103 mg, 0.5 mmol, 2.5 equiv.) were added at room temperature. The reaction mixture was then stirred at room temperature for 24 h to obtain a turbid colorless suspension. NH₂-TEMPO (4-amino TEMPO, 85 mg, 0.5 mmol, 2.5 equiv) was then added and the solution was stirred at room temperature for another 24 h. The EtOAc was removed by rotavap and the crude was dissolved in water and purified by dialysis (membrane MWCO = 3500 Da) against de-ionized (DI) water for 3 days. The resulting suspension was finally filtered through a por4 fritted funnel and water was removed by freeze drying.

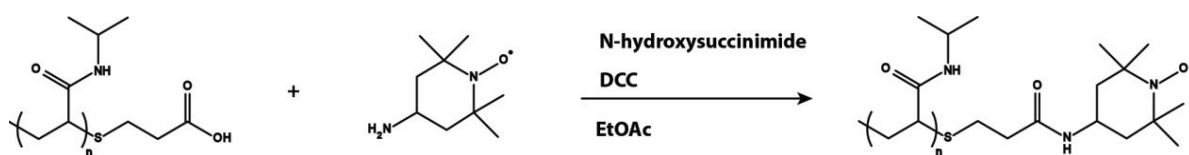


Fig. 6.4: Synthesis of FLAP.

Hyperpolarization of water with 25 % spin-labeled FLAP and 75 % *p*NiPAM-COOH: 12.5 mg FLAP and 37.5 mg of *p*NiPAM-COOH were mixed together and impregnated with 100 μ l 1 M NaCl in H₂O (11.6 mg/100 μ l). The sample was centrifuged at 2000 g for 30 s so that the polymer was uniformly wetted. The white powder was shock-frozen in liquid helium in the DNP polarizer.

Osteopontin was expressed and purified by the group of Prof. Robert Konrat in Vienna as published earlier. [7]

Dissolution-DNP experiments:

DNP was performed at 1.2 K with $f_{\mu\text{W}} = 187.9$ GHz and $P_{\mu\text{W}} = 87.5$ mW using frequency-modulated microwave irradiation (modulation frequency 10 kHz and modulation amplitude ± 100 MHz). 50 μ l of the polarized samples were quickly heated in 700 ms by 5 ml of superheated D₂O ($T = 413$ K and $p = 10$ bar). A small cellulose filter was placed at the bottom of the dissolution stick (close to the magnetic center of the polarizer) to separate properly the insoluble FLAP polymer from the solution. The remaining hyperpolarized solution was then transferred in 10 s through a 1.5 mm inner diameter PTFE tube lined with 0.9 T permanent magnets, pushed by helium gas at 6 bar to a 500 MHz NMR spectrometer at a distance of *ca.* 5 m. The injection into the NMR tube took place in 1 s and the decay of the hyperpolarized signal of ¹H was monitored by applying 0.1° detection pulses at intervals of 2 s.

Selective SOFAST-HMQC experiments [8] were performed as described by Frydman *et al.* [9] using 64 increments in the indirect dimension, with 1 scan per increment and gradient selection of the ¹⁵N and ¹H coherences with a recycling time of 0.2 s.

6.1.7 Hyperpolarization of frozen hydrocarbon gases

Sample preparation:

A mixture of *n*-butane, isobutane, and propane ("butane refill gas", Migros, 50 mL, 127 mg) was condensed with 10.2 mg of HYP SO-1 (loading capacity 1.8 mL/g) and only 11 mg of the gas entered the pores of the material.

Ethylene (Carbagas, 50 mL, 59 mg) was condensed with 22.5 mg HYP SO-3 (loading capacity 0.47 mL/g); only 5.9 mg of the gas entered the pores of the material.

DNP experiments:

DNP was performed by applying frequency-modulated microwave irradiation at $f_{\mu\text{W}} = 188.3$ GHz (with a modulation frequency 10 kHz and a modulation amplitude ± 100 MHz) and $P_{\mu\text{W}} = 87.5$ mW. Adiabatic CP contacts were established at intervals of 5 min or 10 min.

6.1.8 Hyperpolarization of biological extracts

Sample preparation:

Tomato plants were prepared at the Université de Nantes as described in the Supporting Information of reference [10]. The resulting extract was dissolved in 200 μ l of a mixture of H₂O/D₂O/glycerol-*d*₈ (v/v/v : 20/30/50) doped with 25 mM TEMPOL (Sigma Aldrich).

Two breast cancer cell cultures (one culture with natural abundance, the other grown in an enriched medium) were prepared and extracted at the Université de Nantes following the protocol summarized in reference [10]. Each extract was dissolved in 200 μ l of a mixture of H₂O/D₂O/glycerol-*d*₈ (v/v/v : 20/30/50) doped with 25 mM TEMPOL (Sigma Aldrich).

Dissolution-DNP experiments:

DNP was performed at 1.2 K and $B_0 = 6.7$ T with $f_{\mu\text{W}} = 188.3$ GHz and $P_{\mu\text{W}} = 87.5$ mW using frequency-modulated microwave irradiation (modulation frequency 10 kHz and modulation amplitude ± 100 MHz). Cross-Polarization from ¹H to ¹³C was performed at intervals of 5 min and the samples were dissolved with 5 ml of superheated D₂O ($T = 413$ K and $p = 10$ bar) after 30 min of polarization. The hyperpolarized solution was then transferred in 10 s through a 1.5 mm inner diameter PTFE tube lined with 0.9 T permanent magnets [3] pushed by helium gas at 6 bar to a 500 MHz NMR spectrometer. The injection into the NMR tube took place in 1 s.

6.1.9 In-Cell dissolution Dynamic Nuclear Polarization

Sample preparation:

Macrophage cell cultures were provided by Dr. Michael H. Sieweke, Marseille, and grown following the protocol of reference [11]. On the day of our d-DNP experiments, 80 millions of these cells were re-suspended in 280 μl of a medium suitable for NMR (DMEM, 44 mM sodium bicarbonate, 10 % FCS, 1 mM glutamine, 10 % D_2O) and transferred to a 5 mm NMR tube containing 120 μl D_2O . The sample was incubated during 15 min at 37° C prior to injection to avoid their degradation and apoptosis.

A first DNP sample containing 867 mM [$U\text{-}^2\text{H}$, ^{13}C] glucose (Cambridge Isotopes) in $\text{H}_2\text{O}/\text{D}_2\text{O}/\text{glycerol-}d_8$ (v/v/v : 10/40/50) with 50 mM TEMPOL (Sigma Aldrich) was prepared, as well as a second sample containing 1.5 M [$1\text{-}^{13}\text{C}$] sodium pyruvate (Cambridge Isotopes) in a mixture of $\text{D}_2\text{O}/\text{glycerol-}d_8$ (v/v : 1/1) with 25 mM TEMPOL (Sigma Aldrich).

Dissolution-DNP experiments:

DNP was performed at 1.2 K and $B_0 = 6.7$ T with $f_{\mu\text{W}} = 188.3$ GHz and $P_{\mu\text{W}} = 87.5$ mW using frequency-modulated microwave irradiation (modulation frequency 10 kHz and modulation amplitude ± 50 MHz). Direct ^{13}C polarization was performed on the sample containing glucose and Cross-Polarization from ^1H to ^{13}C at intervals of 5 min was performed on the sample containing pyruvate. Both samples were dissolved by 5 ml of superheated D_2O ($T = 413$ K and $p = 10$ bar). The hyperpolarized solution was then transferred in 10 s through a 1.5 mm inner diameter PTFE tube lined with 0.9 T permanent magnets [3] pushed by helium gas at 6 bar to a 500 MHz NMR spectrometer containing 400 μl of the suspension of macrophages at 37° C in D_2O .

References

1. A. Bornet, J. Milani, B. Vuichoud, A. J. P. Linde, G. Bodenhausen and S. Jannin, *Microwave Frequency Modulation to enhance Dissolution Dynamic Nuclear Polarization*, 2014, Chem. Phys. Lett. 602, 63-67.
2. P. Miéville, P. Ahuja, R. Sarkar, S. Jannin, P. R. Vasos, S. Gerber-Lemaire, M. Mishkovsky, A. Comment, R. Gruetter, O. Ouari, P. Tordo and G. Bodenhausen, *Scavenging Free Radicals To Preserve Enhancement and Extend Relaxation Times in NMR using Dynamic Nuclear Polarization*, 2010, Angew. Chem. Int. Edit. 49, 7834-7834.
3. J. Milani, B. Vuichoud, A. Bornet, P. Miéville, R. Mottier, S. Jannin and G. Bodenhausen, *A magnetic tunnel to shelter hyperpolarized fluids*, 2015, Rev. Sci. Instrum. 86, 024101.
4. S. J. Clark, M. D. Segall, C. J. Pickard, P. J. Hasnip, M. J. Probert, K. Refson and M. C. Payne, *First principles methods using CASTEP*, 2005, Z. Kristallogr. 220, 567-570.
5. SpinDynamica code for Mathematica, programmed by Malcolm H. Levitt, with contributions from Jyrki Rantaharju, Andreas Brinkmann, and Soumya Singha Roy, available at www.SpinDynamica.soton.ac.uk
6. D. Gajan, M. Schwarzwälder, M. P. Conley, W. R. Grüning, A. J. Rossini, A. Zagdoun, M. Lelli, M. Yulikov, G. Jeschke, C. Sauvée, O. Ouari, P. Tordo, L. Veyre, A. Lesage, C. Thieuleux, L. Emsley and C. Copéret, *Solid-Phase Polarization Matrixes for Dynamic Nuclear Polarization from Homogeneously Distributed Radicals in Mesostuctured Hybrid Silica Materials*, 2013, J. Am. Chem. Soc. 135, 15459-15466. (b) D. Gajan, A. Bornet, B. Vuichoud, J. Milani, R. Melzi, H. A. van Kalkeren, L. Veyre, C. Thieuleux, M. P. Conley, W. R. Grüning, M. Schwarzwälder, A. Lesage, C. Copéret, G. Bodenhausen, L. Emsley and S. Jannin, *Hybrid polarizing solids for pure hyperpolarized liquids through dissolution dynamic nuclear polarization*, 2014, P. Natl. Acad. Sci. USA 111, 14693-14697.
7. G. Platzer, A. Schedlbauer, A. Chemelli, P. Ozdowy, N. Coudeville, R. Auer, G. Kontaxis, M. Hartl, A. J. Miles, B. A. Wallace, O. Glatter, K. Bister and R. Konrat, *The Metastasis-Associated Extracellular Matrix Protein Osteopontin Forms Transient Structure in Ligand Interaction Sites*, 2011, Biochemistry 50, 6113-6124.
8. P. Schanda, E. Kupce and B. Brutscher, *SOFAST-HMQC experiments for recording two-dimensional heteronuclear correlation spectra of proteins within a few seconds*, 2005, J. Biomol. NMR 33, 199-211.
9. G. Olsen, E. Markhasin, O. Szekely, C. Bretschneider and L. Frydman, *Optimizing water hyperpolarization and dissolution for sensitivity-enhanced 2D biomolecular NMR*, 2016, J. Magn. Reson. 264, 49-58.
10. J. N. Dumez, J. Milani, B. Vuichoud, A. Bornet, J. Lalande-Martin, I. Tea, M. Yon, M. Maucourt, C. Deborde, A. Moing, L. Frydman, G. Bodenhausen, S. Jannin and P. Giraudeau, *Hyperpolarized NMR of plant and cancer cell extracts at natural abundance*, 2015, Analyst 140, 5860-5863.
11. M. Callon, B. Vuichoud, M. Rosas-Ballina, A. Bornet, L. He, J. Milani, M. Baudin, G. Bodenhausen, D. Bumann, S. Jannin and S. Hiller, *Real-Time Observation by NMR of Slow Metabolic Events in Living Mammalian Macrophages by Dissolution Dynamic Nuclear Polarization*, 2016, in preparation.

Remerciements

Je tiens tout d'abord à remercier les différents membres de mon jury de thèse, **Sandrine Gerber-Lemaire** (présidente du jury), **Jean-Philippe Ansermet** (co-directeur de thèse), **Lothar Helm** (rapporteur interne), **Alvar Gossert** (rapporteur externe) et **James Kempf** (rapporteur externe) pour avoir pris le temps de lire et de corriger ma thèse, ainsi que pour la captivante discussion et leurs différentes remarques qui ont suivi mon examen oral.

Je tiens ensuite à remercier mon directeur de thèse, **Geoffrey Bodenhausen**, de m'avoir permis de travailler durant quatre longues et passionnantes années dans son laboratoire. Ayant une liberté presque totale au sein de son groupe, j'ai eu la chance de pouvoir entreprendre les expériences que je désirais. Je ne le remercierai jamais assez de m'avoir fait confiance tout au long de mon travail de thèse.

Je voudrais aussi remercier **Lyndon Emsley** pour m'avoir intégré dans son groupe le LRM(A) durant la fin de ma thèse et m'avoir permis de continuer à travailler sur mes différents projets tout en m'incluant dans la vie et l'ambiance de son laboratoire.

Je tiens à remercier **Béatrice Bliesener** pour l'organisation toujours impeccable de mes voyages à l'étranger et pour tous les problèmes de bureaucratie qu'elle a su gérer avec grande efficacité. Et je remercie aussi **Nadia Gauljaux** qui fut "*forcée*" de s'occuper de tous ces problèmes durant les 6 derniers mois de ma thèse. Merci aussi à **Anne Lene Odegaard** pour la gestion de tous mes problèmes liés à l'école doctorale.

Le service RMN ne serait pas ce qu'il est aujourd'hui sans **Pascal Miéville**, **Martial Rey**, **Emilie Baudat** et **Anto Barisic** et tous les efforts qu'ils fournissent lorsque les spectromètres décident de se mettre en grève (ce qui arrive aussi souvent que les grèves en France). Merci à toute l'équipe de l'atelier mécanique et plus spécialement à **André Fattet**, **Roger Mottier** et **Gil Corbaz** pour avoir fait preuve de patience lors de mes différentes commandes de pièces. Merci à **Donald Zbinden** pour tous les problèmes liés à l'informatique et les debuggages de mon ordinateur, et merci aussi à **Patrick Favre** et **Frédéric Gumy** qui nous ont laissé pour aller vivre et exercer dans des pâturages plus ensoleillés.

Je voudrais maintenant saluer les différentes personnes avec qui j'ai travaillé au cours de ces 4 dernières années et je voudrais commencer bien entendu avec le "*gang des barbus*" de la DNP.

J'ai eu la chance de pouvoir travailler avec **Sami Jannin**, un incroyable conférencier et imitateur hors pair de grands scientifiques, qui m'a aidé et encadré tout au long de ma thèse et sans qui je n'aurais pas eu autant de plaisir à faire de la dissolution-DNP. J'attends toujours avec impatience l'organisation de son très célèbre Beaufathlon™.

Merci aussi à **Aurélien Bornet** qui, malgré le fait d'être né valaisan, fut un excellent collègue, camarade et concurrent à la Nintendo 64 et aussi un fervent admirateur de la Lex Weber qui permit une meilleure entente entre nos cantons respectifs (bande de culs de valaisans).

Je remercie **Jonas Milani** pour sa bonne humeur naturelle dans le laboratoire et pour les soirées de chants passées après les longues journées de conférences (vent frais, vent du matin). Sa voix discrète et mélodieuse dans les couloirs va terriblement me manquer, de même que les repas de Saint Martin au Jura (c'est nous qu'on chante).

Je salue aussi **Quentin Chappuis** qui a arrêté malheureusement trop tôt la dissolution-DNP dans notre laboratoire, mais avec qui je garde néanmoins de bons souvenirs.

Je voudrais remercier maintenant les membres et ex-membres du LRMB en commençant par **Mathieu Baudin** qui est toujours présent et se bat quotidiennement avec détermination afin de faire fonctionner le nouveau polariseur (je lui souhaite bon courage). Merci à **Xiao Ji**, le plus suisse des chinois, pour sa bonne humeur journalière et ses étranges positions lors des groupmeetings. Merci aussi à **Estel Canet**, pour l'interminable travail que l'on a fait ensemble sur l'hyperpolarisation des gaz (et vive la Catalogne libre!). Je remercie aussi **Angel Joaquin Perez Linde**, AJ, pour les multiples conversations que nous avons eu autour de la science et de l'Espagne (doublecheck). Un grand merci aux italiens du labo, **Daniele Mammoli**, toujours bon second aux concours de vins, et **Roberto Buratto**, à qui j'ai pu faire découvrir les délicieux vins vaudois et leur supériorité aux vins fades italiens. Et finalement merci aux anciens disparus du LRMB avec qui j'ai brièvement travaillé, **Takuya Segawa**, **Pavel Sekatski**, **Diego Carnevale**, **Srinivas Chinthapalli** et **Nicola Salvi**.

Je voudrais souhaiter bonne chance aux nouveaux membres du LRM(A), **Jasmine Viger-Gravel**, **Claudia Avalos**, **Snaedis Björgvinsdóttir**, **Dominik Kubicki**, **Federico Paruzzo**, **Albert Hofstetter**, **Brennan Walder**, **Jayasubba Yarava**, **Gabriele Stevanato**, **Baptiste Buzi** (champion du monde de pompes sur une main) et un grand merci tout particulièrement à **Arthur César Pinon** pour sa motivation "*to never skip leg day*" et pour l'incroyable soirée à Pittsburgh après le dîner interminable de la conférence.

Je remercie aussi toute l'équipe du groupe "*Misère*" constitué de **Mickael**, **Stéphanie**, **Léonard**, **Felix**, **Florian**, **Antoine**, **Mathieu** et **Nicolas** pour toutes les palpitantes parties de cartes faites à l'Arcadie en dégustant de délicieux hamburgers froids.

Finalement j'aimerais remercier **toute ma famille** pour leur soutien et aussi de tout mon cœur **Mirella** qui m'a soutenu et supporté pendant ces 4 ans et qui n'a jamais cessé de croire en moi.

Curriculum Vitae

Last Name Vuichoud
First Name Basile
Date of birth 04.05.1988
Address Chemin du Mottey 35, 1020 Renens (CH)
E-mail basile.vuichoud@epfl.ch
basile.vuichoud@gmail.com
Cellphone +41 79 567 31 26



Professional Objective

- Post Doctoral Research Position in Dissolution Dynamic Nuclear Polarization
- Development of novel techniques and implementations in Nuclear Magnetic Resonance

Research and Formation

- **Ph. D Thesis Assistant** of Prof. G. Bodenhausen 2013 - Present
Laboratory of Biomolecular Magnetic Resonance LRMB, EPFL
- **Master Thesis Student** of Prof. K. Severin 2012 - 2013
Laboratory of Supramolecular Chemistry LCS, EPFL
- **Semester Project Student** of Prof. K. Severin 2012
Laboratory of Supramolecular Chemistry LCS, EPFL

Academic Degrees

- **Ph. D Thesis** Expected 2017
Thesis entitled "*Novel Sample Formulations for Pure and Persistent Hyperpolarized Solutions via Dissolution Dynamic Nuclear Polarization*"
Under the supervision of Prof. G. Bodenhausen, LRMB, EPFL
- **Master of Science MSc in Molecular and Biological Chemistry** October 2013
Thesis entitled "*Activation of Nitrous Oxide by Organic Compounds*"
Under the supervision of Prof. K. Severin, LCS, EPFL
- **Bachelor of Science BSc in Molecular and Biological Chemistry** Août 2011
Section de Chimie et Génie Chimique, EPFL
- **Maturité Fédérale** June 2006
Bilingual Diploma (French/German), Gymnase Auguste Piccard

Work Experiences

- **Firefighter with SCBA formation** (self-contained breathing apparatus) 2009 - 2014
1st Aid Detachment, SDIS Paudèze, Pully
- **Night Warden** 2007 - 2009
CHUV, Psychiatric Hospital Cery, Lausanne
- **Propaedeutic Course in Medicine** June 2007
CHUV, Psychiatric Hospital Cery, Lausanne

Teaching Experiences

- **Teaching Assistant**

Laboratory work for undergraduate student in Chemistry, Scientific Police, Geology and Pharmacology 2012 - Present

Exercices for Structural Analysis lecture in Chemistry

Experimental Molecular Sciences lecture for Master Students

Guidance for a Master Project at the EPFL

"The preparation of hyperpolarized water and its use to enhance Water-LOGSY drug screening"

Instructor and designer of a Massively Open Online Course MOOC

"Basic Steps in Magnetic Resonance"

- **Ph. D Assistants Representative**

2014 - 2016

Schedule Management for Chemistry and Ph. D Students at the EPFL

Languages and Skills

- **French** Mother tongue

- **English** Fluent

- **German** Conversational (Bilingual Diploma)

- **Computer** Matlab, Origin, Mathematica, Adobe Illustrator, MestreNova, Bruker TopSpin programming, MS Office, ChemDraw, EndNote

Scientific Track Record

- **Publications**

18 published articles, 4 as first author, 3 as corresponding author (*h* index = 8)

- **Conference Papers**

3 oral presentations, 8 poster presentations

Prizes and Awards

- **Best Poster Prize**, 4th International DNP Symposium, Helsingor, Denmark, 2013

- **Second Poster Prize**, Master Project Ceremony, EPFL, Switzerland, 2013

- **Best Teaching Award**, EPFL

- **Student Travel Stipend** at ENC Conference, 2016, Pittsburgh, Pennsylvania, USA

- **Student Travel Stipend** at EUROMAR Conference, 2015, Prague, Czech Republic

Extra-Curricular Activities

- PADI Advanced Open Water Scuba Diver

- Martial Arts, Jujitsu, 1st Kyu (brown belt)

- Music, guitar player, 12 years studies, Ecole de Musique de Pully

- Skiing, Outdoor Climbing and Hiking

Personal Detail

28 years, single, Swiss, native Montreux, driving license motorbike A1 and car B

Publications List

- 1) Tskhovrebov Alexander G., **Vuichoud Basile**, Solari Euro, Scopelliti Rosario, Severin Kay*, *Adducts Of Nitrous Oxide and N-Heterocyclic Carbenes: Syntheses, Structures, and Reactivity*, **Journal of the American Chemical Society**, 2013, 135, 9486-9492.
- 2) **Vuichoud Basile**, Milani Jonas, Bornet Aurélien*, Melzi Roberto, Jannin Sami*, Bodenhausen Geoffrey, *Hyperpolarization of Deuterated Metabolites via Remote Cross-Polarization and Dissolution Dynamic Nuclear Polarization*, **The Journal of Physical Chemistry B**, 2014, 18, 1411-1415.
- 3) Gajan David, Bornet Aurélien, **Vuichoud Basile**, Milani Jonas, Melzi Roberto, van Kalkeren Henri A., Veyre Laurent, Thieuleux Chloé, Conley Matthew P., Grüning Wolfram R., Schwarzwälder Martin, Lesage Anne, Copéret Christophe, Bodenhausen Geoffrey, Emsley Lyndon*, Jannin Sami, *Hybrid Polarizing Solids for Pure Hyperpolarized Liquids through Dissolution Dynamic Nuclear Polarization*, **Proceedings of the National Academy of Sciences**, 2014, 111, 14693-14697.
- 4) Buratto Roberto, Bornet Aurélien*, Milani Jonas, Mammoli Daniele, **Vuichoud Basile**, Salvi Nicola, Singh Maninder, Laguerre Aurélien, Passemard Solène, Gerber-Lemaire Sandrine, Jannin Sami, Bodenhausen Geoffrey*, *Drug Screening Boosted by Hyperpolarized Long-Lived States in NMR*, **ChemMedChem**, 2014, 9, 2509-2515.
- 5) Bornet Aurélien, Milani Jonas, **Vuichoud Basile**, Perez Linde Angel J., Bodenhausen Geoffrey, Jannin Sami*, *Microwave Frequency Modulation to Enhance Dissolution Dynamic Nuclear Polarization*, **Chemical Physics Letters**, 2014, 602, 63-67.
- 6) Perez Linde Angel J.*, Bornet Aurélien, Milani Jonas, **Vuichoud Basile**, Melzi Roberto, Jannin Sami, Bodenhausen Geoffrey, *Cross Polarization from ^1H to quadrupolar ^6Li nuclei for Dissolution DNP*, **Physical Chemistry Chemical Physics**, 2014, 16, 24813-24817.
- 7) Bornet Aurélien*, Ji Xiao, Mammoli Daniele, **Vuichoud Basile**, Milani Jonas, Bodenhausen Geoffrey*, Jannin Sami, *Long-Lived States of Magnetically Equivalent Spins Populated by Dissolution-DNP and Revealed by Enzymatic Reactions*, **Chemistry a European Journal**, 2014, 20, 17113-17118.
- 8) Chappuis Quentin, Milani Jonas, **Vuichoud Basile**, Bornet Aurélien, Gossert Alvar D.*, Bodenhausen Geoffrey, Jannin Sami*, *Hyperpolarized Water to Study Protein-Ligand Interactions*, **The Journal of the Physical Chemistry Letters**, 2015, 6, 1674-1678.
- 9) Milani Jonas*, **Vuichoud Basile**, Bornet Aurélien, Miéville Pascal, Mottier Roger, Jannin Sami, Bodenhausen Geoffrey, *A Magnetic Tunnel to Shelter Hyperpolarized Fluids*, **Review of Scientific Instruments**, 2015, 86, 024101.
- 10) Mammoli Daniele*, **Vuichoud Basile**, Bornet Aurélien, Milani Jonas, Dumez Jean-Nicolas, Jannin Sami, Bodenhausen Geoffrey, *Hyperpolarized para-Ethanol*, **The Journal of Physical Chemistry B**, 2015, 119, 4048-4052.
- 11) Dumez Jean-Nicolas, Milani Jonas, **Vuichoud Basile**, Bornet Aurélien, Lalande-Martin Julie, Tea Illa, Yon Maxime, Maucourt Mickaël, Deborde Catherine, Moing Annick, Frydman Lucio, Bodenhausen Geoffrey, Jannin Sami*, Giraudeau Patrick*, *Hyperpolarized NMR of Plant and Cancer Cell extracts at Natural Abundance*, **Analyst**, 2015, 140, 5860-5863.
- 12) **Vuichoud Basile***, Milani Jonas, Chappuis Quentin, Bornet Aurélien, Bodenhausen Geoffrey, Jannin Sami*, *Measuring Absolute Spin Polarization in Dissolution-DNP by Spin Polarimetry Magnetic Resonance (SPY-MR)*, **Journal of Magnetic Resonance**, 2015, 260, 127-135.
- 13) Pöschko Maria Theresia, **Vuichoud Basile**, Milani Jonas, Bornet Aurélien, Bechmann Matthias, Bodenhausen Geoffrey, Jannin Sami*, Müller Norbert*, *Spin Noise Detection of Nuclear Hyperpolarization at 1.2 K*, **ChemPhysChem**, 2015, DOI:10.1002/cphc.20150805.
- 14) Bornet Aurélien, Maucourt Mickaël, Deborde Catherine, Jacob Daniel, Milani Jonas, **Vuichoud Basile**, Ji Xiao, Dumez Jena-Nicolas, Moing Annick, Bodenhausen Geoffrey, Jannin Sami*, Giraudeau Patrick*, *Highly Repeatable Dissolution Dynamic Nuclear Polarization for Heteronuclear NMR Metabolomics*, **Analytical Chemistry**, 2016, 88, 6179-6183.

- 15) Baudouin David*, van Kalker Henri A, Bornet Aurélien, **Vuichoud Basile**, Veyre Laurent, Cavailles Matthieu, Schwarzwälder Martin, Liao Wei-Chih, Gajan David, Bodenhausen Geoffrey, Emsley Lyndon, Lesage Anne, Jannin Sami, Copéret Christophe, Thieuleux Chloé*, *Cubic three-dimensional hybrid silica solids for nuclear hyperpolarization*, **Chemical Science**, 2016, DOI: 10.1039/c6sc02055k.
- 16) **Vuichoud Basile***, Bornet Aurélien, de Nanteuil Florian, Milani Jonas, Canet Estel, Ji Xiao, Miéville Pascal, Weber Emmanuelle, Kurzbach Dennis, Flamm Andrea, Konrat Robert, Gossert Alvar, Jannin Sami*, Bodenhausen Geoffrey, *Filterable Agents for hyperpolarization of Water, Metabolites, and Proteins*, **Chemistry A European Journal**, 2016, 22, 14696-14700.
- 17) **Vuichoud Basile***, Canet Estel, Milani Jonas, Bornet Aurélien, Baudouin David, Veyre Laurent, Gajan David, Emsley Lyndon, Lesage Anne, Copéret Christophe, Thieuleux Chloé, Bodenhausen Geoffrey, Koptuyug Igor, Jannin Sami*, *Hyperpolarization of Frozen Hydrocarbon Gases by Dynamic Nuclear Polarization at 1.2 K*, **Journal of Physical Chemistry Letters**, 2016, 7, 3235-3239.
- 18) Grüning Wolfram R., Bieringer Harald, Schwarzwälder Martin, Gajan David, Bornet Aurélien, **Vuichoud Basile**, Milani Jonas, Baudouin David, Veyre Laurent, Lesage Anne, Jannin Sami, Bodenhausen Geoffrey, Thieuleux Chloé*, Copéret Christophe*, *Phenylazide Hybrid-Silica – Polarization Platform for Dynamic Nuclear Polarization at Cryogenic Temperatures*, **Helvetica Chimica Acta**, 2016, DOI: 10.1002/hlca.201600122.

Conference Talks

Microwave Frequency Modulation to Enhance Dissolution Dynamic Nuclear Polarization, Bornet Aurélien, Milani Jonas, **Vuichoud Basile**, Perez Linde Angel J., Bodenhausen Geoffrey, Jannin Sami*, 5th International DNP Symposium, Egmond aan Zee, Netherlands, 2015.

Spin Polarimetry Magnetic Resonance (SPY-MR): Measuring Absolute Spin Polarization in Dissolution Dynamic Nuclear Polarization, **Vuichoud Basile***, Milani Jonas, Chappuis Quentin, Bornet Aurélien, Bodenhausen Geoffrey, Jannin Sami*, European congress on magnetic resonance EUROMAR, Prague, Czech Republic, 2015.

Microwave Frequency Modulation to Enhance Dissolution Dynamic Nuclear Polarization, Bornet Aurélien, Milani Jonas, **Vuichoud Basile**, Perez Linde Angel J., Bodenhausen Geoffrey, Jannin Sami*, COST Meeting, Zürich, Switzerland, 2014.

Conference Posters

Filterable Labeled Agents for Hyperpolarization of Water, Metabolites, and Proteins, **Vuichoud Basile***, Bornet Aurélien, de Nanteuil Florian, Milani Jonas, Canet Estel, Ji Xiao, Miéville Pascal, Weber Emmanuelle, Kurzbach Dennis, Flamm Andrea, Konrat Robert, Gossert Alvar, Jannin Sami*, Bodenhausen Geoffrey, 57th Experimental Nuclear Magnetic Resonance Conference ENC, Pittsburgh, Pennsylvania, USA, 2016.

Spin Polarimetry Magnetic Resonance (SPY-MR): Measuring Absolute Spin Polarization in Dissolution Dynamic Nuclear Polarization, **Vuichoud Basile***, Milani Jonas, Chappuis Quentin, Bornet Aurélien, Bodenhausen Geoffrey, Jannin Sami*, 5th International DNP Symposium, Egmond aan Zee, Netherlands, 2015.

Hybrid Polarizing Solids for Pure Hyperpolarized Liquids through Dissolution Dynamic Nuclear Polarization, Gajan David, Bornet Aurélien, **Vuichoud Basile**, Milani Jonas, Melzi Roberto, van Kalker Henri A., Veyre Laurent, Thieuleux Chloé, Conley Matthew P., Grüning Wolfram R., Schwarzwälder Martin, Lesage Anne, Copéret Christophe, Bodenhausen Geoffrey, Emsley Lyndon*, Jannin Sami, COST Training School Hyperpolarization Techniques, Marseille, France, 2014.

Microwave Frequency Modulation to Enhance Dissolution Dynamic Nuclear Polarization, Bornet Aurélien, Milani Jonas, **Vuichoud Basile**, Perez Linde Angel J., Bodenhausen Geoffrey, Jannin Sami*, European congress on magnetic resonance EUROMAR, Zürich, Switzerland, 2014.

Spin Polarimetry Magnetic Resonance (SPY-MR): Measuring Absolute Spin Polarization in Dissolution Dynamic Nuclear Polarization, **Vuichoud Basile***, Milani Jonas, Chappuis Quentin, Bornet Aurélien, Bodenhausen Geoffrey, Jannin Sami*, European congress on magnetic resonance EUROMAR, Zürich, Switzerland, 2014.

Microwave Frequency Modulation to Enhance Dissolution Dynamic Nuclear Polarization, Bornet Aurélien, Milani Jonas, **Vuichoud Basile**, Perez Linde Angel J., Bodenhausen Geoffrey, Jannin Sami*, 55th Experimental Nuclear Magnetic Resonance Conference ENC, Boston, Massachusetts, USA, 2014.

Cross Polarization of Deuterated Pyruvate for Dissolution-DNP at 188 GHz, **Vuichoud Basile**, Milani Jonas, Bornet Aurélien*, Melzi Roberto, Jannin Sami*, Bodenhausen Geoffrey, 4th International DNP Symposium, Helsingør, Denmark, 2013.

Activation of Nitrous Oxide by Organic Compounds, Tskhovrebov Alexander G., **Vuichoud Basile**, Solari Euro, Scopelliti Rosario, Severin Kay*, Master Project Ceremony, EPFL, Switzerland, 2013.